



# Cryptates and Pendant Arm Ligand Complexes

by

Ashley Stephens B.Sc. (Hons.) (Adelaide)

Thesis submitted for the degree of

Doctor of Philosophy

in

The University of Adelaide

(Faculty of Science)

Department of Chemistry

September, 1994

Awarded 1995

# Contents:

<b>Contents:</b>	i
<b>Abstract:</b>	v
<b>Acknowledgements:</b>	vii
<b>Statement:</b>	viii
<b>Abbreviations:</b>	ix
<b>Chapter 1: Introduction</b>	1
1.1 Cryptands and Supramolecular Chemistry	1
1.2 Applications of Supramolecular Chemistry	8
1.3 Structural Aspects of Cryptates	10
Bibliography	19
<b>Chapter 2: Equilibrium Studies of Monovalent Metal Cryptates</b>	23
2.1 Introduction	23
2.2 Stability of $[MC22C_2]^+$ in Non-Aqueous Solution	28
2.3 Stability of $[MC22C_8]^+$ in Non-Aqueous Solution	34
2.4 $Ag^+$ and $Tl^+$ Cryptates	34
2.5 Effect of Solvent on Cryptate Stability	37
2.6 Effect of the Length of the $C_n$ Bridge on the Stability of $[MC22C_n]^+$	40
Bibliography	42
<b>Chapter 3: Equilibrium Studies of Divalent Metal Cryptates</b>	45
3.1 Protonation Constants of $C22C_2$ and $C22C_8$	45
3.2 Stability Constants of the Divalent Metal Cryptates $[MC22C_2]^{2+}$ and $[MC22C_8]^{2+}$	48
3.2.1 Cryptates of the Alkaline Earth Metal Ions	51
3.2.2 Cryptates of the Heavy Metal Ions $Cd^{2+}$ , $Hg^{2+}$ and $Pb^{2+}$	54
3.2.3 Cryptates of the First-Row Transition Metal Ions	55
3.3 $[M(HC22C_n)]^{3+}$ , $[M(OH)C22C_n]^+$ and $[M(OH)C22C_n]_2^{2+}$ Complexes	60
Bibliography	64
<b>Chapter 4: Cryptate Complexation Dynamics</b>	65
4.1 Introduction	65
4.2 Mechanistic Aspects of Cryptates	66
4.3 Exchange Kinetics of $Na^+$ on $[NaC22C_2]^+$	70

4.4	Exchange Kinetics of Related Cryptate Systems	75
4.5	Exchange Kinetics of Na <sup>+</sup> on [NaC <sub>22</sub> C <sub>8</sub> ] <sup>+</sup>	79
4.6	Exchange Kinetics of Li <sup>+</sup> on [LiC <sub>22</sub> C <sub>8</sub> ] <sup>+</sup>	79
4.7	Exchange Kinetics of Related Cryptate Systems	84
4.8	Effect of Solvent on Cryptate Lability	88
4.9	Effect of the Length of the C <sub>n</sub> Bridge on the Lability of [NaC <sub>22</sub> C <sub>n</sub> ] <sup>+</sup>	91
	Bibliography	93
<b>Chapter 5: Introduction to Pendant Arm Tetraaza Macrocyclic Ligand Complexes</b>		96
	Bibliography	103
<b>Chapter 6: Equilibrium Studies of Monovalent Metal Complexes of TMEC12</b>		106
6.1	Introduction	106
6.2	Stability of [M(TMEC12)] <sup>+</sup> in Non-Aqueous Solution	108
6.3	Effect of Solvent on Complex Stability	111
6.4	Effect of Solvent on Selectivity	112
6.5	A Comparison of the Alkali Metal Complexes of TMEC12, C221 and C22C <sub>2</sub>	117
6.6	Stability of [M(cyclen)] <sup>+</sup> in Non-Aqueous Solution	119
6.7	Effect of the Nature of the Pendant Arm on Complex Stability	120
6.8	Effect of Macrocyclic Ring Size on Complex Stability	122
6.9	Ag <sup>+</sup> Complexes	122
	Bibliography	124
<b>Chapter 7: Equilibrium Studies of Divalent Metal Complexes of TMEC12</b>		126
7.1	Protonation Constants of TMEC12	126
7.2	Stability Constants of Divalent Metal Complexes of TMEC12	129
7.2.1	Alkaline Earth Complexes	129
7.2.2	Complexes of the Heavy Metal Ions Cd <sup>2+</sup> , Hg <sup>2+</sup> and Pb <sup>2+</sup>	132
7.2.3	Complexes of the First-Row Transition Metal Ions	133
7.3	Effect of the Pendant Arm on Complex Stability	134

7.4	Effect of the Nature of the Pendant Arm on Complex Stability	135
7.5	Effect of Macrocyclic Ring Size on Complex Stability	137
7.6	$[M(\text{HTMEC12})]^{(n+1)+}$ and $[M(\text{OH})\text{TMEC12}]^+$ Complexes	138
	Bibliography	141
<b>Chapter 8: Complexation Dynamics of <math>[M(\text{TMEC12})]^+</math></b>		143
8.1	Introduction	143
8.2	Exchange Kinetics of $\text{Na}^+$ on $[\text{Na}(\text{TMEC12})]^+$	144
8.3	Exchange Kinetics of $\text{Li}^+$ on $[\text{Li}(\text{TMEC12})]^+$	149
8.4	Mechanism of Exchange of $\text{M}^+$ on $[M(\text{TMEC12})]^+$	154
8.5	Effect of Solvent on the Lability of $[M(\text{TMEC12})]^+$	154
8.6	Exchange Kinetics of $[M(\text{TMEC12})]^+$ and Related Systems	157
	Bibliography	163
<b>Chapter 9: Intramolecular Exchange in Metal Complexes of TMEC12</b>		165
9.1	Introduction	165
9.2	Solution Structures of Heavy Metal $[M(\text{TMEC12})]^{2+}$	165
9.3	Intramolecular Exchange in Heavy Metal $[M(\text{TMEC12})]^{2+}$	168
9.4	Intramolecular and Intermolecular Exchange in $[\text{Li}(\text{TMEC12})]^+$ and $[\text{Na}(\text{TMEC12})]^+$	175
9.5	A $^{13}\text{C}$ NMR Study of $[\text{Zn}(\text{TMEC12})]^{2+}$	178
	Bibliography	180
<b>Chapter 10: Experimental</b>		181
10.1	Non-Aqueous Titrations	181
10.1.1	Materials	181
10.1.2	Determination of Stability Constants	181
10.2	Aqueous Titrations	184
10.2.1	Materials	184
10.2.2	Determination of Stability Constants	184
10.3	Heavy Metal Complexes of TMEC12	186
10.3.1	Materials	186
10.3.2	Preparation of Complexes	186
10.4	NMR Measurements	187
10.4.1	$^7\text{Li}$ and $^{23}\text{Na}$ NMR Measurements of Intermolecular Metal Ion Exchange	187



10.4.2	$^{13}\text{C}$ NMR Measurements of Intramolecular Exchange in Metal Complexes of TMEC12	188
10.5	Synthesis of Ligands	188
10.5.1	Synthesis of the Cryptand C22C <sub>2</sub>	188
10.5.2	Synthesis of the Cryptand C22C <sub>8</sub>	189
10.5.3	Synthesis of 1,4,7,10-tetrakis(2-methoxyethyl)-1,4,7,10-tetraazacyclododecane (TMEC12)	190
10.5.3.1	Synthesis of <i>NOO'</i> -tris(toluene- <i>p</i> -sulphonyl)bis-(2-hydroxyethyl)amine	191
10.5.3.2	Synthesis of 1,4,7-tris(toluene- <i>p</i> -sulphonyl)-1,4,7-triazaheptane and its Disodium Salt	191
10.5.3.3	Synthesis of 1,4,7,10-tetraazacyclododecane (Cyclen)	191
10.5.3.4	Synthesis of TMEC12	192
	Bibliography	194
<b>Chapter 11: Analysis of Data from Potentiometric Titrations</b>		196
11.1	Determination of Stability Constants of Metal Complexes in Non-Aqueous Solution	196
11.1.1	Direct Titration	197
11.1.2	Competitive Titration	199
11.1.3	Determination of Stability Constants by Curve Fitting	201
11.2	Determination of Stability Constants of Metal Complexes in Aqueous Solution	213
	Bibliography	220
<b>Chapter 12: Kinetic Applications of NMR Spectroscopy</b>		221
12.1	Theory of Two-Site Chemical Exchange	221
12.1.1	Slow Exchange	226
12.1.2	Intermediate Rates of Exchange; Coalescence	227
12.1.3	Fast Exchange	229
12.2	Pulsed Fourier Transform NMR	230
12.3	Lineshape Analysis	231
12.4	Calculation of Activation Parameters	232
	Bibliography	234
<b>Appendix i: The Gutmann Donor Number</b>		236
	Bibliography	238
<b>Publications:</b>		239

## Abstract:

In the first part of this work, the complexation of a range of monovalent and divalent metal ions by the aliphatic bridge cryptands C22C<sub>2</sub> and C22C<sub>8</sub> has been investigated. The results are compared with those for similar cryptands in order to determine the effect of specific structural variations on the complexation properties of cryptands.

The stability constants of the alkali metal cryptates of C22C<sub>2</sub> and C22C<sub>8</sub> and those of Ag<sup>+</sup> and Tl<sup>+</sup> were determined by potentiometric titration in water and a range of non-aqueous solvents. The kinetics of decomplexation of the Li<sup>+</sup> and Na<sup>+</sup> cryptates of C22C<sub>2</sub> and C22C<sub>8</sub> were studied using variable temperature <sup>7</sup>Li and <sup>23</sup>Na NMR spectroscopy, respectively, in several solvents and the kinetic parameters for decomplexation were determined by complete lineshape analysis. The results of these kinetic and equilibrium studies are discussed in terms of metal ion size, metal ion solvation energy, cryptand topology and the solid state structures of these cryptates.

The protonation constants of C22C<sub>2</sub> and C22C<sub>8</sub> and the stability constants of a number of divalent metal complexes of these ligands were determined in aqueous solution using a pH titration method. The metal ions studied include the alkaline earth metal ions, first-row transition metal ions and heavy metal ions. A comparison of these results with those for the alkali metal ions allows an assessment of the influence of the nature of the metal ion on the selectivity of C22C<sub>2</sub> and C22C<sub>8</sub> in their complexation of metal ions.

The second part of this study deals with the complexation of metal ions by the pendant arm tetraaza macrocycle 1,4,7,10-tetrakis(2-methoxyethyl)-1,4,7,10-tetraazacyclododecane (TMEC12). The complexation of alkali metal ions by this type of ligand is a relatively new field of chemistry, and the factors effecting complex stability and lability are investigated.

The stability constants of the alkali metal and Ag<sup>+</sup> complexes of TMEC12 have been determined by potentiometric titration in aqueous solution and several non-aqueous solvents. The kinetics of decomplexation of the Li<sup>+</sup> and Na<sup>+</sup> complexes of TMEC12 were studied using variable temperature <sup>7</sup>Li and <sup>23</sup>Na NMR spectroscopy, respectively, in several solvents. The results are first compared with those for the Na<sup>+</sup> selective cryptands C22C<sub>2</sub> and C221 and the effect of the greater flexibility of TMEC12 on its complexation properties

is considered. The results for TMEC12 are then compared with those for the unsubstituted tetraaza macrocycle cyclen and the related pendant arm ligands THEC12 and TMEC14, which allows an assessment of the effect of the pendant arms and macrocyclic ring size on the complexation properties of these ligands.

The protonation constants of TMEC12 and the stability constants of some alkaline earth, first-row transition metal and heavy metal complexes of TMEC12 were determined by pH titration in aqueous solution. These results are compared with similar results for cyclen, THEC12 and TMEC14, and are considered in terms of the current knowledge on the selective complexation of metal ions by tetraaza and pendant arm tetraaza macrocycles.

An intramolecular exchange process in the  $\text{Cd}^{2+}$ ,  $\text{Hg}^{2+}$  and  $\text{Pb}^{2+}$  complexes of TMEC12 in  $d_4$ -methanol was investigated using variable temperature  $^{13}\text{C}$  NMR, with the kinetic parameters for this exchange process determined by complete lineshape analysis. From these results, the solution structures of these complexes were determined and it was concluded that the mechanism for the intramolecular exchange process involves the exchange between two square antiprismatic enantiomers. The kinetic parameters characterising the intramolecular exchange process for the  $\text{Li}^+$  and  $\text{Na}^+$  complexes taken from the literature are compared with the kinetic parameters for the intermolecular exchange of  $\text{Li}^+$  and  $\text{Na}^+$  between the solvated and complexed states, and it is apparent that these intra- and intermolecular exchange processes occur independently.

## Acknowledgements:

I would like to sincerely thank my supervisor, Professor Stephen Lincoln, for his encouragement, support and direction over the period of this work.

I would also like to recognize my co-workers, especially Philip Clarke, Jeremy Lucas, Ramesh Dhillon and more recently Samer Madbak, for their friendship and support, which has certainly made life more interesting over the last few years. In addition, I thank the general staff of the department for their assistance during this time.

Finally, I would like to thank my parents for their constant interest and encouragement, not only during the course of this study, but throughout the last twenty five years.

## Statement:

This work contains no material which has been accepted for the award of any other degree or diploma in any university or other tertiary institution and, to the best of my knowledge and belief, contains no material previously published or written by another person, except where due reference is made in the text.

I give consent to this copy of my thesis, when deposited in the University Library, being available for loan and photocopying.

Ashley Stephens  
September, 1994

## Abbreviations:

The following abbreviations have been used in this study:

15C5	1,4,7,10,13-pentaoxacyclopentadecane
18C6	1,4,7,10,13,16-hexaoxacyclooctadecane
DB-18C6	2,3,11,12-dibenzo-1,4,7,10,13,16-hexaoxacyclooctadeca-2,11-diene
C21	4,7,13-trioxa-1,10-diazacyclopentadecane
C22	4,7,13,16-tetraoxa-1,10-diazacyclooctadecane
C21C <sub>5</sub>	4,7,13-trioxa-1,10-diazabicyclo[8.5.5]eicosane
C211	4,7,13,18-tetraoxa-1,10-diazabicyclo[8.5.5]eicosane
C22C <sub>2</sub>	4,7,13,16-tetraoxa-1,10-diazabicyclo[8.8.2]eicosane
C22C <sub>5</sub>	4,7,13,16-tetraoxa-1,10-diazabicyclo[8.8.5]tricosane
C221	4,7,13,16,21-pentaoxa-1,10-diazabicyclo[8.8.5]tricosane
C22C <sub>8</sub>	4,7,13,16-tetraoxa-1,10-diazabicyclo[8.8.8]hexacosane
C222	4,7,13,16,21,24-hexaoxa-1,10-diazabicyclo[8.8.8]hexacosane
DB-C222	5,6,14,15-dibenzo-4,7,13,16,21,24-hexaoxa-1,10-diazabicyclo[8.8.8]hexacosa-5,14-diene
C22C <sub>n</sub>	either C22C <sub>2</sub> or C22C <sub>5</sub> or C22C <sub>8</sub>
C <sub>n</sub>	the -(CH <sub>2</sub> ) <sub>n</sub> - moiety (of C22C <sub>n</sub> )
en	1,2-diaminoethane
theen	N,N,N',N'-tetrakis(2-hydroxyethyl)-1,2-diaminoethane
oxalate	ethanedioate
detoda	3,6,9-trioxa-undecanedioate
BHE-C21	1,7-bis(2-hydroxyethyl)-4,10,13-trioxa-1,7-diazacyclopentadecane
BME-C21	1,7-bis(2-methoxyethyl)-4,10,13-trioxa-1,7-diazacyclopentadecane
BHE-C22	1,10-bis(2-hydroxyethyl)-4,7,13,16-trioxa-1,10-diazacyclooctadecane
BME-C22	1,10-bis(2-methoxyethyl)-4,7,13,16-trioxa-1,10-diazacyclooctadecane
cyclen	1,4,7,10-tetraazacyclododecane
THEC12	1,4,7,10-tetrakis(2-hydroxyethyl)-1,4,7,10-tetraazacyclododecane
TMEC12	1,4,7,10-tetrakis(2-methoxyethyl)-1,4,7,10-tetraazacyclododecane
S-THPC12	1,4,7,10-tetrakis((S-) 2-hydroxypropyl)-1,4,7,10-tetraazacyclododecane

cyclam	1,4,8,11-tetraazacyclotetradecane
THEC14	1,4,8,11-tetrakis(2-hydroxyethyl)-1,4,8,11-tetraazacyclotetradecane
TMEC14	1,4,8,11-tetrakis(2-methoxyethyl)-1,4,8,11-tetraazacyclotetradecane
dimethyl-formamide	N,N-dimethylformamide
propylene-carbonate	1,2-propanediol cyclic carbonate
NEt <sub>4</sub> ClO <sub>4</sub>	tetraethylammonium perchlorate
NEt <sub>4</sub> OH	tetraethylammonium hydroxide
NEt <sub>4</sub> Cl	tetraethylammonium chloride
NEt <sub>4</sub> Br	tetraethylammonium bromide
tosyl	<i>p</i> -toluene sulfonyl
tosylate	<i>p</i> -toluene sulfonate
triflate	trifluoromethane sulfonate
L	unspecified ligand
S	unspecified solvent
Å	ångström (10 <sup>-10</sup> m)
r	radius (Å)
D <sub>N</sub>	Gutmann donor number
d <sub>n</sub>	n-deuterated
D	deuterium (2H); as in CDCl <sub>3</sub> and D <sub>2</sub> O
Conc.	concentration (mol dm <sup>-3</sup> )
Expt	experimental
Calc	calculated
VDU	visual display unit
ln	logarithm (base e)
log	logarithm (base 10)
mm Hg	1 mm Hg = 101325 kg m <sup>-1</sup> s <sup>-2</sup>
ms	milliseconds (10 <sup>-3</sup> s)
mV	millivolts (10 <sup>-3</sup> volts)
ISE	ion selective electrode
EMF	potential (volts)
I	ionic strength
E	electrode potential (volts)
E <sub>0</sub>	standard electrode potential (volts)
pH	-log <sub>10</sub> [H <sup>+</sup> ]
pOH	-log <sub>10</sub> [OH <sup>-</sup> ]

$pK_w$	$-\log_{10}[K_w]$
$K_w$	equilibrium constant for self ionisation of water
$T$	temperature (K)
$R$	gas constant ( $J\ mol^{-1}\ K^{-1}$ )
$\Delta G^0$	free energy of complexation ( $kJ\ mol^{-1}$ )
$\Delta G^\ddagger$	free energy of activation ( $kJ\ mol^{-1}$ )
$\Delta H^\ddagger$	enthalpy of activation ( $kJ\ mol^{-1}$ )
$\Delta S^\ddagger$	entropy of activation ( $J\ mol^{-1}\ K^{-1}$ )
$K$	equilibrium (stability) constant
$k$	rate constant ( $s^{-1}$ )
$\tau$	mean lifetime (s)
NMR	nuclear magnetic resonance (spectroscopy)
DNMR	dynamic nuclear magnetic resonance (spectroscopy)
Hz	hertz ( $s^{-1}$ )
MHz	megahertz ( $10^6\ s^{-1}$ )
$\delta$	chemical shift (ppm)
ppm	parts per million
$\chi$	mole fraction
$\omega$	frequency ( $rad\ s^{-1}$ )
$\nu$	frequency ( $s^{-1}$ )
$W_{1/2}$	full width at half maximum amplitude
$T_1$	longitudinal relaxation time (s)
$T_2$	transverse relaxation time (s)
$\gamma$	gyromagnetic ratio



# Chapter 1: Introduction

## 1.1 Cryptands and Supramolecular Chemistry

The current interest in the coordination chemistry of the alkali metal ions originates largely from the research of Pedersen, who was the first to investigate the complexation of alkali metal ions by macrocyclic polyethers.<sup>1-4</sup> Pedersen was interested in preparing non-cyclic phenolic ligands for the complexation of various divalent cations, especially the vanadyl (VO) group. In 1967, he attempted to prepare bis[2-(*o*-hydroxyphenoxy)ethyl]ether by the reaction of partially protected catechol (containing about 10% unreacted catechol) with bis(2-chloroethyl)ether in the presence of sodium hydroxide in *n*-butanol. However, the result was a small quantity of white fibrous crystals, which turned out to be the compound 2,3,11,12-dibenzo-1,4,7,10,13,16-hexaoxacyclooctadeca-2,11-diene (Figure 1.1), later to be known as dibenzo-18-crown-6 or DB-18C6. This compound had the property of being insoluble in methanol, but became readily soluble on the addition of sodium salts.

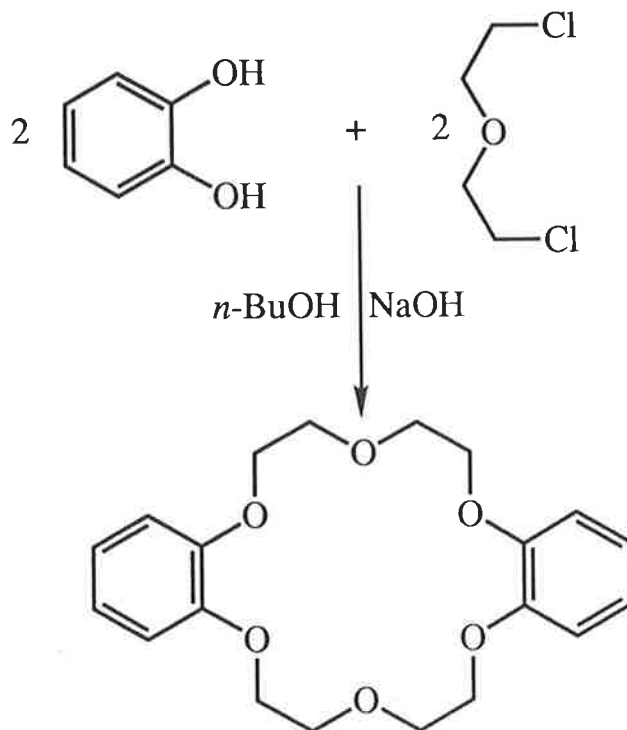


**Figure 1.1.** Formation of the crown ether 2,3,11,12-dibenzo-1,4,7,10,13,16-hexaoxacyclooctadeca-2,11-diene or DB-18C6 from catechol and bis(2-chloroethyl)ether.

Pedersen subsequently published the synthesis and complexing properties of thirty three cyclic polyethers, many of which complexed strongly with alkali, alkaline earth and other metal ions.<sup>1-3</sup> This class of compounds was named crown ethers or coronands (Figure 1.2), because of the crown like appearance of molecular models, and the way they appeared to crown the complexed cation.

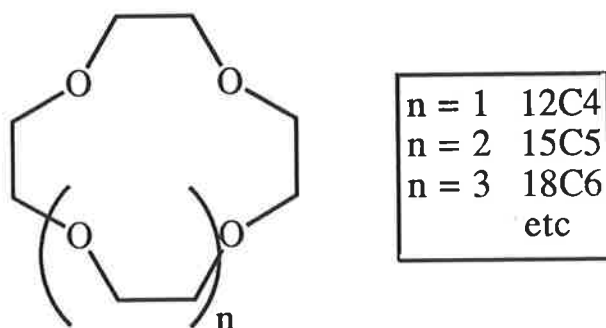
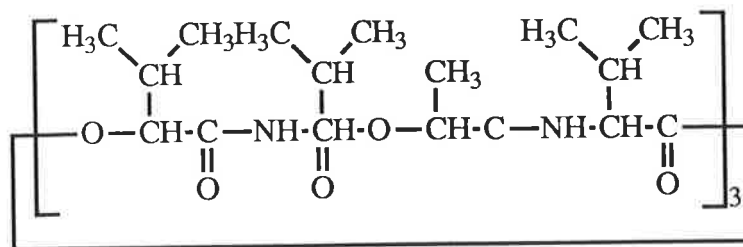


**Figure 1.2.** General structure and trivial nomenclature for the crown ethers, where  $aCb$  is a crown ether containing  $a$  atoms in the macrocyclic ring and  $b$  oxygen donor atoms.

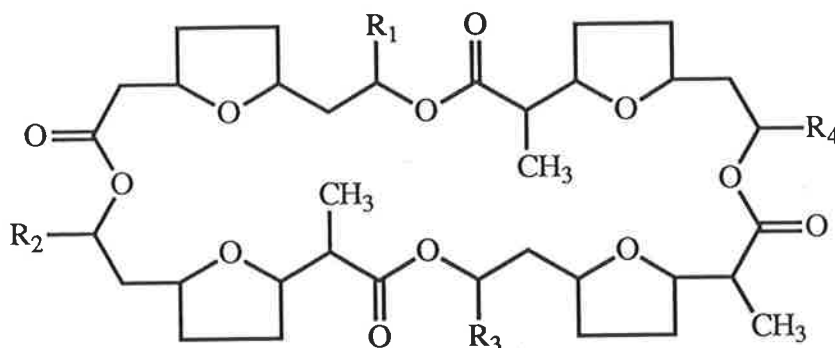
Much of the importance of Pedersen's work (aside from its intrinsic interest) stemmed from the fact that the crown ethers formed stable complexes with the alkali metal ions, which were known to be of biological importance.<sup>5-7</sup> In 1964, it was discovered that the antibiotic valinomycin selectively induces the uptake of  $K^+$  in mitochondria.<sup>8</sup> Further research demonstrated the selective complexation of alkali metal ions by naturally occurring antibiotics such as valinomycin, enniatins A and B, beauvericin and the nactins (Figure 1.3). In addition, these antibiotics and many newly synthesized compounds were found to facilitate the transport of alkali metal ions across natural and artificial lipid membranes.<sup>9-16</sup> Such molecules are known as ionophores.

Valinomycin is a 36 membered cyclic depsipeptide whose structure is shown in Figure 1.3. In the  $K^+$  complex of valinomycin,<sup>17</sup> the ligand folds around the  $K^+$  ion, which is located at the centre of a three dimensional cavity and is octahedrally coordinated to the six ester carbonyl oxygen donor atoms which line the cavity. All the lipophilic side chains point towards the exterior of the complex, which solubilizes the complex in the membrane medium and

(a)



(b)



$R_1 = R_2 = R_3 = R_4 = \text{CH}_3$	Nonactin
$R_1 = R_2 = R_3 = \text{CH}_3$ $R_4 = \text{C}_2\text{H}_5$	Monactin
$R_1 = R_3 = \text{CH}_3$ $R_2 = R_4 = \text{C}_2\text{H}_5$	Dinactin
$R_1 = \text{CH}_3$ $R_2 = R_3 = R_4 = \text{C}_2\text{H}_5$	Trinactin
$R_1 = R_2 = R_3 = R_4 = \text{C}_2\text{H}_5$	Tetranactin

(c)

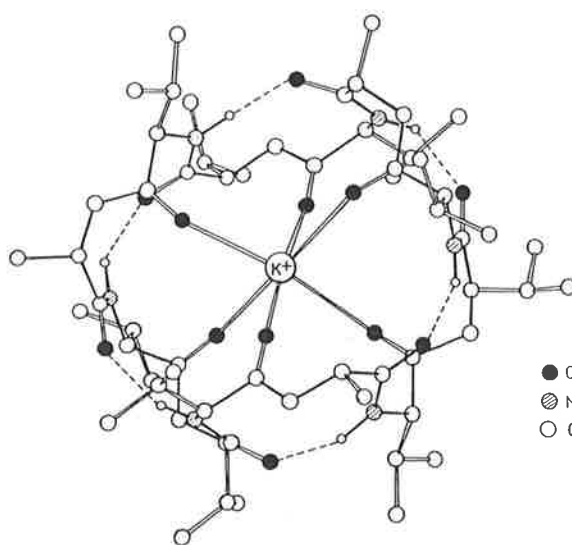
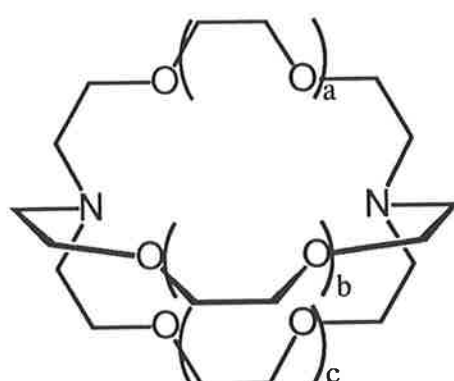


**Figure 1.3.** (a) Structure of valinomycin. (b) Structure of nonactin and its derivatives. (c) Crystal structure of the  $\text{K}^+$  complex of valinomycin.

allows transport of the cation through the membrane. Six intramolecular hydrogen bonds between the amide C=O and NH groups stabilise the ring conformation of the complex and result in limited flexibility. Thus, the size of the intramolecular cavity, which is close to that of  $K^+$ , cannot readily contract, resulting in the observed selectivity of valinomycin for  $K^+$  over  $Na^+$ .<sup>18</sup>

As a result of his fascination with the behaviour of the antibiotics and coincident with the discovery of the crown ethers, Lehn envisaged a ligand that would combine the complexing ability of the antibiotics with the chemical stability of the crown ethers.<sup>4,19</sup> The principle behind the design of such a ligand was to encapsulate the cation within a rigid three dimensional cavity and replace the first solvation shell of the cation with ligand donor atoms, since such a ligand should form more stable complexes than the crown ethers, which possess two dimensional cavities.<sup>19-20</sup> In 1968, Lehn synthesized the first of these ligands; 4,7,13,16-hexaoxa-1,10-diazabicyclo[8.8.8]hexacosane (C222), in which the two nitrogen bridgeheads were linked by three polyether arms.<sup>21</sup> As expected, C222 formed highly stable complexes with a number of monovalent and divalent metal ions, with a pronounced selectivity for  $K^+$  over the other alkali metal ions.<sup>22</sup> It was anticipated that the structure of these ligands would result in the complexed cation being enclosed within the intramolecular cavity and accordingly, these ligands were named cryptands (from the Greek for hidden) and their metal complexes were named cryptates. Subsequently, several more cryptands were synthesized and were shown to form highly stable complexes with numerous metal ions.<sup>23-35</sup> The most striking feature of these ligands was a marked selectivity in their complexation of the alkali metal ions, which was dependent on the relative sizes of the metal ion and the intramolecular cryptand cavity.<sup>25-26</sup>

The trivial name of the cryptand C222 indicates that each polyether chain contains two oxygen donor atoms. The general structural formula and trivial nomenclature of the cryptands are shown in Figure 1.4, together with some aliphatic bridge cryptands. These cryptands differ from the other cryptands in Figure 1.4 simply by the replacement of a polyether bridge by a purely hydrocarbon bridge. For example, C21C<sub>5</sub> and C22C<sub>5</sub> may be derived from C211 and C221, respectively, by the replacement of an ether oxygen by a methylene group. Similarly, C22C<sub>8</sub> is derived from C222 by the replacement of two ether oxygen donor atoms by methylene groups.



a	b	c	cryptand	donor atoms
0	0	0	C111	5 (2N, 3O)
1	0	0	C211	6 (2N, 4O)
1	1	0	C221	7 (2N, 5O)
1	1	1	C222	8 (2N, 6O)
2	1	1	C322	9 (2N, 7O)
2	2	1	C332	10 (2N, 8O)
2	2	2	C333	11 (2N, 9O)
1	0	C <sub>5</sub>	C21C <sub>5</sub>	5 (2N, 3O)
1	1	C <sub>2</sub>	C22C <sub>2</sub>	6 (2N, 4O)
1	1	C <sub>5</sub>	C22C <sub>5</sub>	6 (2N, 4O)
1	1	C <sub>8</sub>	C22C <sub>8</sub>	6 (2N, 4O)

**Figure 1.4.** Structures and trivial nomenclature for some typical cryptands. Here, C<sub>n</sub> denotes an aliphatic bridge, (CH<sub>2</sub>)<sub>n</sub> units in length.

The cryptands have been the centre of substantial research since their synthesis by Lehn in 1968. This is not only a result of their own intrinsic interest, which lies in their ability to form selective and highly stable complexes with the alkali metal ions, but also because their complexation properties resemble those of naturally occurring antibiotics such as valinomycin, which are important in the selective complexation and transport of alkali metal ions across biological membranes. The aim of this section of the study is to improve the current understanding of the thermodynamic, kinetic and mechanistic aspects of cryptate chemistry. In particular, this study explores the complexation properties of the aliphatic bridge cryptands 4,7,10,13-tetraoxa-1,10-diazabicyclo[8.8.2]eicosane (C22C<sub>2</sub>) and 4,7,10,13-tetraoxa-1,10-diazabicyclo[8.8.8]hexacosane (C22C<sub>8</sub>) (Figure 1.5) with some monovalent and divalent metal ions in a range of solvents. Both C22C<sub>2</sub> and C22C<sub>8</sub> differ from conventional cryptands in that the third arm connecting the two nitrogen bridgeheads contains no donor atoms. Thus, C222 and other conventional cryptands (Figure 1.5), with oxygen donor atoms in each of their three arms, are able to enclose a cation within a spherical array of donor atoms, whereas C22C<sub>2</sub> and C22C<sub>8</sub> cannot. Consequently, C22C<sub>2</sub>, C22C<sub>8</sub> and the other aliphatic bridge cryptands shown in Figure 1.5 allow a direct assessment of the effect of specific structural variations on the complexation properties of cryptands.

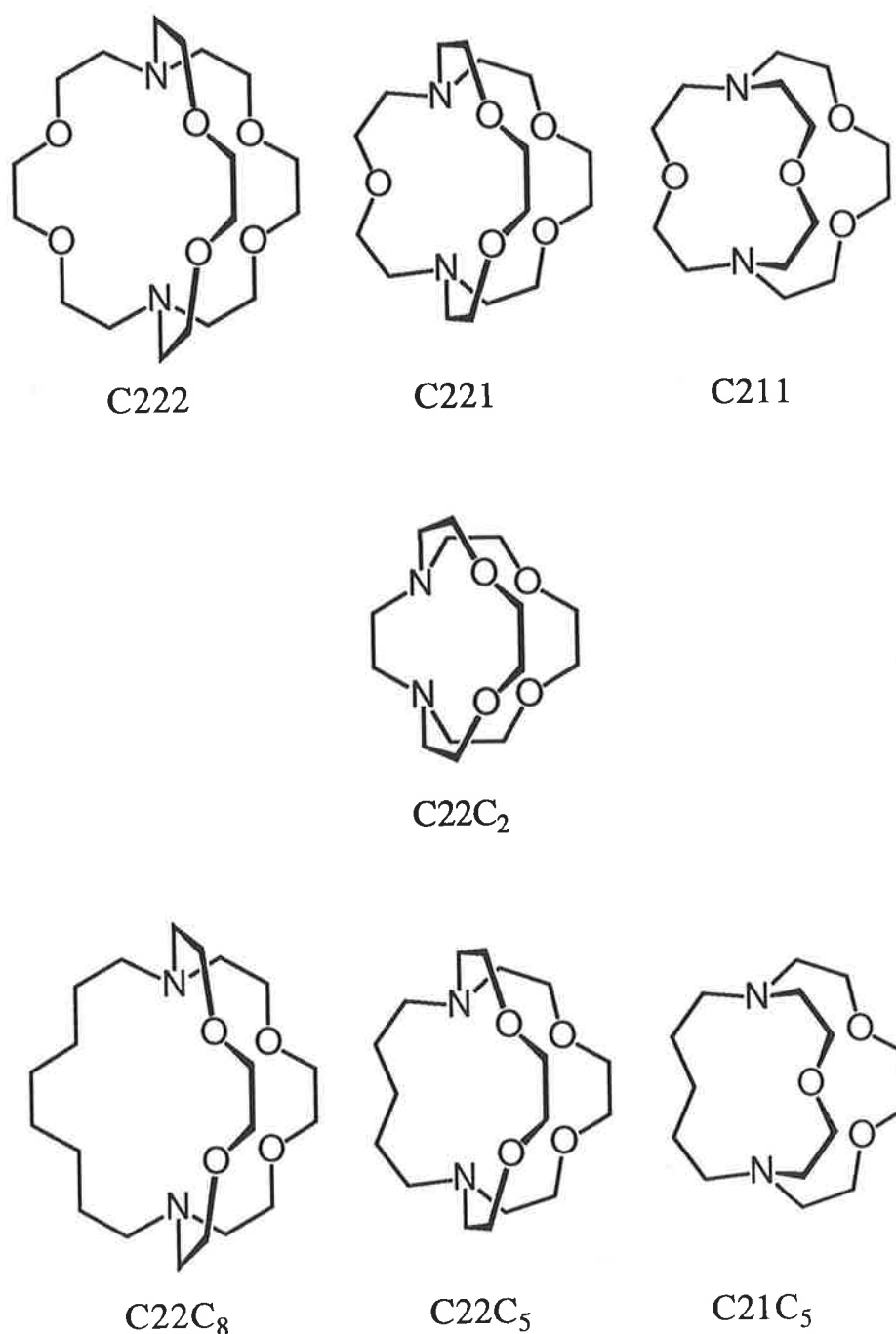


**Figure 1.5.** Structures of some conventional and aliphatic bridge cryptands. The structural relationships between C211 and C21C<sub>5</sub>, C221 and C22C<sub>5</sub> and C222 and C22C<sub>8</sub>, respectively, are clear, whereas C22C<sub>2</sub> has a unique structure as a consequence of the shortness of the  $-(\text{CH}_2)_2-$  moiety connecting the two nitrogen bridgeheads.

The complexation of metal ions by cryptands is part of a wider field of chemistry described by Lehn as supramolecular chemistry.<sup>19,27-28</sup> Lehn defined supramolecular chemistry as the association of two or more chemical species held together by intermolecular forces. When a molecular receptor (*ie* a cryptand) binds a substrate (*ie* a metal ion) a supermolecule is formed; the selective complexation of a substrate by a receptor is known as molecular recognition.<sup>19,25,28</sup> The selective complexation of alkali metal ions by cryptands is an example of spherical recognition; as a result of its spherical intramolecular cavity, the cryptand selectively complexes (recognizes) a spherical alkali metal ion whose size matches that of the cryptand cavity.<sup>19,25-26</sup> The cryptates demonstrate one of the principles of receptor design; that of preorganisation.<sup>19</sup> This simply means that the binding sites of the receptor are prearranged for the recognition (binding) of the substrate. The concept of preorganisation was extended by Cram with the spherands,<sup>29-30</sup> an example of which appears in Figure 1.6. The crystal structure of this ligand is almost identical to that of its  $\text{Li}^+$  complex, which demonstrates that complexation results in almost no conformational change.<sup>31</sup> In the free state the cavity is already present and its dimensions are well suited to the complexation of  $\text{Li}^+$  and  $\text{Na}^+$ . This is reflected in the stabilities of the  $\text{Li}^+$  and  $\text{Na}^+$  complexes of this spherand, which are far greater than those of their cryptate analogues.<sup>32</sup> As a result of the very high rigidity of the cavity, the selectivity of this ligand is so great that the other alkali metal ions do not appear to form complexes at all.<sup>32</sup>

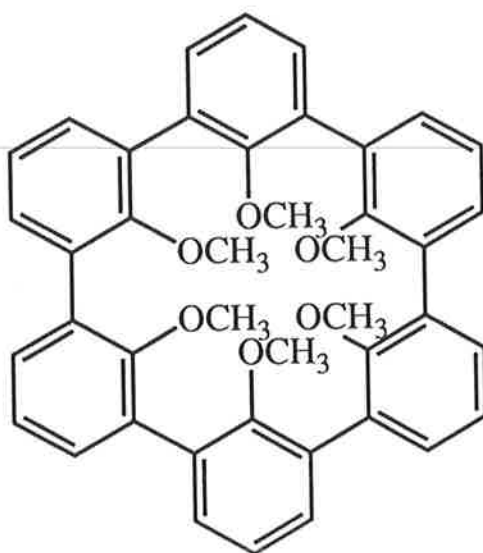


Figure 1.6. Structure of a spherand synthesized by Cram.

Supramolecular chemistry extends far beyond the simple binding of a cation by a ligand. The cryptands were precursors in the development of new ideas in creating receptors for the specific binding of substrates.<sup>25</sup> Specific design strategies have led to the synthesis of macrocyclic and macropolycyclic receptors which selectively complex ammonium ions, organic ions, anions and molecules.<sup>19,27,33-34</sup> Multiple recognition may be achieved with macropolycyclic ligands containing several different receptor sites for the simultaneous recognition of different substrates.<sup>19,27,34</sup> If the receptor contains reactive functions, it may effect a chemical transformation on the bound species and a membrane soluble receptor may effect the translocation of the bound substrate.<sup>19,28</sup> Indeed, Lehn has defined the basic functions of a supramolecular species to be molecular recognition, transformation and translocation.<sup>19</sup> In 1987, Pedersen, Cram and Lehn were awarded the Nobel prize for chemistry for their contribution to supramolecular chemistry. The effective and potential applications resulting from their work include areas such as catalysis, analytical, polymer and separation chemistry, immunobiology, non-linear optics, molecular electronics and artificial photosynthesis.<sup>4</sup>

## 1.2 Applications of Supramolecular Chemistry

The description of some of the applications of supramolecular chemistry which appears below serves to illustrate the diversity and importance of this area of pure and applied research. The examples given here are by no means exhaustive.

**Anion Activation:** Complexation of the cation of a salt by a macrocycle or macropolycycle increases the solubility of that salt in organic solvents. Separation of the cation-anion pair is achieved, which results in anion activation.<sup>20,27,33</sup> This phenomenon may be used in many organic syntheses in which the low solubility of the anion results in very slow reaction rates. It is also applied in phase transfer catalysis, where cryptands assist the transfer of anionic reactants, either from solid to liquid or from liquid to liquid phases.<sup>34</sup> Cryptands have also many applications in the field of anion polymerisation, where they are used to activate anion initiators.<sup>33</sup>

**Anion Complexation:** In chemistry, anions play many roles, including that of nucleophiles, bases, redox agents and phase transfer catalysts and in biology, enzyme substrates are more usually anions than cations.<sup>33</sup> Complexation of



anions can bring about changes in chemical reactivity as does cation complexation.<sup>33</sup> Macrocycles have been synthesized that selectively complex halide ions, carboxylates and phosphates, where the last two species are of special interest as they serve as anchoring sites for numerous biological substrates.<sup>19,35-37</sup>

**Chiral Recognition:** Chiral crown ethers and macropolycyclic ligands have been synthesized that selectively bind one enantiomer of a racemic mixture over the other. Such compounds have been used to separate racemic mixtures of alkyl ammonium salts and amino acids.<sup>20,28,38-39</sup>

**Chromatography:** Because of their selective complexation ability, monomeric cyclic polyethers or polymeric cyclic polyethers and cryptands allow the separation of cations, anions and organic compounds in chromatography.<sup>20,40</sup> For example, cryptands bound to a polymeric solid support act as an ion exchange resin and may be used to separate alkali, alkaline earth, heavy or precious metals.

**Detoxification:** Pollution from heavy metals and radioactive materials are an increasing environmental problem.<sup>27</sup> Cryptands may be used to selectively bind the toxic heavy metals  $\text{Cd}^{2+}$ ,  $\text{Hg}^{2+}$  and  $\text{Pb}^{2+}$ , while leaving the biologically essential cations  $\text{Na}^+$ ,  $\text{K}^+$ ,  $\text{Mg}^{2+}$ ,  $\text{Ca}^{2+}$  and  $\text{Zn}^{2+}$ .<sup>33</sup> Removal of the radioactive cations  $^{85}\text{Sr}^{2+}$ ,  $^{224}\text{Ra}^{2+}$  and  $^{140}\text{Ba}^{2+}$  has been achieved using the cryptand C222.<sup>40-44</sup>

**Electrochemical Determination Methods:** Cation concentration may be determined by potentiometric, conductometric, polarographic and voltammetric determinations.<sup>40</sup> For example,  $\text{Na}^+$  and  $\text{K}^+$  solutions may be standardized by titration with aqueous solutions of C221 and C222, respectively, in weakly alkaline solution, using a cation selective electrode. Conductometric titrations of alkali metal salts with crown ethers or cryptands may also be used.

**Ion Selective Electrodes:** Cyclic polyethers may be used as carrier molecules in ion selective electrodes.<sup>5,19</sup>

**Isotopic Separation:** Crown ethers and cryptands have been used to separate  $^{22}\text{Na}^+$  /  $^{24}\text{Na}^+$  and  $^{40}\text{Ca}^{2+}$  /  $^{44}\text{Ca}^{2+}$ .<sup>27,33</sup>

**Membrane Transport Processes:** The transport of ions and molecules across membranes is of fundamental importance in biological systems.<sup>7,48-49</sup> A large number of macrocycles have been used as ionophores in membrane transport studies, with the cryptands acting as efficient carriers for the alkali metal ions.<sup>37</sup> Anion transport, cation-anion cotransport and the transport of amino acids have also been achieved.<sup>28,39,50-51</sup> Such studies give a deeper insight into transport mechanism, in the development of selective carriers for pharmacology, in analytical chemistry, or in separation science.<sup>28</sup>

**Molecular and Supramolecular Devices:** The combination of receptors, carriers and catalysts with polymolecular organized assemblies creates molecular and supramolecular devices; structures capable of performing operations such as energy, electron or ion transfer, information storage and signal transduction.<sup>19</sup>

**Selective Chromogenic Reagents:** Crown ethers and cryptands to which chromophoric functional groups are attached have been developed. These compounds undergo specific colour changes when binding alkali or alkaline earth metal ions and can serve as probes or photometric reagents selective for these metal ions.<sup>52-53</sup>

**Supramolecular Reactivity and Catalysis:** Molecular receptors bearing appropriate reactive groups have been synthesized that selectively complex a substrate, react with it and release the products.<sup>19</sup> The design of efficient and selective supramolecular reagents and catalysts may give mechanistic insight into the elementary steps of catalysis, provide new types of chemical reagents and lead to a better understanding of enzymatic catalysis.<sup>19,28</sup> Examples of reactions catalysed by receptor molecules include ester cleavage, hydrogen transfer and the hydrolysis of adenosine triphosphate.<sup>54-57</sup>

### 1.3 Structural Aspects of Cryptates

The selective complexation of alkali metal ions by cryptands arises from the ability of the ligand to completely encapsulate the appropriately sized metal ion within the intramolecular cryptand cavity. Crystallographic studies of the cryptates have been extensive, and this has resulted in considerable knowledge of the structural characteristics of these complexes in the solid state.<sup>58-73</sup> These characteristics are largely determined by the relative sizes of the metal ions and the cryptand cavity, as discussed below.

Cryptands may exist in any of three conformations, depending on the configuration of the nitrogen bridgeheads (Figure 1.7). These are the *endo-endo* conformation, in which the lone pair of electrons of both nitrogen donor atoms are directed towards the centre of the cryptand cavity and the *endo-exo* and *exo-exo* conformations, in which one or both nitrogen lone pairs are directed away from the cavity. The *endo-endo* conformation is the conformer observed in the cryptates, since this allows all of the ligand donor atoms to interact with the metal ion.<sup>58-73</sup> The solid state structure of C222 shows that the free ligand adopts the *endo-endo* conformation that is observed in the solid state structures of its cryptates.<sup>60</sup> However, the uncomplexed cryptand is somewhat extended compared with the cryptate, and compensates for the vacant cavity by rotating a methylene group inward, with some of the oxygen lone pairs directed away from the cavity centre.<sup>60</sup> This demonstrates that some conformational changes must occur during the complexation of a metal ion.

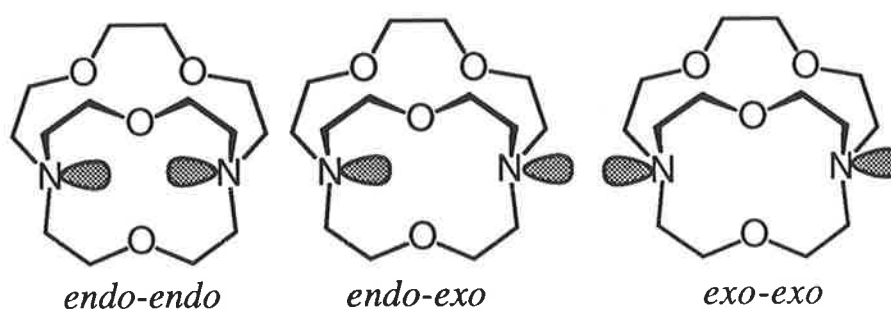


**Figure 1.7.** The cryptand C211 is used to illustrate the three possible cryptand conformations; *endo-endo*, *endo-exo* and *exo-exo*.

Cryptates may exist in two forms, *inclusive* and *exclusive*, depending on the relative sizes of the metal ion and the cryptand cavity. In general, *inclusive* cryptates form when the size of the metal ion is less than or equal to the size of the cryptand cavity, whereas *exclusive* cryptates form when the metal ion is too large to reside within the cavity. These size correlations are illustrated in Table 1.1;  $[\text{LiC211}]^+$ ,  $[\text{LiC21C}_5]^+$ ,  $[\text{NaC221}]^+$  and  $[\text{KC222}]^+$  all form *inclusive* cryptates, whereas  $[\text{NaC211}]^+$ ,  $[\text{NaC21C}_5]^+$  and  $[\text{KC221}]^+$  are *exclusive* cryptates.<sup>59,64,69-71</sup> In *inclusive* cryptates, the cation is completely included within the intramolecular cavity (Figure 1.8) whereas in *exclusive* cryptates, the metal ion resides on a face of the cryptand, which is delineated by two of the three nitrogen to nitrogen polyether bridges, as shown in Figure 1.8. In *inclusive* cryptates, the first coordination sphere of the metal ion is solely

occupied by ligand donor atoms and the cation has minimal interaction with the anion (in the solid state) or with the solvent (in solution). In contrast, the exposed nature of the metal ion in an *exclusive* cryptate allows direct contact with the anion or solvent. This is illustrated in Figure 1.9, which shows space-filling representations of  $[\text{NaC221}]^+$  (*inclusive*) and  $[\text{NaC211}]^+$  (*exclusive*). The structural characteristics of some specific cryptates are now discussed in more detail.

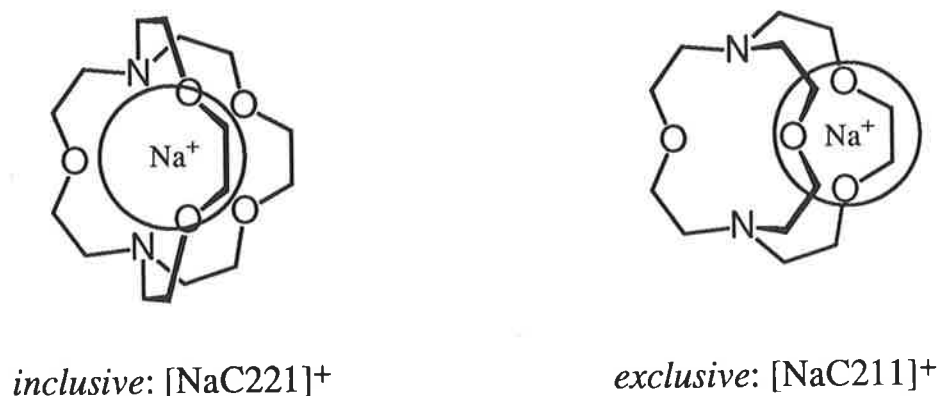


**Figure 1.8.** Examples of *inclusive* and *exclusive* cryptates whose structures have been determined by X-ray crystallography.<sup>69-70</sup>

The cryptand C221 has an intramolecular cavity radius of  $\sim 1.1 \text{ \AA}$ ,<sup>26</sup> which is closest to the ionic radius of  $\text{Na}^+$  ( $1.02 \text{ \AA}$ )<sup>74</sup> and as a consequence, it forms *inclusive*  $[\text{NaC221}]^+$ .<sup>69</sup> However, the larger  $\text{K}^+$ , with an ionic radius of  $1.38 \text{ \AA}$ ,<sup>74</sup> is too large to be included within the cavity of C221 and thus,  $[\text{KC221}]^+$  is an *exclusive* cryptate.<sup>69</sup> These structural characteristics of  $[\text{MC221}]^+$  are reflected in the relative stabilities of  $[\text{MC221}]^+$  in solution, where the stability sequence  $\text{Li}^+ < \text{Na}^+ > \text{K}^+$  is observed in several solvents.<sup>26,75</sup> This is consistent with  $\text{Li}^+$  ( $0.76 \text{ \AA}$ )<sup>74</sup> forming an *inclusive* cryptate but being too small to establish optimum bonding distances with the cryptand donor atoms and the optimum bonding distances and *inclusive* structure of  $[\text{NaC221}]^+$  conferring a greater stability on this cryptate than that characterising *exclusive*  $[\text{KC221}]^+$ .

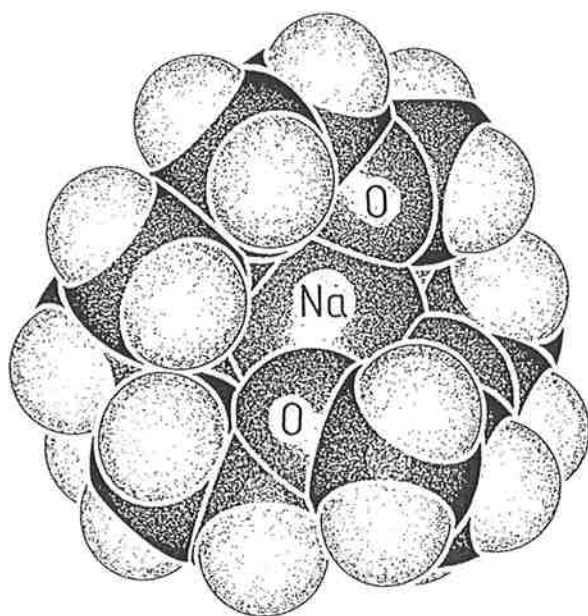
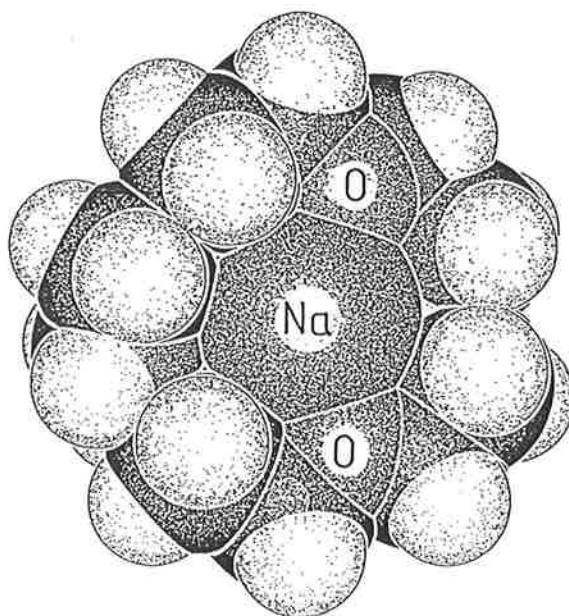
The larger, more flexible cryptand C222 shows significantly different behaviour to that exhibited by C221. The cavity size of C222 ( $1.4 \text{ \AA}$ )<sup>26</sup> lies closest to the ionic radius of  $\text{K}^+$  ( $1.38 \text{ \AA}$ )<sup>74</sup> and  $\text{Rb}^+$  ( $1.52 \text{ \AA}$ )<sup>74</sup> and thus, these metal ions form *inclusive* cryptates with C222 without undue distortion of the

**Table 1.1.** Approximate Cavity Radii and Number of Binding Sites of Selected Cryptands and the Ionic Radii of Selected Monovalent Metal Ions for Various Coordination Numbers.

Cryptand	Cavity Radius <sup>a</sup> Å	No. of Binding Sites	Cation	Ionic Radius (Å) <sup>b</sup> for Coordination Number		
				6	7	8
C111	0.5	5	Li <sup>+</sup>	0.76		0.92
C211, C21C <sub>5</sub> <sup>c</sup>	0.8	6, 5	Na <sup>+</sup>	1.02	1.12	1.18
C221, C22C <sub>5</sub> <sup>c</sup>	1.1	7, 6	K <sup>+</sup>	1.38	1.46	1.51
C222, C22C <sub>8</sub> <sup>c</sup>	1.4	8, 6	Rb <sup>+</sup>	1.52	1.56	1.61
C322	1.8	9	Cs <sup>+</sup>	1.67		1.74
C332	2.1	10	Ag <sup>+</sup>	1.15	1.22	1.28
C333	2.4	11	Tl <sup>+</sup>	1.50		1.59

<sup>a</sup> Reference 26. The cavity radii of these aliphatic bridge cryptands are based on their isostructural cryptands.

<sup>b</sup> Reference 74. The alkali metal ions show variable coordination numbers in their complexes, with K<sup>+</sup>, Rb<sup>+</sup> and Cs<sup>+</sup> often exhibiting coordination numbers greater than six. In this study, all ionic radii quoted are for a coordination number of six, unless stated otherwise.

 $[\text{NaC221}]^+$  $[\text{NaC211}]^+$ 

**Figure 1.9.** Space-filling representations of  $[\text{NaC221}]^+$  (*inclusive*) and  $[\text{NaC211}]^+$  (*exclusive*) generated from the crystal structures<sup>69</sup> by the program SCHAKAL<sup>76</sup> using spheres of appropriate radii.

ligand.<sup>58-59</sup> However, the  $\text{Na}^+$  and  $\text{Cs}^+$  cryptates of C222 are also *inclusive*,<sup>59</sup> even though the ligand must undergo a considerable amount of distortion to accommodate the smaller  $\text{Na}^+$  (1.02 Å)<sup>74</sup> or larger  $\text{Cs}^+$  (1.67 Å)<sup>74</sup> ions, which shows that the cryptand cavity can adapt, within certain limits, to the ionic radius of the metal ion.<sup>33</sup> Nevertheless, in solution, there is a temperature dependent equilibrium between *inclusive* and *exclusive*  $[\text{CsC222}]^+$ .<sup>77-79</sup> These observations account for the stability sequence  $\text{Na}^+ < \text{K}^+ > \text{Rb}^+ > \text{Cs}^+$  for these cryptates that is observed in solution.<sup>26,75</sup> No solid state structures of the alkali metal cryptates of C22C<sub>8</sub> have been reported in the literature. Nevertheless, as a consequence of their structural similarities, both C222 and C22C<sub>8</sub> possess similar cavity sizes (1.4 Å) and structural flexibilities. Thus, it may be anticipated that C22C<sub>8</sub> is able to form *inclusive* cryptates with  $\text{Na}^+$ ,  $\text{K}^+$ ,  $\text{Rb}^+$  and  $\text{Cs}^+$ , as observed with C222. However, the absence of oxygen donor atoms in one arm of C22C<sub>8</sub> may reduce the tendency of the cation to reside within the cryptand cavity, especially in solution, where the metal ion may complete its coordination shell with solvent molecules.

The solid state structures of C22C<sub>2</sub>,  $[\text{LiC22C}_2]\text{NCS}$ ,  $[\text{NaC22C}_2]\text{NCS}$  and  $[\text{KC22C}_2]\text{NCS}$  appear in Figure 1.10.<sup>80-82</sup> In the free ligand and in all of its metal complexes, C22C<sub>2</sub> has adopted the *endo-endo* conformation, although the ligand conformation differs in each structure. As a result of the short  $-(\text{CH}_2)_2-$  moiety linking the two nitrogen bridgeheads, C22C<sub>2</sub> is not a typical cryptand, and does not possess a well defined three dimensional cavity with which to encapsulate the metal ion. It is apparent that a series of bond angle changes allows optimal bonding distances between the metal ion and the ligand donor atoms in these cryptates. In  $[\text{LiC22C}_2]^+$ ,  $\text{Li}^+$  is coordinated to all six ligand donor atoms but there is minimal interaction between the complexed cation and the  $\text{NCS}^-$  anion. In  $[\text{NaC22C}_2]^+$  and  $[\text{KC22C}_2]^+$ ,  $\text{Na}^+$  and  $\text{K}^+$  are also bound to all six donor atoms of C22C<sub>2</sub> and the  $\text{NCS}^-$  anion. As the size of the metal ion increases, there is a progressive movement of the metal ion from below the plane of the four oxygens in the  $\text{Li}^+$  complex to above the plane in the  $\text{K}^+$  complex. Space-filling representations of  $[\text{LiC22C}_2]^+$  and  $[\text{NaC22C}_2]^+$  appear in Figure 1.11.

From the preceding discussions, it is apparent that there is a strong correlation between cation size, cryptand cavity size, cryptate structure and cryptate stability in solution. Generally, it cannot be assumed that the solid state structure of a metal complex is maintained in solution, since various solvational and conformational changes accompany dissolution. Nevertheless, a

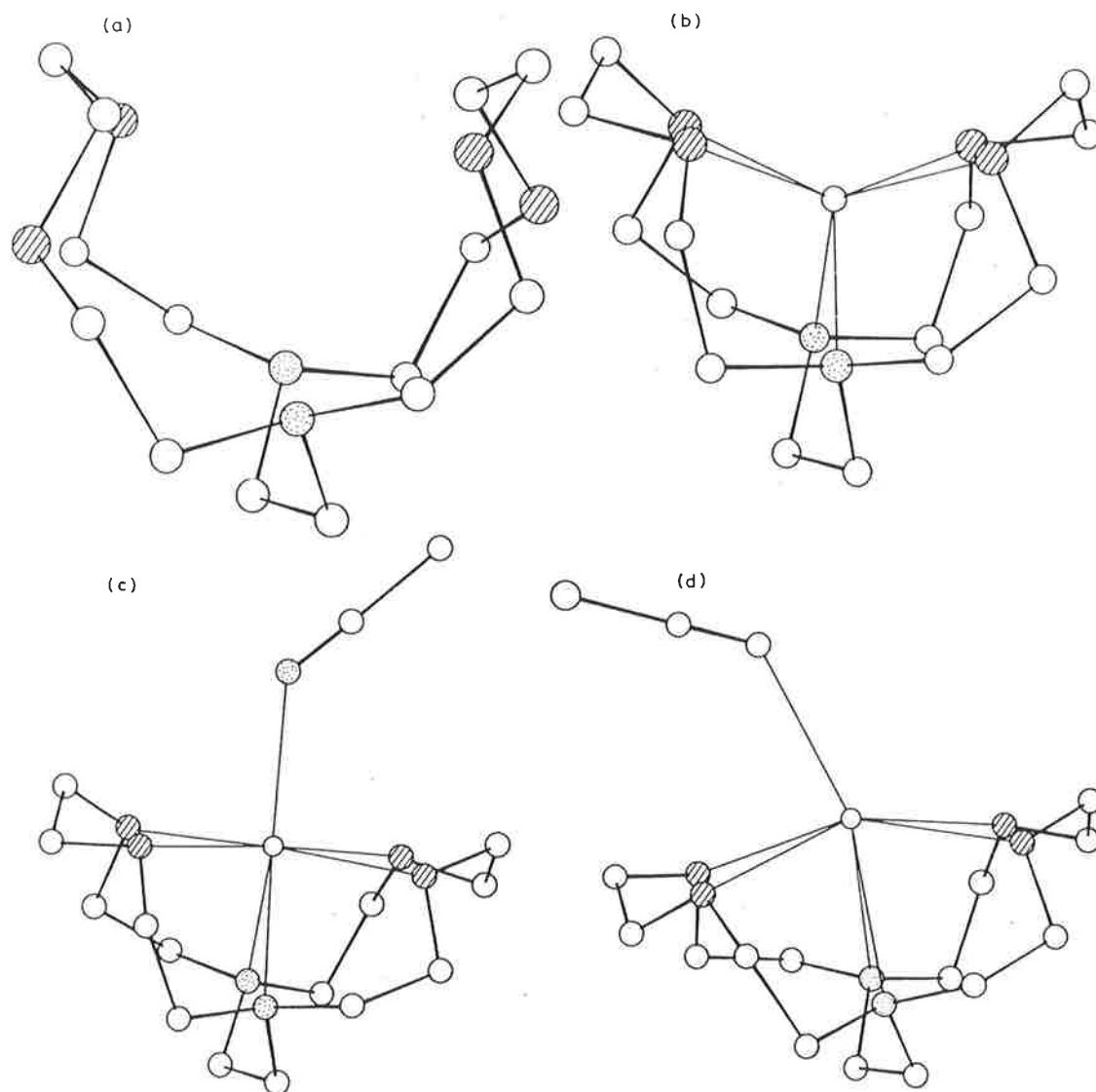


**Figure 1.10.** Solid state structures of  $C_{22}C_2$  and some of its alkali metal complexes. (a)  $C_{22}C_2$ .<sup>80</sup> (b)  $[LiC_{22}C_2]NCS$ .<sup>82</sup> (c)  $[NaC_{22}C_2]NCS$ .<sup>81</sup> (d)  $[KC_{22}C_2]NCS$ .<sup>81</sup>



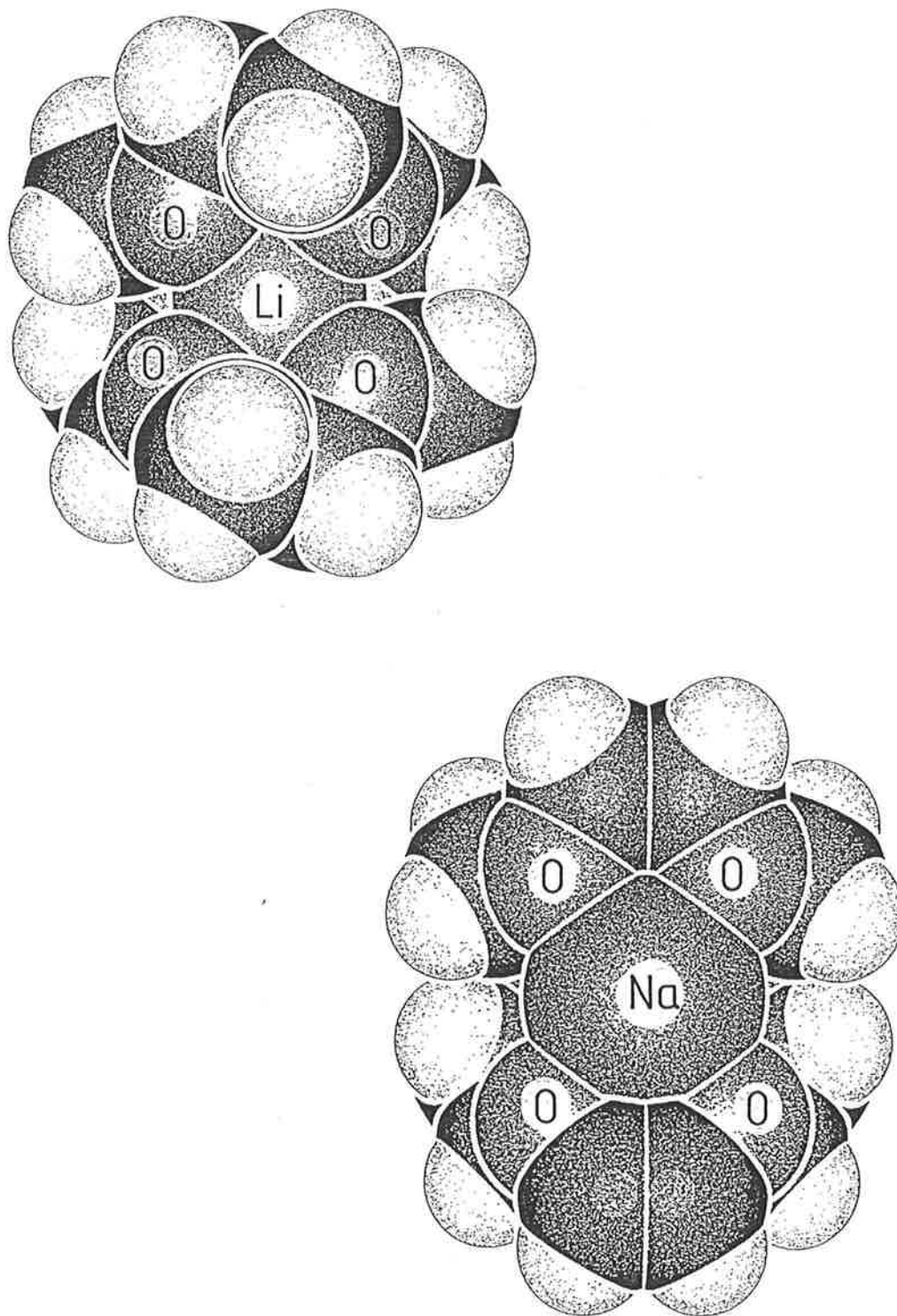


**Figure 1.11.** Space-filling representations of  $[\text{LiC}_{22}\text{C}_2]^+$  and  $[\text{NaC}_{22}\text{C}_2]^+$  generated from the crystal structures<sup>81-82</sup> by the program SCHAKAL<sup>76</sup> using spheres of appropriate radii.

number of NMR studies<sup>70,83-85</sup> have demonstrated that the *inclusive / exclusive* structure of the cryptate in the solid state is retained in solution. In the following chapters, these solid state structural characteristics are invaluable in the interpretation of the thermodynamic and kinetic properties of the cryptates of  $C_{22}C_2$  and  $C_{22}C_8$ .

- 1 Pedersen, C.J. *J. Am. Chem. Soc.* **1967**, 89, 2495-2496.
- 2 Pedersen, C.J. *J. Am. Chem. Soc.* **1967**, 89, 7017-7036.
- 3 Pedersen, C.J.; Frensdorff, H.K. *Angew. Chem. Int. Ed. Engl.* **1972**, 11, 16-25.
- 4 Dietrich, B.; Sauvage, J-P. *New. J. Chem.* **1988**, 12, 725-728.
- 5 Burgermeister, W.; Winkler-Ostwatitsch. *Top. Curr. Chem.* **1977**, 69, 93-196.
- 6 Eigen, M.; Winkler, R. "*The Neurosciences, Second Study Program*", Rockefeller University Press, New York, **1970**.
- 7 Williams, R.J.P. *Chem. Soc. Rev.* **1980**, 9, 281.
- 8 Moore, C.; Pressman, B.C. *Biochem. Biophys. Res. Commun.* **1964**, 15, 562.
- 9 Graven, S.N.; Lardy, H.A.; Johnson, D.; Rutter, A. *Biochemistry*, **1966**, 5, 1729-1735.
- 10 Stefanac, Z.; Simon, W. *Microchem. J.* **1967**, 12, 125.
- 11 Mueller, P.; Rudin, D.O. *Biochem. Biophys. Res. Comm.* **1967**, 26, 398.
- 12 Estrada, O.S.; Gomez-Louero, C.; Montal, M. *Bioenergetics.* **1972**, 3, 417.
- 13 Simon, W.; Morf, W.E.; Meier, P.C. *Struct. Bonding (Berlin)*. **1973**, 16, 113.
- 14 Kirch, M.; Lehn, J-M. *Angew. Chem. Int. Ed. Engl.* **1975**, 14, 555-556.
- 15 Pressman, B.C. *Annu. Rev. Biochem.* **1976**, 45, 501.
- 16 Dietrich, B.; Viout, P.; Lehn, J-M. "*Macrocyclic Chemistry*", VCH, Weinheim, **1993**.
- 17 Neupert-Laves, K.; Dobler, M. *Helv. Chim. Acta.* **1975**, 58, 432.
- 18 Grell, E.; Funck, T.; Eggers, F. "*Membranes Vol 3*", Dekker, New York. **1975**.
- 19 Lehn, J-M. *Angew. Chem. Int. Ed. Engl.* **1988**, 27, 89-112.
- 20 Gokel, G. "*Crown Ethers and Cryptands*", The Royal Society of Chemistry, Cambridge, **1991**.
- 21 Dietrich, B.; Lehn, J-M.; Sauvage, J-P. *Tetrahedron. Lett.* **1969**, 2885.
- 22 Dietrich, B.; Lehn, J-M.; Sauvage, J-P. *Tetrahedron. Lett.* **1969**, 2889.
- 23 Dietrich, B.; Lehn, J-M.; Sauvage, J-P.; Blanzat, J. *Tetrahedron.* **1973**, 29, 1629-1645.
- 24 Dietrich, B.; Lehn, J-M.; Sauvage, J-P.; Blanzat, J. *Tetrahedron.* **1973**, 29, 1647-1658.
- 25 Lehn, J-M. *Struct. Bonding (Berlin)*. **1973**, 16, 1-69.
- 26 Lehn, J-M.; Sauvage, J-P. *J. Am. Chem. Soc.* **1975**, 97, 6700-6707.
- 27 Lehn, J-M. *Acc. Chem. Res.* **1978**, 11, 49-57.

- 28 Lehn, J-M. *Pure. Appl. Chem.* **1979**, 51, 979-997.
- 29 Cram, D.J.; Kaneda, T.; Helgeson, R.C.; Lein, G.M. *J. Am. Chem. Soc.* **1979**, 101, 6752.
- 30 Trueblood, K.N.; Knobler, C.B.; Maverick, E.; Helgeson, R.C.; Brown, S.B.; Cram, D.J. *J. Am. Chem. Soc.* **1981**, 103, 5594.
- 31 Cram, D.J. *Angew. Chem. Int. Ed. Engl.* **1986**, 25, 1039.
- 32 Cram, D.J.; Lein, G.M. *J. Am. Chem. Soc.* **1985**, 107, 3657.
- 33 Atwood, J.L.; Davies, J.E.D.; MacNicol, D.D. "*Inclusion Compounds*", Volume 2. Academic Press, London, **1984**.
- 34 Izatt, R.M.; Christensen, J.J. "*Synthesis of Macrocycles: The Design of Selective Complexing Agents*", Wiley-Interscience, New York, **1987**.
- 35 Kimura, E. *Top. Curr. Chem.* **1985**, 128, 113.
- 36 Hosseini, M.W.; Lehn, J-M. *Helv. Chim. Acta.* **1987**, 70, 1312.
- 37 Vögtle, F.; Sieger, H.; Müller, W.M. *Top. Curr. Chem.* **1981**, 98, 107-161.
- 38 Weber, E.; Vögtle, F. *Top. Curr. Chem.* **1981**, 98, 3-41.
- 39 Lehn, J-M.; Simon, J.; Moradpour, A. *Helv. Chim. Acta.* **1978**, 61, 2407.
- 40 Blasius, E.; Janzen, K-P. *Top. Curr. Chem.* **1981**, 98, 163-189.
- 41 Müller, W.H. *Naturwissenschaften.* **1970**, 57,248.
- 42 Müller, W.H.; Müller, W.A. *Naturwissenschaften.* **1974**, 61,455.
- 43 Müller, W.H. *Strahlentherapie.* **1977**, 570.
- 44 Müller, W.H.; Müller, W.A.; Linzner, U. *Naturwissenschaften.* **1977**, 64, 96.
- 45 Jepson, B.E.; DeWitt, R. *J. Inorg. Nucl. Chem.* **1976**, 38, 1175.
- 46 Heumann, K.G.; Schiefer, H.P. *Angew. Chem. Int. Ed. Engl.* **1980**, 19, 406.
- 47 Knochel, A.; Wilken, R.D. *J. Am. Chem. Soc.* **1981**, 103, 5707.
- 48 Keynes, R.D. *Scientific American.* **1979**, 240, 98.
- 49 Hinkle, P.C.; McCarty, R.E. *Scientific American.* **1978**, 238, 104.
- 50 Lehn J-M.; Spach, G. (Ed). "*Physical Chemistry of Transmembrane Ion Motions*", Elsevier, Amsterdam, **1983**.
- 51 Tsukube, H. *Angew. Chem. Int. Ed. Engl.* **1982**, 21, 304.
- 52 Bartsch, R.A.; Babb, D.A.; Czech, B.P.; Desai, D.H.; Chapoteau, E.; Gebauer, C.R.; Zazulak, W.; Kumar, A. *J. Inclusion. Phenom. Mol. Recognit.Chem.* **1990**, 9, 113-123.
- 53 Tagaki, M.; Ueno, M. *Top. Curr. Chem.* **1984**, 121, 39.
- 54 Chao, Y. Weisman, G.R.; Sogah, G.D.Y.; Cram, D.J. *J. Am. Chem. Soc.* **1979**, 101, 4948.
- 55 Lehn, J-M.; Sirlin, C. *New. J. Chem.* **1987**, 11 693.

- 56 Behr, J-P.; Lehn, J-M. *J. Chem. Soc., Chem. Commun.* **1978**, 143.
- 57 Hosseini, M.W.; Lehn, J-M.; Maggiora, L.; Mertes, K.B.; Mertes, M.P. *J. Am. Chem. Soc.* **1987**, 109, 537.
- 58 Metz, B.; Moras, D.; Weiss, R. *J. Chem. Soc., Chem. Commun.* **1970**, 217.
- 59 Metz, B.; Moras, D.; Weiss, R. *J. Chem. Soc., Chem. Commun.* **1971**, 444.
- 60 Metz, B.; Moras, D.; Weiss, R. *J. Chem. Soc., Pekin Trans 2.* **1976**, 423.
- 61 Moras, D.; Metz, B.; Weiss, R. *Acta. Crystallogr.* **1973**, B29, 383.
- 62 Moras, D.; Metz, B.; Weiss, R. *Acta. Crystallogr.* **1973**, B29, 388.
- 63 Moras, B.; Weiss, R. *Acta. Crystallogr.* **1973**, B29, 396.
- 64 Moras, B.; Weiss, R. *Acta. Crystallogr.* **1973**, B29, 400.
- 65 Moras, B.; Weiss, R. *Acta. Crystallogr.* **1973**, B29, 1059.
- 66 Metz, B.; Weiss, R. *Inorg. Chem.* **1974**, 13, 2094.
- 67 Moras, B.; Weiss, R. *Acta. Crystallogr.* **1973**, B29, 1382.
- 68 Moras, B.; Weiss, R. *Acta. Crystallogr.* **1973**, B29, 1388.
- 69 Mathieu, F.; Metz, B.; Moras, D.; Weiss, R. *J. Am. Chem. Soc.* **1978**, 100, 4412-4416.
- 70 Lincoln, S.F.; Horn, E.; Snow, M.R.; Hambley, T.W.; Brereton, I.M.; Spotswood, T.M. *J. Chem. Soc., Dalton Trans.* **1986**, 1075-1080.
- 71 Lincoln, S.F.; Horn, E.; Snow, M.R.; Hambley, T.W.; Brereton, I.M.; Spotswood, T.M. *J. Chem. Soc., Dalton Trans.*, **1987**, 489.
- 72 Abou-Hamdan, A.; Hounslow, A.M.; Lincoln, S.F.; Hambley, T.W. *J. Chem. Soc., Dalton Trans.* **1987**, 489.
- 73 Clarke, P.; Gulbis, J.M.; Lincoln, S.F.; Tiekink, E.R.T. *Inorg. Chem.* **1992**, 31, 3398.
- 74 Shannon, R.D. *Acta Crystallogr., Sect. A: Cryst. Phys. Diffr., Theor Gen. Crystallogr.* **1976**, A32, 751.
- 75 Cox, B.G.; Garcia-Rosas, J.; Schneider, H. *J. Am. Chem. Soc.* **1981**, 103, 1384-1389.
- 76 Keller, E. SCHAKAL, A Fortran-77 program. Inorganic Chemistry Institute, University of Freiburg, Freiburg, Germany.
- 77 Mei, E.; Popov, A.I.; Dye, J.L. *J. Am. Chem. Soc.* **1977**, 99, 6532.
- 78 Mei, E.; Liu, L.; Dye, J.L.; Popov, A.I. *J. Solution. Chem.* **1977**, 6, 771.
- 79 Kauffmann, E.; Dye, J.L.; Lehn, J-M.; Popov, A.I. *J. Am. Chem. Soc.* **1980**, 102, 2274-2278.
- 80 Groth, P. *Acta Chem. Scand.* **1985**, A39, 59-62.
- 81 Groth, P. *Acta Chem. Scand.* **1985**, A39, 68-72.
- 82 Groth, P. *Acta Chem. Scand.* **1985**, A39, 73-76.

- 83 Cahen, Y.M.; Dye, J.L.; Popov, A.I. *J. Phys. Chem.* **1975**, 79, 1289-1291.
- 84 Schmidt, E.; Tremillon, J-M.; Kintzinger, J-P.; Popov, A.I. *J. Am. Chem. Soc.* **1983**, 105, 7563-7566.
- 85 Echegoyen, L.; Kaifer, A.; Durst, H.D.; Gokel, G.W. *J. Org. Chem.* **1984**, 49, 688.

# Chapter 2: Equilibrium Studies of Monovalent Metal Cryptates

## 2.1 Introduction

One of the major objects of numerous studies<sup>1-12</sup> of the cryptates of alkali and other metal ions has been the determination of the factors governing cryptate stability, measured by the magnitude of the stability constant,  $K_s$ , (Equation 2.2) for the equilibrium shown in Equation 2.1. These factors include the relative sizes of the metal ion and the cryptand cavity, the solvation energy of the metal ion, the structure and flexibility of the cryptand and the number and type of cryptand donor atoms, as discussed below.



$$K_s = \frac{[ML^+]}{[M^+][L]} \quad 2.2$$

The alkali metal ion cryptates are characterised by stability constants several orders of magnitude higher than those of the complexes of natural or synthetic monocyclic ligands.<sup>1-2,13-14</sup> For example, the  $K^+$  complex of the bicyclic cryptand C222 is  $10^5$  times more stable than the  $K^+$  complex of its monocyclic analogue.<sup>1</sup> This phenomenon is known as the macrobicyclic or cryptate effect and is even greater than the related macrocyclic effect (Figure 2.1). The macrobicyclic effect is attributable to the bicyclic topology of the cryptands, whose preformed three dimensional intramolecular cavities are ideally suited to the complexation of the spherical alkali metal ions.<sup>1-2,13-15</sup> Thus, the cryptands are able to fully encapsulate the complexed cation within a rigid, three dimensional array of donor atoms, conferring greater stability on their alkali metal complexes than the two dimensional cavities of monocyclic ligands. The bicyclic cryptands are also more able to discriminate between the various alkali metal ions, when compared with the more flexible monocyclic ligands, which may more readily adapt to variations in the size of the metal ion. Thus, alkali metal cryptates are characterised by greater selectivity than their monocyclic analogues.<sup>1-2</sup>

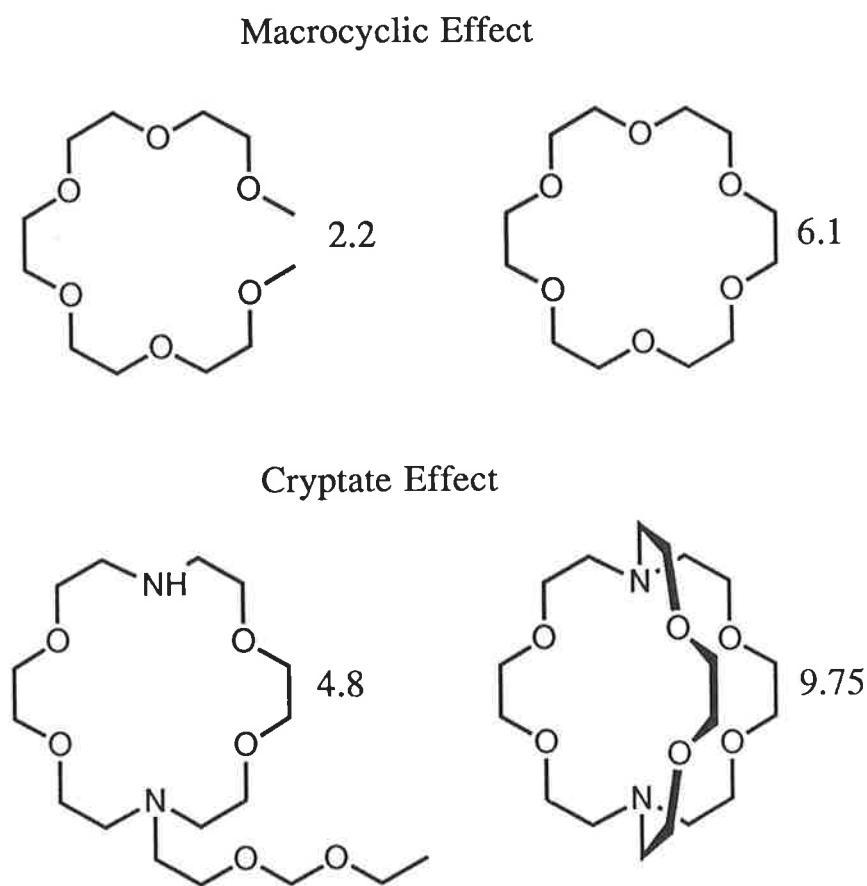


**Figure 2.1.** The macrocyclic effect is demonstrated by the greater stability of the crown ether complex formed with  $K^+$  by comparison with that formed by the linear polyether. The cryptate effect is demonstrated by the greater stability of the  $[KC222]^+$  cryptate by comparison with the complex formed by  $K^+$  with the analogous monocyclic ligand. The numbers quoted are the stability constants,  $\log(K_s/\text{dm}^3 \text{ mol}^{-1})$ , for the  $K^+$  complexes of these ligands in methanol (top) and methanol / water (95:5) (bottom).<sup>13</sup>



The bicyclic nature of the cryptands renders expansion and contraction of the cavity difficult, so that a cavity size selectivity is observed, with the most stable cryptate being that in which the complexed metal ion most closely fits the cryptand cavity.<sup>1-2,6,13,15-17</sup> Inclusion of cations larger than the cavity size would lead to destabilization of the cryptate as a result of ligand deformation and as a consequence, such complexes are *exclusive* in nature, as discussed in Chapter 1. Similarly, cations smaller than the optimum size also form less stable complexes, since the cryptand cavity cannot contract in order to maintain optimum contact between the metal ion and ligand binding sites. This is exemplified by C221, where the variation of  $K_s$  in the sequence  $\text{Li}^+ < \text{Na}^+ > \text{K}^+$  is consistent with  $\text{Li}^+$  ( $r = 0.76 \text{ \AA}$ ) being able to enter the cavity of C221 ( $r = 1.1 \text{ \AA}$ ) but being too small to establish optimum bonding distances,  $\text{Na}^+$  ( $r = 1.02 \text{ \AA}$ ) being of optimum size and forming *inclusive*  $[\text{NaC221}]^+$  and  $\text{K}^+$  ( $r = 1.38 \text{ \AA}$ ) being too large to enter the cavity and forming the less stable *exclusive*  $[\text{KC221}]^+$ . A similar explanation holds for the other cryptates in Table 2.1. As the size of the cavity is increased further, selectivity shifts to the larger  $\text{Cs}^+$  ion, but the high selectivity shown by smaller, less flexible cryptands is lost, since the larger, more flexible cryptands can more readily adapt to variations in the size of the metal ion.<sup>2,13,16</sup>

**Table 2.1.** Variation in Cryptate Stability with Cavity Radius<sup>a</sup> and Metal Ion Radius<sup>b</sup> in Methanol.

Cryptand (donor atoms)	Cavity Radius $\text{\AA}$	$\log(K_s/\text{dm}^3 \text{ mol}^{-1})$				
		$\text{Li}^+$ ( $0.76 \text{ \AA}$ )	$\text{Na}^+$ ( $1.02 \text{ \AA}$ )	$\text{K}^+$ ( $1.38 \text{ \AA}$ )	$\text{Rb}^+$ ( $1.52 \text{ \AA}$ )	$\text{Cs}^+$ ( $1.67 \text{ \AA}$ )
C211 <sup>c</sup> (6)	0.8	8.04	7.09	$\leq 2.6$		
C221 <sup>c</sup> (7)	1.1	5.38	9.65	8.54	6.74	4.33
C222 <sup>c</sup> (8)	1.4	2.6	7.98	10.41	8.98	4.4
C322 <sup>d</sup> (9)	1.8	2.3	5.0	7.6	7.9	$\sim 8.0$
C332 <sup>d</sup> (10)	2.1		3.2	6.0	6.15	6.15
C333 <sup>d</sup> (11)	2.4		2.7	5.4	5.7	5.9
C22 <sup>e</sup> (6)	$\sim 1.5$		1.0	2.0	1.2	

<sup>a</sup> Cavity radii from reference 2. <sup>b</sup> Six coordinate ionic radii from reference 19.

<sup>c</sup> Reference 6. <sup>d</sup> Reference 1. <sup>e</sup> Reference 18.

Complexation involves substitution of several solvent molecules from the inner coordination sphere of the metal ion and may be regarded as a competition between the solvent and the ligand for coordination of the metal ion.<sup>20-21</sup> Thus, the overall stability of the cryptate largely results from the differences between the binding energy of the ligand and the solvation energy of the metal ion.<sup>6</sup> As the solvation energy of the cation increases, complex stability tends to decrease.<sup>6,20-26</sup> However, despite the large variations in the solvation energies of the alkali metal ions among different solvents,<sup>27-28</sup> the selectivity shown by cryptands is essentially independent of solvent.<sup>6</sup>

This study seeks to better assess the contribution of these factors to the stability of cryptates through ligands based on the eighteen membered 1,4,7,10-tetraoxa-1,10-diazacyclooctadecane (C22). The ligands C22C<sub>2</sub>, and C22C<sub>8</sub>, together with C22C<sub>5</sub>,<sup>29-30</sup> form a series of cryptands resulting from structural modifications of the parent macrocycle C22 (Figure 2.2), where the two amine protons have been replaced by the  $-(\text{CH}_2)_n-$  moiety (where  $n = 2, 5$  or 8). All four ligands possess the same number and type of donor atoms, but the  $-(\text{CH}_2)_n-$  linkage systematically modifies the flexibility of the parent C22 moiety as  $n$  is varied, which may be reflected in the stabilities and selectivities of their complexes. As a result, this series of ligands should enhance the understanding of the contribution of ligand topology and flexibility to the macrobicyclic effect.

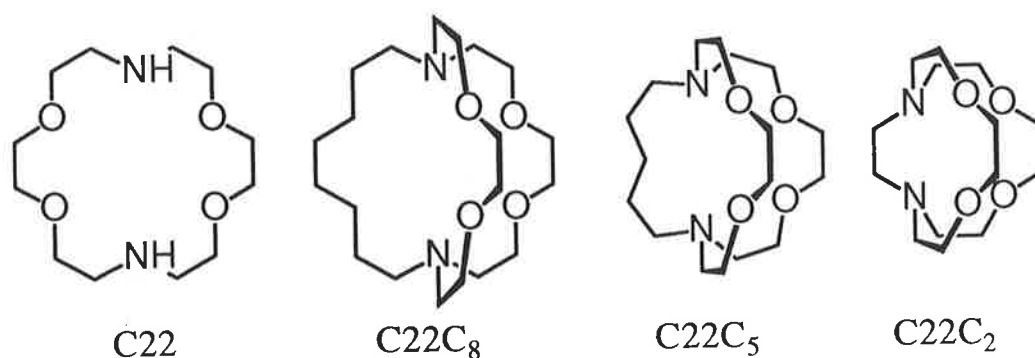


**Figure 2.2.** The cryptands C22C<sub>2</sub>, C22C<sub>5</sub> and C22C<sub>8</sub> may be viewed as structural modifications of the diaza crown ether C22, where the two amine protons have been replaced by the  $-(\text{CH}_2)_n-$  moiety.

The cryptand C22C<sub>2</sub>, has a unique, clam-like structure, resulting from the shortness of the C<sub>2</sub> arm. It is of considerable interest to investigate the effect of this characteristic of C22C<sub>2</sub> on its selectivity for metal ions. An additional feature of C22C<sub>2</sub> is that its bicyclic structure contains one arm that possesses no donor atoms, as does the structure of C22C<sub>8</sub>. Together with C21C<sub>5</sub> and C22C<sub>5</sub>, these ligands represent an intermediate structural stage between the diaza crown ether C22 and the cryptands C211, C221 and C222, in which all three arms possess donor atoms.

In this chapter, the stabilities of the complexes [MC22C<sub>2</sub>]<sup>+</sup> and [MC22C<sub>8</sub>]<sup>+</sup>, where M<sup>+</sup> = Li<sup>+</sup>, Na<sup>+</sup>, K<sup>+</sup>, Rb<sup>+</sup>, Cs<sup>+</sup>, Ag<sup>+</sup> and Tl<sup>+</sup> have been determined in several solvents and the results are related to the preceding discussion. In Chapter 3, these aspects of cryptate chemistry are investigated through the stabilities of a number of divalent metal cryptates of C22C<sub>2</sub> and C22C<sub>8</sub>. These ions are characterised by greater surface charge densities, a wider variation in their hard/soft acid nature by comparison with the alkali metal ions, and in some cases by directional bonding and crystal field effects, which may superimpose on the metal ion/cryptand cavity size ratio which tends to dominate the chemistry of alkali metal cryptates.

## 2.2 Stability of $[MC22C_2]^+$ in Non-Aqueous Solution

The stabilities of  $[MC22C_2]^+$ , where  $M^+ = Na^+, K^+, Rb^+, Cs^+$ , and  $Tl^+$  have been determined by potentiometric titration in numerous non-aqueous solvents and water (Table 2.2). The selectivity of  $C22C_2$  for  $Na^+$  over the other alkali metal ions is demonstrated by the variation of the stability of  $[MC22C_2]^+$  in the sequence  $Li^+ < Na^+ > K^+ > Rb^+ > Cs^+$  in acetonitrile and dimethylformamide. This may be explained by reference to the solid state structures of  $C22C_2$  and its alkali metal cryptates<sup>31-32</sup> (Figure 1.10), which were discussed in Chapter 1. It may be recalled that in  $[LiC22C_2]NCS$ ,  $Li^+$  is 6 coordinate, being bound to two nitrogens and four oxygens of  $C22C_2$ .<sup>32</sup> In  $[NaC22C_2]NCS$  and  $[KC22C_2]NCS$ , both  $Na^+$  and  $K^+$  are 7 coordinate, being bound to all six ligand donor atoms and to the  $NCS^-$  anion.<sup>31</sup> The ligand has a clam-like structure, with the two  $-(CH_2)_2O(CH_2)_2O(CH_2)_2-$  jaws hinged about the  $>N(CH_2)_2N<$  moiety (Figures 1.10 and 2.2). It is apparent that a series of bond angle changes effectively narrow or widen the angle between the ligand jaws depending on the size of the metal ion.<sup>33</sup>

From the crystallographic data, it is possible to calculate the angle between each jaw of  $C22C_2$ , which is defined as the dihedral angle between the mean planes defined by the two nitrogens and each pair of oxygens (Figure 2.4). This angle was calculated to be  $70.9^\circ$ ,  $89.6^\circ$ ,  $100.0^\circ$  and  $88.4^\circ$  for  $[LiC22C_2]^+$ ,  $[NaC22C_2]^+$ ,  $[KC22C_2]^+$  and the free ligand  $C22C_2$ , respectively. This variation in the jaw-angle with the size of  $M^+$  may be clearly seen in Figure 2.3. It is apparent that the complex in which this dihedral angle is closest to that in the free ligand will experience least strain and hence greatest stability. The angle in  $[LiC22C_2]^+$  is considerably lower than that in  $C22C_2$ , and the consequent increase in strain has a destabilizing effect on this complex. In  $[NaC22C_2]^+$ , the angle is similar to that in  $C22C_2$  and as a result, the stability of  $[NaC22C_2]^+$  is greatest, coincident with stability reaching a maximum as a result of strain being minimum in this complex. In  $[KC22C_2]^+$ , the larger size of  $K^+$  results in an increase in jaw-angle and the corresponding increase in strain experienced in this complex results in a decrease in stability. The further decrease in stability observed with  $[RbC22C_2]^+$  and  $[CsC22C_2]^+$  is probably coincident with a further increase in jaw-angle. Thus, the selectivity of  $C22C_2$  for  $M^+$  results from a conformational preference, which, although based on the size of  $M^+$ , differs from the mode of selectivity exhibited by the cryptands, where cryptate stability is determined by the fit of the cation into the preformed cryptand cavity.

**Table 2.2.** Stability Constants<sup>a</sup> for the Complexation of Monovalent Metal Ions by 4,7,13,16-Tetraoxa-1,10-diazabicyclo[8.8.2]eicosane (C22C2) at 298.2 K.

solvent	$D_N^b$	$\log(K_f/\text{dm}^3 \text{ mol}^{-1})$						
		$[\text{LiC22C2}]^+{}^c$	$[\text{NaC22C2}]^+{}^d$	$[\text{KC22C2}]^+{}^d$	$[\text{RbC22C2}]^+{}^d$	$[\text{CsC22C2}]^+{}^d$	$[\text{AgC22C2}]^+{}^c$	$[\text{TlC22C2}]^+{}^c$
acetonitrile	14.1	$7.8 \pm 0.1$	$9.4 \pm 0.3$	$7.2 \pm 0.1$	$5.9 \pm 0.1$	$5.0 \pm 0.1$	$9.4 \pm 0.1^c$	$10.4 \pm 0.3^d$
methanol	19.0 (23.5) <sup>f</sup>	$4.0 \pm 0.1$	$6.6 \pm 0.1$				$10.2 \pm 0.1^c$	$7.8 \pm 0.1^d$
dimethyl- formamide	26.6	$3.5 \pm 0.1$	$6.1 \pm 0.1$	$3.2 \pm 0.1$	$2.8 \pm 0.1$	$2.7 \pm 0.1$	$9.4 \pm 0.1^c$	$6.7 \pm 0.1^d$
dimethyl- sulfoxide	29.8		$5.6 \pm 0.1$					
pyridine	33.1	4.0	$8.4 \pm 0.1$				$5.0^c$	
water	18.0 (33.0) <sup>f</sup>	<2	$3.2 \pm 0.1$	<2	<2	<2	$8.80 \pm 0.05^e$	$5.46 \pm 0.05^e$

<sup>a</sup> In  $0.050 \text{ mol dm}^{-3} \text{ NEt}_4\text{ClO}_4$  supporting electrolyte except where stated otherwise. <sup>b</sup> Gutmann donor numbers from reference 35. <sup>c</sup> Reference 22. <sup>d</sup> This work. <sup>e</sup> Determined by pH titration in  $0.10 \text{ mol dm}^{-3} \text{ NEt}_4\text{ClO}_4$  supporting electrolyte. <sup>f</sup> In references 36 and 37, it has been suggested that  $D_N = 33.0$  and  $23.5$  are more appropriate in water and methanol solutions rather than  $D_N = 18.0$  and  $19.0$ , respectively, obtained for water and methanol in 1,2-dichloroethane solution, where the hydrogen-bonding structure of these solvents is disrupted.

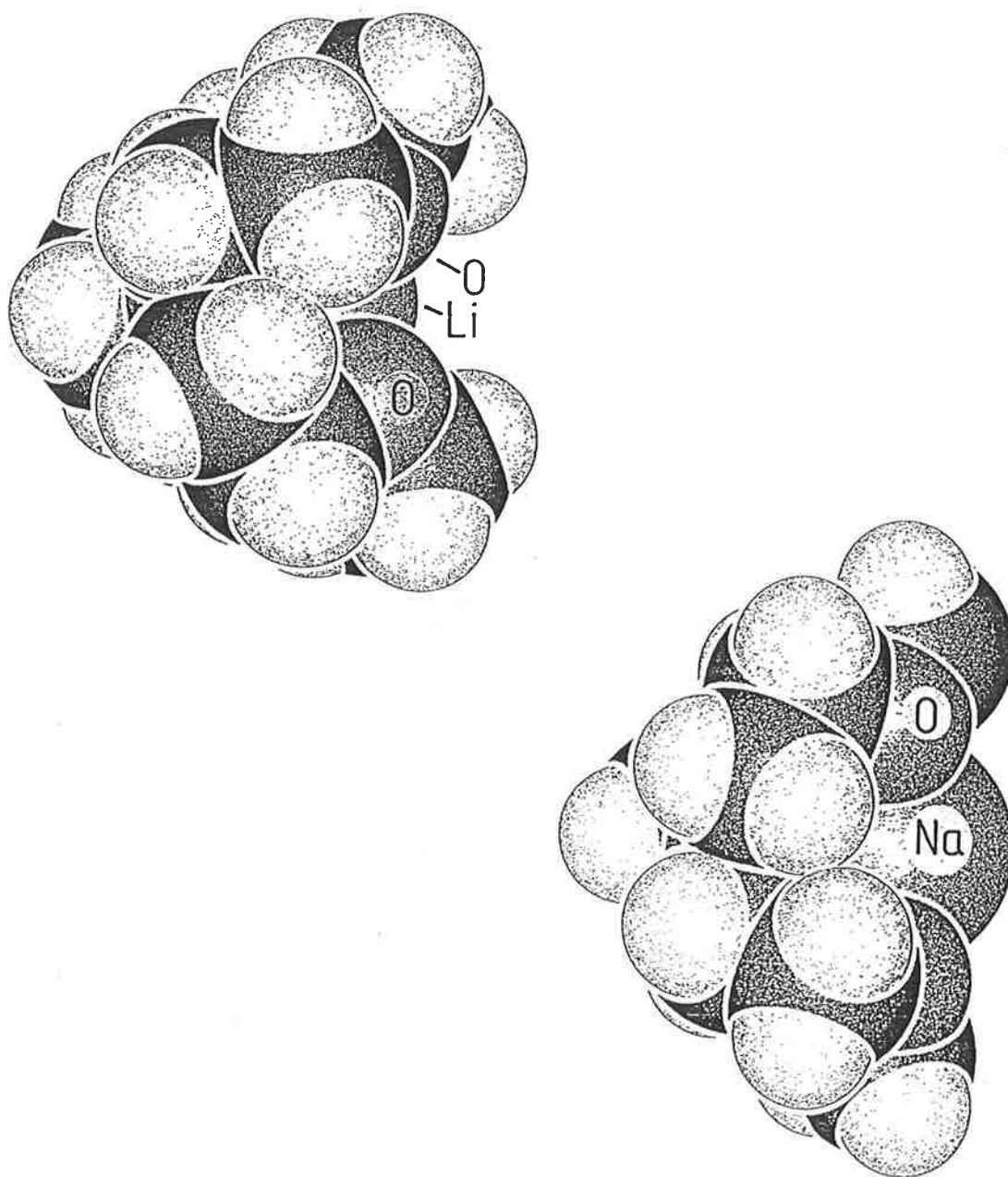


**Figure 2.3.** Space-filling representations of  $[\text{LiC}_{22}\text{C}_2]^+$  and  $[\text{NaC}_{22}\text{C}_2]^+$  generated from the crystal structures<sup>31-32</sup> by the program SCHAKAL<sup>38</sup> using spheres of appropriate radii. The jaw-angles in  $[\text{LiC}_{22}\text{C}_2]^+$  and  $[\text{NaC}_{22}\text{C}_2]^+$  are  $70.9^\circ$  and  $89.6^\circ$ , respectively.

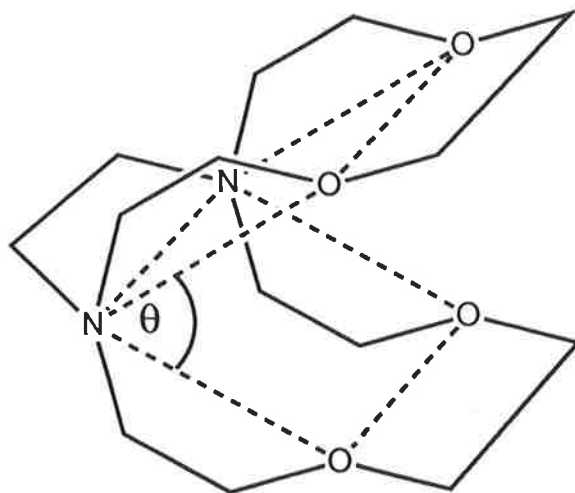


**Figure 2.4.** The jaw-angle,  $\theta$ , in  $C22C_2$  and its complexes is defined as the dihedral angle between the mean planes delineated by the two hinge nitrogens and the pair of oxygens in each jaw. In both the  $Na^+$  and  $K^+$  complexes, these atoms define perfect planes.

The effect of variations in cryptand structure on cryptate stability is shown in Table 2.3, which shows the variations in the stabilities of several different cryptates with  $M^+$  in a range of solvents. In general, the variation in stability for a given metal ion results from a combination of the fit of  $M^+$  into the cryptand cavity and the number of cryptand donor atoms interacting with  $M^+$ . The variation in stability of the alkali metal ion cryptates of C221 is  $Li^+ < Na^+ > K^+ > Rb^+ > Cs^+$ , which is identical to the selectivity pattern shown by  $C22C_2$ . The stabilities of  $[MC221]^+$  are generally higher than those of  $[MC22C_2]^+$ , probably as a consequence of the greater electrostatic attraction between  $M^+$  and C221 compared with  $C22C_2$ , which possesses one less oxygen donor atom. In the solid state,  $[NaC221]NCS$  forms an *inclusive* cryptate, resulting from the matching of the sizes of  $Na^+$  and the cavity of C221 and there is minimal interaction between  $Na^+$  and the thiocyanate anion.<sup>39</sup> This *inclusive* structure (Figure 1.9) probably also enhances the stability of  $[NaC221]^+$  compared with the more open structure of  $[NaC22C_2]^+$ , (Figure 1.11) which results in the coordination of the thiocyanate anion to  $Na^+$  in  $[NaC22C_2]NCS$ . The  $Na^+/Li^+$  selectivity of  $C22C_2$  is, in general, considerably less than that of C221. This is consistent with the ability of  $C22C_2$  to optimise its coordination of  $Li^+$  by a decrease in the jaw-angle, whereas the cavity of

**Table 2.3.** Stability Constants for the Complexation of Monovalent Metal Ions by 4,7,13,16-Tetraoxa-1,10-diazabicyclo[8.8.2]eicosane (C22C2) and Other Cryptands at 298.2 K.

	log( $K_s$ /dm <sup>3</sup> mol <sup>-1</sup> ) (298.2 K)						
	Li <sup>+</sup>	Na <sup>+</sup>	K <sup>+</sup>	Rb <sup>+</sup>	Cs <sup>+</sup>	Ag <sup>+</sup>	Tl <sup>+</sup>
acetonitrile							
C22C <sub>2</sub>	7.8 <sup>a</sup>	9.4 <sup>b</sup>	7.2 <sup>b</sup>	5.9 <sup>b</sup>	5.0 <sup>b</sup>	9.4 <sup>a</sup>	10.4 <sup>b</sup>
C22C <sub>5</sub>	6.07 <sup>c</sup>	7.55 <sup>c</sup>	6.26 <sup>d</sup>	5.5 <sup>d</sup>	4.57 <sup>d</sup>	8.27 <sup>c</sup>	
C221	10.33 <sup>e</sup>	>11.3 <sup>e</sup>	9.5 <sup>e</sup>	7.27 <sup>e</sup>	5.15 <sup>e</sup>	11.24 <sup>e</sup>	11.92 <sup>f</sup>
C211	>10 <sup>e</sup>	>9 <sup>e</sup>	2.84 <sup>e</sup>			7.70 <sup>e</sup>	7.02 <sup>f</sup>
C21C <sub>5</sub> <sup>g</sup>	4.15	5.08				4.29	
methanol							
C22C <sub>2</sub>	4.0 <sup>a</sup>	6.6 <sup>b</sup>				10.2 <sup>a</sup>	7.8 <sup>b</sup>
C22C <sub>5</sub>	2.30 <sup>c</sup>	5.41 <sup>c</sup>	5.8 <sup>c</sup>	5.7 <sup>c</sup>	4.8 <sup>c</sup>	11.13 <sup>c</sup>	6.48 <sup>c</sup>
C221	5.38 <sup>e</sup>	9.65 <sup>e</sup>	8.54 <sup>e</sup>	6.74 <sup>e</sup>	4.33 <sup>e</sup>	14.64 <sup>e</sup>	10.76 <sup>f</sup>
C211	8.04 <sup>e</sup>	6.1 <sup>e</sup>	2.3 <sup>e</sup>	1.9 <sup>e</sup>		10.60 <sup>e</sup>	5.65 <sup>f</sup>
C21C <sub>5</sub> <sup>g</sup>	3.00	3.76				7.69	
dimethylformamide							
C22C <sub>2</sub>	3.5 <sup>a</sup>	6.1 <sup>b</sup>	3.2 <sup>b</sup>	2.8 <sup>b</sup>	2.7 <sup>b</sup>	9.4 <sup>a</sup>	6.7 <sup>b</sup>
C22C <sub>5</sub>	2.21 <sup>c</sup>	3.66 <sup>c</sup>	3.85 <sup>c</sup>	3.82 <sup>c</sup>	2.90 <sup>c</sup>	9.40 <sup>c</sup>	5.05 <sup>c</sup>
C221	3.58 <sup>e</sup>	7.93 <sup>e</sup>	6.66 <sup>e</sup>	5.35 <sup>e</sup>	3.61 <sup>e</sup>	12.41 <sup>e</sup>	8.61 <sup>f</sup>
C211	6.99 <sup>e</sup>	5.23 <sup>e</sup>	<2.5 <sup>e</sup>			8.62 <sup>e</sup>	3.15 <sup>f</sup>
C21C <sub>5</sub> <sup>g</sup>	1.80	2.87				5.23	

<sup>a</sup> Reference 22. <sup>b</sup> This work. <sup>c</sup> Reference 30. <sup>d</sup> Reference 21. <sup>e</sup> Reference 6.

<sup>f</sup> Reference 44. <sup>g</sup> Reference 9.



C221 is too large for the optimum coordination of  $\text{Li}^+$ . However the  $\text{Na}^+/\text{K}^+$  selectivity is greater for C22C<sub>2</sub> than for C221, which suggests that the different structures of these ligands probably influences their relative abilities to complex cations of larger than optimum size; C221 does not include  $\text{K}^+$  within its cavity but forms an *exclusive* cryptate, whereas C22C<sub>2</sub> is able to adjust to the larger  $\text{K}^+$  by an increase in jaw-angle. Although the stabilities of  $[\text{MC221}]^+$  are greater than those of  $[\text{MC22C}_2]^+$ , as  $\text{M}^+$  increases in size from  $\text{K}^+$  to  $\text{Cs}^+$ , the stabilities of these cryptates decrease and become increasingly similar, consistent with specific interactions becoming less important as the sizes of  $\text{M}^+$  and the cryptand cavity become increasingly dissimilar.

The other cryptands in Table 2.3 serve to illustrate the effect of varying ligand structure while maintaining the same number and type of donor atoms (six in the case of C22C<sub>2</sub>, C22C<sub>5</sub> and C211) and the inclusion of C21C<sub>5</sub> demonstrates the effect of a decrease in the number of ligand donor atoms to five. For  $\text{Li}^+$ , the stability sequence  $[\text{LiC211}]^+ > [\text{LiC22C}_2]^+ > [\text{LiC22C}_5]^+ > [\text{LiC21C}_5]^+$  is obtained. The high stability of  $[\text{LiC211}]^+$  results from the optimum fit of  $\text{Li}^+$  into the C211 cavity to form an *inclusive* cryptate, where  $\text{Li}^+$  resides at the centre of the cryptand cavity, and interacts with six donor atoms.<sup>40-41</sup> Both C22C<sub>2</sub> and C22C<sub>5</sub> are too large to effectively coordinate  $\text{Li}^+$ . However, the ability of C22C<sub>2</sub> to adjust its jaw-angle to fit  $\text{Li}^+$  probably accounts for the greater stability of  $[\text{LiC22C}_2]^+$  compared with that of  $[\text{LiC22C}_5]^+$ . An optimal fit of  $\text{Li}^+$  into the C21C<sub>5</sub> cavity also occurs, but the presence of only five donor atoms results in  $[\text{LiC21C}_5]^+$  forming an *exclusive* cryptate in solution, with the consequence that its stability is the lowest for this series of ligands.<sup>42</sup> For the larger  $\text{Na}^+$ , the stability sequence changes to  $[\text{NaC22C}_2]^+ > [\text{NaC211}]^+ > [\text{NaC22C}_5]^+ > [\text{NaC21C}_5]^+$ . This is consistent with  $\text{Na}^+$  being too large to enter the cavities of C211 and C21C<sub>5</sub> so that their cryptates are *exclusive* in nature<sup>43</sup> and are much less stable than  $[\text{NaC22C}_2]^+$ , where  $\text{Na}^+$  fits the cryptand cavity optimally. The cavity size of C22C<sub>5</sub> is similar to that of C221 and should therefore be ideal for complexation of  $\text{Na}^+$ . However, in the solid state,  $[\text{NaC22C}_5]^+$  is an *exclusive* cryptate and  $\text{Na}^+$  interacts significantly only with the four oxygens of C22C<sub>5</sub>, whereas in  $[\text{NaC22C}_2]^+$ , all six donor atoms are within bonding distances.<sup>29</sup> The stabilities of  $[\text{MC211}]^+$  are too low to be determined for  $\text{M}^+ = \text{K}^+, \text{Rb}^+$  and  $\text{Cs}^+$ ,<sup>6</sup> consistent with the large differences in the size of the metal ion and cryptand cavity destabilising these complexes. The other  $[\text{MC22C}_2]^+$  and  $[\text{MC22C}_5]^+$  cryptates are discussed in detail later.

## 2.3 Stability of $[\text{MC22C}_8]^+$ in Non-Aqueous Solution

The stabilities of the alkali metal cryptates,  $[\text{MC22C}_8]^+$ , appear in Table 2.4. A small selectivity for  $\text{K}^+$  is shown by  $\text{C22C}_8$ , as demonstrated by the variation of the stability of  $[\text{MC22C}_8]^+$  in the sequence  $\text{Li}^+ < \text{Na}^+ < \text{K}^+ > \text{Rb}^+ > \text{Cs}^+$  in acetonitrile and dimethylformamide. This is similar to the pattern of selectivity exhibited by  $[\text{MC222}]^+$  (Table 2.5), which suggests that the similarity of the cavity sizes of  $\text{C22C}_8$  and  $\text{C222}$  ( $r = 1.4 \text{ \AA}$ ), which match that of  $\text{K}^+$  ( $r = 1.38 \text{ \AA}$ ) is the main factor in determining the stabilities of  $[\text{MC22C}_8]^+$  and  $[\text{MC222}]^+$ . As is the case with  $\text{C222}$ ,  $\text{Li}^+$  and  $\text{Na}^+$  are smaller than the cavity size and consequently form complexes less stable than does  $\text{K}^+$ , which is of optimum size. The larger  $\text{Rb}^+$  and  $\text{Cs}^+$  also form less stable complexes than does  $\text{K}^+$ , since they are larger than the cavity size of  $\text{C22C}_8$ . Although the selectivities of  $\text{C22C}_8$  and  $\text{C222}$  for the alkali metal ions are similar, the stabilities of  $[\text{MC22C}_8]^+$  are several orders of magnitude lower than those of  $[\text{MC222}]^+$ . This is a result of the weaker electrostatic attraction between  $\text{M}^+$  and  $\text{C22C}_8$  compared with  $\text{C222}$ , as a result of  $\text{C22C}_8$  possessing two less ether oxygens. However, this effect is modified by the relative sizes of the metal ion and the cryptand cavity. Thus, the differences in the stabilities of  $[\text{MC22C}_8]^+$  and  $[\text{MC222}]^+$  are greatest for  $\text{K}^+$ , corresponding to the optimum fit of  $\text{K}^+$  into the cavity of  $\text{C222}$  and the establishment of optimum bonding distances between  $\text{K}^+$  and all eight cryptand donor atoms. A similar relationship holds between the stabilities of  $[\text{MC22C}_5]^+$  and  $[\text{MC221}]^+$ , although the magnitude of the effect is smaller, since  $\text{C22C}_5$  and  $\text{C221}$  differ only by one oxygen donor atom. In this case, the maximum difference between the stabilities of  $[\text{MC22C}_5]^+$  and  $[\text{MC221}]^+$  occurs with  $\text{Na}^+$ , which is of optimum size for complexation by  $\text{C221}$ .

## 2.4 $\text{Ag}^+$ and $\text{Tl}^+$ Cryptates

In the oxygen donor solvents methanol, dimethylformamide and water,  $[\text{AgC22C}_2]^+$ ,  $[\text{AgC22C}_8]^+$ ,  $[\text{TlC22C}_2]^+$  and  $[\text{TlC22C}_8]^+$  are more stable than their alkali metal ion analogues. The very high stability of the  $\text{Ag}^+$  cryptates is a result of the soft acid nature of  $\text{Ag}^+$ ,<sup>45-46</sup> which enables it to bind more effectively with the cryptand nitrogen donor atoms than can the hard acid alkali metal ions.<sup>47-48</sup> However, in the nitrogen donor solvents acetonitrile and pyridine, the stabilities of the alkali metal species  $[\text{MC22C}_2]^+$  and  $[\text{MC22C}_8]^+$  increase relative to the analogous  $\text{Ag}^+$  complexes, since these nitrogen donor solvents solvate  $\text{Ag}^+$  far more strongly than they do the alkali metal ions.  $\text{Tl}^+$

**Table 2.4.** Stability Constants<sup>a</sup> for the Complexation of Monovalent Metal Ions by 4,7,13,16-Tetraoxa-1,10-diazabicyclo[8.8.8]-hexacosane (C22C<sub>8</sub>) at 298.2 K.

solvent	$D_N^b$	$\log(K_s/\text{dm}^3 \text{ mol}^{-1})$						
		[LiC22C <sub>8</sub> ] <sup>+</sup>	[NaC22C <sub>8</sub> ] <sup>+</sup>	[KC22C <sub>8</sub> ] <sup>+</sup>	[RbC22C <sub>8</sub> ] <sup>+</sup>	[CsC22C <sub>8</sub> ] <sup>+</sup>	[AgC22C <sub>8</sub> ] <sup>+</sup>	[TlC22C <sub>8</sub> ] <sup>+</sup>
acetonitrile	14.1	3.7 ± 0.1	4.86 ± 0.05	5.09 ± 0.05	3.85 ± 0.05	3.13 ± 0.05	6.23 ± 0.05	6.19 ± 0.05
methanol	19.0 (23.5) <sup>d</sup>	2.2 ± 0.1	3.4 ± 0.1				10.0 ± 0.1	
dimethyl- formamide	26.6	1.9 ± 0.1	2.3 ± 0.1	2.6 ± 0.1	2.2 ± 0.1	2.0 ± 0.1	7.7 ± 0.1	3.1 ± 0.1
pyridine	33.1		3.94 ± 0.05					
water	18.0 (33.0) <sup>d</sup>	<2 <sup>c</sup>	<2 <sup>c</sup>	<2 <sup>c</sup>	<2 <sup>c</sup>	<2 <sup>c</sup>		

<sup>a</sup> In 0.050 mol dm<sup>-3</sup> NEt<sub>4</sub>ClO<sub>4</sub> supporting electrolyte except where stated otherwise. <sup>b</sup> Gutmann donor number from reference 35.

<sup>c</sup> Determined by pH titration in 0.10 mol dm<sup>-3</sup> NEt<sub>4</sub>ClO<sub>4</sub> supporting electrolyte. <sup>d</sup> In references 36 and 37 it has been suggested that  $D_N = 33.0$  and  $23.5$  are more appropriate in water and methanol solutions rather than  $D_N = 18.0$  and  $19.0$ , respectively, obtained for water and methanol in 1,2-dichloroethane solution where the hydrogen bonding structure of these solvents is disrupted.

**Table 2.5.** Stability Constants for the Complexation of Monovalent Metal Ions by 4,7,13,16-Tetraoxa-1,10-diazabicyclo[8.8.8]hexacosane (C22C8) and Other Cryptands at 298.2 K.

	log( $K_s$ /dm <sup>3</sup> mol <sup>-1</sup> ) (298.2K)						
	Li <sup>+</sup>	Na <sup>+</sup>	K <sup>+</sup>	Rb <sup>+</sup>	Cs <sup>+</sup>	Ag <sup>+</sup>	Tl <sup>+</sup>
acetonitrile							
C22C <sub>2</sub>	7.8 <sup>a</sup>	9.4 <sup>b</sup>	7.2 <sup>b</sup>	5.9 <sup>b</sup>	5.0 <sup>b</sup>	9.4 <sup>a</sup>	10.4 <sup>b</sup>
C22C <sub>5</sub>	6.07 <sup>c</sup>	7.55 <sup>c</sup>	6.26 <sup>d</sup>	5.5 <sup>d</sup>	4.57 <sup>d</sup>	8.27 <sup>c</sup>	
C22C <sub>8</sub>	3.7 <sup>b</sup>	4.86 <sup>b</sup>	5.09 <sup>b</sup>	3.85 <sup>b</sup>	3.13 <sup>b</sup>	6.23 <sup>b</sup>	6.19 <sup>b</sup>
C222	6.97 <sup>e</sup>	9.63 <sup>e</sup>	11.3 <sup>e</sup>	9.50 <sup>e</sup>	4.57 <sup>e</sup>	8.99 <sup>e</sup>	12.30 <sup>f</sup>
C22	4.39 <sup>g</sup>	4.49 <sup>h</sup>	4.35 <sup>h</sup>	3.37 <sup>i</sup>	2.25 <sup>h</sup>	7.94 <sup>j</sup>	6.82 <sup>j</sup>
methanol							
C22C <sub>2</sub>	4.0 <sup>a</sup>	6.6 <sup>b</sup>				10.2 <sup>a</sup>	7.8 <sup>b</sup>
C22C <sub>5</sub>	2.30 <sup>c</sup>	5.41 <sup>c</sup>	5.8 <sup>c</sup>	5.7 <sup>c</sup>	4.8 <sup>c</sup>	11.13 <sup>c</sup>	6.48 <sup>c</sup>
C22C <sub>8</sub>	2.2 <sup>b</sup>	3.4 <sup>b</sup>				10.0 <sup>b</sup>	
C222	2.6 <sup>e</sup>	7.98 <sup>e</sup>	10.41 <sup>e</sup>	8.98 <sup>e</sup>	4.4 <sup>e</sup>	12.20 <sup>e</sup>	10.28 <sup>f</sup>
C22		1.0 <sup>k</sup>	2.0 <sup>k</sup>	1.2 <sup>k</sup>		9.99 <sup>j</sup>	3.54 <sup>j</sup>
dimethylformamide							
C22C <sub>2</sub>	3.5 <sup>a</sup>	6.1 <sup>b</sup>	3.2 <sup>b</sup>	2.8 <sup>b</sup>	2.7 <sup>b</sup>	9.4 <sup>b</sup>	6.7 <sup>b</sup>
C22C <sub>5</sub>	2.21 <sup>c</sup>	3.66 <sup>c</sup>	3.85 <sup>c</sup>	3.82 <sup>c</sup>	2.90 <sup>c</sup>	9.40 <sup>c</sup>	5.05 <sup>c</sup>
C22C <sub>8</sub>	1.9 <sup>b</sup>	2.3 <sup>b</sup>	2.6 <sup>b</sup>	2.2 <sup>b</sup>	2.0 <sup>b</sup>	7.7 <sup>b</sup>	3.1 <sup>b</sup>
C222		6.17 <sup>e</sup>	7.98 <sup>e</sup>	6.78 <sup>e</sup>	2.16 <sup>e</sup>	10.07 <sup>e</sup>	8.06 <sup>f</sup>
C22	~0 <sup>g</sup>	<2 <sup>l</sup>	<2 <sup>l</sup>		0.61 <sup>g</sup>	9.91 <sup>j</sup>	3.41 <sup>j</sup>

<sup>a</sup> Reference 22. <sup>b</sup> This work. <sup>c</sup> Reference 30. <sup>d</sup> Reference 21. <sup>e</sup> Reference 6. <sup>f</sup> Reference 44.

<sup>g</sup> Reference 49. <sup>h</sup> Reference 26. <sup>i</sup> Reference 50. <sup>j</sup> Reference 51. <sup>k</sup> Reference 18.

<sup>l</sup> Reference 52.

is intermediate between  $\text{Ag}^+$  and the alkali metal ions in its soft/hard acid nature<sup>44,53</sup> and as a consequence, binds less strongly to the cryptand nitrogen donor atoms than does  $\text{Ag}^+$ . Thus, the stabilities of  $[\text{TlC22C}_2]^+$  and  $[\text{TlC22C}_8]^+$  are lower than those of the corresponding cryptates of  $\text{Ag}^+$  in the oxygen donor solvents methanol, dimethylformamide and water, but in acetonitrile the stabilities of the  $\text{Tl}^+$  cryptates approach or exceed those of the  $\text{Ag}^+$  cryptates. The soft acid nature of  $\text{Ag}^+$  and  $\text{Tl}^+$  superimposes on the effect of cation size. Thus, the stabilities of the  $\text{Tl}^+$  cryptates are generally several orders of magnitude greater than those of  $\text{Rb}^+$  ( $r = 1.52 \text{ \AA}$ ), which is the alkali metal ion closest in size to  $\text{Tl}^+$  ( $r = 1.50 \text{ \AA}$ ). In fact,  $[\text{TlC22C}_2]^+$  is more stable than  $[\text{NaC22C}_2]^+$ , despite the larger than optimum size of  $\text{Tl}^+$  and hence greater strain in  $[\text{TlC22C}_2]^+$ . Similarly,  $[\text{AgC22C}_8]^+$  and  $[\text{TlC22C}_8]^+$  are more stable than  $[\text{KC22C}_8]^+$ , despite  $\text{Ag}^+$  ( $r = 1.15 \text{ \AA}$ ) and  $\text{Tl}^+$  being too small and too large, respectively, to fit the cavity of  $\text{C22C}_8$ , whereas  $\text{K}^+$  is of optimum size. The most stable  $\text{Ag}^+$  and  $\text{Tl}^+$  cryptates in Tables 2.3 and 2.5 are  $[\text{AgC221}]^+$  and  $[\text{TlC222}]^+$ , respectively, which corresponds to the optimum matching of ionic radius to cryptand cavity size, probably because this coincides with the maximum interaction between these metal ions and the two cryptand nitrogens.

## 2.5 Effect of Solvent on Cryptate Stability

From Tables 2.2 and 2.4, it can be seen that there is considerable variation in the stability of  $[\text{MC22C}_2]^+$  and  $[\text{MC22C}_8]^+$  with solvent. On complexation, the metal ion becomes largely desolvated, with solvent molecules in the first coordination sphere of the metal ion being replaced by ligand donor atoms. The Gutmann donor number,<sup>35</sup>  $D_N$  (Appendix i), is proportional to the electron-donating strength of the solvent and may be used as a measure of cation solvation energy.<sup>7-9,20-23,26,50,54-58</sup> Thus, the stabilities of  $[\text{MC22C}_2]^+$  and  $[\text{MC22C}_8]^+$  tend to decrease as  $D_N$  increases, consistent with increasingly strong  $\text{M}^+$  solvation causing a decrease in cryptate stability. Similar results are obtained with the other cryptates in Tables 2.3 and 2.5. The apparently anomalous position of water in this sequence may be resolved when a  $D_N$  value of 33.0 is employed. This value, and the  $D_N$  value of 23.5 quoted for methanol in Tables 2.2 and 2.4, are probably the most appropriate, since they refer to the bulk solvent, whereas the values 19.0 and 18.0 are determined in 1,2-dichloroethane, where the intermolecular hydrogen bonding of these protic solvents is disrupted.<sup>36-37</sup>

A similar variation in stability with  $D_N$  is observed with the analogous  $\text{Ag}^+$  and  $\text{Tl}^+$  cryptates in the oxygen donor solvents, but not in the nitrogen donor solvents as discussed previously. The stabilities of the alkali metal cryptates in pyridine are much greater than expected on the basis of its  $D_N$  of 33.1. However, the relation between  $D_N$  and solvent donor strength may not always be applicable in determining the magnitude of cation-solvent interactions for the alkali metal ions. The hard acid alkali metal ions show a preference for binding with hard base oxygen donor atoms, so that the cation may be more strongly solvated in these solvents than in the softer base pyridine.<sup>59-60</sup> It must also be remembered that  $D_N$  is proportional to the electron-donating strength of a single solvent molecule, whereas the number of solvent molecules coordinating to a metal ion in solution depends on the size of the metal ion and also the size and structure of the solvent. It may be that the incorporation of the nitrogen donor atom within the aromatic ring leads to steric hindrance between adjacent pyridines coordinated to the central ion, whereas no such difficulty occurs with the other solvents studied. However, the stability of  $[\text{AgC}_{22}\text{C}_2]^+$  is lower in pyridine than in the weaker donor solvent acetonitrile,<sup>22</sup> since  $\text{Ag}^+$  has a tendency to form two strong bonds in a linear array,<sup>47</sup> which would reduce the effect of steric crowding present with higher coordination numbers. Similar results have been obtained for other alkali metal complexes in pyridine.<sup>22,29,49,56</sup> In order to quantify this phenomenon, some estimates of the metal ion solvation energies in pyridine are necessary. Unfortunately, no such data was available in the literature.

In general, solvation of the cryptand and its cryptate are less significant than solvation of the metal ion in determining cryptate stability. A number of studies have demonstrated that the difference in the solvation free energies of the cryptand L and its cryptate  $[\text{ML}]^+$  (where  $\text{M}^+$  is an alkali metal ion,  $\text{Ag}^+$  or  $\text{Tl}^+$ ) for a given metal ion, is constant for aprotic, non-aqueous solvents.<sup>5,6,28,61-63</sup> This implies that the variations in cryptate stability among different non-aqueous solvents are almost entirely due to variations in the solvation energy of  $\text{M}^+$ . However, in protic solvents, such as methanol and water, this relationship is no longer valid. It has been shown that the Gibbs free energy of transfer of the cryptand C222 from water to various non-aqueous solvents is positive,<sup>6,12,61</sup> which shows that the ligand is more strongly solvated in water than in non-aqueous solution. This is probably a result of hydrogen bonding between the solvent and the cryptand donor atoms, which may lead to a reduction in cryptate stability, since such interactions will be disrupted on complex formation. This would also account for the

particularly low stabilities of alkali metal cryptates in water, as exemplified by  $[\text{NaC22C}_2]^+$  in aqueous solution. Values of the Gibbs free energies of transfer of alkali metal ions from water to various non-aqueous solvents,  $\Delta G_{\text{tr}}(\text{M}^+)$ , appear in Table 2.6. There is a clear correlation between  $D_{\text{N}}$  and the solvation energy of  $\text{M}^+$  in non-aqueous solvents, but not in water. The solvation energies of the alkali metal ions are higher in  $\text{H}_2\text{O}$  than in methanol and lie between those of the strong donor solvents dimethylformamide and dimethylsulfoxide, and those of the weak donor solvents acetonitrile and propylene carbonate. Thus, it would seem that neither  $D_{\text{N}} = 18.0$  nor  $D_{\text{N}} = 33.0$  are accurate measures of the solvation energies of the alkali metal ions in aqueous solution, which is probably a reflection of the hydrogen bonded structure of water.

**Table 2.6.** Gibbs Free Energies of Transfer<sup>a</sup> ( $\Delta G_{\text{tr}}(\text{M}^+)$ ) ( $\text{kJ mol}^{-1}$ ) from Water to Non-Aqueous Solvents

$\text{M}^+$	dimethyl- sulfoxide (29.8 <sup>b</sup> )	dimethyl- formamide (26.6 <sup>b</sup> )	methanol (19.0 <sup>b</sup> , 23.5 <sup>c</sup> )	propylene- carbonate (15.1 <sup>b</sup> )	acetonitrile (14.1 <sup>b</sup> )
$\text{Li}^+$	-17.5	-9.1	4.1	21.7	22.8
$\text{Na}^+$	-15.0	-8.7	9.2	15.5	13.6
$\text{K}^+$	-14.3	-7.8	10.4	7.0	7.3
$\text{Rb}^+$	-12.4	-7.6	11.1	4.6	6.4
$\text{Cs}^+$	-15.2	-8.0	10.6	3.1	4.0
$\text{Ag}^+$	-34.9	-16.6	7.8	19.3	-23.0
$\text{Tl}^+$	-25.1	-11.7	4.2	8.4	9.2

<sup>a</sup> All values of  $\Delta G_{\text{tr}}(\text{M}^+)$  are from reference 28 except for  $\text{Tl}^+$  which are from reference 27.

<sup>b</sup> Gutmann donor number from reference 35. <sup>c</sup> Gutmann donor number from references 36-37.

## 2.6 Effect of the Length of the $C_n$ Bridge on the Stability of $[MC22C_n]^+$

It is apparent from Table 2.5 that the different stereochemistries of the  $C22C_n$  cryptands are reflected in the substantial differences among the stabilities of their cryptates. There is a clear trend in the alkali metal complexes  $[MC22C_n]^+$ ; as  $n$  increases, the stabilities and selectivities of  $[MC22C_n]^+$  tend to decrease and approach those of the complexes of the parent macrocycle C22 (Figure 2.5). This is consistent with an increase in the length of the aliphatic  $-(CH_2)_n-$  arm resulting in a consequent increase in the flexibility of the  $C22C_n$  ligand. In the solid state structures of  $[MC22C_5]^+$ , the major interaction is between  $M^+$  and the four oxygens of the eighteen membered C22 ring and the distances between  $M^+$  and the mean plane of the four oxygens range from 0.0112 Å below the plane in  $[NaC22C_5]^+$  to 1.2996 Å above the plane in  $[CsC22C_5]^+$ .<sup>30</sup> Thus, in the absence of donor atoms in the  $-(CH_2)_5-$  bridge, the tendency for  $M^+$  to reside within the cavity of  $C22C_5$  is reduced, and as a consequence, the stabilities of  $[MC22C_5]^+$  are no longer determined by the relative sizes of  $M^+$  and the cavity of  $C22C_5$ . This is reflected by the change in selectivity from  $Na^+ > K^+ > Rb^+$  for  $[MC221]^+$  to  $Na^+ \leq K^+ \geq Rb^+$  for  $[MC22C_5]^+$ . (In acetonitrile, the stabilities of  $[MC22C_5]^+$  are in the sequence  $Na^+ > K^+ > Rb^+$  as discussed in reference 21). The stabilities of  $[MC22C_8]^+$  fall below those of both  $[MC22C_5]^+$  and  $[MC22C_2]^+$ , even for  $M^+ = K^+, Rb^+$  and  $Cs^+$ , although the larger cavity size of  $C22C_8$  should favour the complexation of these larger metal ions. In addition, the stabilities of  $[MC22C_8]^+$  and  $[MC22]^+$  are usually within an order of magnitude, in spite of the three dimensional intramolecular cavity of bicyclic  $C22C_8$ . This suggests that the selectivity of  $[MC22C_8]^+$  is no longer solely determined by the relative sizes of  $M^+$  and the cavity of  $C22C_8$ , which may explain the lower selectivity of  $C22C_8$  compared with that of C22.

The macrobicyclic effect is exemplified by the greater stabilities of the alkali metal ion cryptates of C221 and C222 by comparison with those of the diaza crown ether C22. The greater stability of  $[MC221]^+$  and  $[MC222]^+$  compared with  $[MC22]^+$  results from the three dimensional cavity, the decreased flexibility and the greater number of donor atoms of C221 and C222 compared with C22. In the absence of oxygen donor atoms in the aliphatic  $-(CH_2)_5-$  arms of  $C22C_5$ , the effect of the bicyclic cavity of this cryptand is reduced, because  $M^+$  tends to move away from the centre of the cryptand cavity, and the major interaction is between  $M^+$  and the C22 moiety of  $C22C_5$ .



The small differences in the stabilities of the complexes of bicyclic C22C<sub>8</sub> and monocyclic C22 probably results from a similar origin. In contrast, the clam-like structure of C22C<sub>2</sub>, which is a consequence of the shortness of the aliphatic -(CH<sub>2</sub>)<sub>2</sub>- arm, results in the stability and selectivity of [MC22C<sub>2</sub>]<sup>+</sup> being comparable to those of [MC221]<sup>+</sup> and [MC222]<sup>+</sup>.

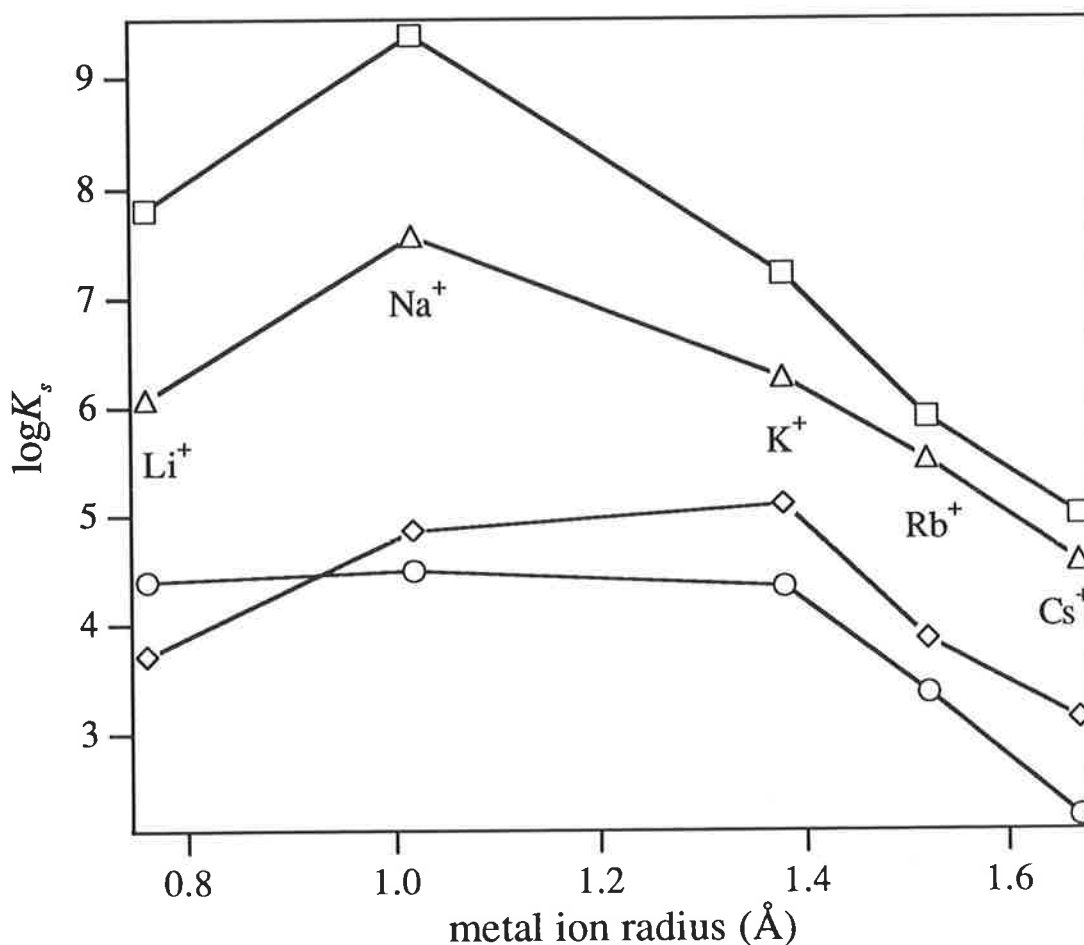


**Figure 2.5.** A plot of  $\log K_s$  versus metal ion radius for [MC22C<sub>2</sub>]<sup>+</sup> (squares), [MC22C<sub>5</sub>]<sup>+</sup> (triangles), [MC22C<sub>8</sub>]<sup>+</sup> (diamonds) and [MC22]<sup>+</sup> (circles) in acetonitrile. It is apparent that as the length of the aliphatic -(CH<sub>2</sub>)<sub>n</sub>- arm of C22C<sub>n</sub> increases, the stabilities and selectivities of [MC22C<sub>n</sub>]<sup>+</sup> decrease and approach those of [MC22]<sup>+</sup>.

- 1 Lehn, J-M. *Struct. Bonding (Berlin)*. **1973**, 16, 1-69.
- 2 Lehn, J-M.; Sauvage, J-P. *J. Am. Chem. Soc.* **1975**, 97, 6700-6707.
- 3 Dietrich, B.; Lehn, J-M.; Sauvage, J.P. *J. Chem. Soc., Chem. Commun.* **1973**, 15-16.
- 4 Cox, B.G.; Schneider, H.; Stroka, J. *J. Am. Chem. Soc.* **1978**, 100, 4746-4749.
- 5 Gutknecht, J.; Schneider, H.; Stroka, J. *Inorg. Chem.* **1978**, 17, 3326-3329.
- 6 Cox, B.G.; Garcia-Rosas, J.; Schneider, H. *J. Am. Chem. Soc.* **1981**, 103, 1384-1389.
- 7 Lincoln, S.F.; Brereton, I.M.; Spotswood, T.M. *J. Am. Chem. Soc.* **1986**, 108, 8134-8138.
- 8 Clarke, P.; Abou-Hamdan, A.; Hounslow, A.M.; Lincoln, S.F. *Inorg. Chim. Acta.* **1988**, 154, 83-87.
- 9 Lincoln, S.F.; Abou-Hamdan, A. *Inorg. Chem.* **1990**, 29, 3584-3589.
- 10 Mathieu, F.; Metz, B.; Moras, D.; Weiss, R. *J. Am. Chem. Soc.* **1978**, 100, 4412-4416.
- 11 Buschmann, H-J. *Inorg. Chim. Acta.* **1986**, 125, 31-35.
- 12 de Namor, A.F.D.; Ghousseini, L.; Lee, W.H. *J. Chem. Soc., Faraday Trans. 1.* **1985**, 81, 781-791.
- 13 Lehn, J-M. *Acc. Chem. Res.* **1978**, 11, 49-57.
- 14 Gokel, G.W. "*Crown Ethers and Cryptands*", The Royal Society of Chemistry, Cambridge, **1991**.
- 15 Dietrich, B.; Viout, P.; Lehn, J-M. "*Macrocyclic Chemistry*", VCH, Weinheim, **1993**.
- 16 Lamb, J.D.; Izatt, R.M.; Christensen, J.J.; Eatough, D.J. "*Coordination Chemistry of Macrocyclic Compounds*", Plenum Press, New York, **1979**.
- 17 Buschmann, H-J. "*Thermodynamic and Stereochemical Aspects of the Macrocyclic and Cryptate Effects*" in "*Stereochemical and Stereophysical Behaviour of Macrocycles*", Elsevier, Amsterdam, **1987**.
- 18 Frensdorff, H.K. *J. Am. Chem. Soc.* **1971**, 93, 600-606.
- 19 Shannon, R.D. *Acta Crystallogr., Sect. A: Cryst. Phys. Diffr., Theor. Gen. Crystallogr.* **1976**, A32, 751-767.
- 20 Lincoln, S.F.; Stephens, A.K.W. *Inorg. Chem.* **1991**, 30, 3529-3537.
- 21 Dhillon, R.; Lincoln, S.F. *Aust. J. Chem.* **1994**, 47, 123-130.
- 22 Lincoln, S.F.; Abou-Hamdan, A. *Inorg. Chem.* **1991**, 30, 462-466.
- 23 Lincoln, S.F.; Steel, B.J.; Brereton, I.M.; Spotswood, T.M. *Polyhedron.* **1986**, 5, 1597-1600.

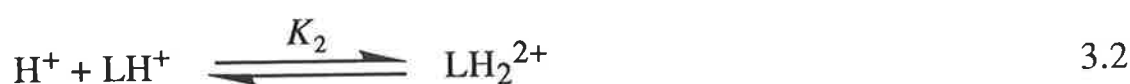
- 24 Cox, B.G.; van Truong, N.; Schneider, H. *J. Am. Chem. Soc.* **1984**, 106, 1273-1280.
- 25 Buschmann, H-J. *Inorg. Chim. Acta.* **1986**, 120, 125-129.
- 26 Boss, R.D.; Popov, A.I. *Inorg. Chem.* **1986**, 25, 1747-1750.
- 27 Cox, B.G. *Annu. Rep. Prog. Chem., Sect. A, Phys. Inorg. Chem.* **1973**, 70, 249-274.
- 28 Cox, B.G.; Firman, P.; Garcia-Rosas, J.; Schneider, H. *Tetrahedron Lett.* **1982**, 23, 3777-3780.
- 29 Clarke, P.; Lincoln, S.F.; Tiekink, E.R.T. *Inorg. Chem.* **1991**, 30, 2747-2751.
- 30 Clarke, P.; Gulbis, J.M.; Lincoln, S.F.; Tiekink, E.R.T. *Inorg. Chem.* **1992**, 31, 3398-3404.
- 31 Groth, P. *Acta Chem. Scand.* **1985**, A39, 68-72.
- 32 Groth, P. *Acta Chem. Scand.* **1985**, A39, 73-76.
- 33 Alfheim, T.; Dale, J.; Groth, P.; Krautwurst, K.D. *J. Chem. Soc., Chem. Commun.* **1984**, 1502-1504.
- 34 Groth, P. *Acta Chem. Scand.* **1985**, A39, 59-62.
- 35 Gutmann, V. "*Coordination Chemistry in Non-Aqueous Solutions*"; Springer-Verlag: Wien, **1968**.
- 36 Erlich, R.H.; Roach, E.; Popov, A.I. *J. Am. Chem. Soc.* **1970**, 92, 4989-4990.
- 37 Dewitte, W.J.; Popov, A.I. *J. Soln. Chem.* **1976**, 5, 231-240.
- 38 Keller, E. SCHAKAL, A Fortran-77 program. Inorganic Chemistry Institute, University of Freiburg, Freiburg, Germany.
- 39 Mathieu, F.; Metz, B.; Moras, D.; Weiss, R. *J. Am. Chem. Soc.* **1978**, 100, 4412-4416.
- 40 Cahen, Y.M.; Dye, J.L.; Popov, A.I. *J. Phys. Chem.* **1975**, 79, 1289-1291.
- 41 Moras, D.; Weiss, R. *Acta. Crystallogr., Sect. B: Struct. Crystallogr. Cryst. Chem.* **1973**, B29, 400-403.
- 42 Abou-Hamdan, A.; Hambley, T.W.; Hounslow, A.M.; Lincoln, S.F. *J. Chem. Soc., Dalton Trans.* **1987**, 492-498.
- 43 Lincoln, S.F.; Horn, E.; Snow, M.R.; Hambley, T.W.; Brereton, I.M.; Spotswood, T.M. *J. Chem. Soc., Dalton Trans.* **1986**, 1075-1080.
- 44 Cox, B.G.; Stroka, J.J.; Schneider, I.; Schneider, H. *J. Chem. Soc., Faraday Trans 1.* **1989**, 85, 187-198.
- 45 Pearson, R.G. *J. Am. Chem. Soc.* **1963**, 85, 3533-3539.
- 46 Pearson, R.G. *Coord. Chem. Rev.* **1990**, 100, 403-425.

- 47 Cotton, F.A.; Wilkinson, G. *"Advanced Inorganic Chemistry"*, 3rd ed, Interscience, New York, **1980**.
- 48 Buschmann, H-J. *Inorg. Chim. Acta.* **1985**, 102, 95-98.
- 49 Shamsipur, M.; Popov, A.I. *Inorg. Chim. Acta.* **1980**, 43, 243-247.
- 50 Kulstad, S.; Malmsten, L.A. *J. Inorg. Nucl. Chem.* **1980**, 42, 573-578.
- 51 Cox, B.G.; Firman, P.; Horst, H.; Schneider, H. *Polyhedron*, **1983**, 2, 343-347.
- 52 Morolleau, I.; Gisselbrecht, J.P.; Gross, M.; Arnaud-Neu, F.; Schwing-Weill, M.T. *J. Chem. Soc., Dalton Trans.* **1989**, 367-370.
- 53 Taylor, E.C.; McKillop, A. *Acc. Chem. Res.* **1970**, 3, 338-346.
- 54 Lin, J.D.; Popov, A.I. *J. Am. Chem. Soc.* **1981**, 103, 3773-3777.
- 55 Strasser, B.O.; Popov, A.I.; *J. Am. Chem. Soc.* **1985**, 107, 7921-7924.
- 56 Shamsipur, M.; Popov, A.I. *J. Phys. Chem.* **1986**, 90, 5997-5999.
- 57 Shamsipur, M.; Popov, A.I. *J. Phys. Chem.* **1987**, 91, 447-451.
- 58 Cahen, Y.M.; Dye, J.L.; Popov, A.I. *J. Phys. Chem.* **1975**, 79, 1292-1295.
- 59 Popov, A.I. *Pure Appl. Chem.* **1979**, 51, 101-110.
- 60 Ahmed, N.; Day, M.C. *J. Am. Chem. Soc.* **1977**, 99, 941
- 61 de Namor, A.F.D.; Ghousseini, L.; Lee, W.H. *J. Chem. Soc., Faraday Trans. 1.* **1985**, 81, 2495-2502.
- 62 de Namor, A.F.; Salazar, F.F.; Greenwood, P. *J. Chem. Soc., Faraday Trans 1.* **1987**, 83, 2663-2670.
- 63 Chanttoni, M.K.; Kolthoff, I.M. *J. Solution. Chem.* **1985**, 14, 1-12.

## Chapter 3: Equilibrium Studies of Divalent Metal Cryptates

### 3.1 Protonation Constants of C22C<sub>2</sub> and C22C<sub>8</sub>

In aqueous solution at 298.2 K and  $I = 0.10 \text{ mol dm}^{-3}$  ( $\text{NEt}_4\text{ClO}_4$ ), the cryptands C22C<sub>2</sub> and C22C<sub>8</sub> behave as dibasic species characterised by the protonation constants  $K_1$  and  $K_2$  as defined in Equations 3.1 - 3.4. The protonation constants of both C22C<sub>2</sub> and C22C<sub>8</sub> appear in Table 3.1, together with those of some related cryptands and diaza crown ethers (Figure 3.1).



$$K_1 = \frac{[\text{LH}^+]}{[\text{H}^+][\text{L}]} \quad 3.3$$

$$K_2 = \frac{[\text{LH}_2^{2+}]}{[\text{H}^+][\text{LH}^+]} \quad 3.4$$

**Table 3.1.** Protonation Constants for the Cryptands C22C<sub>2</sub>, C22C<sub>8</sub> and other Ligands at 298.2 K in 0.10 mol dm<sup>-3</sup>  $\text{NEt}_4\text{ClO}_4$  Aqueous Solution.

Ligand	$\log(K_1/\text{dm}^3 \text{ mol}^{-1})$	$\log(K_2/\text{dm}^3 \text{ mol}^{-1})$
C22C <sub>2</sub> <i>a</i>	10.92 ± 0.05	3.42 ± 0.05
C22C <sub>5</sub> <i>b</i>	11.43 ± 0.05	8.10 ± 0.05
C22C <sub>8</sub> <i>a</i>	11.06 ± 0.05	8.41 ± 0.05
C221 <i>c</i>	11.02	7.74
C222 <i>c</i>	10.00	7.53
C21 <i>c</i>	8.76	8.04
C22 <i>c</i>	9.20	8.02

*a* This work. *b* Reference 1. *c* Reference 2.

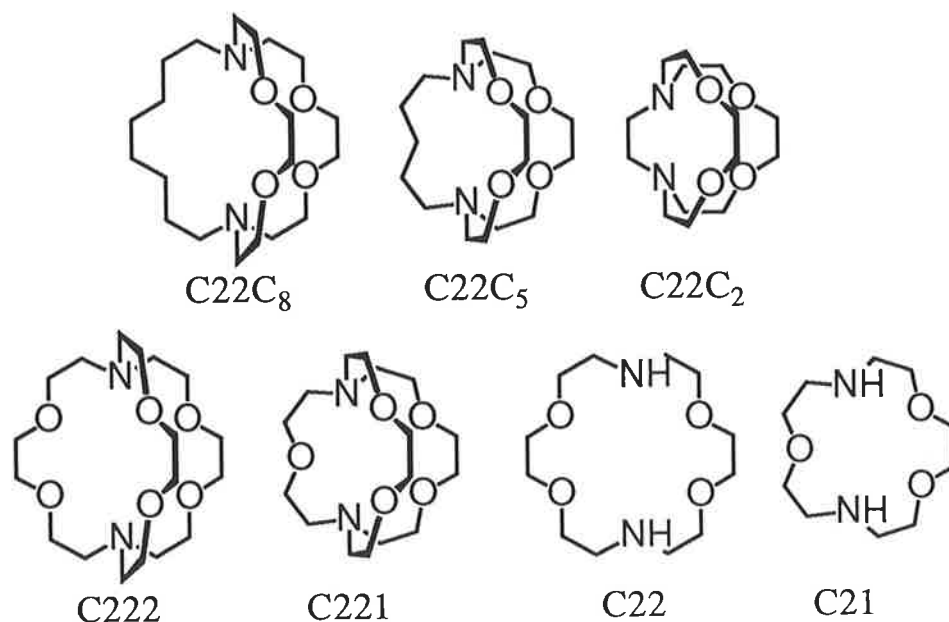


**Figure 3.1.** The cryptands C22C<sub>2</sub>, C22C<sub>5</sub>, C22C<sub>8</sub>, C221 and C222 and the diaza crown ethers C21 and C22.

The solid state structure of  $[(\text{H}_3\text{O})\text{C22C}_5]\text{ClO}_4$  shows the oxygen of  $\text{H}_3\text{O}^+$  to be  $0.666 \text{ \AA}$  above the plane of the four coplanar C22C<sub>5</sub> oxygens, with the lone pairs of the nitrogens directed toward the centre of the cryptand cavity in the *endo-endo* conformation, maximising the interactions of these lone pairs with the positive charge of the proton of  $\text{H}_3\text{O}^+$ .<sup>3</sup> In solution, the *endo-endo* conformation will probably be in equilibrium with the *endo-exo* and *exo-exo* conformations, but it is expected that the *endo-endo* conformation will predominate for  $\text{HC22C}_5^+$  and the other monoprotonated cryptands in Table 3.1. The small variations in  $K_1$  among the five cryptands in Table 3.1 probably indicates that both nitrogen lone pairs are able to interact with the proton and that the differences in  $K_1$  are due to structural variations. The lower values of  $K_1$  for C222 and C221 compared with those for C22C<sub>8</sub> and C22C<sub>5</sub>, respectively, may result from the greater hydrogen bonding capacity arising from the extra ether oxygen(s) of the first pair of cryptands. A similar relationship exists among the  $K_2$  values of these ligands. The protonation constant  $K_1$  for both the diaza crown ethers C21 and C22 is lower than for the cryptands in Table 3.1. This is consistent with the proton in the

monoprotonated cyclic crown ether interacting with water to a greater extent than in the bicyclic cryptands as a result of the more open structure of the monocyclic ligand. This may be likened to the macrobicyclic effect seen with the alkali metal cryptates, where an increase in stability is seen in going from the diaza crown ether complex to the cryptate (see Chapter 2).

The statistical effect arising from the availability of one and two protonatable nitrogens in  $\text{HC22C}_n^+$  and  $\text{C22C}_n$ , respectively, predicts that  $\log K_1$  should exceed  $\log K_2$  by 0.3 log units, but the greater difference is a result of the electrostatic repulsion between the two protons in  $\text{H}_2\text{C22C}_n^{2+}$ . The substantial difference between  $K_1$  and  $K_2$  for  $\text{C22C}_2$  probably results from the very close proximity of the two protons in  $\text{H}_2\text{C22C}_2^{2+}$ , which is a consequence of the short aliphatic  $\text{C}_2$  arm in this ligand (Figure 3.1). The increase in the length of the aliphatic arm, and thus the separation of the two bridgehead nitrogens, causes a corresponding increase in  $K_2$  on going from  $\text{C22C}_2$  through  $\text{C22C}_5$  to  $\text{C22C}_8$ . An additional effect of this electrostatic repulsion is that  $\text{H}_2\text{C22C}_n^{2+}$  may assume an *exo-endo* or *exo-exo* conformation, where one or both nitrogens direct their electron lone pair away from the cryptand cavity, so that the interaction distance between the protons is increased. (If the *endo-endo*, *exo-endo* and *exo-exo* conformations coexist for each  $\text{HC22C}_n^+$  or  $\text{H}_2\text{C22C}_n^{2+}$  species, the observed  $K_1$  and  $K_2$  values are the weighted means of the different  $K_1$  and  $K_2$  characterising these conformers in labile equilibrium with each other). There is a much smaller variation in  $K_2$  for the cryptands in Table 3.1 (except for  $\text{C22C}_2$ ), with all  $K_2$  values similar to those of the diaza crown ethers  $\text{C21}$  and  $\text{C22}$ . This indicates that the solvent interaction with this second protonated site is similar for all of these diprotonated ligands, which suggests that at least one of the protonated nitrogens is in the *exo* conformation.

### 3.2 Stability Constants of the Divalent Metal Cryptates $[\text{MC22C}_2]^{2+}$ and $[\text{MC22C}_8]^{2+}$

The complexation of a divalent metal ion  $\text{M}^{2+}$  by a cryptand L may be expressed as;



where the stability constant,  $K_s$ , is given by;

$$K_s = \frac{[\text{ML}^{2+}]}{[\text{M}^{2+}][\text{L}]} \quad 3.6$$

The stability constants of a number of divalent metal cryptates of  $\text{C22C}_2$  and  $\text{C22C}_8$  have been determined in aqueous solution and appear in Table 3.2. It is apparent that the magnitude of  $K_s$  varies substantially with the nature of the ligand and the metal ion. By comparison with  $[\text{MC22}]^{2+}$  and the other  $[\text{MC22C}_n]^{2+}$  complexes, the stability of  $[\text{MC22C}_2]^{2+}$  is the highest for all of the metal ions studied (except for  $\text{Hg}^{2+}$ ), although all four ligands have the same number and type of donor atoms. From studies of metal complexes with linear bidentate ligands, it has been observed that ligands that result in five and six membered chelate rings, when binding  $\text{M}^{2+}$ , form more stable complexes than those containing smaller or larger chelate rings.<sup>4</sup> Thus, the optimum "bite-size" of the  $>\text{NCH}_2\text{CH}_2\text{N}<$  moiety (which forms a five membered chelate ring with  $\text{M}^{2+}$ ) engenders greater stability on its metal complexes compared with that of the complexes formed by  $\text{C22}$ ,  $\text{C22C}_5$  and  $\text{C22C}_8$ , where only nitrogen to nitrogen chelate rings of eight or more members are possible when complexing  $\text{M}^{2+}$ . The exception to this is the lower stability of  $[\text{HgC22C}_2]^{2+}$ . This may be a reflection of the tendency of  $\text{Hg}^{2+}$  to form two linear bonds with the nitrogen donor atoms of these ligands,<sup>5</sup> which cannot occur in  $[\text{HgC22C}_2]^{2+}$  as a result of the close proximity of the two nitrogens, which are separated only by the  $-(\text{CH}_2)_2-$  moiety.

The factors responsible for variations in  $K_s$  with the nature of  $\text{M}^{2+}$  are as follows: i) the relative size of the metal ion<sup>6</sup> and the cryptand cavity;<sup>7</sup> ii) the metal ion solvation energies;<sup>8</sup> iii) the hard or soft acid nature of the metal ions and the consequent variations in their affinity for oxygen or nitrogen donor atoms<sup>9-10</sup> and iv) variations in ligand field stabilisation energies.<sup>5</sup> The



**Table 3.2.** Stability Constants for the Complexation of Divalent Metal Ions ( $M^{2+}$ ) by the Cryptands C22C<sub>2</sub>, C22C<sub>5</sub>, C22C<sub>8</sub>, C221, C222 and the Diaza Crown Ether C22 at 298.2 K in Aqueous Solution.

$M^{2+}$	Ionic Radius <sup>a</sup> (Å)	$\log(K_s/\text{dm}^3 \text{ mol}^{-1})$					
		[MC22C <sub>2</sub> ] <sup>2+</sup> <sup>b</sup>	[MC22C <sub>5</sub> ] <sup>2+</sup> <sup>c</sup>	[MC22C <sub>8</sub> ] <sup>2+</sup> <sup>b</sup>	[MC22] <sup>2+</sup>	[MC221] <sup>2+</sup>	[MC222] <sup>2+</sup>
Mg <sup>2+</sup>	0.72	3.5 ± 0.1	2.1 ± 0.1	2.8 ± 0.1		≤2 <sup>h</sup>	≤2 <sup>h</sup>
Ca <sup>2+</sup>	1.00 (1.12)	4.68 ± 0.05	2.0 ± 0.2	2.6 ± 0.1	1.8 <sup>d</sup>	6.95 <sup>h</sup>	4.4 <sup>h</sup>
Sr <sup>2+</sup>	1.18 (1.26)	4.3 ± 0.1	3.0 ± 0.1	2.8 ± 0.1	2.57 <sup>d</sup>	7.35 <sup>h</sup>	8.0 <sup>h</sup>
Ba <sup>2+</sup>	1.35 (1.42)	5.28 ± 0.05	2.8 ± 0.1	<2	2.98 <sup>d</sup>	6.30 <sup>h</sup>	9.5 <sup>h</sup>
Co <sup>2+</sup>	0.75	6.8 ± 0.1	5.0 ± 0.1	<6	≤2.5 <sup>e</sup>	5.40 <sup>e</sup>	≤2.5 <sup>e</sup>
Ni <sup>2+</sup>	0.69		5.5 ± 0.2	5.4 ± 0.1	≤2.5 <sup>e</sup>	4.28 <sup>e</sup>	≤3.5 <sup>e</sup>
Cu <sup>2+</sup>	0.73	9.4 ± 0.1	9.0 ± 0.2	8.7 ± 0.1	6.18 <sup>e</sup> 7.59 <sup>f</sup>	7.56 <sup>e</sup>	6.81 <sup>e</sup>
Zn <sup>2+</sup>	0.74	7.1 ± 0.1	6.4 ± 0.1	6.3 ± 0.1	3.19 <sup>e</sup> 4.13 <sup>f</sup>	5.41 <sup>e</sup>	≤2.5 <sup>e</sup>
Cd <sup>2+</sup>	0.95 (1.10)	9.0 ± 0.2	5.18 ± 0.05	4.5 ± 0.1	5.31 <sup>e</sup>	10.04 <sup>e</sup>	7.10 <sup>e</sup>
Hg <sup>2+</sup>	1.02 (1.14)	13.4 ± 0.1		16.5 ± 0.1	17.85 <sup>d</sup>	19.97 <sup>g</sup>	18.2 <sup>d</sup>
Pb <sup>2+</sup>	1.19 (1.29)	11.1 ± 0.1	8.1 ± 0.3	8.02 ± 0.05	6.90 <sup>e</sup>	13.12 <sup>e</sup>	12.72 <sup>e</sup>

<sup>a</sup> Reference 6. Ionic radii for six coordination are quoted for all metal ions and in the case of  $\text{Ca}^{2+}$ ,  $\text{Sr}^{2+}$ ,  $\text{Ba}^{2+}$ ,  $\text{Cd}^{2+}$ ,  $\text{Hg}^{2+}$  and  $\text{Pb}^{2+}$ , the radii quoted in brackets refer to eight coordination. <sup>b</sup> This work. <sup>c</sup> Reference 1. <sup>d</sup> Reference 11. <sup>e</sup> Reference 2. <sup>f</sup> Reference 12. <sup>g</sup> Reference 13. <sup>h</sup> Reference 7. With the exception of references 7 and 11 which were obtained in  $0.1 \text{ mol dm}^{-3} \text{ NMe}_4\text{Cl}$  and  $0.05 \text{ mol dm}^{-3} \text{ NMe}_4\text{Br}$  supporting electrolyte, respectively, all other data were obtained in  $0.10 \text{ mol dm}^{-3} \text{ NEt}_4\text{ClO}_4$ .

Irving-Williams series<sup>14-15</sup> is largely derived from effects ii) - iv) and predicts the sequence  $Ba^{2+} < Sr^{2+} < Ca^{2+} < Mg^{2+} < Mn^{2+} < Fe^{2+} < Co^{2+} < Ni^{2+} < Cu^{2+} > Zn^{2+}$  for the stabilities of  $M^{2+}$  complexes with a given ligand. The cryptates of  $C22C_2$  and  $C22C_8$  follow this sequence for the similarly sized first-row transition metal ions  $Co^{2+}$ ,  $Ni^{2+}$ ,  $Cu^{2+}$  and  $Zn^{2+}$ , but the alkaline earth cations do not. The variation of  $K_s$  in the sequence  $Mg^{2+} < Co^{2+} < Ni^{2+} < Cu^{2+} > Zn^{2+}$  agrees with that predicted from the Irving-Williams series. This is consistent with the hard acid  $Mg^{2+}$  binding less strongly with the nitrogen donor atoms than do the borderline soft acid divalent transition metal ions. The stabilities of the  $Co^{2+}$ ,  $Ni^{2+}$  and  $Cu^{2+}$  complexes are also enhanced by their ligand field effects. No such stabilisation exists for  $Mg^{2+}$  and  $Zn^{2+}$ . The other alkaline earth cryptates and those of  $Cd^{2+}$ ,  $Hg^{2+}$  and  $Pb^{2+}$  are discussed in more detail below.

### 3.2.1 Cryptates of the Alkaline Earth Metal Ions

The alkaline earth cryptates of  $C22C_2$  and  $C22C_8$  are in general characterised by lower stabilities than are their transition metal analogues and the cryptates of the heavy metal ions  $Cd^{2+}$ ,  $Hg^{2+}$  and  $Pb^{2+}$ . This is a result of the hard acid alkaline earth cations binding less strongly to the cryptand nitrogen donor atoms than do the softer acids  $Co^{2+}$ ,  $Ni^{2+}$ ,  $Cu^{2+}$ ,  $Zn^{2+}$ ,  $Cd^{2+}$ ,  $Hg^{2+}$  and  $Pb^{2+}$ . The alkaline earth cations also lack the additional stability conferred by ligand field effects.

The variation of  $K_s$  in the sequence  $Mg^{2+} < Ca^{2+} > Sr^{2+} < Ba^{2+}$  for  $[MC22C_2]^{2+}$  is similar to the stability sequence  $Li^+ < Na^+ > K^+ > Rb^+ > Cs^+$ , observed in Chapter 2 for the alkali metal cryptates of  $C22C_2$ . The selectivity of  $C22C_2$  for  $Na^+$  results from the jaw-angle in  $[NaC22C_2]^+$  being closest to that in free  $C22C_2$ , whereas cations smaller and larger, respectively, than  $Na^+$ , induce strain in  $C22C_2$  by causing the jaws of  $C22C_2$  to assume less and more than the optimum angle. Thus, the high stability of  $[CaC22C_2]^{2+}$  is consistent with the strain energy in  $C22C_2$  being minimised with  $Ca^{2+}$ , which has a similar ionic radius to  $Na^+$ . The smaller and larger  $Mg^{2+}$  and  $Sr^{2+}$ , respectively, induce strain in  $C22C_2$ , since the jaw-angle is smaller than the optimum value in  $[MgC22C_2]^{2+}$  and larger than the optimum value in  $[SrC22C_2]^{2+}$ . However, the increase in stability observed with  $[BaC22C_2]^{2+}$  does not fit this trend and in addition, the formation of  $[Ba(C22C_2)_2]^{2+}$  (Equation 3.7) (characterised by  $\log(K'_s/dm^3 mol^{-1}) = 4.65$ ) indicates that the relationship between stability and jaw-angle no longer holds.



where the stability constant  $K'_s$  is given by;

$$K'_s = \frac{[\text{Ba}(\text{C22C}_2)_2]^{2+}}{[\text{BaC22C}_2]^{2+}[\text{C22C}_2]} \quad 3.8$$

A similar tendency to form 1:2 complexes with increasing metal ion size is observed with the 15C5 and 18C6 crown ethers in methanol, where  $[\text{M15C5}]^{2+}$  and  $[\text{M18C6}]^{2+}$  complexes form when  $\text{M}^{2+} = \text{Ca}^{2+}, \text{Sr}^{2+}$  and  $\text{Ba}^{2+}$  but  $[\text{M}(\text{15C5})_2]^{2+}$  and  $[\text{M}(\text{18C6})_2]^{2+}$  complexes form only for the larger  $\text{Sr}^{2+}$  and  $\text{Ba}^{2+}$ .<sup>16</sup> It is possible that the large size of  $\text{Ba}^{2+}$  results in only a weak interaction with the nitrogens of  $\text{C22C}_2$  such that the four oxygens bind to  $\text{Ba}^{2+}$  without disrupting the optimum jaw-angle of the cryptand, and the second  $\text{C22C}_2$  binds similarly (Figure 3.2). In this case, approach of a second  $\text{C22C}_2$  may readily occur as shown by  $K'_s$  being less than an order of magnitude smaller than  $K_s$ . Thus, the greater stability of  $[\text{BaC22C}_2]^{2+}$  compared with  $[\text{CaC22C}_2]^{2+}$  may result from the absence of strain in  $[\text{BaC22C}_2]^{2+}$ , together with the lower solvation energy of  $\text{Ba}^{2+}$ , compared with that of the smaller  $\text{Ca}^{2+}$ . A speciation plot for the formation of  $[\text{BaC22C}_2]^{2+}$  and  $[\text{Ba}(\text{C22C}_2)_2]^{2+}$  appears in Figure 3.3.

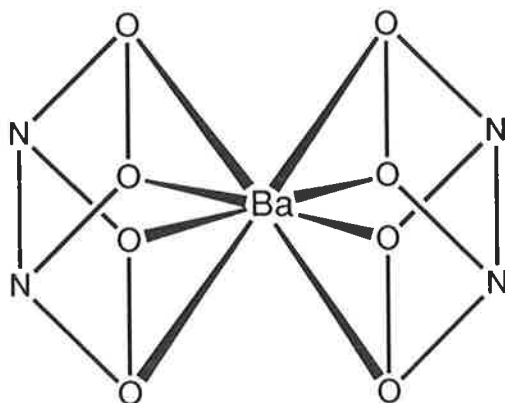


**Figure 3.2.** Possible structure of the complex  $[\text{Ba}(\text{C22C}_2)_2]^{2+}$ .

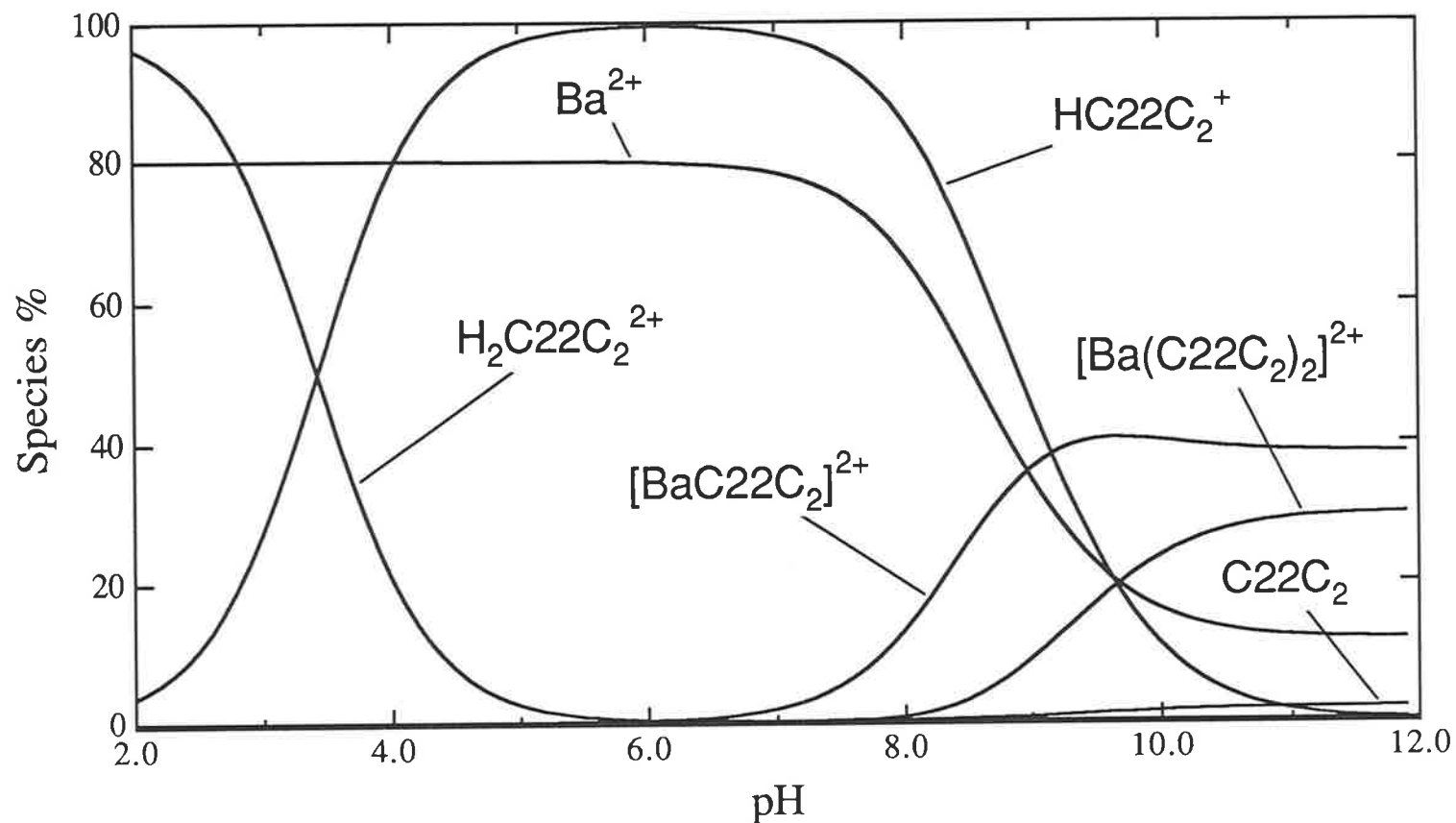


**Figure 3.3.** Speciation curves for Ba<sup>2+</sup> cryptates of C<sub>22</sub>C<sub>2</sub> at 298.2 K in 0.10 mol dm<sup>-3</sup> NEt<sub>4</sub>ClO<sub>4</sub> aqueous solution where percentages are expressed in terms of the total C<sub>22</sub>C<sub>2</sub> concentration being 100%. The total Ba<sup>2+</sup> and C<sub>22</sub>C<sub>2</sub> concentrations are 8.83 × 10<sup>-4</sup> mol dm<sup>-3</sup> and 1.104 × 10<sup>-3</sup> mol dm<sup>-3</sup>, respectively.

In contrast to C22C<sub>2</sub>, C22C<sub>5</sub> and C22C<sub>8</sub> show very little selectivity in their complexation of the alkaline earth metal ions. The stabilities of the alkali metal cryptates, [MC22C<sub>5</sub>]<sup>+</sup> and [MC22C<sub>8</sub>]<sup>+</sup>, are in the sequence Li<sup>+</sup> < Na<sup>+</sup> < K<sup>+</sup> > Rb<sup>+</sup> > Cs<sup>+</sup> (Chapter 2). However, there is no apparent trend in the stabilities of the alkaline earth cryptates, [MC22C<sub>5</sub>]<sup>2+</sup> and [MC22C<sub>8</sub>]<sup>2+</sup>, which are all within an order of magnitude of the stabilities of the diaza crown ethers [MC22]<sup>2+</sup>. Thus, for the hard acid alkali and alkaline earth metal ions, a similar trend is observed for the complexes of the C22C<sub>n</sub> series of ligands, where, as n is increased, the stability and selectivity of the cryptates of C22C<sub>n</sub> decrease and approach those of the parent macrocycle C22. As discussed in Section 2.6, this may be a consequence of the absence of ether oxygens in the aliphatic C<sub>5</sub> and C<sub>8</sub> arms of C22C<sub>5</sub> and C22C<sub>8</sub>, which decreases the tendency of the alkali metal ions to reside within the cavities of these bicyclic ligands.

### 3.2.2 Cryptates of the Heavy Metal Ions Cd<sup>2+</sup>, Hg<sup>2+</sup> and Pb<sup>2+</sup>

The variation in stability of  $K_s$  for [MC22C<sub>2</sub>]<sup>2+</sup> and [MC221]<sup>2+</sup> is in the sequence Cd<sup>2+</sup> < Hg<sup>2+</sup> > Pb<sup>2+</sup>. This is consistent with Hg<sup>2+</sup> (with an ionic radius similar to that of Na<sup>+</sup>) being of optimum size to complex with C22C<sub>2</sub> and C221 as assessed from the jaw-angle requirements of the former ligand and the estimated cavity size of the latter. In contrast, Cd<sup>2+</sup> and Pb<sup>2+</sup> are too small and too large, respectively, for the cavities of C22C<sub>2</sub> and C221, but for both ligands, the stability of the Pb<sup>2+</sup> complex is greater than that of the Cd<sup>2+</sup> complex, consistent with the lower hydration energy of the larger Pb<sup>2+</sup>. For the other ligands in Table 3.2, it appears that a combination of Hg<sup>2+</sup> being closer to optimum size than is Cd<sup>2+</sup>, and the lower hydration energy of Hg<sup>2+</sup> compared with Cd<sup>2+</sup>, are the major factors causing the Hg<sup>2+</sup> complexes to be more stable than the Cd<sup>2+</sup> analogues. On this basis, Pb<sup>2+</sup> should be closer to optimum size for complexation by C22C<sub>8</sub> and C222 than is Hg<sup>2+</sup>, but this is not reflected in the relative stabilities of their cryptates. This may be a consequence of the soft acid Hg<sup>2+</sup> binding with the nitrogens more strongly than do the borderline soft acids Cd<sup>2+</sup> and Pb<sup>2+</sup>. This is supported by the fact that the complexes of Cd<sup>2+</sup> and Pb<sup>2+</sup> are more dependent on the number of ether oxygens in the cryptand than is Hg<sup>2+</sup>. Thus, the stabilities of [MC22C<sub>5</sub>]<sup>2+</sup> and [MC22C<sub>8</sub>]<sup>2+</sup> are far lower than those of [MC221]<sup>2+</sup> and [MC222]<sup>2+</sup>, respectively, when M<sup>2+</sup> = Cd<sup>2+</sup> and Pb<sup>2+</sup> than is the case when M<sup>2+</sup> = Hg<sup>2+</sup>.

### 3.2.3 Cryptates of the First-Row Transition Metal Ions

As the cryptand cavities of C22C<sub>5</sub> and C22C<sub>8</sub> are both larger than the optimum size required to accommodate Co<sup>2+</sup>, Ni<sup>2+</sup>, Cu<sup>2+</sup> and Zn<sup>2+</sup>, it may be inferred from the similar stabilities of [MC22C<sub>5</sub>]<sup>2+</sup> and [MC22C<sub>8</sub>]<sup>2+</sup> that the major interaction is between M<sup>2+</sup> and the eighteen membered C22 ring of both cryptands and that this is dominated by the interaction with the cryptand nitrogens. This is as expected, since these metal ions are borderline soft acids and interact more strongly with nitrogen donor atoms than with the harder oxygen donor atoms. The greater stabilities of [MC22C<sub>5</sub>]<sup>2+</sup> and [MC22C<sub>8</sub>]<sup>2+</sup> compared with those of their [MC22]<sup>2+</sup> analogues indicate that the -(CH<sub>2</sub>)<sub>n</sub>- moiety has the effect of shielding M<sup>2+</sup> from interaction with water and possibly produces a more favourable conformation for complexation.

The presence of oxygens in all three arms of C221 and C222 appears in most cases to have a destabilising effect on their cryptates, when compared with those of C22C<sub>5</sub> and C22C<sub>8</sub>. This may be as a result of M<sup>2+</sup> being attracted further toward the centre of the cryptand cavity than is the case in [MC22C<sub>5</sub>]<sup>2+</sup> and [MC22C<sub>8</sub>]<sup>2+</sup> and as a consequence, interactions between M<sup>2+</sup> and the cryptand nitrogens are decreased. The metal ions Co<sup>2+</sup>, Ni<sup>2+</sup> and Cu<sup>2+</sup> will attempt to impose the coordination geometries which maximise the ligand field stabilisation energy in their complexes. This may result in steric strain in complexes of rigid ligands such as cryptands. This is exemplified by [CoC221][Co(SCN)<sub>4</sub>], where Co<sup>2+</sup> lies within the cryptand cavity, coordinated to all seven cryptand donor atoms in a distorted pentagonal bipyramid, with the ligand experiencing considerable strain.<sup>17</sup> Thus, the ability of the cryptand to adopt to the required geometry without strain will have a large influence on the stability of its cryptates. It may be that these geometries are more readily adopted in [MC22C<sub>5</sub>]<sup>2+</sup> and [MC22C<sub>8</sub>]<sup>2+</sup>, when compared with those of [MC221]<sup>2+</sup> and [MC222]<sup>2+</sup>. These geometric requirements may also result in only some of the ligand donor atoms coordinating to M<sup>2+</sup>, which would have a destabilising effect when compared with cryptates of d<sup>10</sup> Zn<sup>2+</sup>, which has no such geometric requirements for the coordination of the ligand. Thus, the combination of these two effects may explain why the stabilities of the Zn<sup>2+</sup> cryptates in Table 3.2 are generally greater than those of their Co<sup>2+</sup> and Ni<sup>2+</sup> analogues.

A comparison of the stabilities of [MC22C<sub>5</sub>]<sup>2+</sup> and [MC22C<sub>8</sub>]<sup>2+</sup> with those of their respective analogues [MC221]<sup>2+</sup> and [MC222]<sup>2+</sup>, where the

number of ether oxygens has been increased by one and two respectively, shows that the divalent metal ions in Table 3.2 can be placed in two distinct groups. When  $M^{2+} = Ca^{2+}, Sr^{2+}, Ba^{2+}, Cd^{2+}, Hg^{2+}$  and  $Pb^{2+}$ , the stabilities of  $[MC22C_5]^{2+}$  and  $[MC22C_8]^{2+}$  are considerably lower than those of  $[MC221]^{2+}$  and  $[MC222]^{2+}$ , respectively. This is consistent with the increased stabilities of the second pair of cryptates being a result of their extra oxygen donor atoms increasing the binding of the metal ion. In contrast, the stabilities of  $[MC22C_5]^{2+}$  and  $[MC22C_8]^{2+}$  for  $Co^{2+}, Ni^{2+}, Cu^{2+}, Zn^{2+}$  and  $Mg^{2+}$  are either greater than or similar to those of  $[MC221]^{2+}$  and  $[MC222]^{2+}$ .

The separation of the divalent  $M^{2+}$  into these two groups is also observed in a number of studies on the effect of oxygen donor atoms in divalent metal complexes.<sup>18-22</sup> It was found that in almost all cases, alteration of a ligand by the addition of groups containing oxygen donor atoms causes an increase in the selectivity of the modified ligand for large metal ions relative to small metal ions, irrespective of the nature of  $M^{2+}$  (Figures 3.4 and 3.5). One reason for this is that large metal ions, with higher coordination numbers, more readily accommodate the larger number of donor atoms that result from these modifications of the ligand.<sup>18-22</sup> This is certainly important with the complexes of C221 and C222, where the number of donor atoms (seven and eight, respectively) exceeds the common coordination numbers of small metal ions such as the first-row transition metal ions and  $Mg^{2+}$ . Another important factor is that in all the ligands involved in these studies, the oxygen donor atom is coordinated to  $M^{2+}$  as part of a five membered chelate ring.<sup>18-22</sup> Molecular mechanics calculations have shown that the minimum strain energy in five membered chelate rings occurs with metal-donor atom bond lengths of 2.5 - 2.8 Å, corresponding to a large metal ion with an ionic radius of  $\sim 1.0$  Å.<sup>23-25</sup> Thus, the ability of larger metal ions to coordinate more strongly with five membered chelate rings containing oxygen donor atoms derives from the fact that these larger metal ions coordinate with the production of less strain energy than smaller metal ions.<sup>20</sup> As the adjacent oxygen donor atoms of the cryptands C22C<sub>5</sub>, C22C<sub>8</sub>, C221 and C222 would be coordinated to  $M^{2+}$  as part of a five membered chelate ring, this effect may account for the decrease in stability for the complexes of  $Co^{2+}, Ni^{2+}, Cu^{2+}, Zn^{2+}$  and  $Mg^{2+}$  that is observed in going from C22C<sub>5</sub> to C221 and from C22C<sub>8</sub> to C222.



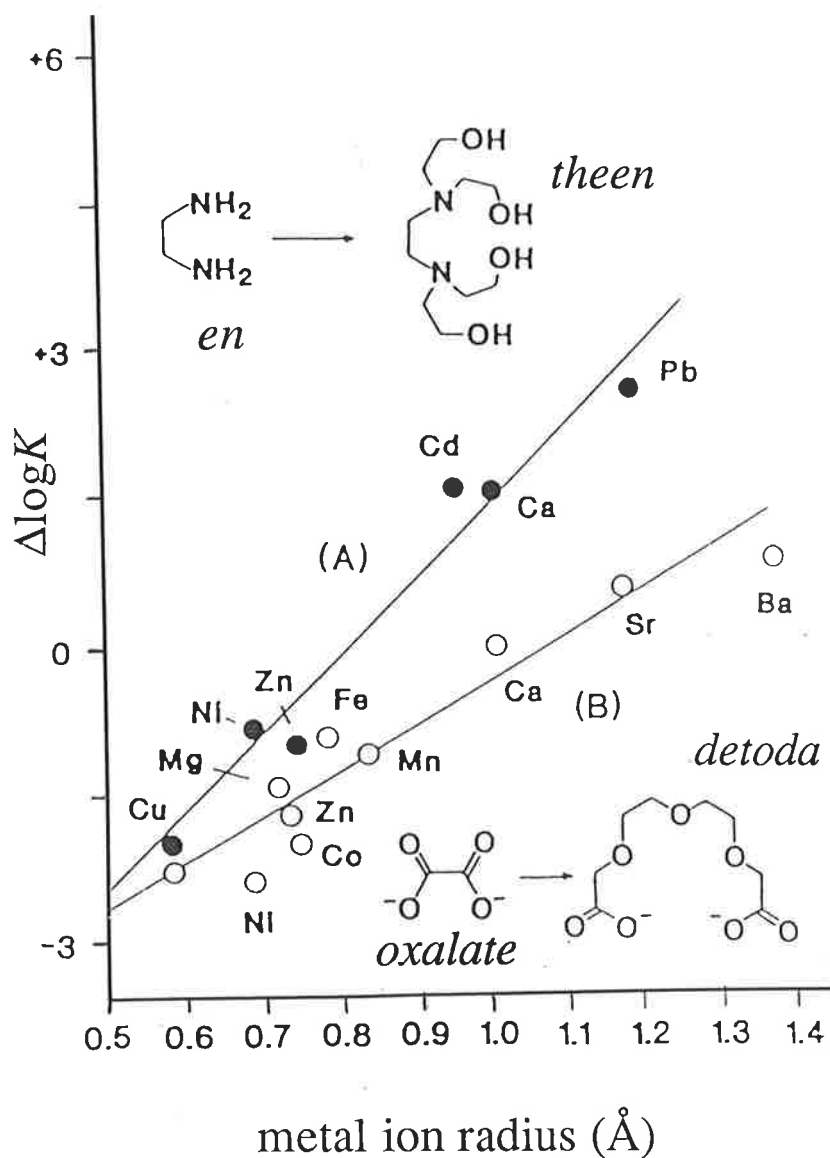


**Figure 3.4.** (Reproduced from reference 22). The effect of oxygen donor atoms on the complex stability of open chain ligands as a function of metal ion size. The change in stability,  $\Delta \log K$ , that occurs (A) on passing from divalent metal complexes of *en* to those of *then* (•) and (B) from divalent metal complexes of *oxalate* to those of *detoda* (o), is plotted as a function of metal ion radius. The value of  $\Delta \log K$  for each metal ion is simply  $\log K_s$  for the second complex minus  $\log K_s$  for the first complex.

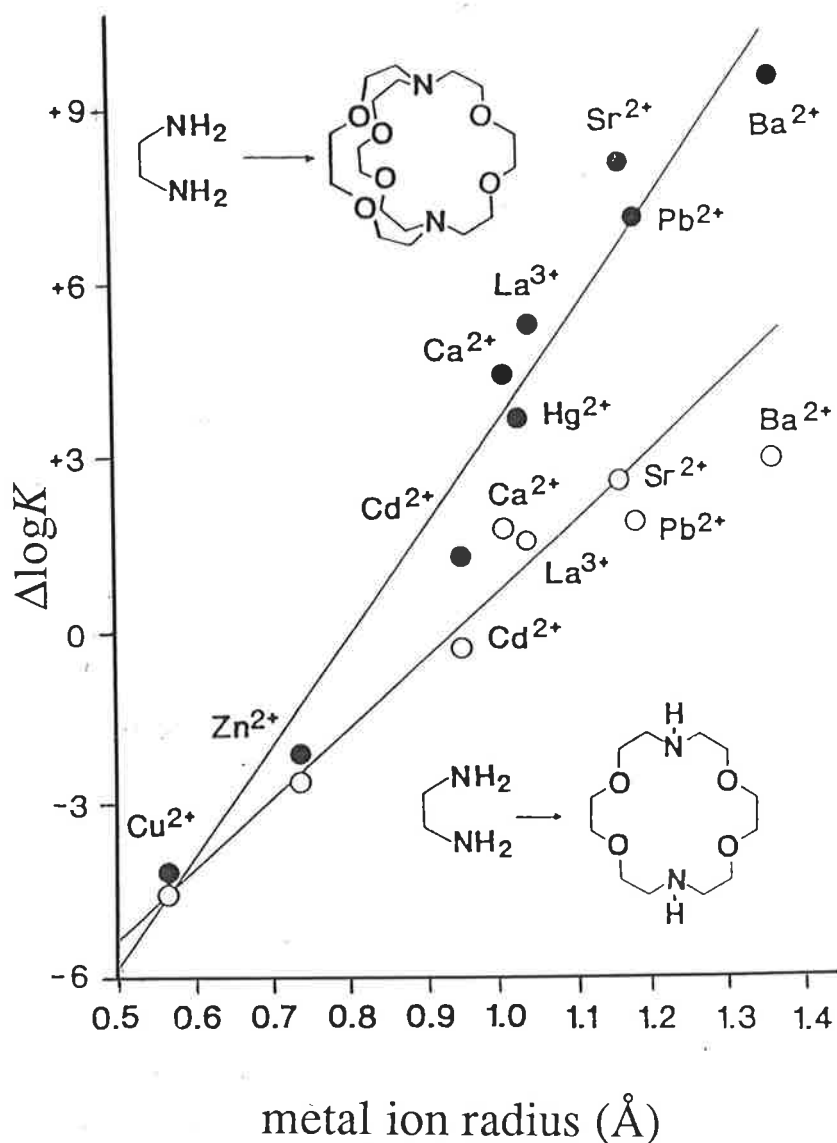


**Figure 3.5.** (Reproduced from reference 22). The effect of oxygen donor atoms on complex stability when incorporated into macrocyclic ligands. The change in stability,  $\Delta \log K$ , that occurs on passing from divalent metal complexes of *en* to those of C22 (o) and from divalent metal complexes of *en* to those of C222 (•), is plotted as a function of metal ion radius. The value of  $\Delta \log K$  for each metal ion is simply  $\log K_s$  for the second complex minus  $\log K_s$  for the first complex.

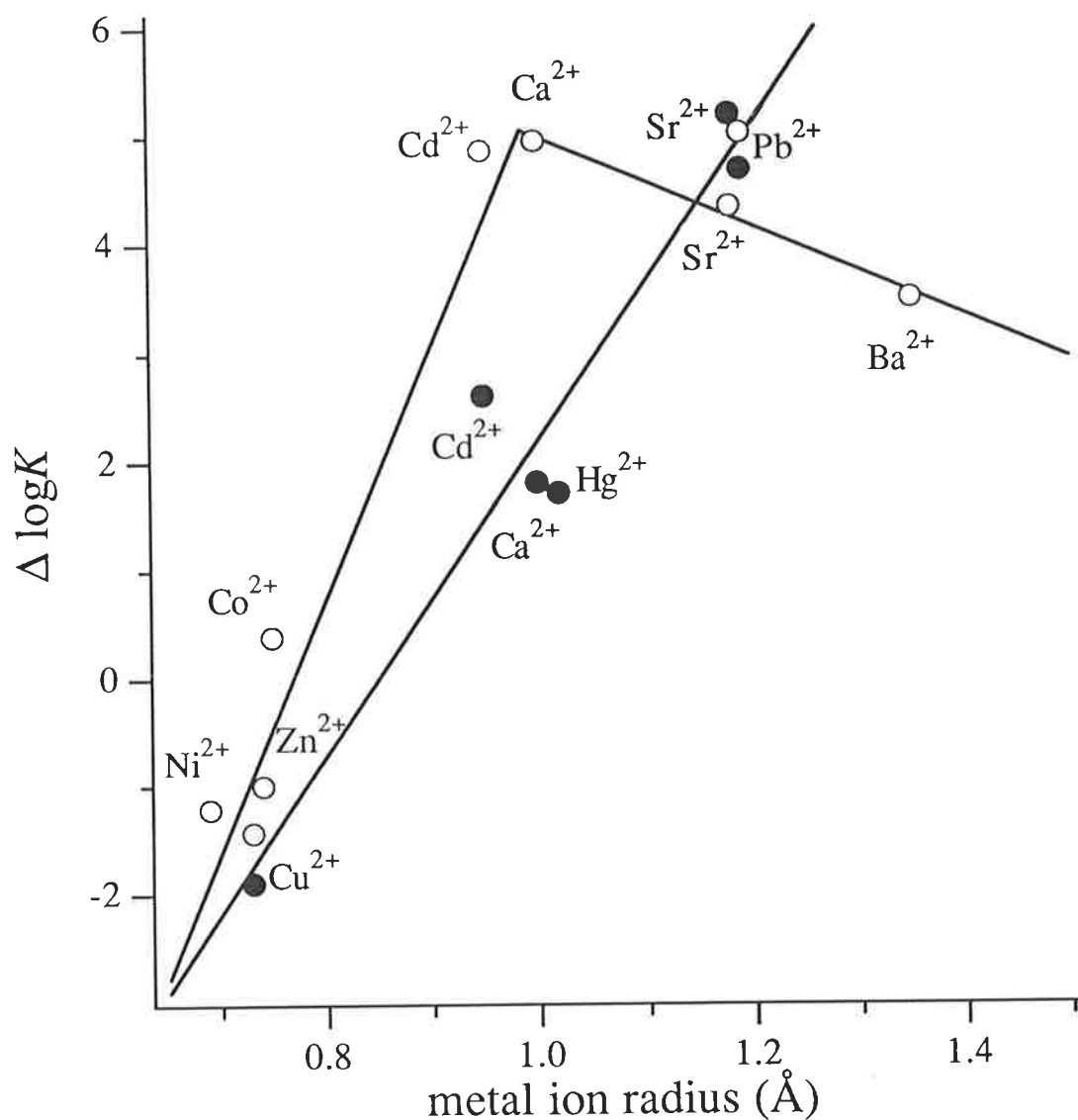


**Figure 3.6.** The effect of oxygen donor atoms on the stability of cryptate complexes as a function of metal ion size. The change in stability,  $\Delta\log K$ , that occurs on passing from divalent metal cryptates of C22C<sub>5</sub> to those of C221 (○) and from divalent metal cryptates of C22C<sub>8</sub> to those of C222 (●), is plotted as a function of metal ion radius. The value of  $\Delta\log K$  for each metal ion is simply  $\log K_s$  for the second complex minus  $\log K_s$  for the first complex.

Figure 3.6 shows that the pair of ligands C22C<sub>8</sub> and C222 show behaviour similar to that exhibited in Figures 3.4 and 3.5, with  $\Delta \log K$  increasing with increasing ionic radius, but the pair of ligands C22C<sub>5</sub> and C221 do not. In this case, there is a maximum in  $\Delta \log K$  at an ionic radius of about 1 Å, which is close to the estimated cavity size of C221 (1.1 Å). As a result of the rigid structure of these ligands, it is unlikely that optimum metal-donor atom bonding distances could be approached for all of the ligand donor atoms, except for metal ions of similar size to the cryptand cavity. It is apparent that the tendency for  $\Delta \log K$  to increase with increasing ionic radius will be modified for metal ions larger than the cavity size of the cryptand. Thus, the maximum in  $\Delta \log K$  at  $\sim 1.0$  Å observed in Figure 3.6 probably corresponds to the matching of the size of M<sup>2+</sup> to the size of the C221 cavity.

### 3.3 [M(HC22C<sub>n</sub>)]<sup>3+</sup>, [M(OH)C22C<sub>n</sub>]<sup>+</sup> and [M(OH)C22C<sub>n</sub>]<sub>2</sub><sup>2+</sup> Complexes

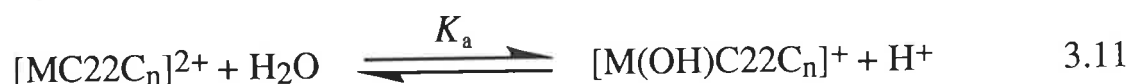
The equilibrium:



$$\text{where } K_{OH} = \frac{[M(OH)C22C_n^{+}]}{[M^{2+}][OH^{-}][C22C_n]} \quad 3.10$$

is characterised by  $\log(K_{OH}/\text{dm}^6 \text{ mol}^{-2}) = 11.9 \pm 0.1$  and  $21.4 \pm 0.1$  when  $M^{2+} = \text{Zn}^{2+}$  and  $\text{Hg}^{2+}$  for C22C<sub>2</sub> and  $22.20 \pm 0.05$  and  $13.9 \pm 0.1$  when  $M^{2+} = \text{Hg}^{2+}$  and  $\text{Pb}^{2+}$  for C22C<sub>8</sub>, respectively.

The complex [MC22C<sub>n</sub>]<sup>2+</sup> acts as an acid as expressed in Equation 3.11

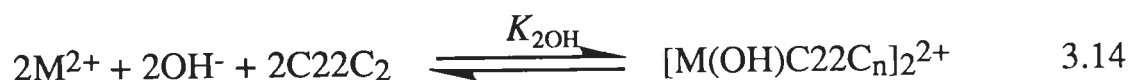


$$\text{where } K_a = \frac{[M(OH)C22C_n^{+}][H^{+}]}{[MC22C_n^{2+}]} \quad 3.12$$

$$\text{and } pK_a = -\log K_a \quad 3.13$$

The  $pK_a$  values for  $[MC22C_n]^{2+}$  appear in Table 3.3. The  $pK_a$  of a hydrated metal ion should decrease as the ionic radius decreases. However, there is no apparent trend in the  $pK_a$  values of  $[MC22C_n]^{2+}$  with ionic radius. This is consistent with the acidity of  $M^{2+}\text{-OH}_2$  depending on its environment, being different when coordinated by  $C22C_n$  than in the hydrated metal ion, as demonstrated by the large difference between the  $pK_a$  values of  $[HgC22C_2]^{2+}$  and  $[HgC22C_8]^{2+}$ .

The equilibrium:



$$\text{where } K_{2OH} = \frac{[[M(OH)C22C_2]_2^{2+}]}{[M^{2+}]^2[OH^-]^2[C22C_2]^2} \quad 3.15$$

is characterised by  $\log(K_{2OH}/\text{dm}^{15} \text{ mol}^{-5}) = 33.5 \pm 0.2$  and  $26.6 \pm 0.1$  when  $M^{2+} = \text{Cu}^{2+}$  and  $\text{Zn}^{2+}$ . The  $[M(OH)C22C_n]_2^{2+}$  species probably consists of two  $[MC22C_n]^{2+}$  complexes linked by two bridging hydroxide ions. Similar species have been observed in the related  $C21C_5$  system.<sup>26</sup> These species may well be present for some of the other metal ions studied but their detection would have been prevented by precipitation of the metal hydroxide at high pH. A speciation plot showing the various complex species formed between  $\text{Cu}^{2+}$  and  $C22C_2$  appears in Figure 3.7.

No complexation of  $M^{2+}$  by the monoprotonated ligand was observed for  $C22C_2$  and  $C22C_8$ . This is not surprising in the case of  $C22C_2$ , where the close proximity of the two nitrogens makes it unlikely that the species  $[M(\text{HC}22\text{C}_2)]^{3+}$  would form. The criterion for the detection of such species was that they be present in  $\geq 10\%$  of the total metal ion concentration. Thus the failure to detect this species with  $C22C_8$  simply means that they were insufficiently stable to form in significant concentrations before formation of  $[MC22C_8]^{2+}$  occurred.

**Table 3.3.**  $pK_a$  values<sup>a</sup> of  $[MC22C_n]^{2+}$  at 298.2 K.

$M^{2+}$	ionic radius <sup>b</sup> (Å)	$pK_a$ ( $K_a/\text{mol dm}^{-3}$ )	
		C22C <sub>2</sub>	C22C <sub>8</sub>
Zn <sup>2+</sup>	0.74	$9.0 \pm 0.1$	
Hg <sup>2+</sup>	1.02 (1.14)	$5.8 \pm 0.1$	$8.1 \pm 0.05$
Pb <sup>2+</sup>	1.19 (1.29)		$7.9 \pm 0.1$

<sup>a</sup> In  $0.10 \text{ mol dm}^{-3}$   $\text{NEt}_4\text{ClO}_4$  supporting electrolyte.

<sup>b</sup> Reference 6. Six coordinate ionic radii are quoted for all metal ions. The numbers in parentheses are the eight coordinate ionic radii for these metal ions.

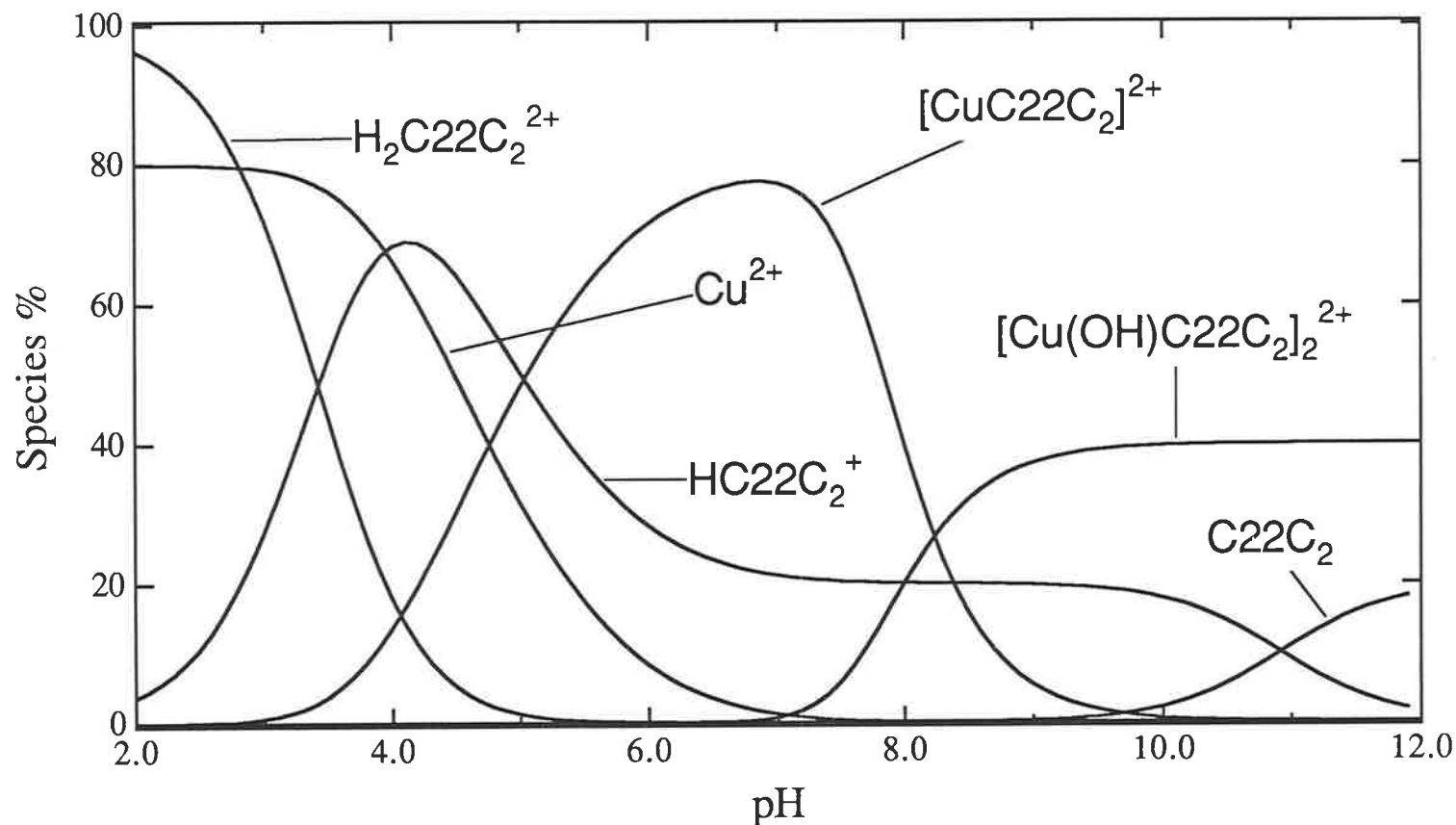


**Figure 3.7.** Speciation curves for  $\text{Cu}^{2+}$  cryptates of  $\text{C}_{22}\text{C}_2$  at 298.2 K in  $0.10 \text{ mol dm}^{-3}$   $\text{NEt}_4\text{ClO}_4$  aqueous solution where percentages are expressed in terms of the total  $\text{C}_{22}\text{C}_2$  concentration being 100%. The total  $\text{Cu}^{2+}$  and  $\text{C}_{22}\text{C}_2$  concentrations are  $8.02 \times 10^{-4} \text{ mol dm}^{-3}$  and  $1.003 \times 10^{-3} \text{ mol dm}^{-3}$ , respectively.

- 1 Dhillon, R.S.; Lincoln, S.F.; Stephens, A.K.W. *Inorg. Chim. Acta.* **1994**, 215, 79-84.
- 2 Arnaud-Neu, F.; Spiess, B.; Schwing-Weill, M.J. *Helv. Chim. Acta.* **1977**, 60, 2633.
- 3 Clarke, P.; Gulbis, J.M.; Lincoln, S.F.; Tiekink, E.R.T. *Inorg. Chem.* **1992**, 31, 3398.
- 4 Shriver, D.F.; Atkins, P.W.; Langford, C.H. "Inorganic Chemistry". Oxford University Press, **1990**.
- 5 Cotton, F.A.; Wilkinson, G. "Advanced Inorganic Chemistry", 4th ed, Interscience, New York, **1980**.
- 6 Shannon, R.D. *Acta. Crystallogr., Sect. A: Cryst. Phys. Diffr., Theor. Gen. Crystallog.* **1976**, A32, 751.
- 7 Lehn, J-M.; Sauvage, J-P. *J. Am. Chem. Soc.* **1975**, 97, 6700.
- 8 Burgess, J. "Metal Ions in Solution", Ellis Horwood, Chichester, **1978**.
- 9 Pearson, R.G. *J. Am. Chem. Soc.* **1963**, 85, 3533.
- 10 Pearson, R.G. *Coord. Chem. Rev.* **1990**, 100, 403.
- 11 Anderegg, G. *Helv. Chim. Acta.* **1975**, 58, 1218.
- 12 Luboch, E.; Cygan, A.; Biernat, J.F. *Inorg. Chim. Acta.* **1983**, 68, 201.
- 13 Arnaud-Neu, F.; Spiess, B.; Schwing-Weill, M.J. *J. Am. Chem. Soc.* **1982**, 104, 5641.
- 14 Irving, H.; Williams, R.J.P. *Nature (London)*. **1948**, 162, 746.
- 15 Irving, H.; Williams, R.J.P. *J. Chem. Soc.* **1953**, 3192.
- 16 Buschmann, H-J. *J. Sol. Chem.* **1986**, 15, 453.
- 17 Mathieu, F.; Weiss, W. *J. Chem. Soc., Chem. Commun.* **1973**, 816.
- 18 Hancock, R.D. *Pure Appl. Chem.* **1986**, 58, 1445-1452.
- 19 Hancock, R.D.; Martell, A.E. *Chem. Rev.* **1989**, 89, 1875-1914.
- 20 Hancock, R.D.; Bhavan, R.; Wade, P.W.; Boeyens, J.C.A.; Dobson, S.M. *Inorg. Chem.* **1989**, 28, 187-194.
- 21 Hancock, R.D. *Pure Appl. Chem.* **1993**, 65, 941-946.
- 22 Hancock, R.D. *Perspect. Coord. Chem.* **1993**, 129-151.
- 23 Hancock, R.D. *Prog. Inorg. Chem.* **1989**, 37, 187.
- 24 Hancock, R.D. *Acc. Chem. Res.* **1990**, 23, 253-257.
- 25 Hancock, R.D.; Wade, P.W.; Ngwenya, M.P.; de Sousa, A.S.; Damu, K.V. *Inorg. Chem.* **1990**, 29, 1968-1974.
- 26 Duckworth, P.A.; Lincoln, S.F.; Lucas, J. *Inorg. Chim. Acta.* **1991**, 188, 55.

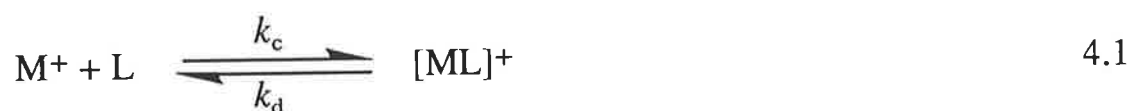


# Chapter 4: Cryptate Complexation Dynamics

## 4.1 Introduction

The high thermodynamic stability exhibited by the alkali metal cryptates has resulted in considerable research into the kinetics of complexation and decomplexation of these complexes, in order to give a more complete understanding of the cryptates and to allow mechanistic deductions about the complexation and decomplexation processes. These studies are also important in relating the behaviour of the alkali metal cryptates to that of antibiotics and other carrier molecules, which regulate the transport of alkali metal ions across membranes in biological systems.

The kinetic and thermodynamic aspects of complexation are interrelated, as may be seen from the complexation reaction shown in Equation 4.1, where the stability constant,  $K_s$ , can be expressed in terms of the complexation rate constant,  $k_c$ , and the decomplexation rate constant,  $k_d$ :



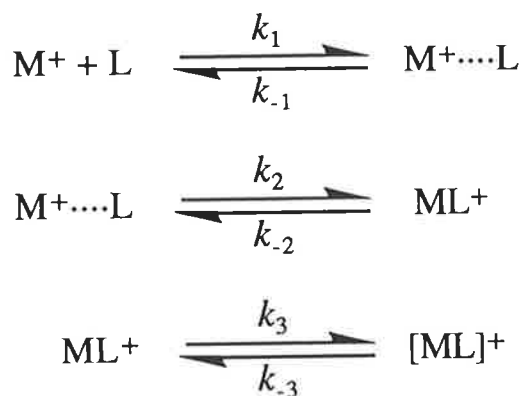
$$K_s = \frac{k_c}{k_d} \quad 4.2$$

Cryptate lability is influenced by a number of different factors, including the relative sizes of the metal ion and the cryptand cavity, the flexibility of the cryptand, the number and type of cryptand donor atoms and the solvation energy of the metal ion.<sup>1-22</sup> In Chapter 2, these factors were considered in discussing the variations in thermodynamic stability of the alkali metal cryptates of clam-like C22C<sub>2</sub> and also C22C<sub>8</sub>. In this chapter, the influence of these factors on the lability of their cryptates will be investigated. Thus, the exchange of Na<sup>+</sup> on [NaC22C<sub>2</sub>]<sup>+</sup> and [NaC22C<sub>8</sub>]<sup>+</sup> and the exchange of Li<sup>+</sup> on [LiC22C<sub>8</sub>]<sup>+</sup> have been studied in several solvents by <sup>23</sup>Na and <sup>7</sup>Li NMR spectroscopy and are compared with similar data for other cryptates.

## 4.2 Mechanistic Aspects of Cryptates

In solution, cryptate formation involves a combination of solvational changes in the metal ion and ligand and conformational changes in the ligand. The complexation process may be represented by a simplified reaction scheme, the Eigen-Winkler mechanism (Scheme 4.1), derived from studies of the complexation of alkali metal ions by biofunctional ionophores.<sup>23-25</sup>

Scheme 4.1



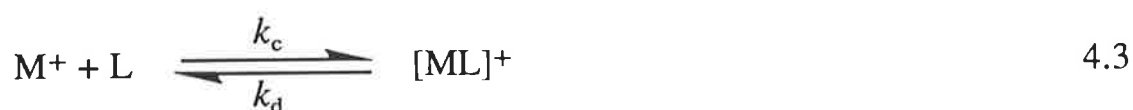
This mechanism is somewhat simplified; replacement of a solvent molecule by a ligand donor atom in the first coordination sphere of the metal ion may only occur in a single step, so that the overall complexation probably involves several steps.<sup>23-25</sup> However, the steps may be combined into three main sequences, as indicated in Scheme 4.1. The first sequence consists of the diffusion controlled formation of an outer sphere complex ( $\text{M}^+ \cdots \text{L}$ ) between the fully solvated metal ion and the solvated ligand, characterised by the rate constant  $k_1$ . The second sequence involves formation of the first metal-ligand bonds, partial rearrangement of the ligand and partial cation desolvation, characterised by  $k_2$ . The final sequence corresponds to the formation of the remaining metal-ligand bonds and the final solvational changes of the metal ion, characterised by  $k_3$ .

A number of ultrasonic absorption measurements on alkali metal complexes of cryptands and crown ethers have been interpreted in terms of the Eigen-Winkler mechanism.<sup>26-32</sup> These studies have shown that the rate determining step in Scheme 4.1 may involve either cation desolvation or ligand rearrangement, depending on the relative energies of these processes. An

ultrasonic absorption study of the complexation of alkali metal ions by C222 has identified two ligand conformational changes during the complexation process. These were attributed to the conversion of the *exo-exo* conformation to the *exo-endo* conformation and the conversion of the *exo-endo* conformation to the *endo-endo* conformation, with the latter process coincident with the inclusion of  $M^+$  within the cavity of C222.<sup>33</sup> In this study, only two rate constants are determined;  $k_c$  and  $k_d$ , which cannot be identified with any particular step in Scheme 4.1, but characterise the rate-determining steps for the complexation and decomplexation processes.

The exchange of an alkali metal ion,  $M^+$ , between the complexed and solvated states may proceed by two possible mechanisms in which the role of the solvent is not specifically considered.<sup>11,34-35</sup>

Mechanism I The unimolecular mechanism, a first-order process where the rate determining step for decomplexation does not involve solvated  $M^+$  or L. Mechanism I is described by Equation 4.3;



where;

$k_c$  is the complexation rate constant

$k_d$  is the decomplexation rate constant

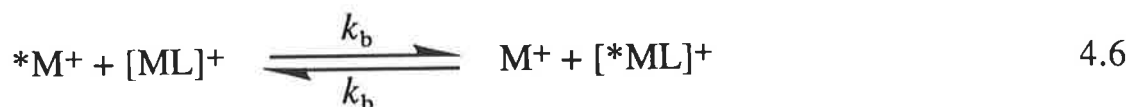
$K_s = \frac{k_c}{k_d}$  is the stability constant

For the unimolecular mechanism, the rate of exchange is independent of the concentration of solvated  $M^+$ ;

$$\text{rate} = k_d[ML]^+ \quad 4.4$$

$$\tau_c = \frac{1}{k_d} \quad 4.5$$

Mechanism II The second order bimolecular mechanism, where decomplexation involves displacement of the complexed metal ion by a second metal ion. Mechanism II is described by Equation 4.6;



where  $k_b$  is the bimolecular exchange rate constant.

In this case, the exchange rate depends on the solvated  $M^+$  concentration as follows;

$$\text{rate} = k_b[ML^+] [M^+] \quad 4.7$$

and the following relationship holds;

$$\tau_c = \frac{1}{k_b[ML^+]} \quad 4.8$$

For both mechanisms, the following relationship holds between the mean site lifetimes of  $M^+$  in the complexed and solvated states;

$$\frac{\tau_c}{\chi_c} = \frac{\tau_s}{\chi_s} \quad 4.9$$

where  $\tau_c$  and  $\tau_s$  are the mean lifetimes of  $[ML]^+$  and  $M^+$ , respectively, and  $\chi_c$  and  $\chi_s$  are the corresponding mole fractions.

In some cases, both mechanisms I and II may operate simultaneously, in which case the observed rate of exchange is given by;

$$\text{rate} = k_{\text{obs}}[ML^+] \quad 4.10$$

$$= (k_d + k_b[M^+]) [ML^+] \quad 4.11$$

and the corresponding observed lifetime,  $\tau_c$ , is given by;

$$\tau_c = \frac{1}{k_{\text{obs}}} = \frac{1}{(k_d + k_b[M^+])} \quad 4.12$$

The mechanism observed depends on a number of factors, including temperature, concentration and the nature of the solvent and the anion.<sup>11,16,26-34</sup>

For most cryptate systems studied, the unimolecular exchange mechanism is observed.<sup>3-4,9,13,15,17,20-22</sup> For this mechanism, the standard state activation parameters characterising the exchange process may be derived from the temperature dependence of  $\tau_c$  according to Equations 4.13 and 4.14. The method of calculating these parameters is described in Chapter 12.

$$k_d = \frac{1}{\tau_c} = \frac{k_B T}{h} \exp\left(\frac{-\Delta G_d^\ddagger}{RT}\right) \quad 4.13$$

$$= \frac{k_B T}{h} \exp\left(\frac{-\Delta H_d^\ddagger}{RT} + \frac{\Delta S_d^\ddagger}{R}\right) \quad 4.14$$

where;

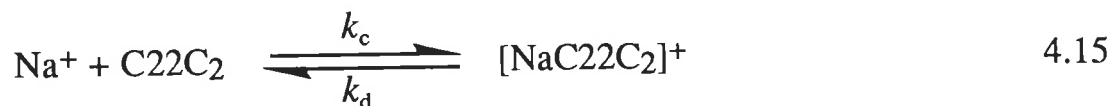
$k_B$  is Boltzmann's constant

$h$  is Planck's constant

$\Delta G_d^\ddagger$ ,  $\Delta H_d^\ddagger$  and  $\Delta S_d^\ddagger$  are the free energy, enthalpy and entropy of activation, respectively, for the decomplexation process.

### 4.3 Exchange Kinetics of Na<sup>+</sup> on [NaC<sub>22</sub>C<sub>2</sub>]<sup>+</sup>

The temperature dependent coalescence of the <sup>23</sup>Na resonances arising from solvated Na<sup>+</sup> and [NaC<sub>22</sub>C<sub>2</sub>]<sup>+</sup> in dimethylformamide, dimethylsulfoxide and water yields the kinetic parameters (Table 4.1) for the decomplexation of [NaC<sub>22</sub>C<sub>2</sub>]<sup>+</sup> for the equilibrium shown in Equation 4.15



The temperature dependent exchange of Na<sup>+</sup> between the solvated and complexed environments in dimethylformamide appears in Figure 4.1. The kinetic parameters were obtained from the temperature dependence of  $\tau_c$ , the mean lifetime of [NaC<sub>22</sub>C<sub>2</sub>]<sup>+</sup>, through Equation 4.14. The decomplexation rate constant,  $k_d$ , is quoted at two temperatures; (i) the coalescence temperature, where the exchange induced modification of the spectra is at a maximum and hence the most reliable values of  $k_d$  are obtained and (ii) at 298.2 K, for the purpose of comparison with other systems. The  $\tau_c$  values were determined by complete lineshape analysis (Chapter 12) of the coalescing <sup>23</sup>Na resonances observed for each of the solutions (i) - (x), whose compositions appear in Table 4.1. The magnitudes and temperature variations of  $\tau_c$  for each of the solutions studied for a given solvent are indistinguishable (Figure 4.2). Thus,  $\tau_c$  is independent of the concentration of solvated Na<sup>+</sup>, consistent with the operation of a monomolecular mechanism for the decomplexation of Na<sup>+</sup> from [NaC<sub>22</sub>C<sub>2</sub>]<sup>+</sup> (Equation 4.3). The free Na<sup>+</sup> concentration was varied by a factor of two or more (Table 4.1), so that any significant contribution from a bimolecular decomplexation process would have been apparent (Equation 4.12).

Cryptate decomplexation appears to operate predominantly via a monomolecular mechanism but this is not invariably the case. For example, the decomplexation of Li<sup>+</sup> from [LiC<sub>22</sub>1]<sup>+</sup> is characterised by a monomolecular mechanism in methanol, which has a dielectric constant ( $\epsilon$ ) of 32.7, whereas the bimolecular mechanism is favoured in acetonitrile and propylene carbonate ( $\epsilon = 38.0$  and 69.0 respectively), consistent with solvents having a higher dielectric constant stabilising a transition state in which both the entering and leaving Li<sup>+</sup> are bound.<sup>14</sup>

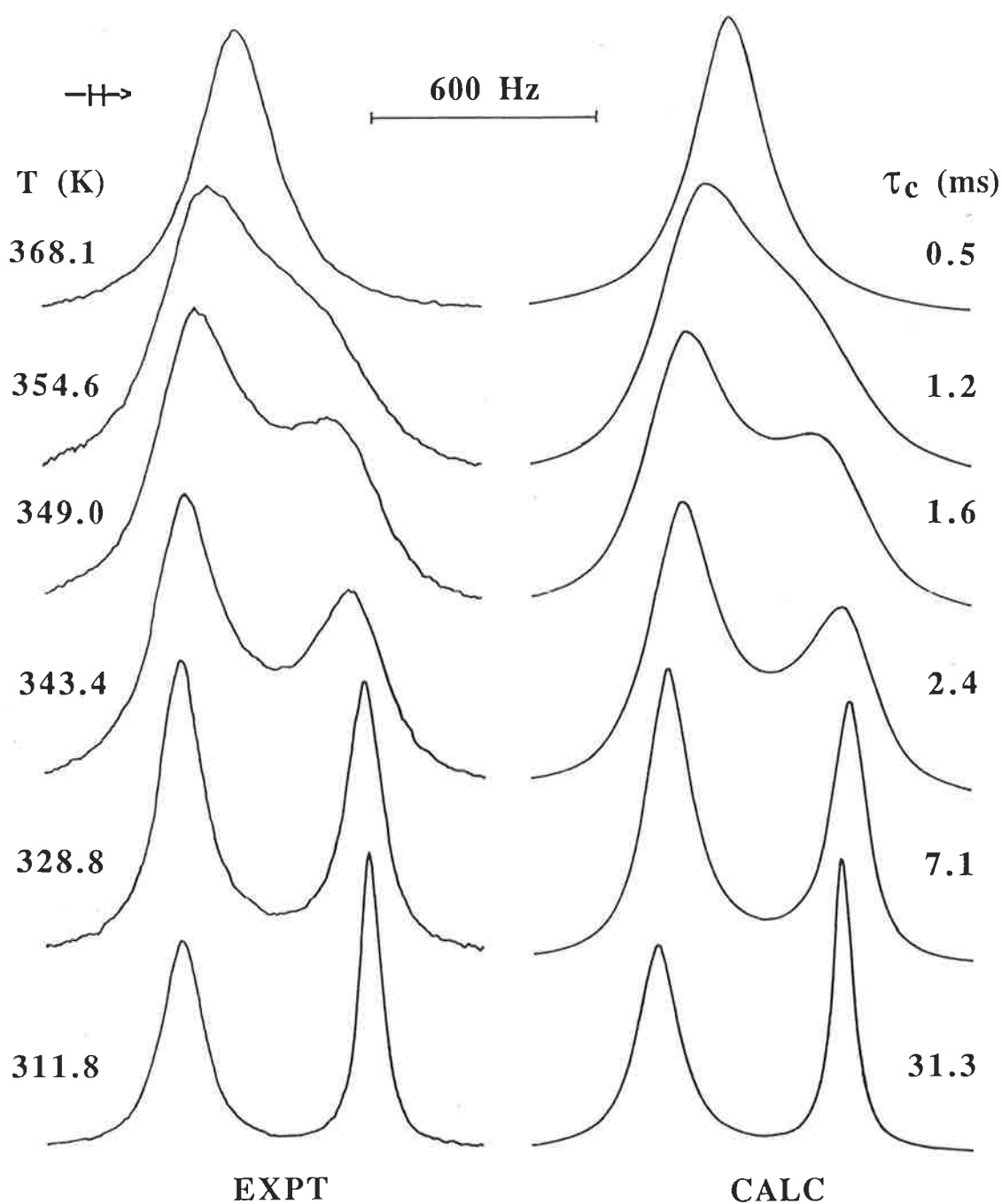


**Figure 4.1.** Typical exchange-modified 79.39 MHz  $^{23}\text{Na}$  NMR spectra of a dimethylformamide solution of solvated  $\text{Na}^+$  ( $0.041 \text{ mol dm}^{-3}$ ) and  $[\text{NaC}_{22}\text{C}_2]^+$  ( $0.059 \text{ mol dm}^{-3}$ ). Experimental temperatures and spectra appear to the left of the figure and the best fit calculated line shapes and corresponding  $\tau_c$  values appear to the right. The resonance of  $[\text{NaC}_{22}\text{C}_2]^+$  appears downfield from that of solvated  $\text{Na}^+$ .

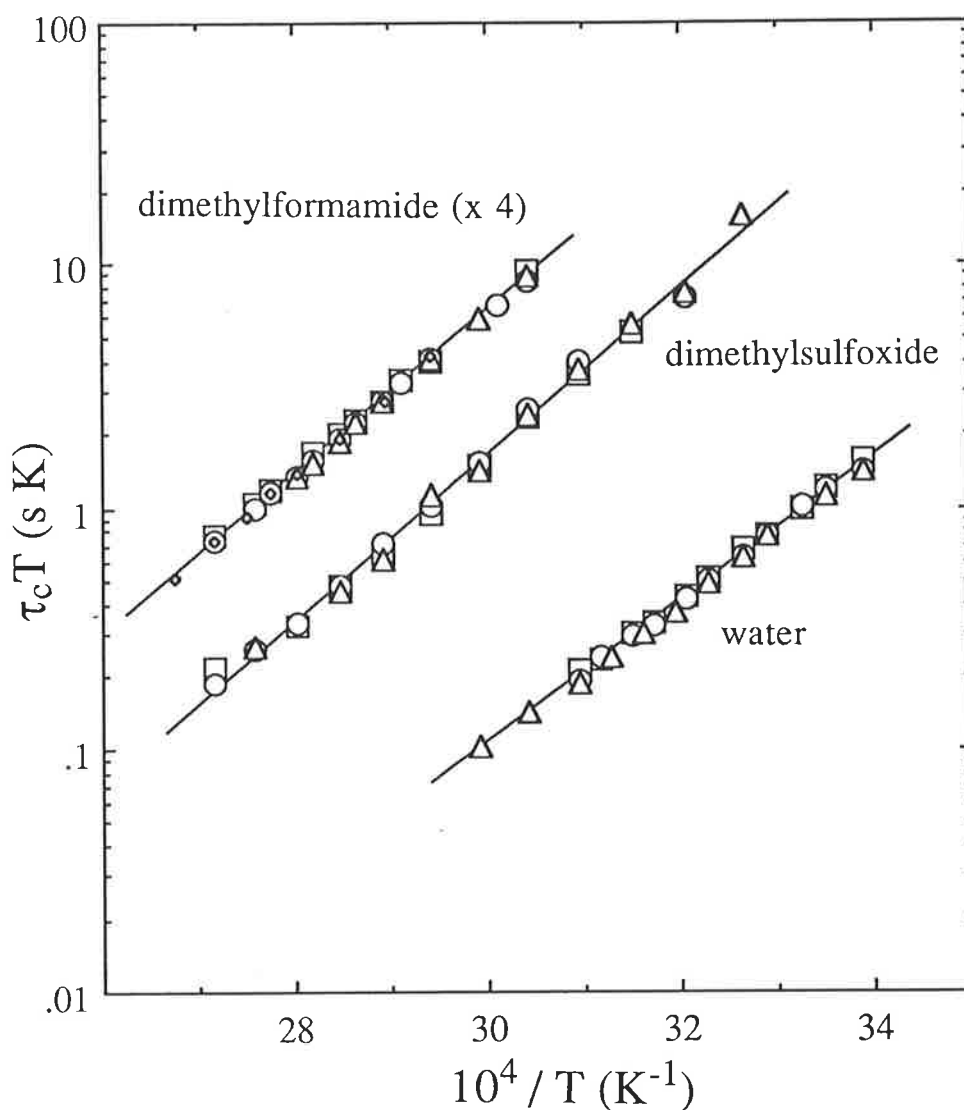


**Figure 4.2.** Temperature variation of  $\tau_c$  for  $[NaC_{22}C_2]^+$  in water, dimethylformamide and dimethylsulfoxide. Data points for aqueous solutions i-iii are represented by triangles, squares and circles, respectively. Data points for dimethylformamide solutions iv-vii are represented by triangles, squares, diamonds and circles, respectively. Data points for dimethylsulfoxide solutions viii-x are represented by triangles, squares and circles, respectively. The solid lines represent the best fits of the combined data for each group to Equation 4.14.



**Table 4.1.** Sodium Ion Exchange on  $[\text{NaC22C}_2]^+$  in Water, Dimethylformamide and Dimethylsulfoxide. Solution Composition and Kinetic Parameters.<sup>a</sup>

soln.	solvent	$[\text{Na}^+_{\text{solvated}}]$ mol dm <sup>-3</sup>	$[\text{NaC22C}_2^+]$ mol dm <sup>-3</sup>	$k_d(\text{T})$ s <sup>-1</sup>	$k_d(298.2 \text{ K})$ s <sup>-1</sup>	$\Delta H_d^\ddagger$ kJ mol <sup>-1</sup>	$\Delta S_d^\ddagger$ J mol <sup>-1</sup> K <sup>-1</sup>
				$k_d(309.6 \text{ K})$			
i	water	0.0360	0.0177	621 ± 7	254 ± 5	57.1 ± 1.1	-7.5 ± 3.3
ii		0.0307	0.0231	632 ± 7	264 ± 5	55.7 ± 0.8	-11.7 ± 2.5
iii		0.0204	0.0333	606 ± 5	249 ± 4	56.8 ± 0.8	-8.5 ± 2.5
(i - iii) <sup>b</sup>				619 ± 4	255 ± 3	56.6 ± 0.5	-9.4 ± 1.7
				$k_d(351.2 \text{ K})$			
(iv)	dimethyl- formamide	0.076	0.024	721 ± 7	12.3 ± 0.7	64.1 ± 0.9	-20.6 ± 1.3
(v)		0.059	0.041	727 ± 4	12.8 ± 0.3	63.6 ± 0.4	-9.0 ± 2.5
(vi)		0.041	0.059	701 ± 7	12.9 ± 0.7	62.9 ± 0.9	-10.5 ± 1.3
(vii)		0.035	0.065	743 ± 3	11.0 ± 0.3	66.4 ± 0.5	-12.7 ± 2.9
(iv - vii) <sup>b</sup>				717 ± 4	12.3 ± 0.4	64.0 ± 0.5	-9.5 ± 1.5
				$k_d(334.4 \text{ K})$			
viii	dimethyl- sulfoxide	0.0675	0.0333	227 ± 4	10.7 ± 0.6	67.4 ± 1.2	0.7 ± 3.4
ix		0.0504	0.0504	221 ± 5	11.7 ± 0.7	64.6 ± 1.3	-7.9 ± 3.5
x		0.0343	0.0665	219 ± 7	10.6 ± 0.9	66.7 ± 2.0	-1.6 ± 5.8
(viii - x) <sup>b</sup>				222 ± 3	11.1 ± 0.5	65.8 ± 0.9	-4.1 ± 2.6

<sup>a</sup> Errors represent one standard deviation from the least-squares fit of the experimental  $\tau_c$  data to Equation 4.14. <sup>b</sup> Simultaneous fit of all data for this solvent.

The  $^{23}\text{Na}$  NMR spectra of solutions containing  $\text{Na}^+ / [\text{NaC22C}_2]^+$  in acetonitrile, methanol and pyridine show two well resolved resonances, which exhibit no apparent broadening at temperatures approaching the boiling point of these solvents (355 K, 338 K and 388 K, respectively). Thus, the rate of exchange of  $\text{Na}^+$  between the solvated and complexed environments is in the very slow exchange region of the NMR timescale in these solvents. However, conservative lower limits for  $\tau_c$  of 28.7, 11.4 and 10.8 ms, respectively, could be estimated using the slow-exchange approximation (Equation 12.23, Chapter 12), by calculating the  $\tau_c$  value that would cause the width of the  $[\text{NaC22C}_2]^+$  resonance to be broadened by a factor of 1.5. These results are summarised in Table 4.2.

**Table 4.2.** Kinetic Parameters for  $\text{Na}^+$  Exchange on  $[\text{NaC22C}_2]^+$  in a Range of Solvents at 298.2 K.

Solvent	$D_{\text{N}}^a$	$10^{-5} k_c^b$ $\text{dm}^3 \text{mol}^{-1} \text{s}^{-1}$	$k_d$ $\text{s}^{-1}$	$\log K_s$ $(K_s/\text{dm}^3 \text{mol}^{-1})$
acetonitrile	14.1		$<35^c$	9.4
methanol	19.0 (23.5) <sup>d</sup>		$<88^c$	6.6
dimethyl- formamide	26.6	155	12.3	6.1
dimethyl- sulfoxide	29.8	44.2	11.1	5.6
water	18.0 (33.0) <sup>d</sup>	4.04	255	3.2
pyridine	33.1		$<93^c$	8.4

<sup>a</sup> Gutmann donor numbers from reference 45. <sup>b</sup>  $k_c = k_d K_s$ . <sup>c</sup> Calculated from Equation 12.23. The widths at half height of the  $^{23}\text{Na}$  resonances of  $[\text{NaC22C}_2]^+$  ( $W_{1/2a}$ ) in acetonitrile, methanol and pyridine are 22.2 Hz, 55.9 Hz and 59.2 Hz, respectively. <sup>d</sup> In references 46 and 47, it has been suggested that  $D_{\text{N}} = 33.0$  and  $23.5$  are more appropriate than  $D_{\text{N}} = 18.0$  and  $19.0$ , respectively, obtained for water and methanol in 1,2-dichloroethane solution, where the hydrogen-bonding structure of these solvents is disrupted.

## 4.4 Exchange Kinetics of Related Cryptate Systems

The  $[\text{NaC22C}_2]^+$  kinetic data may now be compared with those characterising  $[\text{LiC22C}_2]^+$  and other cryptates, for which monomolecular decomplexation mechanisms also operate in the solvents listed in Table 4.3. The variations in stability among these cryptates have been discussed in Chapter 2. It is now appropriate to determine the relationship between stability and lability for these cryptates. In dimethylformamide, it is apparent that the lower stability of  $[\text{LiC22C}_2]^+$  compared with that of  $[\text{NaC22C}_2]^+$  is a result of both the larger  $k_d$  and smaller  $k_c$  characterising  $[\text{LiC22C}_2]^+$ . The larger  $k_d$  of  $[\text{LiC22C}_2]^+$  is due to the much smaller  $\Delta H_d^\ddagger$ . As described in Chapter 2, the lower stability of  $[\text{LiC22C}_2]^+$  is a consequence of the greater strain in  $[\text{LiC22C}_2]^+$  compared with that in  $[\text{NaC22C}_2]^+$ , which results from the significantly smaller jaw-angle in  $[\text{LiC22C}_2]^+$  compared with that of  $\text{C22C}_2$ . The decomplexation of  $[\text{LiC22C}_2]^+$  may be envisaged to occur through the opening of the cryptand jaws, as the bound cryptand approaches the conformation of the free cryptand in the transition state. Thus, the smaller  $\Delta H_d^\ddagger$  of  $[\text{LiC22C}_2]^+$  probably results from the release of strain associated with this process, together with the partial resolution of  $\text{Li}^+$  in the transition state. From Figure 2.3, it may be seen that  $\text{Li}^+$  lies deep within the cavity of  $\text{C22C}_2$  and is unlikely to interact with solvent. (In the solid state,  $\text{Na}^+$  is coordinated to the  $\text{NCS}^-$  anion in  $[\text{NaC22C}_2]\text{NCS}$  whereas  $\text{Li}^+$  in  $[\text{LiC22C}_2]^+$  is not.<sup>48-49</sup> If these coordination numbers are retained in solution,  $\text{Na}^+$  in  $[\text{NaC22C}_2]^+$  will coordinate a solvent molecule while  $\text{Li}^+$  in  $[\text{LiC22C}_2]^+$  will not). Thus, the large negative  $\Delta S_d^\ddagger$  characterising  $[\text{LiC22C}_2]^+$  may result from the partial resolution of  $\text{Li}^+$  as the transition state forms.

In contrast, the lower strain in  $[\text{NaC22C}_2]^+$  (which results from a similar jaw-angle in the bound and free cryptand) results in a larger  $\Delta H_d^\ddagger$ . The wider jaw-angle in  $[\text{NaC22C}_2]^+$  (Figure 2.3) means that  $\text{Na}^+$  is likely to interact with solvent in the  $[\text{NaC22C}_2]^+$  ground state. Thus, the effect of resolution on  $\Delta H_d^\ddagger$  is likely to be less significant for  $[\text{NaC22C}_2]^+$  than for  $[\text{LiC22C}_2]^+$ . The smaller negative  $\Delta S_d^\ddagger$  characterising  $[\text{NaC22C}_2]^+$  is also attributable to  $\text{Na}^+$  being partially solvated in the  $[\text{NaC22C}_2]^+$  ground state. These arguments are consistent with the complexation of  $\text{Na}^+$  by  $\text{C22C}_2$  being characterised by a larger  $k_c$  than is the complexation of  $\text{Li}^+$ . In addition,  $\text{Li}^+$  cryptates are often characterised by smaller  $k_c$  values than their  $\text{Na}^+$  analogues<sup>9</sup>, because the greater solvation energy of  $\text{Li}^+$  gives rise to a more significant contribution to the activation energy from desolvation during the

**Table 4.3.** Kinetic Parameters for Na<sup>+</sup> Exchange on [NaC22C<sub>2</sub>]<sup>+</sup> and Other Cryptates.

cryptate	solvent	$D_N^a$	$10^{-5} k_c^b$ (298.2 K) dm <sup>3</sup> mol <sup>-1</sup> s <sup>-1</sup>	$k_d$ (298.2 K) s <sup>-1</sup>	$\Delta H_d^\ddagger$ kJ mol <sup>-1</sup>	$\Delta S_d^\ddagger$ J mol <sup>-1</sup> K <sup>-1</sup>	log $K_s$ ( $K_s$ /dm <sup>3</sup> mol <sup>-1</sup> )
[NaC22C <sub>2</sub> ] <sup>+</sup> <sup>c</sup>	methanol	19.0 (23.5) <sup>d</sup>		<88			6.6
[NaC22C <sub>2</sub> ] <sup>+</sup> <sup>c</sup>	water	18.0 (33.0) <sup>d</sup>	4.04	255	56.6	-9.4	3.2
[NaC22C <sub>2</sub> ] <sup>+</sup> <sup>c</sup>	dimethyl- formamide	26.6	155	12.3	64.0	-9.5	6.1
[NaC22C <sub>2</sub> ] <sup>+</sup> <sup>c</sup>	dimethyl- sulfoxide	29.8	44.2	11.1	65.8	-4.1	5.6
[LiC22C <sub>2</sub> ] <sup>+</sup> <sup>e</sup>	methanol	19.0 (23.5) <sup>d</sup>	97.1	971	31.0	-84.0	4.0
[LiC22C <sub>2</sub> ] <sup>+</sup> <sup>e</sup>	dimethyl- formamide	26.6	7.60	240	22.5	-124	3.5
[NaC211] <sup>+</sup>	water	18.0 (33.0) <sup>d</sup>	0.754	47.6 <sup>f</sup>	67.2 <sup>f</sup>	12.6	3.2 <sup>g</sup>
[NaC211] <sup>+</sup>	dimethyl- formamide	26.6	19.2	12.1 <sup>f</sup>	83.5 <sup>f</sup>	55.9	5.23 <sup>g</sup>
[NaC211] <sup>+</sup>	dimethyl- sulfoxide	29.8	14.5	34.0 <sup>f</sup>	69.5 <sup>f</sup>	17.4	4.63 <sup>g</sup>

**Table 4.3** continued.

[NaC21C <sub>5</sub> ] <sup>+</sup> <sup>h</sup>	dimethyl- formamide	26.6	214	28800	40.0	-25.3	2.87
[NaC221] <sup>+</sup>	water	18.0 (33.0) <sup>d</sup>	36	14.5 <sup>i</sup>			5.4 <sup>g</sup>
[NaC221] <sup>+</sup>	dimethyl- formamide	26.6	180	0.25 <sup>i</sup> 0.337 <sup>j</sup>	73.0 <sup>j</sup>	-9 <sup>j</sup>	7.93 <sup>g</sup>
[NaC221] <sup>+</sup>	dimethyl- sulfoxide	29.8	72	0.75 <sup>i</sup> 0.765 <sup>j</sup>	70.4 <sup>j</sup>	-11 <sup>j</sup>	6.98 <sup>g</sup>
[NaC22C <sub>5</sub> ] <sup>+</sup> <sup>k</sup>	methanol	19.0 (23.5) <sup>d</sup>	105	41.0	55.1	-29.2	5.41
[NaC22C <sub>5</sub> ] <sup>+</sup> <sup>k</sup>	dimethyl- formamide	26.6		>500			3.66
[NaC22C <sub>5</sub> ] <sup>+</sup> <sup>k</sup>	dimethyl- sulfoxide	29.8		>3000			3.15

<sup>a</sup> Gutmann donor numbers from reference 45. <sup>b</sup>  $k_c = k_d K_s$ . <sup>c</sup> This work. <sup>d</sup> In references 46 and 47 it has been suggested that  $D_N = 33.0$  and  $23.5$  are more appropriate in water and methanol solutions rather than  $D_N = 18.0$  and  $19.0$ , respectively, obtained for water and methanol in 1,2-dichloroethane solution, where the hydrogen-bonding structure of these solvents is disrupted. <sup>e</sup> Reference 50. <sup>f</sup> Reference 13. <sup>g</sup> Reference 51. <sup>h</sup> Reference 15. <sup>i</sup> Reference 9. <sup>j</sup> Reference 52. <sup>k</sup> Reference 53.

complexation process.

The kinetic parameters characterising  $[\text{NaC22C}_2]^+$  may be compared with those of other  $\text{Na}^+$  cryptates. Factors affecting the comparative lability of cryptate systems are the relative fit of  $\text{Na}^+$  into the cryptand cavity, the flexibility of the cryptand, and the number of cryptand donor atoms interacting with  $\text{Na}^+$ . In water, dimethylformamide and dimethylsulfoxide,  $k_d$  characterising  $[\text{NaC211}]^+$  is 0.19, 0.98 and 3.06 times  $k_d$  characterising  $[\text{NaC22C}_2]^+$ , but  $k_c$  characterising  $[\text{NaC22C}_2]^+$  is always larger, which results in  $[\text{NaC22C}_2]^+$  being either similar to or greater in stability than  $[\text{NaC211}]^+$ . Both C211 and C22C<sub>2</sub> possess six donor atoms, but the cavity of C211 is too small to effectively complex  $\text{Na}^+$  whereas  $\text{Na}^+$  is of optimum size for C22C<sub>2</sub>. Thus, the similar  $k_d$  and larger  $k_c$  characterising  $[\text{NaC22C}_2]^+$  probably result from the open clam-like structure of  $[\text{NaC22C}_2]^+$  and the greater flexibility of C22C<sub>2</sub>, compared with C211. The  $k_c$  and  $k_d$  characterising  $\text{Li}^+$  and  $\text{Na}^+$  cryptates of C211 tend to be smaller than those of larger, more flexible cryptands, consistent with the greater rigidity of C211 presenting a significantly higher steric barrier to the complexation and decomplexation of  $\text{M}^+$ . The smaller electrostatic interaction between  $\text{Na}^+$  and C21C<sub>5</sub>, which possesses only five donor atoms, combined with the exclusive structure<sup>54</sup> of  $[\text{NaC21C}_5]^+$ , results in  $k_d$  for  $[\text{NaC21C}_5]^+$  in dimethylformamide being substantially greater than that characterising  $[\text{NaC22C}_2]^+$ .

The substantially greater stability of  $[\text{NaC221}]^+$  compared with  $[\text{NaC22C}_2]^+$  arises almost entirely from the smaller  $k_d$  characterising  $[\text{NaC221}]^+$ . The lower  $k_d$  characterising  $[\text{NaC221}]^+$  in dimethylformamide and dimethylsulfoxide arise mainly from the higher  $\Delta H_d^\ddagger$ . This is consistent with C221 possessing one more oxygen donor atom than C22C<sub>2</sub> and also the inclusive structure of  $[\text{NaC221}]^+$ .<sup>55</sup> The more open structure of  $[\text{NaC22C}_2]^+$  (Figure 1.11), in which  $\text{Na}^+$  is more accessible to solvent, renders it significantly more labile towards decomplexation.

As discussed in Chapter 2, the lower stability of  $[\text{NaC22C}_5]^+$  compared with  $[\text{NaC22C}_2]^+$  in several solvents may be explained by reference to the solid state structures of these cryptates.<sup>48,53</sup> In  $[\text{NaC22C}_5]^+$ ,  $\text{Na}^+$  has a significant bonding interaction with only the four oxygen donor atoms but interacts with all four oxygen donor atoms and both nitrogen donor atoms in  $[\text{NaC22C}_2]^+$ . These differences in electrostatic attraction between  $\text{Na}^+$  and the two cryptands appear to be largely reflected by the respective  $k_d$  values characterising their

cryptates. Thus,  $k_d$  characterising  $[\text{NaC22C}_5]^+$  is considerably higher than  $k_d$  characterising  $[\text{NaC22C}_2]^+$ .

#### 4.5 Exchange Kinetics of $\text{Na}^+$ on $[\text{NaC22C}_8]^+$

The exchange of  $\text{Na}^+$  on  $[\text{NaC22C}_8]^+$  falls within the NMR time scale in methanol, pyridine and acetonitrile. The temperature dependent coalescence of the  $^{23}\text{Na}$  NMR resonances characterising this exchange in methanol appear in Figure 4.3. The kinetic parameters shown in Table 4.4 were obtained from the temperature dependence of  $\tau_c$ , the mean lifetime of  $[\text{NaC22C}_8]^+$  through Equation 4.14. The  $\tau_c$  values were determined by complete lineshape analysis of the coalescing  $^{23}\text{Na}$  resonances observed for each of the solutions (i) - (ix), whose compositions appear in Table 4.4. From Figure 4.4, it may be seen that the magnitudes and temperature variations of  $\tau_c$  for each of the solutions studied for a given solvent are indistinguishable. This is consistent with the operation of a monomolecular mechanism for the decomplexation of  $\text{Na}^+$  from  $[\text{NaC22C}_8]^+$ . In dimethylformamide, a single narrow  $^{23}\text{Na}$  resonance was observed for a solution containing solvated  $\text{Na}^+ / [\text{NaC22C}_8]^+$  from room temperature to close to the solvent freezing point (226 K). This is consistent with  $\text{Na}^+$  exchange on  $[\text{NaC22C}_8]^+$  being in the very fast exchange limit of the NMR timescale (Chapter 12), where no kinetic data is obtainable. The low solubility of  $\text{C22C}_8$  in water precluded any studies in this solvent.

#### 4.6 Exchange Kinetics of $\text{Li}^+$ on $[\text{LiC22C}_8]^+$

The  $^7\text{Li}$  NMR spectra of solutions containing solvated  $\text{Li}^+ / [\text{LiC22C}_8]^+$  in methanol and pyridine, exhibited a single narrow resonance at temperatures approaching the freezing point of these solvents (175 K and 231 K, respectively). Thus,  $\text{Li}^+$  exchange on  $[\text{LiC22C}_8]^+$  is in the very fast exchange limit of the  $^7\text{Li}$  NMR timescale in these solvents (Chapter 12) and no kinetic data could be derived. In acetonitrile,  $[\text{LiC22C}_8]^+$  was also in the fast exchange limit for much of the accessible temperature range, but at 236.0 K, the coalesced singlet resonance exhibited broadening which appeared to arise from a  $\text{Li}^+$  exchange process and a lower limit of  $k_d > 700 \text{ s}^{-1}$  was derived through the fast-exchange approximation (Equation 12.34). In propylene carbonate, the single  $^7\text{Li}$  resonance broadened with decreasing temperature and eventually resolved into two coalescing resonances just above the solvent freezing point (218 K). An estimate of  $k_d = 1020 \text{ s}^{-1}$  at this temperature was obtained from the square top approximation (Equation 12.28). The kinetic parameters

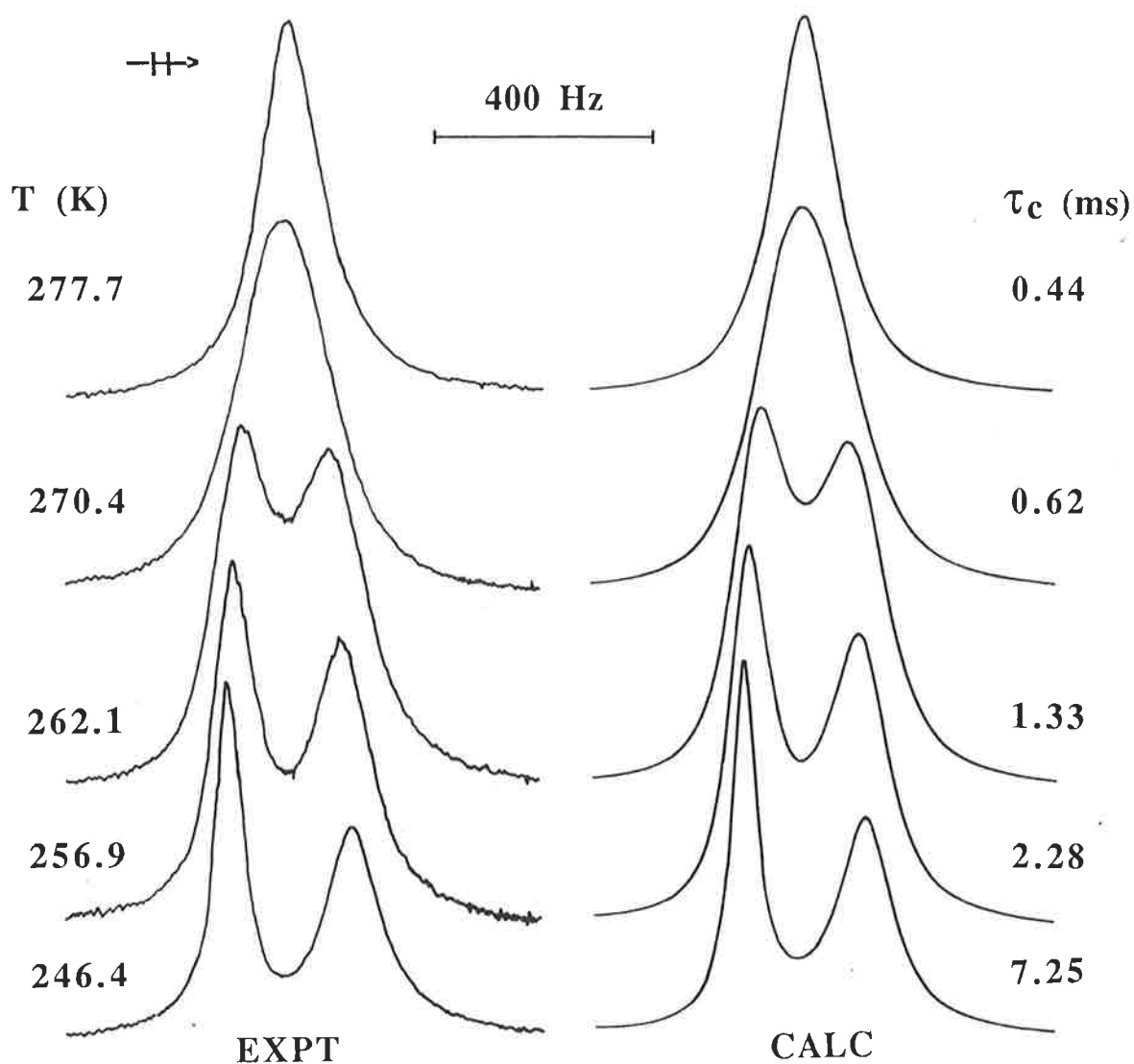


**Figure 4.3.** Typical exchange-modified 79.39 MHz  $^{23}\text{Na}$  NMR spectra of a methanol solution of solvated  $\text{Na}^+$  ( $0.0431 \text{ mol dm}^{-3}$ ) and  $[\text{NaC}_{22}\text{C}_8]^+$  ( $0.0571 \text{ mol dm}^{-3}$ ). Experimental temperatures and spectra appear to the left of the figure and the best fit calculated line shapes and corresponding  $\tau_c$  values appear to the right. The resonance of  $[\text{NaC}_{22}\text{C}_8]^+$  appears upfield from that of solvated  $\text{Na}^+$ .



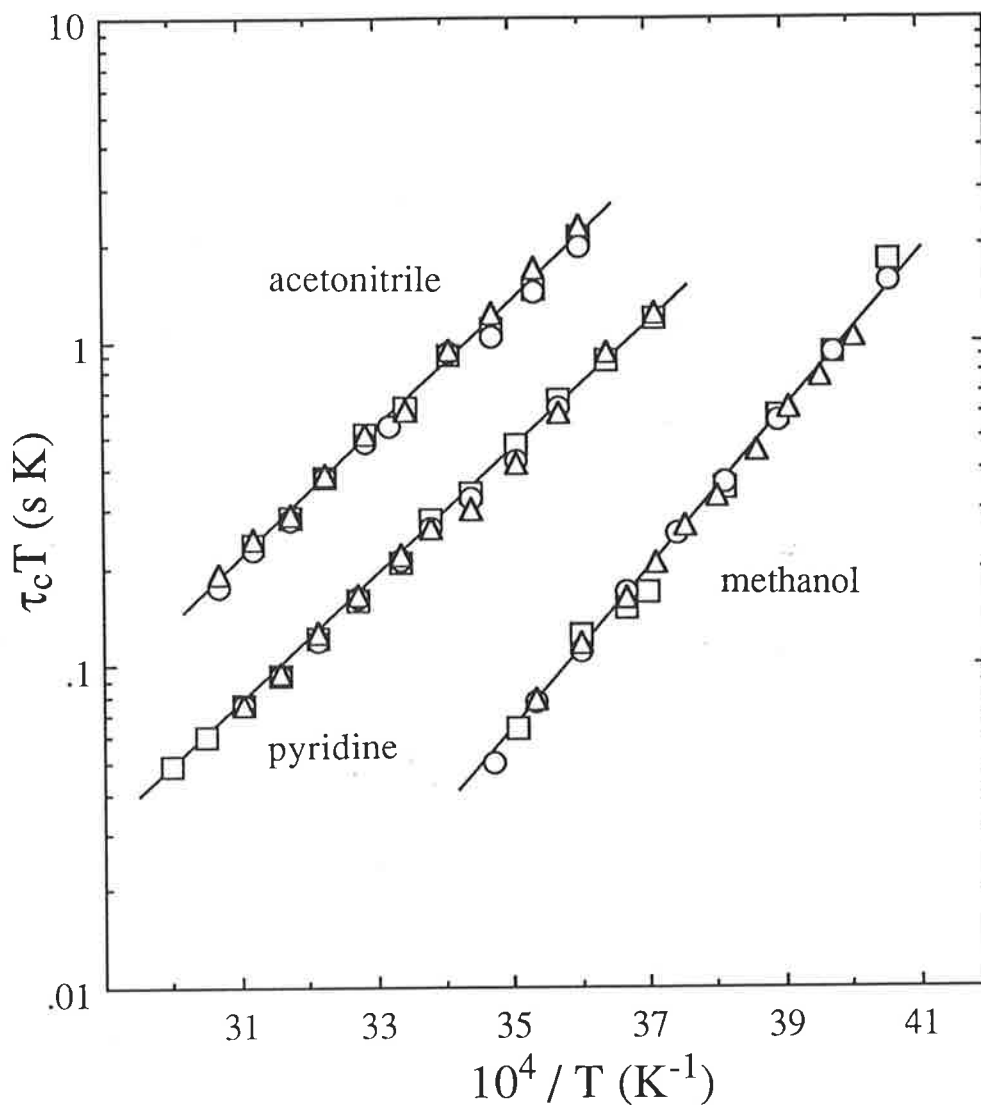


**Figure 4.4.** Temperature variation of  $\tau_c$  for  $[\text{NaC}_{22}\text{C}_8]^+$  in acetonitrile, pyridine and methanol. Data points for acetonitrile solutions i-iii are represented by triangles, squares and circles, respectively. Data points for pyridine solutions iv-vi are represented by triangles, squares and circles, respectively. Data points for methanol solutions vii-ix are represented by triangles, squares and circles, respectively. The solid lines represent the best fits of the combined data for each group to Equation 4.14.

**Table 4.4.** Sodium Ion Exchange on  $[\text{NaC22C}_8]^+$  in Acetonitrile, Pyridine and Methanol. Solution Composition and Kinetic Parameters.<sup>a</sup>

soln.	solvent	$[\text{Na}^+_{\text{solvated}}]$ $\text{mol dm}^{-3}$	$[\text{NaC22C}_8^+]$ $\text{mol dm}^{-3}$	$k_d(T)$ $\text{s}^{-1}$	$k_d(298.2 \text{ K})$ $\text{s}^{-1}$	$\Delta H_d^\ddagger$ $\text{kJ mol}^{-1}$	$\Delta S_d^\ddagger$ $\text{J mol}^{-1} \text{ K}^{-1}$
				$k_d(293.4 \text{ K})$			
i	acetonitrile	0.0216	0.0286	$314 \pm 4$	$421 \pm 5$	$39.1 \pm 0.6$	$-63.7 \pm 2.0$
ii		0.0286	0.0216	$335 \pm 5$	$446 \pm 6$	$37.9 \pm 0.7$	$-67.2 \pm 2.3$
iii		0.0372	0.0131	$347 \pm 7$	$462 \pm 7$	$37.7 \pm 0.8$	$-67.3 \pm 2.6$
(i - iii) <sup>b</sup>				$332 \pm 4$	$443 \pm 5$	$38.2 \pm 0.6$	$-66.1 \pm 1.8$
				$k_d(295.9 \text{ K})$			
(iv)	pyridine	0.0408	0.0613	$1102 \pm 9$	$1250 \pm 10$	$37.8 \pm 0.4$	$-58.9 \pm 1.2$
(v)		0.0582	0.0439	$1100 \pm 10$	$1240 \pm 11$	$37.1 \pm 0.3$	$-61.3 \pm 1.1$
(vi)		0.0766	0.0255	$1144 \pm 16$	$1290 \pm 16$	$36.0 \pm 0.7$	$-64.8 \pm 2.3$
(iv - vi) <sup>b</sup>				$1110 \pm 7$	$1253 \pm 8$	$37.1 \pm 0.3$	$-61.2 \pm 0.9$
				$k_d(267.3 \text{ K})$			
vii	methanol	0.0431	0.0571	$1110 \pm 35$	$11600 \pm 900$	$48.0 \pm 1.7$	$-6.1 \pm 6.0$
viii		0.0581	0.0421	$1090 \pm 12$	$11100 \pm 280$	$47.5 \pm 0.6$	$-8.3 \pm 2.0$
ix		0.0775	0.0226	$1102 \pm 6$	$10000 \pm 170$	$45.1 \pm 0.4$	$-17.1 \pm 1.3$
(vii - ix) <sup>b</sup>				$1100 \pm 12$	$10800 \pm 300$	$46.8 \pm 0.6$	$-11.0 \pm 2.2$

<sup>a</sup> Errors represent one standard deviation from the least-squares fit of the experimental  $\tau_c$  data to Equation 4.14. <sup>b</sup> Simultaneous fit of all data for this solvent.

characterising  $[\text{LiC22C}_8]^+$  and  $[\text{NaC22C}_8]^+$  are summarised in Table 4.5.

**Table 4.5.** Kinetic Parameters for  $\text{M}^+$  Exchange on  $[\text{MC22C}_8]^+$  in a Range of Solvents at 298.2 K.

Solvent	$D_{\text{N}}^a$	$10^{-5} k_{\text{c}}^b$ $\text{dm}^3 \text{mol}^{-1} \text{s}^{-1}$	$k_{\text{d}}$ $\text{s}^{-1}$	$\log K_{\text{s}}$ $(K_{\text{s}}/\text{dm}^3 \text{mol}^{-1})$
$[\text{NaC22C}_8]^+$				
acetonitrile	14.1	321	443	4.86
methanol	19.0 (23.5) <sup>c</sup>	271	10800	3.4
dimethyl- formamide	26.6		fast	2.3
pyridine	33.1	109	1253	3.94
$[\text{LiC22C}_8]^+$				
acetonitrile	14.1		$>700^d$	3.7
propylene- carbonate	15.1		$>1020^e$	
methanol	19.0 (23.5) <sup>c</sup>		fast	2.2
pyridine	33.1		fast	

<sup>a</sup> Gutmann donor numbers from reference 45. <sup>b</sup>  $k_{\text{c}} = k_{\text{d}}K_{\text{s}}$ . <sup>c</sup> In references 46 and 47, it has been suggested that  $D_{\text{N}} = 33.0$  and  $23.5$  are more appropriate than  $D_{\text{N}} = 18.0$  and  $19.0$ , respectively, obtained for water and methanol in 1,2-dichloroethane solution, where the hydrogen-bonding structure of these solvents is disrupted. <sup>d</sup> Calculated from Equation 12.34. Here,  $W'_{1/2} = 77.4$  Hz,  $W_{1/2a} = 18.2$  Hz,  $W_{1/2b} = 1.1$  Hz,  $\Delta\nu = 171$  Hz and  $\chi_{\text{a}} = \chi_{\text{b}} = 0.5$ . The subscripts **a** and **b** refer to the complexed and solvated environments of  $\text{Li}^+$ . <sup>e</sup> Calculated from Equation 12.28. Here,  $\nu_{\text{a}} - \nu_{\text{b}} = 458.3$  Hz.

The greater lability of  $[\text{LiC22C}_8]^+$  compared with that of  $[\text{NaC22C}_8]^+$  probably arises from the smaller size of  $\text{Li}^+$  ( $r = 0.76 \text{ \AA}$ ) which fits the cavity of  $\text{C22C}_8$  ( $r = 1.4 \text{ \AA}$ ) less optimally than does  $\text{Na}^+$  ( $r = 1.02 \text{ \AA}$ ), thus facilitating the decomplexation of  $\text{Li}^+$  from  $\text{C22C}_8$ . Thus, the lower stability of  $[\text{LiC22C}_8]^+$  observed in methanol and acetonitrile is a result of its greater  $k_d$  compared with  $[\text{NaC22C}_8]^+$ . A similar relation holds between  $[\text{LiC222}]^+$  and  $[\text{NaC222}]^+$  (Table 4.6) and results from the same origin, since the cavity sizes of  $\text{C222}$  and  $\text{C22C}_8$  are similar. This is characteristic of other alkali metal cryptates, where the most stable cryptate, corresponding to the metal ion which best fits the cryptand cavity, is also the least labile towards decomplexation.<sup>9</sup>

## 4.7 Exchange Kinetics of Related Cryptate Systems

A greater insight into the factors influencing cryptate lability may be gained by comparison of  $[\text{NaC22C}_8]^+$  with other cryptate systems, for which  $k_d$  also characterises a monomolecular decomplexation process. Table 4.6 includes data for systems covering a wide range of solvents and cryptand structures. One of the major factors that determines cryptate lability is the number of cryptand donor atoms. It may be seen from Table 4.6 that  $[\text{NaC222}]^+$  is characterised by a substantially smaller  $k_d$  than  $[\text{NaC22C}_8]^+$  in methanol and pyridine, whereas differences in  $k_c$  are negligible in methanol. The smaller  $k_d$  of  $[\text{NaC222}]^+$  in pyridine is largely due to a much greater  $\Delta H_d^\ddagger$ . These differences illustrate the importance of bond breaking in the decomplexation process, with the greater electrostatic attraction between  $\text{Na}^+$  and  $\text{C222}$ , compared with  $\text{C22C}_8$ , which possesses two fewer oxygen donor atoms, slowing the rate of release of  $\text{Na}^+$  from the cryptate. A similar relation exists between  $[\text{LiC22C}_8]^+$  and  $[\text{LiC222}]^+$ . Thus, the greater stability of  $[\text{NaC222}]^+$  and  $[\text{LiC222}]^+$  by comparison with their  $\text{C22C}_8$  analogues results largely from differences in  $k_d$  rather than differences in  $k_c$ .

The influence of the number of cryptand donor atoms superimposes onto the fit of the metal ion into the cryptand cavity as may be seen in the variation of  $k_d$  in the sequence :  $[\text{NaC22C}_8]^+ > [\text{NaC22C}_5]^+ > [\text{NaC222}]^+ > [\text{NaC221}]^+$  in methanol. The effect of the extra ether oxygens in the last two cryptates is to slow the release of  $\text{Na}^+$  from the cryptate as a consequence of increased electrostatic interaction between the cryptands  $\text{C222}$  and  $\text{C221}$ , and  $\text{Na}^+$ . However,  $\text{Na}^+$  ( $r = 1.02 \text{ \AA}$ ) fits the cavity of  $\text{C22C}_5$  ( $r = 1.1 \text{ \AA}$ ) more optimally than it does the cavity of  $\text{C22C}_8$  ( $r = 1.4 \text{ \AA}$ ), with the result that  $k_d$

Table 4.6. Kinetic Parameters for M<sup>+</sup> Exchange on [MC22C<sub>8</sub>]<sup>+</sup> and Other Cryptates.

cryptate	solvent	$D_N^a$	$10^{-5} k_c^b$ (298.2 K) dm <sup>3</sup> mol <sup>-1</sup> s <sup>-1</sup>	$k_d$ (298.2 K) s <sup>-1</sup>	$\Delta H_d^\ddagger$ kJ mol <sup>-1</sup>	$\Delta S_d^\ddagger$ J mol <sup>-1</sup> K <sup>-1</sup>	log $K_s$ ( $K_s$ /dm <sup>3</sup> mol <sup>-1</sup> )
[NaC22C <sub>8</sub> ] <sup>+</sup> <sup>c</sup>	methanol	19.0 (23.5) <sup>d</sup>	271	10800	46.8	-11.0	3.4
[NaC22C <sub>8</sub> ] <sup>+</sup> <sup>c</sup>	pyridine	33.1	109	1253	37.1	-61.2	3.94
[LiC22C <sub>8</sub> ] <sup>+</sup> <sup>c</sup>	acetonitrile	14.1		>700			3.7
[LiC22C <sub>8</sub> ] <sup>+</sup> <sup>c</sup>	propylene-carbonate	15.1		>1020			
[NaC222] <sup>+</sup>	methanol	19.0 (23.5) <sup>d</sup>	2700 <sup>e</sup>	2.87 <sup>e</sup>			7.98 <sup>f</sup>
[NaC222] <sup>+</sup> <sup>g</sup>	pyridine	33.1		1.14	56.9	-53	
[LiC222] <sup>+</sup>	acetonitrile	14.1	39197 <sup>h</sup>	420 <sup>h</sup>	11.6 <sup>h</sup>	-156 <sup>h</sup>	6.97 <sup>f</sup>
[LiC222] <sup>+</sup>	propylene-carbonate	15.1	44158 <sup>h</sup>	507 <sup>h</sup>	15.0 <sup>h</sup>	-143 <sup>h</sup>	6.94 <sup>f</sup>
[NaC22C <sub>5</sub> ] <sup>+</sup> <sup>i</sup>	methanol	19.0 (23.5) <sup>d</sup>	105	41.0	55.1	-29.2	5.41
[NaC221] <sup>+</sup>	methanol	19.0 (23.5) <sup>d</sup>	1700 <sup>e</sup>	0.0235 <sup>e</sup>			9.65 <sup>f</sup>

**Table 4.6** continued.

[NaC21C5] <sup>+</sup> <sup>j</sup>	methanol	19.0 (23.5) <sup>d</sup>	104	1800	44.9	-31.9	3.76
[NaC211] <sup>+</sup>	methanol	19.0 (23.5) <sup>d</sup>	31.0 <sup>e</sup>	2.5 <sup>e</sup>			6.1 <sup>f</sup>

<sup>a</sup> Gutmann donor numbers from reference 45. <sup>b</sup>  $k_c = k_d K_s$ . <sup>c</sup> This work. <sup>d</sup> In references 46 and 47, it has been suggested that  $D_N = 33.0$  and  $23.5$  are more appropriate in water and methanol solutions rather than  $D_N = 18.0$  and  $19.0$ , respectively, obtained for water and methanol in 1,2-dichloroethane solution, where the hydrogen-bonding structure of these solvents is disrupted. <sup>e</sup> Reference 9. <sup>f</sup> Reference 51. <sup>g</sup> Reference 4.

<sup>h</sup> Reference 14. <sup>i</sup> Reference 53. <sup>j</sup> Reference 15.

characterising  $[\text{NaC22C}_8]^+$  is greater than  $k_d$  characterising  $[\text{NaC22C}_5]^+$ . However, although  $\text{Na}^+$  fits the cavity of  $\text{C22C}_5$  better than that of  $\text{C222}$ , the extra oxygen donor atoms of  $\text{C222}$  result in  $k_d$  being lower for  $[\text{NaC222}]^+$  than for  $[\text{NaC22C}_5]^+$ . The inclusion of  $[\text{NaC211}]^+$  in Table 4.6 serves to illustrate that a decrease below optimum cavity size to  $r = 0.8 \text{ \AA}$  increases  $k_d$ , and that  $\text{C21C}_5$ , which has the same cavity size, but one less ether oxygen, forms  $[\text{NaC21C}_5]^+$  which is of increased lability. The rate of decomplexation of  $[\text{NaC21C}_5]^+$  is 720 times that of  $[\text{NaC211}]^+$  at 298.2 K in methanol, whereas the rate of decomplexation of  $[\text{NaC22C}_8]^+$  is 3760 times that of  $[\text{NaC222}]^+$ . The greater difference in lability between  $[\text{NaC22C}_8]^+$  and  $[\text{NaC222}]^+$  compared with the other pair of cryptates illustrates the greater difference in electrostatic interaction between  $\text{Na}^+$  and these two cryptands than is the case with the other pair of cryptands, which differ by one ether oxygen only. The variations in  $k_d$  characterising the cryptates in Table 4.6 are predominantly reflected in the variations in  $K_s$ , which illustrates the dominance of the decomplexation process in determining the relative stabilities of these cryptates.

These results may be correlated with studies on the efficacy of cryptands as alkali metal ion carriers in membrane transport studies.<sup>56-57</sup> An effective cation carrier should show high selectivity for the desired metal ion, but sufficiently high rates of complexation and decomplexation for rapid cation exchange at the membrane interface. It was found that the cryptands  $\text{C211}$ ,  $\text{C221}$  and  $\text{C222}$  are good cation receptors but are poor cation carriers, resulting in very slow transport of alkali metal ions across a membrane. In contrast, the cryptands  $\text{C21C}_5$ ,  $\text{C22C}_5$  and  $\text{C22C}_8$  showed a far greater efficiency at transporting alkali metal ions across membranes. This is attributable to a number of factors. The greater lipophilicity of these ligands, by comparison with  $\text{C211}$ ,  $\text{C221}$  and  $\text{C222}$ , results in an increase in the solubility of their cryptates in the membrane media. The greater lability of the cryptates of  $\text{C21C}_5$ ,  $\text{C22C}_5$  and  $\text{C22C}_8$  results in faster cation exchange at the membrane interface, compared with the slower decomplexation rates of the cryptates of  $\text{C211}$ ,  $\text{C221}$  and  $\text{C222}$ . The decreased stability of the cryptates of  $\text{C21C}_5$ ,  $\text{C22C}_5$  and  $\text{C22C}_8$ , compared with those of  $\text{C211}$ ,  $\text{C221}$  and  $\text{C222}$ , results in a greater equilibrium concentration of free ligand, which is available for back-diffusion in order to continue the transport process. This is consistent with the observations of this study, where it is apparent that the lesser electrostatic attraction between  $\text{M}^+$  and the cryptand that occurs with  $\text{C21C}_5$ ,  $\text{C22C}_5$  and  $\text{C22C}_8$ , by comparison with  $\text{C211}$ ,  $\text{C221}$  and  $\text{C222}$ , respectively,

causes a decrease in cryptate stability (Chapter 2) and an increase in cryptate lability.

## 4.8 Effect of Solvent on Cryptate Lability

As may be seen from Tables 4.2 and 4.5, the exchange kinetics of  $[\text{NaC22C}_2]^+$  and  $[\text{NaC22C}_8]^+$  are strongly dependent on the nature of the solvent. The variation in magnitude of  $k_d$  (298.2 K) characterising  $[\text{NaC22C}_2]^+$  is in the sequence methanol < dimethylformamide < water. For  $[\text{NaC22C}_8]^+$ , a similar trend occurs, with  $k_d$  varying in the sequence acetonitrile < methanol < dimethylformamide. In acetonitrile, methanol and pyridine,  $k_d$  characterising  $[\text{NaC22C}_8]^+$  varies by a factor of 24, whereas  $k_c$  varies only by a factor of 3. Thus, the variation in the stability of  $[\text{NaC22C}_8]^+$  in these solvents is predominantly due to variations in  $k_d$ . These observations are similar to the variation of  $k_d$  with the nature of the solvent observed for other  $\text{Na}^+$  cryptates for which it is generally found that the magnitude of  $k_d$  increases with change of solvent as  $D_N$  increases and  $k_c$  is relatively invariant with the nature of the solvent.<sup>9,15,20</sup> Such an observation implies that the transition state for decomplexation is more similar to solvated  $\text{Na}^+$  and the free cryptand than to the cryptate.

The free energies of the solvated metal ion, the ligand, the complex and also the transition state will be determined to a substantial extent by the electron donating ability of the solvent, as characterised by its Gutmann donor number  $D_N$ , and also the number of solvent molecules bound to each of these species. Precise separation of these factors is impossible but the overall trends observed for  $[\text{NaC22C}_2]^+$  and  $[\text{NaC22C}_8]^+$  may be rationalised through a simple model, in which  $k_c$  is deemed invariant and  $\Delta G_{d^\ddagger}$  varies with the nature of the solvent (Figure 4.5). The variation in  $k_d$  may be explained on the basis that the free energy of decomplexation,  $\Delta G_{d^\ddagger}$ , is largely the difference between the free energy change,  $\Delta G_{r^\ddagger}$ , arising from structural rearrangements in the cryptate  $[\text{ML}]^+$  in achieving its transition state stereochemistry in the absence of solvent interaction and  $\Delta G_{s^\ddagger}$ , the involvement of solvent in the activation process, which gives rise to an increased solvation in the transition state (Equation 4.16).

$$\Delta G_{d^\ddagger} = \Delta G_{r^\ddagger} - \Delta G_{s^\ddagger} \quad 4.16$$

The free energy of complexation,  $\Delta G^0$ , is given by equation 4.17;



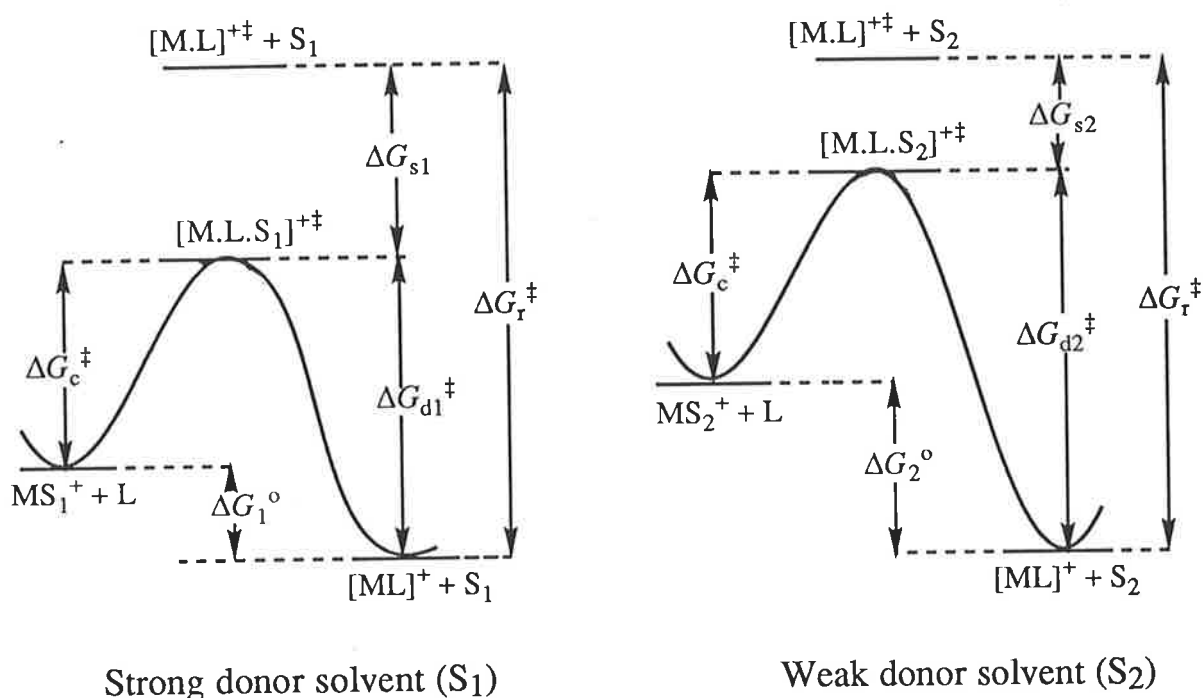


**Figure 4.5.** A simplified reaction profile for the formation and decomplexation of the cryptate  $[ML]^+$  in a strong donor solvent  $S_1$  (left) and a weak donor solvent  $S_2$  (right). The free energies of the  $[ML]^+$  ground states are normalized to the same value in each profile and the free energy of activation for the complexation process ( $\Delta G_c^\ddagger$ ) is taken to be solvent independent, as is found for several cryptate systems.  $MS_n^+$  is the ground state metal ion. Both free ligand  $L$ , cryptate  $[ML]^+$  and transition state  $[M.L.S_n]^{\ddagger}$  are solvated, but no indication of the number of solvent molecules is given, owing to the uncertainty in such a number. The transition state  $[M.L]^{\ddagger}$  occurs only in the absence of solvent.

$$\Delta G^0 = \Delta G_{c^\ddagger} - \Delta G_{d^\ddagger} \quad 4.17$$

The solvent interaction,  $\Delta G_{s^\ddagger}$ , decreases the free energy of the transition state. Therefore an increase in  $D_N$  increases  $\Delta G_{s^\ddagger}$ , and thus  $\Delta G_{d^\ddagger}$  and  $\Delta G^0$  decrease so that  $[ML]^+$  becomes more labile and less stable as  $D_N$  increases. In contrast,  $k_d$  is essentially independent of  $D_N$  when a bimolecular mechanism operates.<sup>37-38</sup> The monomolecular mechanism is favoured in solvents of high donicity because  $\Delta G_{s^\ddagger}$  is large, whereas the bimolecular mechanism is favoured by solvents with high dielectric constants. Thus, in weak donor solvents (where  $\Delta G_{s^\ddagger}$  is small), the activation energy for the monomolecular mechanism may become larger than that of the bimolecular mechanism, which would then dominate the decomplexation process.<sup>37</sup>

The exchange kinetics of  $[\text{NaC22C}_2]^+$  and  $[\text{NaC22C}_8]^+$  are generally in agreement with the preceding arguments, but there are some exceptions. In water,  $k_c$  characterising  $[\text{NaC22C}_2]^+$  tends to be lower than expected on the basis of this model. The desolvation of the metal ion during complexation is thought to be a concerted process, with each of the solvent molecules coordinated to the cation being replaced in a step-wise manner by donor atoms of the ligand. However, such a process may be hindered when the ligand is strongly solvated, as may occur in aqueous solution, with hydrogen bonding between ligand donor atoms and water molecules. Conversely, the solvation of the ligand donor atoms during the decomplexation of  $\text{Na}^+$  from  $[\text{NaC22C}_2]^+$  tends to stabilise the transition state, so that  $\Delta H_{d^\ddagger}$  in water is lower than in dimethylformamide and dimethylsulfoxide, resulting in the larger  $k_d$  characterising  $[\text{NaC22C}_2]^+$  in aqueous solution.

On the basis of Equation 4.16,  $\text{Na}^+$  exchange on  $[\text{NaC22C}_2]^+$  and  $[\text{NaC22C}_8]^+$  in pyridine ( $D_N = 33.1$ ) should be characterised by a much larger  $k_d$  than is observed. Thus, the relatively high stabilities of  $[\text{NaC22C}_2]^+$  and  $[\text{NaC22C}_8]^+$  in pyridine arise from a small  $k_d$ . In Chapter 2, this was attributed to two possible causes; (i) a relatively weak interaction between the hard acid alkali metal ion  $\text{Na}^+$  and the soft base nitrogen donor atom in pyridine and (ii) the inability of pyridine to effectively coordinate to  $\text{Na}^+$  as a result of steric hindrance between adjacent pyridines. Both of these effects may account for the low value of  $k_d$  characterising  $[\text{NaC22C}_2]^+$  and  $[\text{NaC22C}_8]^+$  in pyridine. The anomalous high stability and low lability of alkali metal cryptates in pyridine has been observed for several other systems, including  $[\text{NaC222}]^+$ ,  $[\text{NaC21C}_5]^+$ ,  $[\text{LiC22C}_2]^+$  and  $[\text{NaC22C}_5]^+$ .<sup>4,15,50,53</sup>

The variation in  $k_d$  and  $k_c$  over the range of solvents studied for both  $[\text{NaC22C}_2]^+$  and  $[\text{LiC22C}_2]^+$  is encompassed within the general trend usually observed for cryptates, in which  $k_d$  varies substantially with solvent and  $k_c$  less so, with the result that cryptate stability is largely determined by  $k_d$ . However over the narrower range of solvent donor numbers for which quantitative data is available (Table 4.3), diversions from this trend may occur. This is exemplified by the larger  $k_d$  characterising  $[\text{LiC22C}_2]^+$  in methanol compared with that in dimethylformamide and the lower  $k_d$  characterising  $[\text{NaC22C}_2]^+$  in dimethylsulfoxide compared with that in dimethylformamide. In these solvents,  $k_c$  tends to decrease with increasing  $D_N$ , consistent with the rate-determining step for complexation involving considerable desolvation of  $M^+$ , with the result that  $K_S$  is largely determined by variations in  $k_c$ . In this case, the transition state more closely resembles the cryptate, where the metal ion is substantially desolvated. In the Eigen-Winkler mechanism for cryptate formation, the variation of  $k_c$  and  $k_d$  with solvent will depend on the relative importance of cation desolvation, cryptand conformational changes and the formation or disruption of bonds between the metal ion and the cryptand. From the results characterising  $[\text{NaC22C}_2]^+$  and  $[\text{NaC22C}_8]^+$ , it is apparent that the relative importance of these factors are dependent on the natures of the solvent and the cryptand.

#### 4.9 Effect of the Length of the $C_n$ Bridge on the Lability of $[\text{NaC22C}_n]^+$

One of the main aims of this work is to study the factors determining cryptate stability through the  $C22C_n$  series of ligands, which are based on the diaza crown ether C22. In Chapter 2, it was seen that as  $n$  was increased, the stabilities of  $[\text{MC22C}_n]^+$  decreased and approached those of  $[\text{MC22}]^+$ . It is now appropriate to see how these variations in stability are reflected in the labilities of the  $[\text{NaC22C}_n]^+$  complexes. It is apparent from Table 4.7 that the different stabilities of the  $[\text{NaC22C}_n]^+$  cryptates are predominantly determined by variations in  $k_d$ . The variation of  $k_d$  in the sequence:  $[\text{NaC22C}_8]^+ > [\text{NaC22C}_5]^+ > [\text{NaC22C}_2]^+$  is consistent with the shortening of the  $C_n$  arm slowing the rate of release of  $\text{Na}^+$  from the cryptate, probably coincident with a progressive decrease in flexibility of these cryptates and the loose fit of  $\text{Na}^+$  in  $C22C_8$ . The highest stability and lowest lability towards decomplexation occurs with  $[\text{NaC22C}_2]^+$ , consistent with the optimisation of fit and the interaction of  $\text{Na}^+$  with all six donor atoms of  $C22C_2$ . The cavity of  $C22C_5$  is also of optimum size for  $\text{Na}^+$ , but as described previously, the absence of an

oxygen donor atom in the C<sub>5</sub> arm results in movement of Na<sup>+</sup> away from the centre of the cryptand cavity and a concomitant decrease in the interaction between Na<sup>+</sup> and the C<sub>22</sub>C<sub>5</sub> nitrogens, with the result that  $k_d$  characterising [NaC<sub>22</sub>C<sub>5</sub>]<sup>+</sup> is greater than that characterising [NaC<sub>22</sub>C<sub>2</sub>]<sup>+</sup>. The loose fit of Na<sup>+</sup> in [NaC<sub>22</sub>C<sub>8</sub>]<sup>+</sup>, together with the higher flexibility of C<sub>22</sub>C<sub>8</sub>, result in this cryptate being the most labile towards decomplexation in this series. No quantitative kinetic data is available for the alkali metal complexes of the parent macrocycle C<sub>22</sub>, but for the related crown ether complex [Na18C6]<sup>+</sup>, the following parameters have been determined in methanol at 298.2 K; log  $K_s$  = 4.32,  $k_d$  = 7.2 x 10<sup>4</sup> s<sup>-1</sup> and  $k_c$  = 1.5 x 10<sup>9</sup> dm<sup>3</sup> mol<sup>-1</sup> s<sup>-1</sup>.<sup>58-59</sup> Despite the larger  $k_d$  characterising [Na18C6]<sup>+</sup> by comparison with that for [NaC<sub>22</sub>C<sub>8</sub>]<sup>+</sup>, the larger  $k_c$  characterising [Na18C6]<sup>+</sup> results in [Na18C6]<sup>+</sup> being more stable than [NaC<sub>22</sub>C<sub>8</sub>]<sup>+</sup>. Similarly, the complexation of Na<sup>+</sup> by C<sub>22</sub> is also probably characterised by both a larger  $k_c$  and  $k_d$  than is [NaC<sub>22</sub>C<sub>8</sub>]<sup>+</sup>. This demonstrates the influence of ligand flexibility on complex lability, with the greater flexibility of the monocyclic crown ether rendering both complexation and decomplexation more facile when compared to its bicyclic cryptate analogues.

**Table 4.7.** Kinetic and Equilibrium Parameters for Na<sup>+</sup> Exchange on [NaC<sub>22</sub>C<sub>n</sub>]<sup>+</sup> in Methanol and Dimethylformamide at 298.2 K

cryptate	solvent	10 <sup>5</sup> $k_c$ dm <sup>3</sup> mol <sup>-1</sup> s <sup>-1</sup>	$k_d$ s <sup>-1</sup>	log $K_s$ ( $K_s$ /dm <sup>3</sup> mol <sup>-1</sup> )
[NaC <sub>22</sub> C <sub>2</sub> ] <sup>+</sup> <sup>a</sup>	methanol		slow	6.6
[NaC <sub>22</sub> C <sub>2</sub> ] <sup>+</sup> <sup>a</sup>	dimethyl- formamide	155	12.3	6.1
[NaC <sub>22</sub> C <sub>5</sub> ] <sup>+</sup> <sup>b</sup>	methanol	105	41.0	5.41
[NaC <sub>22</sub> C <sub>5</sub> ] <sup>+</sup> <sup>b</sup>	dimethyl- formamide		>500	3.66
[NaC <sub>22</sub> C <sub>8</sub> ] <sup>+</sup> <sup>a</sup>	methanol	271	10800	3.4
[NaC <sub>22</sub> C <sub>8</sub> ] <sup>+</sup> <sup>a</sup>	dimethyl- formamide		fast	2.3

<sup>a</sup> This work. <sup>b</sup> Reference 53.

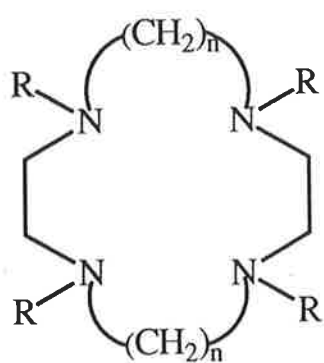
- 1 Lehn, J.-M.; Sauvage, J.-P.; Dietrich, B. *J. Am. Chem. Soc.* **1970**, *92*, 2916-2918.
- 2 Lehn, J.-M. *Struct. Bonding (Berlin)*. **1973**, *16*, 1-69.
- 3 Cahen, Y.M.; Dye, J.L.; Popov, A.I.; *J. Phys. Chem.* **1975**, *79*, 1292-1295.
- 4 Ceraso, J.M.; Smith, P.B.; Landers, J.S.; Dye, J.L. *J. Phys. Chem.* **1977**, 760-766.
- 5 Cox, B.G.; Schneider, H.; Stroka, J. *J. Am. Chem. Soc.* **1978**, *100*, 4746-4749.
- 6 Cox, B.G.; Schneider, I.; Schneider, H. *Ber. Bunsenges. Phys. Chem.* **1980**, *84*, 470-474.
- 7 Cox, B.G.; Garcia-Rosas, J.; Schneider, H. *J. Phys. Chem.* **1980**, *84*, 3178-3183.
- 8 Liesegang, G.W. *J. Am. Chem. Soc.* **1981**, *103*, 953-955.
- 9 Cox, B.G.; Garcia-Rosas, J.; Schneider, H. *J. Am. Chem. Soc.* **1981**, *103*, 1054-1059.
- 10 Lin, J.D.; Popov, A.I. *J. Am. Chem. Soc.* **1981**, *103*, 3773-3777.
- 11 Schmidt, E.; Popov, A.I. *J. Am. Chem. Soc.* **1983**, *105*, 1878-1882.
- 12 Cox, B.G.; van Truong, N.; Schneider, H. *J. Chem. Soc., Faraday Trans 1*. **1984**, *80*, 3285-3293.
- 13 Lincoln, S.F.; Brereton, I.M.; Spotswood, T.M. *J. Chem. Soc., Faraday Trans 1*. **1985**, *81*, 1623-1630.
- 14 Shamsipur, M.; Popov, A.I. *J. Phys. Chem.* **1986**, *90*, 5997-5999.
- 15 Lincoln, S.F.; Brereton, I.M.; Spotswood, T.M. *J. Am. Chem. Soc.* **1986**, *108*, 8134-8138.
- 16 Shamsipur, M.; Popov, A.I. *J. Phys. Chem.* **1987**, *91*, 447-451.
- 17 Clarke, P.; Abou-Hamdan, A.; Hounslow, A.; Lincoln, S.F. *Inorg. Chim. Acta*. **1988**, *154*, 83-87.
- 18 Cox, B.G.; Stroka, J.; Schneider, H. *Inorg. Chim. Acta*. **1988**, *147*, 9-15.
- 19 Cox, B.G.; Stroka, J.; Schneider, I.; Schneider, H. *J. Chem. Soc., Faraday Trans 1*. **1989**, *85*, 187-198.
- 20 Lincoln, S.F.; Abou-Hamdan, A. *Inorg. Chem.* **1990**, *29*, 3584-3589.
- 21 Lincoln, S.F.; Rodopoulos, T. *Inorg. Chim. Acta*. **1993**, *205*, 23-30.
- 22 Dhillon, R.; Lincoln, S.F. *Aust. J. Chem.* **1994**, *47*, 123-130.
- 23 Burgermeister, W.; Winkler-Oswatitsch, R. *Top. Curr. Chem.* **1977**, *69*, 91-196.
- 24 Eigen, M.; Winkler, R. *"The Neurosciences, Second Study Program"*, New York, Rockefeller University Press, **1970**.

- 25 Cox, B.G.; Schneider, H. *Pure Appl. Chem.* **1990**, 62, 2259-2268.
- 26 Chen, C.C.; Petrucci, S. *J. Phys. Chem.* **1982**, 86, 2601-2605.
- 27 Maynard, K.J.; Irish, D.E.; Eyring, E.M.; Petrucci, S. *J. Phys. Chem.* **1984**, 88, 729-736.
- 28 Wallace, W.; Chen, C.; Eyring, E.M.; Petrucci, S. *J. Phys. Chem.* **1985**, 89, 1357-1366.
- 29 Petrucci, S.; Adamic, R.J.; Eyring, E.M. *J. Phys. Chem.* **1986**, 90, 1677-1683.
- 30 Xu, M.; Inoue, N.; Eyring, E.M.; Petrucci, S. *J. Phys. Chem.* **1988**, 92, 2789-2798.
- 31 Cobranchi, D.P.; Phillips, G.R.; Johnson, D.E.; Barton, R.M.; Rose, D.J.; Eyring, E.M.; Rodriguez, L.J.; Petrucci, S. *J. Phys. Chem.* **1989**, 93, 1396-1398.
- 32 Rodriguez, L.J.; Eyring, E.M.; Petrucci, S. *J. Phys. Chem.* **1989**, 93, 5916-5924.
- 33 Schneider, H.; Richmann, K.H.; Funck, T.; Firman, P.; Eggers, F.; Eyring, E.M.; Petrucci, S. *J. Phys. Chem.* **1988**, 92, 2798-2804.
- 34 Shchori, E.; Jagur-Gordzinski, J.; Luz, Z.; Shporer, H. *J. Am. Chem. Soc.* **1971**, 93, 7133-7138.
- 35 Soong, L.L.; Leroi, G.E.; Popov, A.I. *Inorg. Chem.* **1990**, 29, 1366-1370.
- 36 Strasser, B.O.; Hallenga, K.; Popov, A.I. *J. Am. Chem. Soc.* **1985**, 107, 789-792.
- 37 Strasser, B.O.; Popov, A.I. *J. Am. Chem. Soc.* **1985**, 107, 7921-7924.
- 38 Shamsipur, M.; Popov, A.I. *J. Phys. Chem.* **1988**, 92, 147-151.
- 39 Szczygiel, P.; Shamsipur, M.; Popov, A.I. *J. Phys. Chem.* **1987**, 91, 1252-1255.
- 40 Strasser, B.O.; Shamsipur, M.; Popov, A.I. *J. Phys. Chem.* **1985**, 89, 4822-4824.
- 41 Graves, H.P.; Detellier, C. *J. Am. Chem. Soc.* **1988**, 110, 6019-6024.
- 42 Delville, A.; Stover, H.D.H.; Detellier, C. *J. Am. Chem. Soc.* **1985**, 107, 4172-4175.
- 43 Stover, H.D.H.; Detellier, C. *J. Phys. Chem.* **1989**, 93, 3174-3178.
- 44 Briere, K.M.; Detellier, C. *J. Phys. Chem.* **1987**, 91, 6097-6099.
- 45 Gutmann, V. *"Coordination Chemistry in Non-Aqueous Solutions"*, Springer-Verlag, Wien, **1968**.
- 46 Erlich, R.H.; Roach, E.; Popov, A.I. *J. Am. Chem. Soc.* **1970**, 92, 4989-4990.
- 47 Dewitte, W.J.; Popov, A.I. *J. Soln. Chem.* **1976**, 5, 231-240.

- 48 Groth, P. *Acta. Chem. Scand.* **1985**, A39, 68-72.
- 49 Groth, P. *Acta. Chem. Scand.* **1985**, A39, 73-76.
- 50 Lincoln, S.F.; Abou-Hamdan, A. *Inorg. Chem.* **1991**, 30, 462-466.
- 51 Cox, B.G.; Garcia-Rosas, J.; Schneider, H. *J. Am. Chem. Soc.* **1981**, 103, 1384-1389.
- 52 Ishihara, K.; Miura, H.; Funahashi, S.; Tanaka, M. *Inorg. Chem.* **1988**, 27, 1706-1710.
- 53 Clarke, P.; Lincoln, S.F.; Tiekink, E.R.T. *Inorg. Chem.* **1991**, 30, 2747-2751.
- 54 Lincoln, S.F.; Horn, E.; Snow, M.R.; Hambley, T.W.; Brereton, I.M.; Spotswood, T.M. *J. Chem. Soc., Dalton Trans.* **1986**, 1075-1080.
- 55 Mathieu, F.; Metz, B.; Moras, D.; Weiss, R. *J. Am. Chem. Soc.* **1978**, 100, 4412-4416.
- 56 Lehn, J-M. *Pure Appl. Chem.* **1979**, 51, 979-997.
- 57 Kirch, M.; Lehn, J-M. *Angew. Chem., Int. Ed. Engl.* **1975**, 14, 555-556.
- 58 Frensdorff, H.K. *J. Am. Chem. Soc.* **1971**, 93, 600-606.
- 59 Lincoln, S.F.; White, A.; Hounslow, A.M. *J. Chem. Soc., Faraday Trans 1.* **1987**, 83, 2459-2466.

## Chapter 5: Introduction to Pendant Arm Tetraaza Macrocyclic Ligand Complexes

The tetraaza and pendant arm tetraaza macrocyclic ligands are cyclic tetramines with the general structure shown in Figure 5.1. Pendant arm tetraaza macrocyclic ligands are derived from their parent tetraaza macrocycles by the attachment of substituents to the cyclic backbone. The pendant arm ligands discussed in the following chapters are *N*-functionalised tetraaza macrocycles based on the 1,4,7,10-tetraazacyclododecane (cyclen) and 1,4,8,11-tetraazacyclotetradecane (cyclam) structures. The trivial nomenclature adopted for these ligands is shown in Figure 5.1. For example, the systematic name 1,4,8,11-tetrakis(2-hydroxyethyl)-1,4,8,11-tetraazacyclotetradecane is abbreviated as THEC14; tetrahydroxyethylcyclam, where the 14 indicates that the ligand is derived from the 14 membered macrocycle cyclam. Similarly, the ligand 1,4,7,10-tetrakis(2-hydroxyethyl)-1,4,7,10-tetraazacyclododecane is THEC12; tetrahydroxyethylcyclen, which is derived from the 12 membered macrocycle cyclen. In this study, the number of atoms in the macrocyclic ring is always appended to the name of the ligand to avoid confusion between ligands with the same pendant arms, but with different macrocyclic ring size such as THEC12 and THEC14. The structures of the tetraaza ligands discussed in this study appear in Figure 5.2.



n	R	Ligand
2	H	cyclen
2	CH <sub>2</sub> CH <sub>2</sub> OH	THEC12
2	CH <sub>2</sub> CH <sub>2</sub> OCH <sub>3</sub>	TMEC12
3	H	cyclam
3	CH <sub>2</sub> CH <sub>2</sub> OH	THEC14
3	CH <sub>2</sub> CH <sub>2</sub> OCH <sub>3</sub>	TMEC14

**Figure 5.1.** Structure and trivial nomenclature of the tetraaza macrocycles and their pendant arm derivatives.



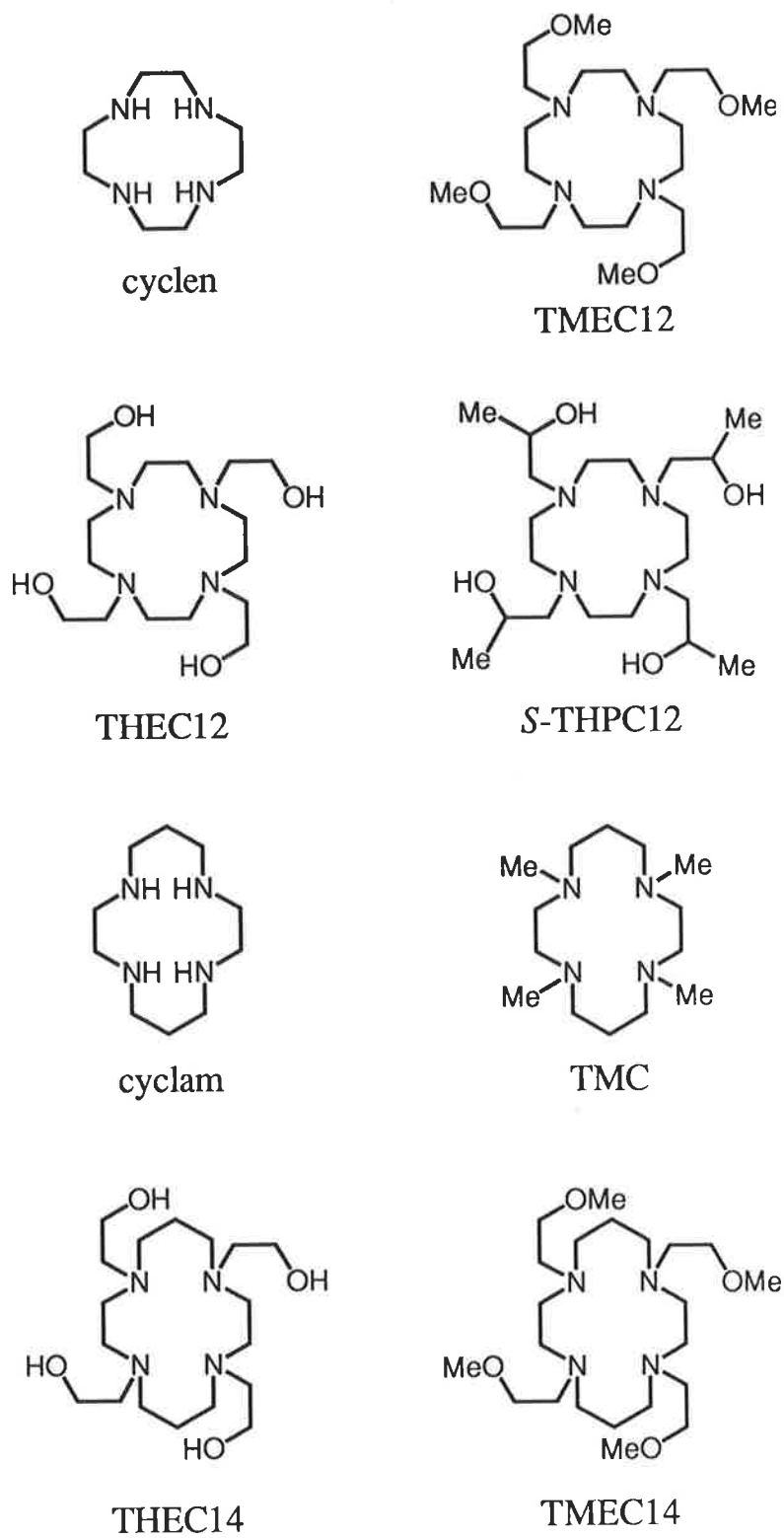


**Figure 5.2.** Structures of the tetraaza and pendant arm tetraaza macrocyclic ligands discussed in this work.

The initial studies of polyaza macrocyclic ligands were stimulated by the interesting properties of their metal complexes, when compared with those of their non cyclic analogues. Such properties include a high degree of thermodynamic and kinetic stability (the macrocyclic effect), unusual spectral and magnetic properties, novel coordination geometries and the ability to stabilise unusual oxidation states.<sup>1-12</sup> Polyaza macrocyclic ligands are also involved in a number of fundamental biological processes such as the mechanism of photosynthesis (the chlorin ring in chlorophyll) and the transport of oxygen in respiratory systems (the porphyrin ring of the iron containing haem proteins).<sup>1</sup> A considerable amount of research involving synthetic polyaza macrocycles has been directed towards the preparation of model compounds for the naturally occurring macrocycles in order to develop the understanding of this type of metal ion environment which is of considerable importance in living systems.<sup>1,13-17</sup>

The pendant arm tetraaza macrocycles and related pendant arm ligands were created with the aim of combining the properties of the relatively rigid and kinetically stable macrocyclic structure with those of the more flexible and labile open chain ligands.<sup>1,18</sup> In recent years, the coordination chemistry of these ligands has received considerable attention.<sup>18-36</sup> By systematic variation of the pendant arm, the properties of the parent macrocycle may be modified at will. This has led to the synthesis of ligands with a number of interesting and useful applications. By covalent coupling of a suitable organic group to the macrocycle, metal ion promoted reactions such as ester, amide and nitrile hydrolysis may be studied.<sup>38-40</sup> Other applications include the synthesis of iron sequestering reagents for the treatment of acute iron poisoning<sup>41</sup> and the development of biofunctional chelating agents which attach metal ions to proteins and may be used as labelling agents for proteins and antibodies<sup>42</sup> and in cancer therapy and diagnosis.<sup>43-44</sup> One of the major areas of current interest<sup>30,45-46</sup> is in the design of ligands for the selective binding of particular metal ions, an area of considerable importance in analytical chemistry. In particular, research has been directed to the design of ligands which are selective for toxic heavy metals such as  $\text{Cd}^{2+}$ ,  $\text{Hg}^{2+}$  and  $\text{Pb}^{2+}$ , over the biologically essential ions such as  $\text{Cu}^{2+}$ ,  $\text{Ca}^{2+}$  and  $\text{Zn}^{2+}$ . In this area, the use of pendant arms containing oxygen donor groups has proven particularly effective at altering the metal ion selectivity of ligands.<sup>30,47-50</sup>

The selective complexation of alkali metal ions by cryptands, crown ethers and similar ligands is well established (Chapters 1 - 4), whereas studies

of metal ion complexation by tetraaza and pendant arm tetraaza macrocycles has generally involved di- and trivalent transition and main group metal ions. Thus, the majority of alkali metal ion complexes have been with ligands containing predominantly oxygen donor atoms, with fewer nitrogen or sulfur donor atoms. Unsubstituted tetraaza macrocycles do not form detectable complexes with alkali metal ions in aqueous solution, whereas they complex strongly with transition metal and heavy metal ions.<sup>18,51</sup> One way to enhance the affinity of these ligands for the alkali metal ions would be the addition of oxygen donor groups. This may be achieved either by incorporation of the oxygen donor into the macrocyclic ring, or, more readily, by the addition of pendant arms containing the oxygen donor atom to form pendant arm tetraazamacrocycles.

One of the first examples of alkali metal ion complexation by this class of ligand is the complexation of  $\text{Li}^+$ ,  $\text{Na}^+$  and  $\text{K}^+$  by 1,4,7,10-tetrakis(2-hydroxyethyl)-1,4,7,10-tetraazacyclododecane (THEC12).<sup>52-55</sup> The solid state structures of these complexes appear in Figure 5.3. In  $[\text{Li}(\text{THEC12})]^+$ ,  $[\text{Na}(\text{THEC12})]^+$  and  $[\text{K}(\text{THEC12})]^+$ ,  $\text{Li}^+$ ,  $\text{Na}^+$  and  $\text{K}^+$  are bound by all four nitrogens of the tetraaza ring and one, three and four oxygens of the hydroxyethyl pendant arms, respectively. It is apparent that the mode of complexation of THEC12 is substantially dependent on the size of the metal ion, with an increase in coordination number as the ionic radius of the metal ion increases. There is clearly a three dimensional arrangement of donor atoms about the complexed cation, which may be compared with the three dimensional arrangement of donor atoms in cryptands. As a consequence, it is anticipated that the pendant arm tetraaza macrocyclic ligands should demonstrate some of the complexation properties of the cryptands, since it is the three dimensional cavity possessed by the cryptands that gives rise to the high thermodynamic stability of their complexes and the high selectivity observed in their complexation of alkali and alkaline earth metal ions. Prior to this work, it has been shown that THEC12 is able to form stable complexes with alkali metal ions, but little is known about their solution chemistry.<sup>56</sup> This study aims to understand the thermodynamic and kinetic aspects of the complexation of alkali metal ions by pendant arm tetraaza macrocycles through 1,4,7,10-tetrakis(2-methoxyethyl)-1,4,7,10-tetraazacyclododecane or TMEC12 (Figure 5.2).

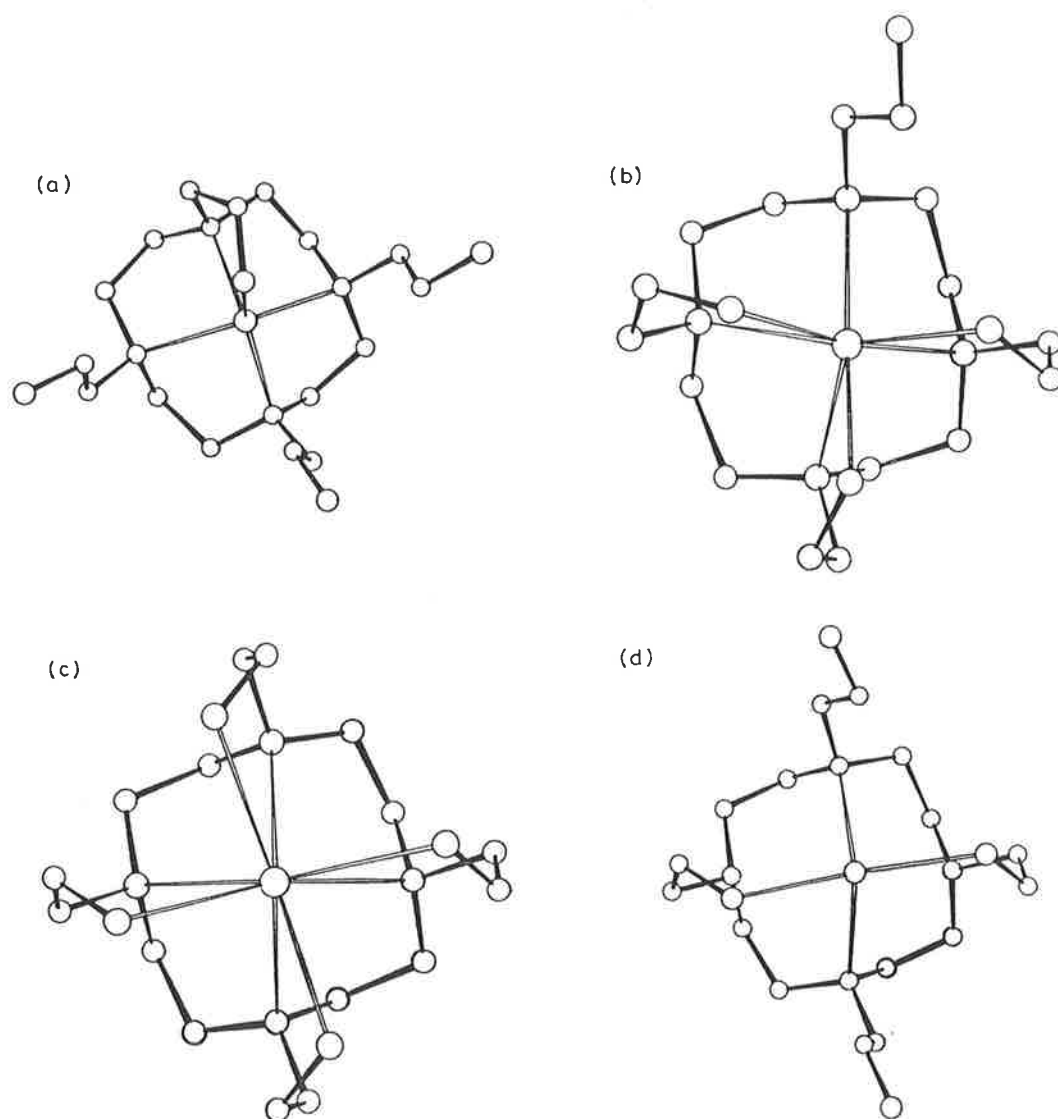


**Figure 5.3.** Solid state structures of the alkali metal complexes of THEC12. (a)  $[\text{Li}(\text{THEC12})]^+ \cdot 0.52$  (b)  $[\text{Na}(\text{THEC12})]^+ \cdot 0.53$  (c)  $[\text{K}(\text{THEC12})]^+ \cdot 0.53$  (d)  $\text{THEC12} \cdot \text{H}_2\text{O} \cdot 0.54$

Pendant arm tetraaza macrocycles such as TMEC12 should prove effective complexing agents for alkali metal ions since they are closely related to Gokel's lariat ethers,<sup>57-58</sup> which are simply crown ethers and polyaza crown ethers with pendant arms (Figure 5.4). These compounds were synthesised in order to study and mimic the antibiotic valinomycin (see Chapter 1) by combining the three dimensionality of the cryptands with the flexibility of the crown ethers.<sup>58</sup> The complexation of alkali metal ions by lariat ethers has been studied extensively in solution and the solid state, where it is apparent that the pendant arms play a major role in the binding of the cation.<sup>58-63</sup> There are a number of thermodynamic and kinetic studies of alkali metal complexes of the bibracchial lariat ethers shown in Figure 5.4.<sup>61-63</sup> In solution, these lariat ethers show similar complexation properties to those exhibited by the cryptands. However, their greater structural flexibility results in these lariat ethers showing less selectivity in their complexation of alkali metal ions and the resultant complexes are considerably less stable and more labile than their cryptate analogues. The relative ease of synthesis and the possibility of varying structural characteristics such as macrocyclic ring size and the number and nature of the coordinating pendant arms suggests that a new field of alkali metal chemistry should evolve with the pendant arm tetraaza macrocyclic ligands.

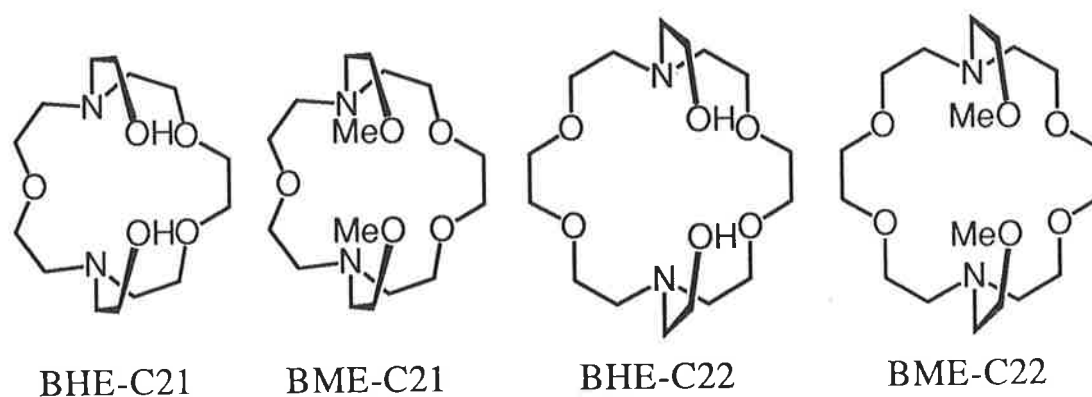


**Figure 5.4.** Structures of *N*-pivot bibracchial lariat ethers based on the diaza crown ethers C21 and C22.

The specific aims of this section of the study are to examine the complexation of a range of monovalent and divalent metal ions by the ligand TMEC12 in aqueous solution and in several non-aqueous solvents. These results are compared with similar data for the parent macrocycle cyclen, THEC12 and the fourteen membered pendant arm tetraaza macrocycle TMEC14 (Figure 5.2). This allows an assessment of the effects of i) the pendant arms; ii) varying the nature of the donor group of the pendant arm and iii) increasing the size of the macrocyclic ring while retaining the same donor group. The complexation of metal ions by TMEC12 and these related ligands should both contrast with and complement the studies of metal ion complexation by the cryptands C22C<sub>2</sub> and C22C<sub>8</sub> discussed in the previous chapters.

- 1 Lindoy, L.F. *"The Chemistry of Macrocyclic Ligand Complexes"*, Cambridge University Press, Cambridge, England, **1989**.
- 2 Melson, G.A. *"Coordination Chemistry of Macrocyclic Compounds"*, Plenum, New York, **1979**.
- 3 Cabiness, D.K.; Margerum, D.W. *J. Am. Chem. Soc.* **1970**, 92, 2151.
- 4 Jackels, S.C.; Farmery, K.; Barefield, E.K.; Rose, N.J.; Busch, D.H. *Inorg. Chem.* **1972**, 11, 2893-2901.
- 5 Hinz, F.P.; Margerum, D.W. *Inorg. Chem.* **1974**, 13, 2941-2949.
- 6 Kodama, M.; Kimura, E. *J. Chem. Soc., Dalton Trans.* **1976**, 116-120.
- 7 Kodama, M.; Kimura, E. *J. Chem. Soc., Dalton Trans.* **1976**, 1720-1724.
- 8 Kodama, M.; Kimura, E. *J. Chem. Soc., Dalton Trans.* **1976**, 2341-2345.
- 9 Anichini, A.; Fabbrizzi, L.; Paoletti, P.; Clay, R.M. *J. Chem. Soc., Dalton Trans.* **1978**, 577-583.
- 10 Clay, R.M.; McCormac, H.; Micheloni, M.; Paoletti, P. *Inorg. Chem.* **1982**, 21, 2494-2496.
- 11 Fabrizzi, L. *Comments Inorg. Chem.* **1985**, 4, 33.
- 12 Barefield, E.K.; Freeman, G.M.; Van Derveer, D.G. *Inorg. Chem.* **1986**, 25, 552-558.
- 13 Kodama, M.; Kimura, E. *J. Chem. Soc., Dalton Trans.* **1980**, 327-333.
- 14 Kato, M.; Ito, T. *Inorg. Chem.* **1985**, 24, 504-508.
- 15 Fujita, E.; Szalda, D.J.; Creutz, C.; Sutin, N. *J. Am. Chem. Soc.* **1988**, 110, 4870-4871.
- 16 Szalda, D.J.; Fujita, E.; Creutz, C. *Inorg. Chem.* **1989**, 28, 1446-1450 and references therein.
- 17 Kimura, E.; Shiota, T.; Koike, T.; Shiro, M.; Kodama, M. *J. Am. Chem. Soc.* **1990**, 112, 5805-5811 and references therein.
- 18 Kaden, T.A. *Top. Curr. Chem.* **1984**, 121, 157-179.
- 19 Murase, I.; Mikuriya, M.; Sonoda, H.; Kida, S. *J. Chem. Soc., Chem. Commun.* **1984**, 692.
- 20 Murase, I.; Mikuriya, M.; Sonoda, H.; Fukuda, Y.; Kida, S. *J. Chem. Soc., Dalton Trans.* **1986**, 953-959.
- 21 Murase, I.; Ueda, I.; Marubayashi, N.; Kida, S.; Matsumoto, N.; Kudo, M.; Toyohara, M.; Hiata, K.; Mikuriya, M. *J. Chem. Soc., Dalton Trans.* **1990**, 2763-2769.
- 22 Asato, E.; Toftlund, H.; Kida, S.; Mikuriya, M.; Murray, K.S. *Inorg. Chim. Acta.* **1989**, 165, 207-214.
- 23 Vuckovic, G.; Asato, E.; Matsumoto, N.; Kida, S. *Inorg. Chim. Acta.* **1990**, 171, 45-52.
- 24 Takahashi, M.; Takamoto, S. *Bull. Chem. Soc. Jpn.* **1977**, 50, 3413-3414.

- 25 Hafliger, H.; Kaden, T.A. *Helv. Chim. Acta.* **1979**, 62, 683-688.
- 26 Alcock, N.W.; Balakrishnan, K.P.; Berry, A.; Moore, P.; Reader, C.J. *J. Chem. Soc., Dalton Trans.* **1988**, 1089-1093.
- 27 Sayer, B.A.; Michael, J.P.; Hancock, R.D. *Inorg. Chim. Acta.* **1983**, 77, 63-64.
- 28 Clarke, P.; Hounslow, A.M.; Keough, R.A.; Lincoln, S.F.; Wainwright, K.P. *Inorg. Chem.* **1990**, 29, 1793-1797.
- 29 Clarke, P.; Lincoln, S.F.; Wainwright, K.P. *Inorg. Chem.* **1991**, 30, 134-139.
- 30 Hancock, R.D. *Perspect. Coord. Chem.* **1993**, 129-151.
- 31 Stetter, H.; Frank, W. *Angew. Chem. Int. Ed. Engl.* **1976**, 15, 686.
- 32 Kapsprzyk, S.P.; Wilkins, R.G. *Inorg. Chem.* **1982**, 21, 3349-3352.
- 33 Madeyski, C.M.; Michael, J.P.; Hancock, R.D. *Inorg. Chem.* **1984**, 23, 1487-1489.
- 34 van der Merwe, M.J.; Boeyens, J.C.A.; Hancock, R.D. *Inorg. Chem.* **1985**, 24, 1208-1213.
- 35 Alcock, N.W.; Balakrishnan, K.P.; Moore, P. *J. Chem. Soc., Dalton Trans.* **1986**, 1743-1745.
- 36 Evers, A.; Hancock, R.D.; Murase, I. *Inorg. Chem.* **1986**, 25, 2160-2163.
- 37 Adam, K.R.; Leong, A.J.; Lindoy, L.F.; Hendry, P.; Smith, S.V.; Yellowlees, D. *J. Coord. Chem.* **1988**, 19, 189-196.
- 38 Tschudin, D.; Kaden, T.A. *Pure. Appl. Chem.* **1988**, 60, 489-493.
- 39 Wainwright, K.P. *J. Chem. Soc., Dalton Trans.* **1980**, 2117-2120.
- 40 Kaden, T.A. *Pure. Appl. Chem.* **1988**, 60, 1117-1122.
- 41 Weitzel, F.L.; Raymond, K.N. *J. Am. Chem. Soc.* **1979**, 101, 2728-2731.
- 42 Studer, M.; Kaden, T.A.; Mäcke, H.R. *Helv. Chim. Acta.* **1990**, 73, 149-153.
- 43 Moi, M.K.; Yanuck, M.; Deshpande, S.V.; Hope, H.; deNardo, S.J.; Meares, C.F. *Inorg. Chem.* **1987**, 26, 3458-3463.
- 44 Parker, D.; Morphy, J.R.; Jankowski, K.; Cox, J. *Pure. Appl. Chem.* **1989**, 61, 1637-1641.
- 45 Adam, K.R.; McCool, B.J.; Leong, A.J.; Lindoy, L.F.; Ansell, C.W.G.; Baillie, P.J.; Dancey, K.P.; Drummond, L.A.; Henrick, K.; McPartlin, M.; Uppal, D.K.; Tasker, P.A. *J. Chem. Soc., Dalton Trans.* **1990**, 3435-3444.
- 46 Adams, H.; Bailey, N.A.; Fenton, D.E.; Ford, I.G.; Kitchen, S.J.; Williams, M.G.; Tasker, P.A.; Leong, A.J.; Lindoy, L.F. *J. Chem. Soc., Dalton Trans.* **1991**, 1665-1674.



- 47 Hancock, R.D. *Pure. Appl. Chem.* **1986**, 58, 1445-1452.
- 48 Hancock, R.D.; Bhavan, R.; Wade, P.W.; Boeyens, J.C.A.; Dobson, S.M. *Inorg. Chem.* **1989**, 28, 187-194.
- 49 Hancock, R.D.; Martell, A.E. *Chem. Rev.* **1989**, 89, 1875-1914.
- 50 Hancock, R.D. *Pure. Appl. Chem.* **1993**, 65, 941-946.
- 51 Izatt, R.M.; Pawlak, K.; Bradshaw, J.S.; Bruening, R.L. *Chem. Rev.* **1991**, 91, 1721.
- 52 Groth, P. *Acta Chem. Scand.* **1983**, A37, 71-74.
- 53 Groth, P. *Acta Chem. Scand.* **1983**, A37, 283-291.
- 54 Groth, P. *Acta Chem. Scand.* **1983**, A37, 75-77.
- 55 Buoen, S.; Dale, J.; Groth, P.; Krane, J. *J. Chem. Soc., Chem. Commun.* **1982**, 1172-1174.
- 56 Turonek, M.L.; Clarke, P.; Laurence, G.S.; Lincoln, S.F.; Pittet, P-A.; Politis, S.; Wainwright, K.P. *Inorg. Chem.* **1993**, 32, 2195-2198.
- 57 Gokel, G. "*Crown Ethers and Cryptands*", The Royal Society of Chemistry, Cambridge, **1991**.
- 58 Gokel, G.W. *Chem. Soc. Rev.* **1992**, 39-47.
- 59 Gandour, R.D.; Fronczek, F.R.; Gatto, V.J.; Minganti, C.; Schultz, R.A.; White, B.D.; Arnold, K.A.; Mazzocchi, D.; Miller, S.R.; Gokel, G.W. *J. Am. Chem. Soc.* **1986**, 108, 4078.
- 60 Arnold, K.A.; Echevoyen, L.; Fronczek, F.R.; Gandour, R.D.; Gatto, V.J.; White, B.D.; Gokel, G.W. *J. Am. Chem. Soc.* **1987**, 109, 3716.
- 61 Rodopoulos, T.; Pittet, P-A.; Lincoln, S.F. *J. Chem. Soc., Dalton Trans.* **1993**, 1055-1060.
- 62 Lucas, J.B.; Lincoln, S.F. *J. Chem. Soc., Dalton Trans.* **1994**, 423-427.
- 63 Lucas, J.B.; Lincoln, S.F. *Inorg. Chim. Acta.* **1994**, 219, 217-220.

# Chapter 6: Equilibrium Studies of Monovalent Metal Complexes of TMEC12

## 6.1 Introduction

The complexation of a monovalent metal ion,  $M^+$ , by TMEC12 is described by Equation 6.1;



where the stability constant,  $K_s$ , is given by;

$$K_s = \frac{[M(\text{TMEC12})^+]}{[M^+][\text{TMEC12}]} \quad 6.2$$

The complexation of alkali metal ions by pendant arm tetraaza macrocyclic ligands has been studied in the solid state,<sup>1-4</sup> but has been sparsely studied in solution.<sup>5</sup> However, many of the factors determining the stabilities of the alkali metal complexes of cryptands<sup>6-14</sup> and lariat ethers<sup>15-17</sup> should also be important for these complexes. These include the ionic radius and solvation energy of the metal ion, the number and type of ligand donor atoms and the flexibility of the ligand.

The dominant factor determining the stabilities of the alkali metal cryptates is the relative sizes of the metal ion and the cryptand cavity.<sup>6-9,13</sup> In contrast, studies of metal complexes of tetraaza macrocyclic ligands have demonstrated that the macrocyclic ring size has little influence on complex stability,<sup>18-26</sup> except for very small rings and where the ring is structurally reinforced, where the macrocyclic ring is particularly rigid.<sup>18,21-26,27</sup> Unlike the cryptands, these ligands do not have a single preferred conformer with a rigid cavity that leads to a size match selectivity for metal ions. Instead, the ligand has several conformers of similar energy, but with different metal ion size preferences, and the metal ion selectivity of these ligands is governed by the relative stabilities of these conformers.<sup>20,23</sup> Metal ions that are too large to fit within the cavity of the tetraaza macrocyclic ligand are simply coordinated out of the plane of the tetraaza ring.<sup>23</sup> In this case, the size of the macrocyclic

cavity is unimportant and complex stability is governed by the same factors that control the stability in open-chain polyamine ligands, namely, the size of the chelate ring formed on complex formation.<sup>18-26</sup> Molecular mechanics calculations<sup>18,26</sup> have shown that the minimum strain energy in five membered chelate rings occurs with metal-nitrogen bond lengths of 2.5 Å and a N-M-N bond angle of 69°. These parameters correspond to the coordination of a fairly large metal ion, with an ionic radius of ~1.0 Å. The corresponding parameters for six membered chelate rings are metal-nitrogen bond lengths of 1.6 Å and a N-M-N bond angle of 109.5°, which are consistent with the coordination of a small metal ion. Thus, the presence of five membered chelate rings increases the selectivity of the tetraaza macrocyclic ligand for large metal ions over small metal ions, whereas the presence of six membered chelate rings favours the complexation of small metal ions.<sup>18-26</sup>

Studies of the complexes of pendant arm tetraaza macrocycles have shown that the metal ion selectivity of the parent macrocycle is often retained by its pendant arm derivative.<sup>21,22,24</sup> Thus, the main factor in determining the stability of these complexes remains the size of the chelate rings formed on complex formation. The attachment of pendant arms containing oxygen donor atoms to a tetraaza macrocycle leads to an increase in the denticity of the parent ligand, but an increase in steric crowding when the metal ion is coordinated. Generally, the effect of these substituents is to increase the selectivity of the ligand for large metal ions over small metal ions, not only because larger metal ions more readily adopt higher coordination numbers without steric strain, but also because the additional oxygen donor atoms form part of a five membered chelate ring when complexing the metal ion.<sup>19,21-22,24</sup> This study examines these aspects through the complexation of a range of monovalent and divalent metal ions by 1,4,7,10-tetrakis(2-methoxyethyl)-1,4,7,10-tetraazacyclododecane (TMEC12). Little is known of the complexation properties of such ligands with the alkali metal ions. Accordingly, this chapter examines the complexation of alkali metal ions and Ag<sup>+</sup> by TMEC12 in aqueous solution and in a range of non-aqueous solvents. In Chapter 7 the factors governing complex stability for a number of divalent transition metal and heavy metal complexes of TMEC12 in aqueous solution are determined and these are contrasted with those for the alkali metal ions.

## 6.2 Stability of $[M(\text{TMEC12})]^+$ in Non-Aqueous Solution

The stability constants of  $[M(\text{TMEC12})]^+$ , where  $M^+ = \text{Li}^+, \text{Na}^+, \text{K}^+, \text{Rb}^+, \text{Cs}^+$  and  $\text{Ag}^+$ , have been determined in a number of non-aqueous solvents and water and appear in Table 6.1. In the oxygen donor solvents studied, TMEC12 shows a moderate selectivity for  $\text{Na}^+$ , with the stabilities of the alkali metal complexes,  $[M(\text{TMEC12})]^+$ , being in the sequence  $\text{Li}^+ < \text{Na}^+ > \text{K}^+ > \text{Rb}^+ > \text{Cs}^+$  in methanol and dimethylformamide. However, in acetonitrile, the selectivity of TMEC12 for  $\text{Na}^+$  over  $\text{Li}^+$  is reversed, and  $[\text{Li}(\text{TMEC12})]^+$  is more stable than  $[\text{Na}(\text{TMEC12})]^+$ . These trends are now discussed in more detail.

In the solid state structures of  $[M(\text{THEC12})]^+$ ,  $\text{Li}^+$ ,  $\text{Na}^+$  and  $\text{K}^+$  are bound by one, three and four hydroxy groups, respectively, and all four nitrogens of the tetraaza ring.<sup>1-3</sup> In these structures, THEC12 (Figure 6.1) adopts the TRANS I conformation (Figure 6.2), where  $M^+$  is bound above the plane of the tetraaza ring. A similar pattern is likely for  $[M(\text{TMEC12})]^+$ . If these coordination numbers are exhibited by  $[M(\text{TMEC12})]^+$  in solution, then the lower coordination number of  $\text{Li}^+$  may account for the selectivity of TMEC12 for  $\text{Na}^+$  over  $\text{Li}^+$ . However, <sup>13</sup>C NMR studies<sup>28</sup> of  $[\text{Li}(\text{TMEC12})]^+$  and  $[\text{Na}(\text{TMEC12})]^+$  in *d*<sub>4</sub>-methanol (see Chapter 9) have demonstrated that although the ligand adopts the TRANS I conformation, both  $\text{Li}^+$  and  $\text{Na}^+$  are eight coordinate. As it is probable that the larger  $\text{K}^+$ ,  $\text{Rb}^+$  and  $\text{Cs}^+$  are also eight coordinate, it is unlikely that the variations in the stabilities of  $[M(\text{TMEC12})]^+$  result from different coordination numbers for  $M^+$ .

It is apparent from molecular models that when TMEC12 adopts the TRANS I conformation, it is able to form a cavity which is defined by the four nitrogens of the macrocyclic ring and the four oxygens of the methoxyethyl pendant arms. The selectivity of TMEC12 for  $\text{Na}^+$  in the oxygen donor solvents suggests that  $\text{Na}^+$  is of optimum size, although the flexibility of the ligand means that this is difficult to rationalise in terms of the matching of the size of  $\text{Na}^+$  and the size of the TMEC12 cavity. This selectivity is probably coincident with  $\text{Na}^+$  establishing optimum bonding distances and minimising strain in  $[\text{Na}(\text{TMEC12})]^+$  by comparison with the other  $[M(\text{TMEC12})]^+$  complexes. In all solvents studied, the stabilities of  $[M(\text{TMEC12})]^+$  decrease in the order  $\text{Na}^+ > \text{K}^+ > \text{Rb}^+ > \text{Cs}^+$ , which is probably consistent with a systematic decrease in the charge density of  $M^+$  and an increase in strain in

**Table 6.1.** Stability Constants<sup>a</sup> for the Complexation of Monovalent Metal Ions<sup>b</sup> by 1,4,7,10-tetrakis(2-methoxyethyl)-1,4,7,10-Tetraazacyclododecane, TMEC12, at 298.2 K.

solvent	$D_N^c$	$\log(K_s/\text{dm}^3 \text{ mol}^{-1})$					
		[Li(TMEC12)] <sup>+</sup>	[Na(TMEC12)] <sup>+</sup>	[K(TMEC12)] <sup>+</sup>	[Rb(TMEC12)] <sup>+</sup>	[Cs(TMEC12)] <sup>+</sup>	[Ag(TMEC12)] <sup>+</sup>
acetonitrile <sup>d</sup>	14.1	9.34 ± 0.05	9.13 ± 0.05	6.07 ± 0.05	4.85 ± 0.05	3.55 ± 0.05	12.30 ± 0.05
propylene-carbonate <sup>e</sup>	15.1	8.0 ± 0.1	8.2 ± 0.1	6.7 ± 0.1	6.1 ± 0.1		15.3 ± 0.1
methanol <sup>d</sup>	19.0	4.1 ± 0.1	6.2 ± 0.1	3.9 ± 0.1	3.0 ± 0.1	2.5 ± 0.1	14.2 ± 0.1
	(23.5) <sup>f</sup>						
dimethyl-formamide <sup>d</sup>	26.6	3.61 ± 0.05	5.68 ± 0.05	3.62 ± 0.05	2.73 ± 0.05	2.28 ± 0.05	13.73 ± 0.05
dimethyl-sulphoxide <sup>d</sup>	29.8	2.82 ± 0.05	4.95 ± 0.05				11.48 ± 0.05
water <sup>d,g</sup>	18.0	<2	2.20 ± 0.05	<2	<2	<2	12.62 ± 0.05
	(33.0) <sup>f</sup>						

<sup>a</sup> In 0.050 mol dm<sup>-3</sup> NEt<sub>4</sub>ClO<sub>4</sub> supporting electrolyte. <sup>b</sup> Reference 29. The six and eight coordinate ionic radii (Å), respectively, are as follows: Li<sup>+</sup>, 0.76 and 0.92; Na<sup>+</sup>, 1.02 and 1.18; K<sup>+</sup>, 1.38 and 1.51; Rb<sup>+</sup>, 1.52 and 1.61; Cs<sup>+</sup>, 1.67 and 1.74; Ag<sup>+</sup>, 1.15 and 1.28. <sup>c</sup> Gutmann donor number from reference 30. <sup>d</sup> This work. <sup>e</sup> Reference 31. <sup>f</sup> Gutmann donor number from references 32 and 33. <sup>g</sup> Determined by pH titration in 0.10 mol dm<sup>-3</sup> NEt<sub>4</sub>ClO<sub>4</sub> supporting electrolyte.

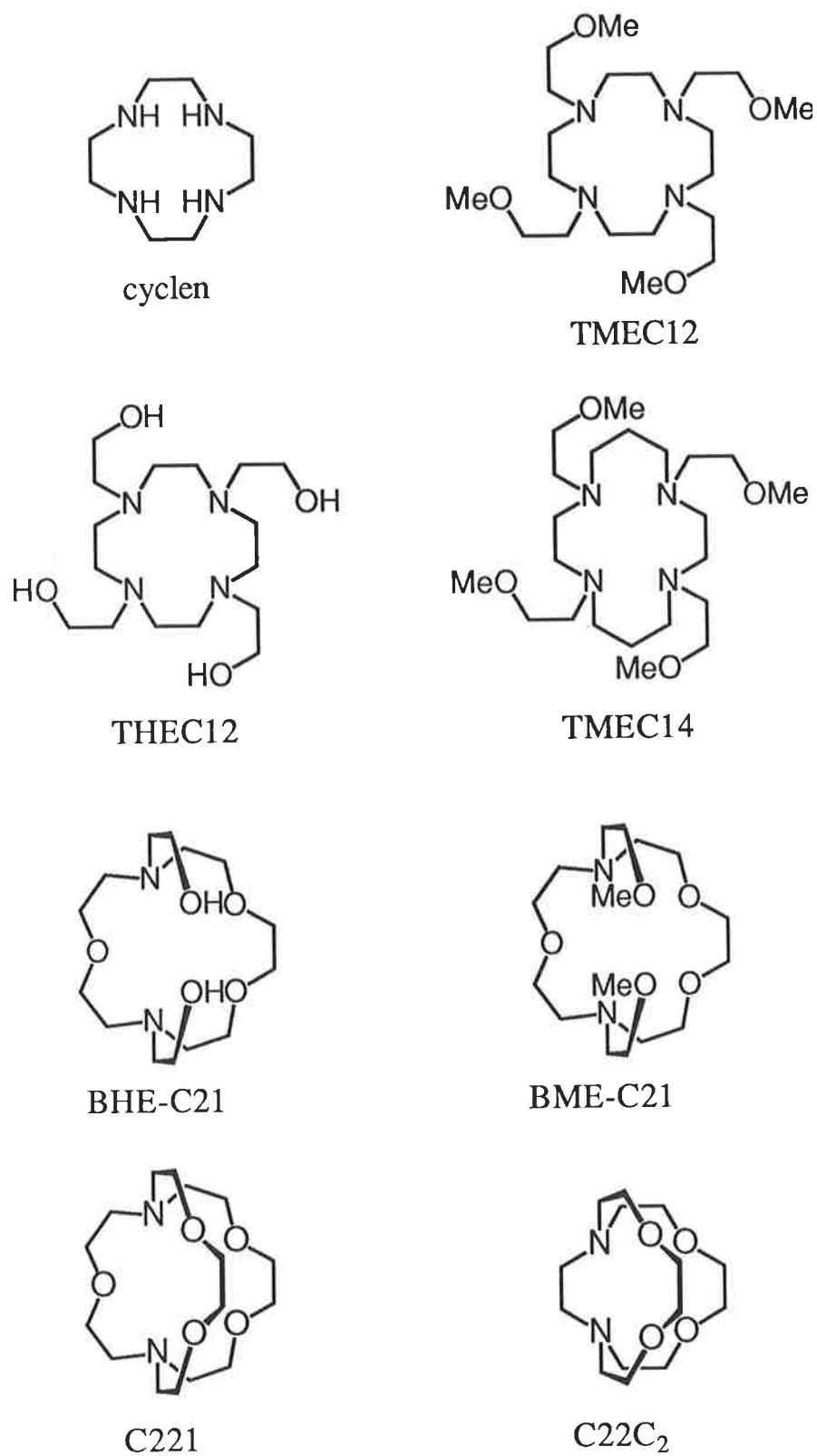


**Figure 6.1.** Structures of TMEC12 and the ligands discussed in this chapter.

$[M(\text{TMEC12})]^+$  as the size of  $M^+$  increases. Despite  $\text{Li}^+$  being eight coordinate, the small size of  $\text{Li}^+$  probably results in greater steric hindrance between coordinating pendant arms in  $[\text{Li}(\text{TMEC12})]^+$  by comparison with the other  $[M(\text{TMEC12})]^+$  complexes. This may prevent  $\text{Li}^+$  from bonding with the oxygen donor atoms of the pendant arms as effectively as the larger alkali metal ions, with the result that  $[\text{Li}(\text{TMEC12})]^+$  is less stable than  $[\text{Na}(\text{TMEC12})]^+$  in the oxygen donor solvents. However, the selectivity of TMEC12 for  $\text{Na}^+$  over  $\text{Li}^+$  is dependent on the nature of the solvent, and in acetonitrile  $[\text{Li}(\text{TMEC12})]^+$  is more stable than  $[\text{Na}(\text{TMEC12})]^+$ , as discussed below.

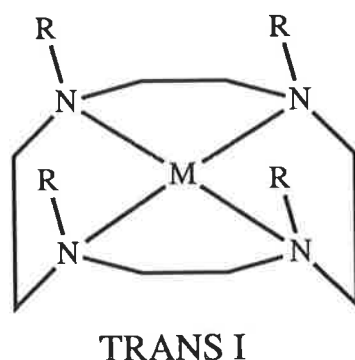


**Figure 6.2.** The TRANS I conformer of the 1,4,7,10-tetraazacyclododecane ring. The pendant arms, R, are shown as uncoordinated.

### 6.3 Effect of Solvent on Complex Stability

The variation in the stability of the alkali metal complexes,  $[M(\text{TMEC12})]^+$ , with the nature of the solvent is similar to that observed with the alkali metal cryptates of  $\text{C22C}_2$  and  $\text{C22C}_8$  in Chapter 2, with complex stability decreasing as the Gutmann donor number<sup>30</sup> of the solvent ( $D_N$ ) increases. The low stabilities of  $[\text{Na}(\text{TMEC12})]^+$  and  $[\text{Ag}(\text{TMEC12})]^+$  in water probably result from a combination of the large  $D_N$  of water, and its ability to form hydrogen bonds. As discussed in Chapter 2, hydrogen bonding between the ligand donor atoms and protic solvents may lead to a decrease in complex stability, since these interactions must be disrupted in complex formation.

A similar variation in stability with  $D_N$  is observed with  $[\text{Ag}(\text{TMEC12})]^+$  in most solvents, but not in acetonitrile and dimethylsulfoxide, where the stabilities of  $[\text{Ag}(\text{TMEC12})]^+$  are particularly low. However, as discussed in Appendix i, the relationship between  $D_N$  and the solvation energy of  $M^+$  is not always applicable. Table 2.6 (Chapter 2) shows that the solvation energy of  $\text{Ag}^+$  in acetonitrile and dimethylsulfoxide is relatively high, when compared with that of the alkali metal ions in these solvents. The high solvation energy of  $\text{Ag}^+$  in acetonitrile may be attributed to the soft acid nature of  $\text{Ag}^+$ ,<sup>34-35</sup> which results in a high affinity of  $\text{Ag}^+$  for the nitrogen donor atom of acetonitrile.<sup>36-37</sup> The apparently anomalous solvation energy of  $\text{Ag}^+$  in dimethylsulfoxide may be resolved when the ambidentate nature of this solvent is taken into account. Dimethylsulfoxide is an ambidentate ligand, and will bind the hard acid alkali metal ions through the hard oxygen donor atom. However, the soft acid  $\text{Ag}^+$  will be bound through the sulfur donor atom,<sup>38</sup> which is a softer base than both oxygen and nitrogen donor atoms and thus, the solvation energy of  $\text{Ag}^+$  in dimethylsulfoxide is very high. A similar effect has been observed for the  $\text{Ag}^+$  cryptates of C211, C221 and C222, which are all less stable in dimethylsulfoxide than in water.<sup>39</sup>

## 6.4 Effect of Solvent on Selectivity

An unusual aspect of the complexation properties of TMEC12 is the influence of the solvent on the relative stabilities of  $[\text{M}(\text{TMEC12})]^+$ . In water, dimethylsulfoxide, dimethylformamide, methanol and propylene carbonate,  $[\text{Na}(\text{TMEC12})]^+$  is more stable than  $[\text{Li}(\text{TMEC12})]^+$ . However in the weak donor solvent acetonitrile, a reversal in the relative stabilities of  $[\text{Na}(\text{TMEC12})]^+$  and  $[\text{Li}(\text{TMEC12})]^+$  occurs, with  $\text{Li}^+$  forming the most stable complex. This contrasts with the alkali metal cryptates, where the selectivity of the cryptands for the alkali metal ions is essentially independent of solvent.<sup>39</sup> It is apparent that the greater structural flexibility of TMEC12 allows the nature of the solvent to have a greater effect on the metal ion selectivity of TMEC12 than is the case with the alkali metal cryptates. This is discussed in detail below.

This phenomenon is best explained by considering the complexation free energy in solution,  $\Delta G^0$ , to be largely the difference between the solvation free energy of  $M^+$ ,  $\Delta G_s$ , and the ligand binding energy,  $\Delta G_b$ . This is simply the complexation free energy in the absence of solvent, and is a measure of the affinity of the ligand for the metal ion. The selectivity of a ligand for  $M^+$



depends on how  $\Delta G_b$  varies with respect to  $\Delta G_s$  and clearly depends on the donor atom stereochemistry and flexibility of the ligand. This is qualitatively illustrated in Figure 6.3, where  $\Delta G_b$  and  $\Delta G^0$  for a rigid and flexible ligand, together with  $\Delta G_s$  for both a strong and a weak donor solvent are plotted as a function of the ionic radius of  $M^+$ . In order to relate the following arguments to experimental results, TMEC12 represents the flexible ligand, whereas the  $Na^+$  selective cryptand, C221, represents the rigid ligand.

Curve (a) of Figure 6.3 shows the variation of  $\Delta G_b$  with ionic radius for C221. The solvation energy of  $M^+$  increases inversely with the ionic radius. The same would be true for  $\Delta G_b$  only if the ligand were able to adjust to all cation sizes. For C221,  $\Delta G_b$  increases as the size of  $M^+$  decreases until it reaches that of  $Na^+$ , corresponding to the optimum fit of this cation into the cavity of C221. For smaller cations,  $\Delta G_b$  levels off and eventually remains constant since the cavity of C221 cannot easily contract in order to maintain optimum contact between  $M^+$  and the cryptand binding sites. There is a critical ionic radius, below which  $\Delta G_b$  no longer increases. Curve (b) shows the variation of  $\Delta G_b$  with ionic radius for TMEC12. Although optimum bonding distances and minimum strain are probably attained in  $[Na(TMEC12)]^+$ , the flexibility of this ligand allows it to adjust its stereochemistry more readily to variations in the size of  $M^+$  than can C221. Thus, for TMEC12, the critical ionic radius will be smaller than that for C221 and the variation of  $\Delta G_b$  with the size of  $M^+$  more closely resembles that of  $\Delta G_s$  (curves (c) and (d)).

The complexation free energies in solution,  $\Delta G^0$ , for  $[MC221]^+$  and  $[M(TMEC12)]^+$ , are essentially the differences between  $\Delta G_b$  and  $\Delta G_s$  for each ligand. Curves (g) and (h) show the variation of  $\Delta G^0$  with ionic radius for C221 and TMEC12, respectively, in a strong donor solvent. The most stable complexes are  $[NaC221]^+$  and  $[Na(TMEC12)]^+$ , which correspond to the maximum differences between  $\Delta G_b$  and  $\Delta G_s$  ( $\Delta G_{max}$ ) for C221 and TMEC12, respectively. For C221, cations larger than  $Na^+$  cannot fit within the cryptand cavity and thus, the stabilities of  $[MC221]^+$  decrease in the sequence  $Na^+ > K^+ > Rb^+ > Cs^+$  in both the strong and the weak donor solvents. For TMEC12, both  $\Delta G_b$  and  $\Delta G_s$  decrease with increasing ionic radius for cations larger than  $Na^+$ . However, since TMEC12 binds  $M^+$  more strongly than does the solvent,  $\Delta G_b$  decreases at a greater rate than does  $\Delta G_s$ . Thus, the stabilities of  $[M(TMEC12)]^+$  decrease in the sequence  $Na^+ > K^+ > Rb^+ > Cs^+$  in both solvents. In the strong donor solvent, both C221 and TMEC12 are selective for  $Na^+$  over  $Li^+$  only as a result of the higher solvation energy of  $Li^+$  compared

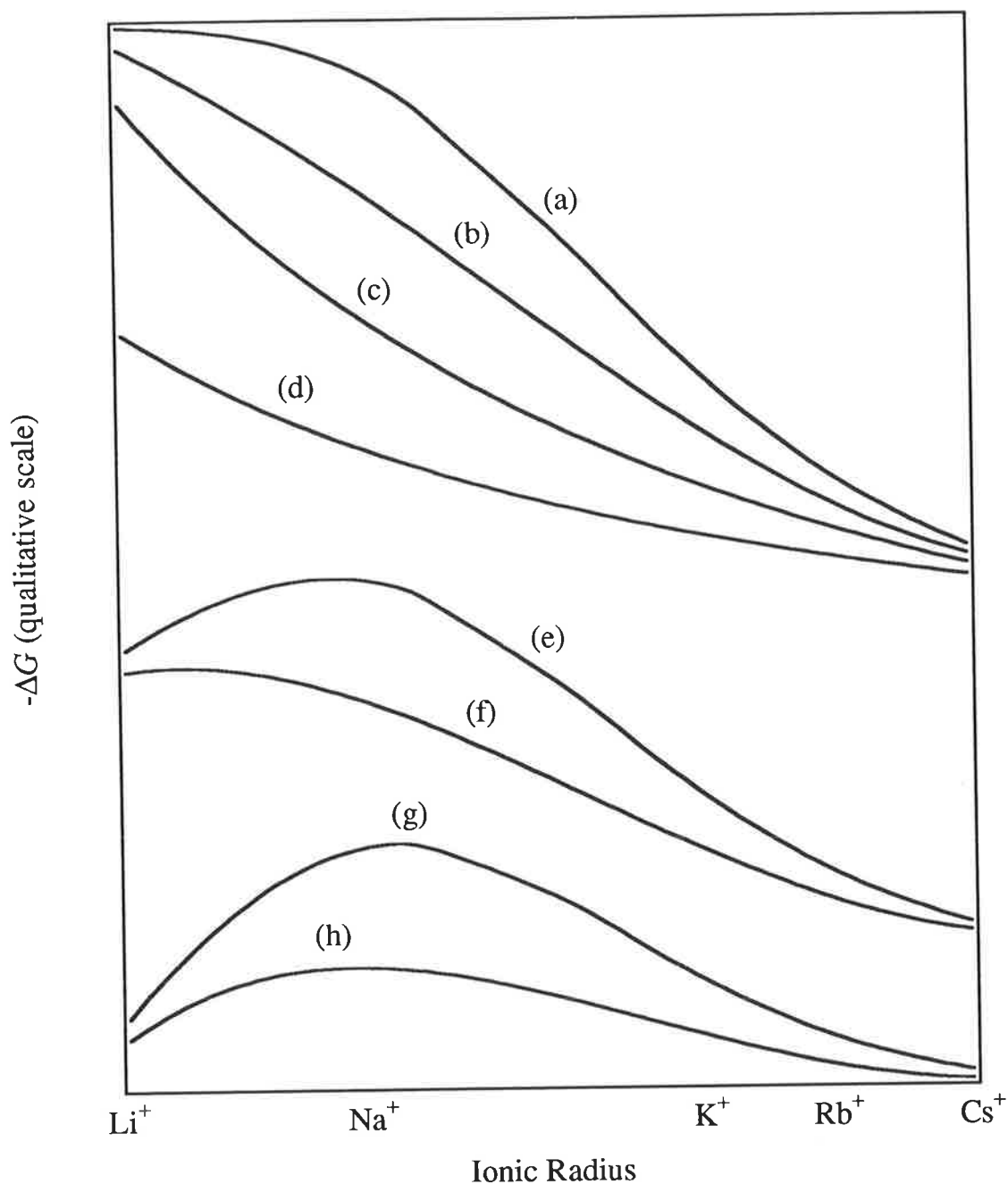


**Figure 6.3.** Curve (a); variation of  $\Delta G_b$  for the rigid ligand C221. (b); variation of  $\Delta G_b$  for the flexible ligand, TMEC12. (c); variation of  $\Delta G_s$  for a strong donor solvent. (d); variation of  $\Delta G_s$  for a weak donor solvent. (e); variation of  $\Delta G^0$  for C221 in a weak donor solvent. (f); variation of  $\Delta G^0$  for TMEC12 in a weak donor solvent. (g); variation of  $\Delta G^0$  for C221 in a strong donor solvent. (h); variation of  $\Delta G^0$  for TMEC12 in a strong donor solvent. Both C221 and TMEC12 are  $\text{Na}^+$  selective in the strong donor solvent. In the weak donor solvent C221 is  $\text{Na}^+$  selective but the selectivity of TMEC12 has shifted from  $\text{Na}^+$  to  $\text{Li}^+$ .

with that of  $\text{Na}^+$ . However, in the absence of solvent, flexible TMEC12 binds  $\text{Li}^+$  more strongly relative to  $\text{Na}^+$  than does the rigid C221 and as a consequence, the selectivity of TMEC12 for  $\text{Na}^+$  over  $\text{Li}^+$  is considerably less than that of C221.

Curves (e) and (f) show the variation of  $\Delta G^0$  with ionic radius for C221 and TMEC12, respectively, in a weak donor solvent. On going from a strong donor solvent to a weak donor solvent, the complexation of  $\text{Li}^+$  is favoured relative to that of  $\text{Na}^+$ . As shown in Figure 6.3, this is because the difference in solvation energy between these ions is smaller in weak donor solvents (curve (d)) than in strong donor solvents (curve (c)).<sup>40</sup> From Figure 6.3 it is apparent that as the solvent varies, the change in the relative solvation energies of  $\text{M}^+$  causes a change in the relative stabilities of both  $[\text{MC221}]^+$  and  $[\text{M}(\text{TMEC12})]^+$  and a concomitant change in the position of  $\Delta G_{\text{max}}$  to a smaller ionic radius. The cavity of C221 is quite rigid, so that changes in solvent are generally unable to significantly alter the position of  $\Delta G_{\text{max}}$  and C221 remains  $\text{Na}^+$  selective in the weak donor solvent. In contrast, small changes in the relative solvation energies of  $\text{Li}^+$  and  $\text{Na}^+$  are able to significantly alter the position of  $\Delta G_{\text{max}}$  for flexible TMEC12. Thus, the selectivity of TMEC12 changes from  $\text{Na}^+$  to  $\text{Li}^+$  in going from the strong donor solvent to the weak donor solvent.

This argument readily accounts for the change in relative stabilities from  $[\text{Na}(\text{TMEC12})]^+ > [\text{Li}(\text{TMEC12})]^+$  in the oxygen donor solvents to  $[\text{Li}(\text{TMEC12})]^+ > [\text{Na}(\text{TMEC12})]^+$  in the weak donor solvent acetonitrile. Quantitative support for this argument is presented in Table 6.2. For example, the difference between the solvation energies of  $\text{Li}^+$  and  $\text{Na}^+$  is  $101.95 \text{ kJ mol}^{-1}$  in dimethylsulfoxide ( $D_{\text{N}} = 29.8$ ), but only  $90.25 \text{ kJ mol}^{-1}$  in acetonitrile ( $D_{\text{N}} = 14.1$ ). Thus,  $\text{Li}^+$  complexes are favoured over  $\text{Na}^+$  complexes by  $11.7 \text{ kJ mol}^{-1}$  in acetonitrile relative to dimethylsulfoxide, which corresponds to a change in relative stability ( $\delta \log K_{\text{S}}$ ) of 2.05 log units. This largely accounts for the change in the stability of  $[\text{Li}(\text{TMEC12})]^+$  relative to  $[\text{Na}(\text{TMEC12})]^+$  ( $\Delta \Delta \log K_{\text{S}}$ ) in going from dimethylsulfoxide to acetonitrile (2.34 log units). The differences between  $\delta \log K_{\text{S}}$  and  $\Delta \Delta \log K_{\text{S}}$  observed in Table 6.2 indicate that for a flexible ligand such as TMEC12, small effects such as variations in the solvation energy of  $[\text{M}(\text{TMEC12})]^+$  may also be important in determining the relative stabilities of the  $[\text{M}(\text{TMEC12})]^+$  complexes.

**Table 6.2.** The Influence of Changes in the Relative Solvation Energies<sup>a</sup> of Alkali Metal Ions on the Stabilities of [M(TMEC12)]<sup>+</sup> at 298.2 K.

solvent	$D_N$	$\Delta\Delta G_s$	$\delta G_s$	$\delta \log K_s$	$\Delta \log K_s$	$\Delta\Delta \log K_s$
		(kJ mol <sup>-1</sup> )	(kJ mol <sup>-1</sup> )			
dimethyl- sulfoxide	29.8 <sup>b</sup>	101.95	11.7	2.05	2.13	2.34
dimethyl- formamide	26.6 <sup>b</sup>	99.85	9.6	1.68	2.07	2.28
methanol	23.5 <sup>c</sup>	104.50	14.25	2.50	2.1	2.31
propylene- carbonate	15.1 <sup>b</sup>	93.25	3.00	0.53	0.20	0.41
acetonitrile	14.1 <sup>b</sup>	90.25	0.00	0.00	-0.21	0.00

<sup>a</sup> Values of the hydration free energies of M<sup>+</sup> were taken from reference 41. These were combined with the transfer free energies of these ions from water to the non-aqueous solvent (reference 42) to give  $\Delta G_s(M^+)$ , the solvation free energy of M<sup>+</sup>. <sup>b</sup>  $D_N$  from reference 30.

<sup>c</sup>  $D_N$  from references 32 and 33.

The symbols in Table 6.2 are defined as follows;

$\Delta\Delta G_s = \Delta G_s(\text{Na}^+) - \Delta G_s(\text{Li}^+)$ , where  $\Delta G_s(M^+)$  is the solvation free energy of M<sup>+</sup>.

$\delta G_s = \Delta\Delta G_s(\text{solvent}) - \Delta\Delta G_s(\text{acetonitrile})$

Thus,  $\delta G_s$  is the difference between  $\Delta\Delta G_s$  for a given solvent and  $\Delta\Delta G_s$  for acetonitrile.

$$\delta \log K_s = \frac{\delta G_s}{2.303RT}$$

$\Delta \log K_s = \log K_s([\text{Na}(\text{TMEC12})]^+) - \log K_s([\text{Li}(\text{TMEC12})]^+)$

Thus,  $\Delta \log K_s$  is the difference in stabilities ( $\log(K_s/\text{dm}^3 \text{ mol}^{-1})$ ) between  $[\text{Na}(\text{TMEC12})]^+$  and  $[\text{Li}(\text{TMEC12})]^+$ .

$\Delta\Delta \log K_s = \Delta \log K_s(\text{solvent}) - \Delta \log K_s(\text{acetonitrile})$

Thus,  $\Delta\Delta \log K_s$  is the difference between  $\Delta \log K_s$  for a given solvent and  $\Delta \log K_s$  for acetonitrile.

Similar changes in selectivity are seen for THEC12 (Table 6.3) and the flexible lariat ethers BHE-C21 and BME-C21 (Figure 6.1), where the stability sequence  $[\text{NaL}]^+ > [\text{LiL}]^+$  in dimethylformamide changes to  $[\text{LiL}]^+ > [\text{NaL}]^+$  in acetonitrile.<sup>16-17,28</sup> In the commonly studied solvents, there is no such reversal in stability for the alkali metal cryptates, where the most stable cryptate always corresponds to the metal ion whose size matches that of the cryptand cavity.<sup>39</sup> However, despite the rigidity of the cryptands, in the very weak donor solvent nitromethane ( $D_N = 2.7$ <sup>30</sup>), the selectivity of C222 for  $\text{K}^+$  shifts to  $\text{Na}^+$ .<sup>43</sup> This is because in such a poorly solvating medium, complexation of  $\text{Na}^+$  is enormously favoured relative to that of  $\text{K}^+$ , when compared with complexation in stronger donor solvents.

The number of pendant arms coordinated to the metal ion may also vary depending on the solvent. This may also tend to influence the selectivity of TMEC12 as the solvent is varied. In *d*<sub>4</sub>-methanol, the <sup>13</sup>C NMR spectra of both  $[\text{Li}(\text{TMEC12})]^+$  and  $[\text{Na}(\text{TMEC12})]^+$  are consistent with  $\text{M}^+$  being eight coordinate (Chapter 9).<sup>28</sup> In solution, the methoxyethyl arms of TMEC12 will be in competition with the solvent for coordination of the metal ion. If no solvent molecule has displaced a pendant arm in methanol, it is unlikely that this will occur in the weaker donor solvents acetonitrile and propylene carbonate. The stronger donor solvents, dimethylformamide, dimethylsulfoxide and water, will compete more strongly with the pendant arms for coordination of  $\text{M}^+$  than will methanol. However, in these solvents, the difference in stability between  $[\text{Li}(\text{TMEC12})]^+$  and  $[\text{Na}(\text{TMEC12})]^+$  is similar to that in methanol, and it is likely that both  $\text{Li}^+$  and  $\text{Na}^+$  remain eight coordinate.

## 6.5 A Comparison of the Alkali Metal Complexes of TMEC12, C221 and C22C<sub>2</sub>

The selectivity pattern of TMEC12 for the alkali metal ions is similar to those of the  $\text{Na}^+$  selective cryptands C22C<sub>2</sub> and C221 (Table 6.3). However, the selectivity of TMEC12 for  $\text{M}^+$  is lower than that exhibited by C22C<sub>2</sub> and C221 and in general the stabilities of the alkali metal complexes of TMEC12 are also lower. A similar relationship exists for THEC12.<sup>5</sup> As discussed previously, the lower selectivity of TMEC12 and THEC12 is a result of their greater flexibility, which allows them to adjust their stereochemistry according to the size of  $\text{M}^+$  more readily than the less flexible C22C<sub>2</sub> and C221. The greater stabilities of these cryptates suggests that the rigid array of donor

**Table 6.3.** Stability Constants<sup>a</sup> for the Complexation of Monovalent Metal Ions by TMEC12 and Other Ligands at 298.2 K

ligand	$\log(K_s/\text{dm}^3 \text{ mol}^{-1})$					
	Li <sup>+</sup>	Na <sup>+</sup>	K <sup>+</sup>	Rb <sup>+</sup>	Cs <sup>+</sup>	Ag <sup>+</sup>
acetonitrile						
TMEC12 <sup>b</sup>	9.34	9.13	6.07	4.85	3.55	12.30
THEC12 <sup>c</sup>	8.07	6.66	3.40	3.00	2.90	9.35
TMEC14 <sup>d</sup>	4.64	4.03	3.37	3.32	3.25	8.48
cyclen <sup>e</sup>	6.90	3.60	2.90	2.82	2.78	9.43
C221 <sup>f</sup>	10.33	>11.3	9.5	7.27	5.15	11.24
C22C <sub>2</sub>	7.88	9.4 <sup>b</sup>	7.2 <sup>b</sup>	5.9 <sup>b</sup>	5.0 <sup>b</sup>	9.48
propylene carbonate						
TMEC12 <sup>b</sup>	8.0	8.2	6.7	6.1		15.3
THEC12 <sup>c</sup>	8.90	7.49	5.91	4.23	4.04	14.00
cyclen <sup>e</sup>	5.60	5.45	4.78	4.10		11.25
C221 <sup>f</sup>	9.60	12.09	9.88	7.03	4.92	18.50
methanol						
TMEC12 <sup>b</sup>	4.1	6.2	3.9	3.0	2.5	14.2
THEC12 <sup>h</sup>	3.09	4.53	2.43	2.20	1.90	12.57
TMEC14 <sup>d</sup>	2.65	2.82	3.02	2.91	2.69	10.32
C221 <sup>f</sup>	5.38	9.65	8.54	6.74	4.33	14.64
dimethylformamide						
TMEC12 <sup>b</sup>	3.61	5.68	3.62	2.73	2.28	13.73
THEC12 <sup>h</sup>	2.99	3.37	1.59	1.39	1.23	11.16
TMEC14 <sup>d</sup>	2.37	2.42	2.48	2.45	2.40	9.70
cyclen <sup>b</sup>	2.1	<2	<2	<2	<2	9.1
C221 <sup>f</sup>	3.58	7.93	6.66	5.35	3.61	12.41
C22C <sub>2</sub>	3.58	6.1 <sup>b</sup>	3.2 <sup>b</sup>	2.8 <sup>b</sup>	2.7 <sup>b</sup>	9.48

<sup>a</sup> In 0.050 mol dm<sup>-3</sup> NEt<sub>4</sub>ClO<sub>4</sub> supporting electrolyte. <sup>b</sup> This work. <sup>c</sup> Reference 28. <sup>d</sup> Reference 44. <sup>e</sup> Reference 31. <sup>f</sup> Reference 39. <sup>g</sup> Reference 45. <sup>h</sup> Reference 5.

atoms and the preformed cavity of C221 and C22C2 engenders a greater stability on their alkali metal complexes than the more flexible array of donor atoms present in the pendant arm tetraaza macrocycles TMEC12 and THEC12. As discussed below, this effect may be of entropic origin.

The stability constants of  $[\text{Na}(\text{TMEC12})]^+$  have also been determined at 288.2 K and 308.2 K in aqueous solution ( $I = 0.10 \text{ mol dm}^{-3} \text{ NEt}_4\text{ClO}_4$ ), in order to determine the enthalpy ( $\Delta H_c$ ) and entropy ( $\Delta S_c$ ) of complexation. At 288.2 K, 298.2 K and 308.2 K,  $\log(K_s/\text{dm}^3 \text{ mol}^{-1}) = 2.27 \pm 0.03$ ,  $2.20 \pm 0.05$  and  $2.03 \pm 0.04$ , respectively. This yields  $\Delta H_c = -20.5 \pm 5.5 \text{ kJ mol}^{-1}$  and  $\Delta S_c = -27.3 \pm 17.8 \text{ J mol}^{-1} \text{ K}^{-1}$ . The negative  $\Delta S_c$  probably arises from the decrease in the number of conformations available to TMEC12 that occurs on complexation of  $\text{Na}^+$ , which counterbalances the increase in entropy that results from the release of water molecules coordinated to  $\text{Na}^+$ . These data contrast with those characterising  $[\text{NaC221}]^+$  in aqueous solution,<sup>46</sup> where  $\Delta H_c = -22.4 \text{ kJ mol}^{-1}$  and  $\Delta S_c = 25.9 \text{ J mol}^{-1} \text{ K}^{-1}$  ( $\log K_s = 5.4$  at 298.2 K<sup>47</sup>). This demonstrates that in aqueous solution, the difference between the stabilities of  $[\text{NaC221}]^+$  and  $[\text{Na}(\text{TMEC12})]^+$  is largely of entropic origin, probably because the loss of conformational entropy that occurs on complexation is greater for the more flexible TMEC12, compared with C221, which possesses a preformed cavity which matches the size of  $\text{Na}^+$ . However, more data in a range of solvents is needed before a more definite conclusion may be drawn, especially considering the large errors associated with the data characterising  $[\text{Na}(\text{TMEC12})]^+$ .

## 6.6 Stability of $[\text{M}(\text{cyclen})]^+$ in Non-Aqueous Solution

The stabilities of  $[\text{M}(\text{cyclen})]^+$  (Figure 6.1), where  $\text{M}^+ = \text{Li}^+, \text{Na}^+, \text{K}^+, \text{Rb}^+, \text{Cs}^+$  and  $\text{Ag}^+$ , have been determined in dimethylformamide and appear in Table 6.3, together with those in acetonitrile and propylene carbonate taken from the literature.<sup>31</sup> The stabilities of  $[\text{M}(\text{cyclen})]^+$  are in the sequence  $\text{Li}^+ > \text{Na}^+ > \text{K}^+ > \text{Rb}^+ > \text{Cs}^+$  in acetonitrile and propylene carbonate. These results suggest that as the ionic radius of  $\text{M}^+$  decreases, there is a corresponding increase in the electrostatic attraction between  $\text{M}^+$  and cyclen. Thus, both the ligand binding energy and the solvation energy of  $\text{M}^+$  increase with decreasing ionic radius. However, as a result of the macrocyclic effect,<sup>36</sup> cyclen binds  $\text{M}^+$  more strongly than does the solvent, so that the stabilities of  $[\text{M}(\text{cyclen})]^+$  increase as the ionic radius of  $\text{M}^+$  decreases.

In dimethylformamide, acetonitrile and propylene carbonate, the stabilities of  $[M(\text{TMEC12})]^+$  are several orders of magnitude greater than those of  $[M(\text{cyclen})]^+$ . This is consistent with the binding of  $M^+$  by the methoxyethyl arms increasing the stabilities of  $[M(\text{TMEC12})]^+$  relative to those of  $[M(\text{cyclen})]^+$ . A similar relationship is observed for  $[M(\text{THEC12})]^+$  (Table 6.3). This effect is also enhanced by the preference of alkali metal ions for the hard oxygen donor atoms over the softer nitrogen donor atoms. As a result of their coordinating pendant arms, TMEC12 and THEC12 are able to form a three dimensional cavity which can encapsulate the metal ion more effectively compared to the two dimensional cavity of cyclen. The presence of this cavity gives rise to the selectivity of the two pendant arm ligands for  $\text{Na}^+$  and also enhances the stability of their complexes by comparison with those of cyclen. This is analogous to the macrobicyclic effect observed with the alkali metal cryptates (Chapter 2).

## 6.7 Effect of the Nature of the Pendant Arm on Complex Stability

In methanol and dimethylformamide, the selectivity patterns of the alkali metal complexes of TMEC12 and THEC12 are similar and both ligands are  $\text{Na}^+$  selective (Table 6.3). This is probably a result of the similar size and arrangement of donor atoms in these two pendant arm tetraaza macrocycles, both of which have the same twelve membered tetraaza ring. The selectivity of TMEC12 and THEC12 for  $\text{Na}^+$  over  $\text{Li}^+$  in these solvents probably results from the ability of these ligands to establish optimum bonding distances with  $\text{Na}^+$  but not  $\text{Li}^+$ . However, it is apparent that this preference of TMEC12 and THEC12 for  $\text{Na}^+$  over  $\text{Li}^+$  is only marginal, since both ligands are selective for  $\text{Li}^+$  in acetonitrile and THEC12 is also selective for  $\text{Li}^+$  in propylene carbonate. This emphasises that while the selectivity of these ligands largely arises from their ability to form a cavity of appropriate size for  $M^+$ , their flexibility means that this is not simply a result of the preference of the ligand for a metal ion of a particular size, as is the case with the cryptands. It is more correct to regard the selectivity of such flexible ligands for alkali metal ions as resulting from the balance between the solvation energy of  $M^+$  and the ligand binding energy, as discussed in Section 6.4.

Although the selectivity patterns of TMEC12 and THEC12 are similar, the selectivity of TMEC12 among the alkali metal ions is greater than that of THEC12 (Table 6.3). Any steric hindrance between coordinating pendant arms



would be greater in  $[M(\text{TMEC12})]^+$  than in  $[M(\text{THEC12})]^+$  as a result of the methyl group on the coordinating oxygen of the pendant arm of TMEC12. Thus, TMEC12 exhibits less stereochemical flexibility than THEC12 and as a result, the selectivity of TMEC12 is greater.

Although the selectivity of TMEC12 for  $M^+$  (where  $M^+$  is an alkali metal ion or  $\text{Ag}^+$ ) resembles that of THEC12, the stabilities of  $[M(\text{TMEC12})]^+$  are significantly higher than those of  $[M(\text{THEC12})]^+$  in all solvents studied (except for  $\text{Li}^+$  in propylene carbonate). The relative stabilities of  $[M(\text{TMEC12})]^+$  and  $[M(\text{THEC12})]^+$  for a given  $M^+$  result from a balance between three major factors; i) the inductive effect of the methyl group; ii) the steric effect of the methyl group and iii) the hydrogen bonding capacity of THEC12.

As a result of the inductive effect of the methyl group, the methoxy donor group is a stronger Lewis base (electron pair donor) than the hydroxy donor group.<sup>24</sup> However, this is counterbalanced by the presence of the methyl group on the coordinating oxygen, which may give rise to steric hindrance and reduce its coordinating ability, particularly with TMEC12, with four pendant arms on the small twelve membered tetraaza ring. The third factor that may contribute to the different stabilities of  $[M(\text{TMEC12})]^+$  and  $[M(\text{THEC12})]^+$  is the ability of the hydroxyethyl pendant arms to form hydrogen bonds. Two types of hydrogen bonding may exist; i) intramolecular hydrogen bonding between the hydroxy groups of the pendant arms of THEC12<sup>4</sup> and ii) intermolecular hydrogen bonding between the hydroxy groups and the solvent. Both of these effects would decrease the tendency of the pendant arms of THEC12 to bind to  $M^+$ , which would have a destabilising effect on  $[M(\text{THEC12})]^+$  by comparison with  $[M(\text{TMEC12})]^+$ , where no possibility for hydrogen bonding exists.

Since the stabilities of  $[M(\text{TMEC12})]^+$  are always greater than those of  $[M(\text{THEC12})]^+$ , it is apparent that the inductive effect of the methyl group and the ability of THEC12 to form hydrogen bonds outweigh the steric effect of the methyl group. However, the differences between the stabilities of  $[M(\text{TMEC12})]^+$  and  $[M(\text{THEC12})]^+$  ( $\Delta\log K_s$ ) are not constant for a given solvent as  $M^+$  is varied. The effect of hydrogen bonding in THEC12 will be constant if all four pendant arms are used to bind  $M^+$ . The inductive effect causes  $\Delta\log K_s$  to increase as the ionic radius of  $M^+$  decreases, whereas the steric effect causes  $\Delta\log K_s$  to decrease as the ionic radius of  $M^+$  decreases. The

result of these two counteracting effects is that  $\Delta \log K_s$  is generally at a maximum for  $\text{Na}^+$ . As  $\Delta \log K_s$  tends to be much smaller for  $\text{Li}^+$  than for the other alkali metal ions, this suggests that the steric effect is much greater for the smaller  $\text{Li}^+$ . Thus, the  $\text{Na}^+/\text{Li}^+$  selectivity is greater for TMEC12 than for THEC12, and a reversal in this selectivity is observed for TMEC12 only in acetonitrile, whereas a reversal occurs for THEC12 in both acetonitrile and propylene carbonate.

## 6.8 Effect of Macrocyclic Ring Size on Complex Stability

The related ligand TMEC14,<sup>44</sup> which has identical pendant arms to TMEC12 but a fourteen membered tetraaza ring (Figure 6.1), forms alkali metal complexes,  $[\text{M}(\text{TMEC14})]^+$ , which are of significantly lower stability than those of  $[\text{M}(\text{TMEC12})]^+$  and the selectivity of TMEC14 for  $\text{M}^+$  is minimal (Table 6.3). It is apparent that the donor atom stereochemistry of TMEC12, which possesses a twelve membered tetraaza ring, is more favourable for the complexation of alkali metal ions than that of TMEC14. Nevertheless, the difference between the stabilities of  $[\text{M}(\text{TMEC14})]^+$  and  $[\text{M}(\text{TMEC12})]^+$  decreases as the size of  $\text{M}^+$  increases, with the result that  $[\text{Cs}(\text{TMEC14})]^+$  is usually more stable than  $[\text{Cs}(\text{TMEC12})]^+$ . This is consistent with TMEC14 being able to form a larger cavity than can TMEC12, which should result in TMEC14 favouring the complexation of larger metal ions, when compared with TMEC12. Unfortunately, the solution structures of  $[\text{M}(\text{TMEC14})]^+$  are unknown, which precludes a more detailed comparison.

## 6.9 $\text{Ag}^+$ Complexes

In all solvents studied,  $[\text{Ag}(\text{TMEC12})]^+$  is more stable than the corresponding alkali metal complexes. This is a result of the soft acid nature of  $\text{Ag}^+$ ,<sup>34-35</sup> which results in  $\text{Ag}^+$  having a far greater affinity for the four nitrogens of the tetraaza ring than the hard acid alkali metal ions.<sup>36-37</sup> However, in the nitrogen donor solvent acetonitrile, the stabilities of the alkali metal species  $[\text{M}(\text{TMEC12})]^+$  increase relative to that of  $[\text{Ag}(\text{TMEC12})]^+$ , since the solvation energy of  $\text{Ag}^+$  is much higher than those of the alkali metal ions in this nitrogen donor solvent. Similar trends are observed for THEC12 and cyclen (Table 6.3).

The observation that the stability of  $[\text{Ag}(\text{TMEC12})]^+$  is greater than that of  $[\text{Ag}(\text{cyclen})]^+$  is consistent with the binding of  $\text{Ag}^+$  by the methoxyethyl pendant arms. In addition, the donor strength of tertiary amines is greater than that of secondary amines,<sup>24</sup> which should result in an increase in stability for complexes of TMEC12 compared with those of cyclen.

The greater stability of  $[\text{Ag}(\text{TMEC12})]^+$  compared with that of  $[\text{Ag}(\text{TMEC14})]^+$  suggests that  $\text{Ag}^+$  ( $r = 1.28 \text{ \AA}$ ), which has a similar ionic radius to  $\text{Na}^+$  ( $r = 1.18 \text{ \AA}$ ), is of closer to optimum size for TMEC12 compared with the larger TMEC14. In addition, five membered chelate rings coordinate large metal ions with less strain than do six membered chelate rings, as discussed in Section 6.1. In  $[\text{Ag}(\text{TMEC12})]^+$ , there are four five membered chelate rings in which both donor atoms are nitrogen (nitrogen chelate rings), whereas in  $[\text{Ag}(\text{TMEC14})]^+$ , there are two five membered and two six membered nitrogen chelate rings, and as a consequence,  $\text{Ag}^+$  is complexed by TMEC12 with less strain when compared with TMEC14. However, the alkali metal complexes of TMEC12 and TMEC14 do not appear to follow these predictions, which should result in the complexes of TMEC14 becoming more stable relative to those of TMEC12 as the size of  $\text{M}^+$  decreases. The effect of the nitrogen chelate ring size appears to be less important for complexes of the hard acid alkali metal ions, which bind preferentially with oxygen donor atoms over nitrogen donor atoms and which lack directionality in their metal-ligand bonds.<sup>18</sup> For the alkali metal complexes of TMEC12 and TMEC14, the ability of the ligand to form a cavity of appropriate size when complexing  $\text{M}^+$  is probably the dominant factor determining complex stability.

- 1 Buøen, S.; Dale, J.; Groth, P.; Krane, J. *J. Chem. Soc., Chem Commun.* **1982**, 1172-174.
- 2 Groth, P. *Acta Chem. Scand.* **1983**, A37, 71-77.
- 3 Groth, P. *Acta Chem. Scand.* **1983**, A37, 283-291.
- 4 Grace, D.S.B.; Krane, J. *J. Chem. Research (S)*. **1983**, 162-163.
- 5 Turonek, M.L.; Clarke, P.; Laurence, G.S.; Lincoln, S.F.; Pittet, P-A.; Politis, S.; Wainwright, K.P. *Inorg. Chem.* **1993**, 32, 2195-2198.
- 6 Lehn, J-M. *Struct. Bonding (Berlin)*. **1973**, 16, 1-69.
- 7 Lehn, J-M.; Sauvage, J-P. *J. Am. Chem. Soc.* **1975**, 97, 6700-6707.
- 8 Cox, B.G.; Garcia-Rosas, J.; Schneider, H. *J. Am. Chem. Soc.* **1981**, 103, 1384-1389.
- 9 Lincoln, S.F.; Brereton, I.M.; Spotswood, T.M. *J. Am. Chem. Soc.* **1986**, 108, 8134-8138.
- 10 Clarke, P.; Abou-Hamdan, A.; Hounslow, A.M.; Lincoln, S.F. *Inorg. Chim. Acta.* **1988**, 154, 83-87.
- 11 Lincoln, S.F.; Abou-Hamdan, A. *Inorg. Chem.* **1990**, 29, 3584-3589.
- 12 Buschmann, H-J. *Inorg. Chim. Acta.* **1986**, 125, 31-35.
- 13 Lehn, J-M. *Acc. Chem. Res.* **1978**, 11, 49-57.
- 14 Lincoln, S.F.; Stephens, A.K.W. *Inorg. Chem.* **1992**, 31, 5067.
- 15 Lincoln, S.F.; Lucas, J.B. *Inorg. Chim. Acta.* **1994**, 219, 217-220.
- 16 Rodopoulos, T.; Pittet, P-A.; Lincoln, S.F. *J. Chem. Soc., Dalton Trans.* **1993**, 1055.
- 17 Lincoln, S.F.; Lucas, J.B. *J. Chem. Soc., Dalton Trans.* **1994**, 423-427.
- 18 Hancock, R.D.; Wade, P.W.; Ngwenya, M.P.; de Sousa, A.S.; Damu, K.V. *Inorg. Chem.* **1990**, 29, 1968-1974.
- 19 Hancock, R.D. *Pure Appl. Chem.* **1993**, 65, 941-946.
- 20 Hancock, R.D. *Acc. Chem. Res.* **1990**, 23, 253-257.
- 21 Hancock, R.D.; Bhavan, R.; Wade, P.W.; Boeyens, J.C.A.; Dobson, S.M. *Inorg. Chem.* **1989**, 28, 187-194.
- 22 Hancock, R.D. *Pure Appl. Chem.* **1986**, 58, 1445-1452.
- 23 Hancock, R.D. Martell, A.E. *Chem. Rev.* **1989**, 89, 1875-1914.
- 24 Hancock, R.D. *Perspect. Coord. Chem.* **1993**, 65, 941-946.
- 25 Thöm, V.J.; Hosken, G.D.; Hancock, R.D. *Inorg. Chem.* **1985**, 24, 3378-3381.
- 26 Hancock, R.D. *Prog. Inorg. Chem.* **1989**, 37, 187.
- 27 Lindoy, L.F. *"The Chemistry of Macrocyclic Ligand Complexes"*, Cambridge University Press, Cambridge, U.K, **1989**.
- 28 Lincoln, S.F.; Dhillon, R. Unpublished material.

- 29 Shannon, R.D.; *Acta Crystallogr., Sect. A.: Cryst. Phys. Diffr., Theor. Gen. Crystallogr.* **1976**, A32, 751-767.
- 30 Gutmann, V. "*Coordination Chemistry in Non-Aqueous Solutions*", Springer-Verlag, Wien, **1968**.
- 31 Lincoln, S.F.; Whitbread, S. Unpublished material.
- 32 Erlich, R.H.; Roach, E.; Popov, A.I. *J. Am. Chem. Soc.* **1970**, 92, 4989-4990.
- 33 Dewitte, W.J.; Popov, A.I. *J. Soln. Chem.* **1976**, 5, 231-240.
- 34 Pearson, R.G. *J. Am. Chem. Soc.* **1963**, 85, 3533.
- 35 Pearson, R.G. *Coord. Chem. Rev.* **1990**, 100, 403.
- 36 Cotton, F.A.; Wilkinson, G. "*Advanced Inorganic Chemistry*", 3rd ed, Interscience, New York, **1980**.
- 37 Buschmann, H-J. *Inorg. Chim. Acta.* **1985**, 102, 95-98.
- 38 Ducommun, Y.; Helm, L.; Merbach, A.E.; Hellquist, B.; Elding, L.I. *Inorg. Chem.* **1989**, 28, 377.
- 39 Cox, B.G.; Garcia-Rosas, J.; Schneider, H. *J. Am. Chem. Soc.* **1981**, 103, 1384-1389.
- 40 Burgess, J. "*Metal Ions in Solution*", Ellis Horwood, Chichester, **1978**.
- 41 Noyes, R.M. *J. Am. Chem. Soc.* **1962**, 84, 513-522.
- 42 Cox, B.G.; Firman, P.; Garcia-Rosas, J.; Schneider, H. *Tetrahedron. Lett.* **1982**, 23, 3777-3780.
- 43 de Namor, A.F.D.; Ghouseini, L.; Lee, W.H. *J. Chem. Soc., Faraday Trans 1.* **1985**, 81, 2495-2502.
- 44 Lincoln, S.F.; Lucas, J.B. Unpublished material.
- 45 Lincoln, S.F.; Abou-Hamdan, A. *Inorg. Chem.* **1991**, 30, 462-466.
- 46 Kauffmann, E.; Lehn, J-M.; Sauvage, J-P. *Helv. Chim. Acta.* **1976**, 59, 1099-1111
- 47 Lehn, J-M.; Sauvage, J-P. *J. Am. Chem. Soc.* **1975**, 97, 6700-6707.

# Chapter 7: Equilibrium Studies of Divalent Metal Complexes of TMEC12

## 7.1 Protonation Constants of TMEC12

In aqueous solution at 298.2 K and  $I = 0.10 \text{ mol dm}^{-3}$  ( $\text{NEt}_4\text{ClO}_4$ ), the pendant arm tetraaza macrocycle TMEC12 behaves as a tetrabasic species. The four protonations of the ligand are described by Equations 7.1 - 7.4 and the protonation constants  $K_1$ ,  $K_2$ ,  $K_3$  and  $K_4$  are defined by Equations 7.5 - 7.8.



$$K_1 = \frac{[\text{HTMEC12}^+]}{[\text{H}^+][\text{TMEC12}]} \quad 7.5$$

$$K_2 = \frac{[\text{H}_2\text{TMEC12}^{2+}]}{[\text{H}^+][\text{HTMEC12}^+]} \quad 7.6$$

$$K_3 = \frac{[\text{H}_3\text{TMEC12}^{3+}]}{[\text{H}^+][\text{H}_2\text{TMEC12}^{2+}]} \quad 7.7$$

$$K_4 = \frac{[\text{H}_4\text{TMEC12}^{4+}]}{[\text{H}^+][\text{H}_3\text{TMEC12}^{3+}]} \quad 7.8$$

The protonation constants of TMEC12 appear in Table 7.1, together with those of some related ligands. The variations in the protonation constants of TMEC12 are consistent with the first two protonations occurring at the amine

groups diagonally opposed across the tetraaza ring such that electrostatic repulsions are minimised. The markedly decreased value of  $K_3$  is largely attributable to the third protonation occurring on an amine group adjacent to those already protonated, with a consequently considerable increase in electrostatic repulsion. An even greater electrostatic repulsion results when the fourth protonation occurs, with the consequence that  $K_4$  characterising TMEC12 is too low to be determined. It is likely that the nitrogens in  $H_3TMEC12^{3+}$  and  $H_4TMEC12^{4+}$  are all in the *exo* conformation, with the lone pairs directed away from the tetraaza ring, in order to minimise repulsions. As the size of the macrocyclic ring is increased, this electrostatic repulsion is decreased, with the consequence that the  $K_3$  and  $K_4$  values of TMEC14 are considerably higher than those of TMEC12.

The protonation constants  $K_1$  and  $K_2$  have also been determined at 288.2 K and 308.2 K ( $I = 0.10 \text{ mol dm}^{-3} \text{ NEt}_4\text{ClO}_4$ ) and appear in Table 7.1. From these data, it is possible to calculate the enthalpy and entropy for the first two protonations of TMEC12. The results calculated are as follows;

$$\begin{aligned}\Delta H_1 &= -34.9 \pm 4.3 \text{ kJ mol}^{-1}, \Delta S_1 = 91.4 \pm 13.8 \text{ J mol}^{-1} \text{ K}^{-1} \\ \Delta H_2 &= -49.3 \pm 4.1 \text{ kJ mol}^{-1}, \Delta S_2 = -10.7 \pm 13.3 \text{ J mol}^{-1} \text{ K}^{-1}\end{aligned}$$

Similar results have been obtained for 1,4,8,11-tetramethyl-1,4,8,11-tetraazacyclotetradecane,<sup>1</sup> and may be rationalised as follows. The first protonation occurs at any of the four equivalent TMEC12 nitrogens, which are in the *endo* conformation, with the lone pairs directed toward the inside of the tetraaza ring. This is an exothermic process, giving rise to the negative  $\Delta H_1$  observed. Under these conditions,  $HTMEC12^+$  will be only weakly solvated, because the small ring size and presence of the methoxyethyl pendant arms limit the extent to which water molecules may hydrogen bond to the protonated amine group. This factor, together with the release of water molecules associated with the proton, gives rise to the large, positive value of  $\Delta S_1$ . The second protonation will occur at the amine group diagonally opposed across the tetraaza ring. However, the  $\Delta H_2$  and  $\Delta S_2$  values are consistent with one or both protonated nitrogens in  $H_2TMEC12^{2+}$  adopting the *exo* conformation, which minimises electrostatic repulsion. In this case,  $H_2TMEC12^{2+}$  will be more extensively solvated than  $HTMEC12^+$ , which gives a negative contribution to both  $\Delta H_2$  and  $\Delta S_2$ , consistent with the observation that  $\Delta H_2 < \Delta H_1$  and  $\Delta S_2 < \Delta S_1$ . It is apparent that the increased solvation of

$H_2TMEC12^{2+}$  compensates for the greater electrostatic repulsion in  $H_2TMEC12^{2+}$ , when compared with  $HTMEC12^+$ .

The pendant arm tetraaza macrocycles TMEC12 and THEC12 show a lower basicity than their parent macrocycle cyclen. This is similar to the decreased basicity of linear tertiary amines compared with their secondary amine analogues.<sup>2-3</sup> The increased inductive effect that occurs with tertiary amine nitrogens is counterbalanced by the greater steric hindrance around a tertiary amine nitrogen, which limits the extent of solvation and hydrogen bonding that the tertiary ammonium group can undergo.<sup>2</sup> A similar relation exists between TMEC14 and cyclam (Table 7.1). (The pendant arm tetraaza macrocycles are strong complexers of alkali metal ions, so that when data is determined using alkali metal salts as the supporting electrolyte, the protonation constants are considerably lower than those determined in inert electrolyte. However, the stabilities of the alkali metal complexes of cyclen and cyclam in aqueous solution are likely to be very low, so that their effect on the protonation constants of cyclen and cyclam is probably negligible).

The protonation constants characterising the twelve membered pendant arm tetraaza macrocycles TMEC12 and THEC12 are quite similar. This demonstrates that the different donor groups (methoxy and hydroxy, respectively) of the pendant arms have little influence on the protonation of these ligands.

**Table 7.1.** Protonation Constants<sup>a</sup> for TMEC12 and Related Ligands at 298.2 K.

Ligand	$\log K_1$ $K_1/\text{dm}^3 \text{ mol}^{-1}$	$\log K_2$ $K_2/\text{dm}^3 \text{ mol}^{-1}$	$\log K_3$ $K_3/\text{dm}^3 \text{ mol}^{-1}$	$\log K_4$ $K_4/\text{dm}^3 \text{ mol}^{-1}$
cyclen <sup>b</sup>	11.32	9.72	<2.30	<2.30
TMEC12 <sup>c</sup>	$10.92 \pm 0.05$	$8.04 \pm 0.05$	$2.17 \pm 0.05$	<2.0
TMEC12 <sup>d</sup>	$11.09 \pm 0.01$	$8.38 \pm 0.02$		
TMEC12 <sup>e</sup>	$10.68 \pm 0.03$	$7.80 \pm 0.03$		
THEC12 <sup>f</sup>	10.74	8.16	1.94	<2.0
TMEC14 <sup>g</sup>	9.04	7.87	4.48	2.29
cyclam <sup>h</sup>	11.59	10.62	1.61	2.42

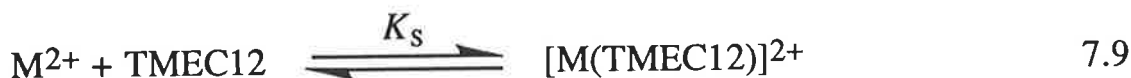
<sup>a</sup> In  $0.10 \text{ mol dm}^{-3} \text{ NEt}_4\text{ClO}_4$  except where stated otherwise. <sup>b</sup> Reference 4,  $0.10 \text{ mol dm}^{-3} \text{ NaNO}_3$ . <sup>c</sup> This work. <sup>d</sup> This work, 288.2 K. <sup>e</sup> This work, 308.2 K. <sup>f</sup> Reference 5.

<sup>g</sup> Reference 6. <sup>h</sup> Reference 7,  $0.5 \text{ mol dm}^{-3} \text{ KNO}_3$ .



## 7.2 Stability Constants of Divalent Metal Complexes of TMEC12

The complexation of a divalent metal ion,  $M^{2+}$ , by TMEC12 may be expressed as;



where the stability constant,  $K_s$ , is given by;

$$K_s = \frac{[M(\text{TMEC12})^{2+}]}{[M^{2+}][\text{TMEC12}]} \quad 7.10$$

The stability constants of a number of divalent metal complexes of TMEC12 have been determined in aqueous solution and appear in Table 7.2. The factors which may cause variations in the magnitude of  $K_s$  with the nature of  $M^{2+}$  are as follows: i) the size of the metal ions;<sup>8</sup> ii) the solvation energies of the metal ions;<sup>9</sup> iii) the relative hardness of the metal ions and their consequent variations in affinity for oxygen or nitrogen donor atoms<sup>10-11</sup> and iv) ligand field effects.<sup>12</sup> The various metal ions in Table 7.2 may be placed in groups according to the nature of  $M^{2+}$ . These groups are discussed in detail below.

### 7.2.1 Alkaline Earth Complexes

The alkaline earth complexes of TMEC12 are characterised by lower stabilities than their first-row transition metal analogues and the complexes of the heavy metal ions  $\text{Cd}^{2+}$ ,  $\text{Hg}^{2+}$  and  $\text{Pb}^{2+}$ . This is a result of the hard acid alkaline earth cations binding less strongly to the ligand nitrogen donor atoms than do the other metal ions in Table 7.2, which are either soft acids or borderline between hard and soft acids.

$^{13}\text{C}$  NMR studies of  $[\text{Ca}(\text{TMEC12})]^{2+}$  in  $d_4$ -methanol have shown  $\text{Ca}^{2+}$  is eight coordinate, bound to the tetraaza ring and all four methoxyethyl arms (Chapter 9).<sup>14</sup> The ligand is in the TRANS I configuration (Figure 7.1), in which the metal ion lies above the plane of the tetraaza ring and the coordination geometry is square antiprismatic. The coordination number and

**Table 7.2.** Stability Constants<sup>a</sup> for the Complexation of Divalent Metal Ions (M<sup>2+</sup>) by TMEC12 and Related Ligands at 298.2 K in Aqueous Solution.

M <sup>2+</sup>	Ionic radius <sup>b</sup> (Å)	log(K <sub>s</sub> /dm <sup>3</sup> mol <sup>-1</sup> )			
		cyclen	TMEC12 <sup>c</sup>	THEC12	TMEC14 <sup>d</sup>
Mg <sup>2+</sup>	0.72	2.25 <sup>e</sup>	2.47 ± 0.03	2.86 <sup>f</sup>	<2
Ca <sup>2+</sup>	1.00 (1.12)	3.12 <sup>g</sup>	5.47 ± 0.06	7.41 <sup>f</sup>	3.22
Sr <sup>2+</sup>	1.18 (1.26)		5.00 ± 0.02	6.47 <sup>f</sup>	2.95
Ba <sup>2+</sup>	1.35 (1.42)		4.72 ± 0.03	4.84 <sup>f</sup>	2.89
Mn <sup>2+</sup>	0.83		7.1 ± 0.1		
Co <sup>2+</sup>	0.75	13.79 <sup>h</sup>	6.6 ± 0.1	6.04 <sup>i</sup>	4.47
Ni <sup>2+</sup>	0.69	16.4 <sup>j</sup>	5.35 ± 0.07	10.76 <sup>i</sup>	3.62
Cu <sup>2+</sup>	0.73	23.3 <sup>k</sup>	13.6 ± 0.1	15.18 <sup>i</sup>	7.04
Zn <sup>2+</sup>	0.74	16.2 <sup>l</sup>	8.58 ± 0.05	12.83 <sup>i</sup>	4.76
Cd <sup>2+</sup>	0.95 (1.10)	14.3 <sup>l</sup>	12.6 ± 0.3	14.63 <sup>i</sup>	4.99
Hg <sup>2+</sup>	1.02 (1.14)		18.57 ± 0.03		15.1
Pb <sup>2+</sup>	1.19 (1.29)	15.9 <sup>l</sup>	14.9 ± 0.1	15.27 <sup>i</sup>	5.78

<sup>a</sup> In 0.10 mol dm<sup>-3</sup> NEt<sub>4</sub>ClO<sub>4</sub> except where stated otherwise. <sup>b</sup> Reference 8. Ionic radii for six-coordination are quoted for all metal ions. The numbers in parentheses are the eight coordinate radii of these ions. <sup>c</sup> This work. <sup>d</sup> Reference 6. <sup>e</sup> Reference 15, 0.5 mol dm<sup>-3</sup> KNO<sub>3</sub>.

<sup>f</sup> Reference 5. <sup>g</sup> Reference 16, 0.1 mol dm<sup>-3</sup> NaNO<sub>3</sub>. <sup>h</sup> Reference 17, 0.2 mol dm<sup>-3</sup> NaClO<sub>4</sub>.

<sup>i</sup> Reference 4, 0.1 mol dm<sup>-3</sup> NaNO<sub>3</sub>. <sup>j</sup> Reference 18, 0.1 mol dm<sup>-3</sup> NaNO<sub>3</sub>. <sup>k</sup> Reference 19, 0.5 mol dm<sup>-3</sup> (HNO<sub>3</sub> + NaNO<sub>3</sub>). <sup>l</sup> Reference 20, 0.1 mol dm<sup>-3</sup> NaNO<sub>3</sub>.

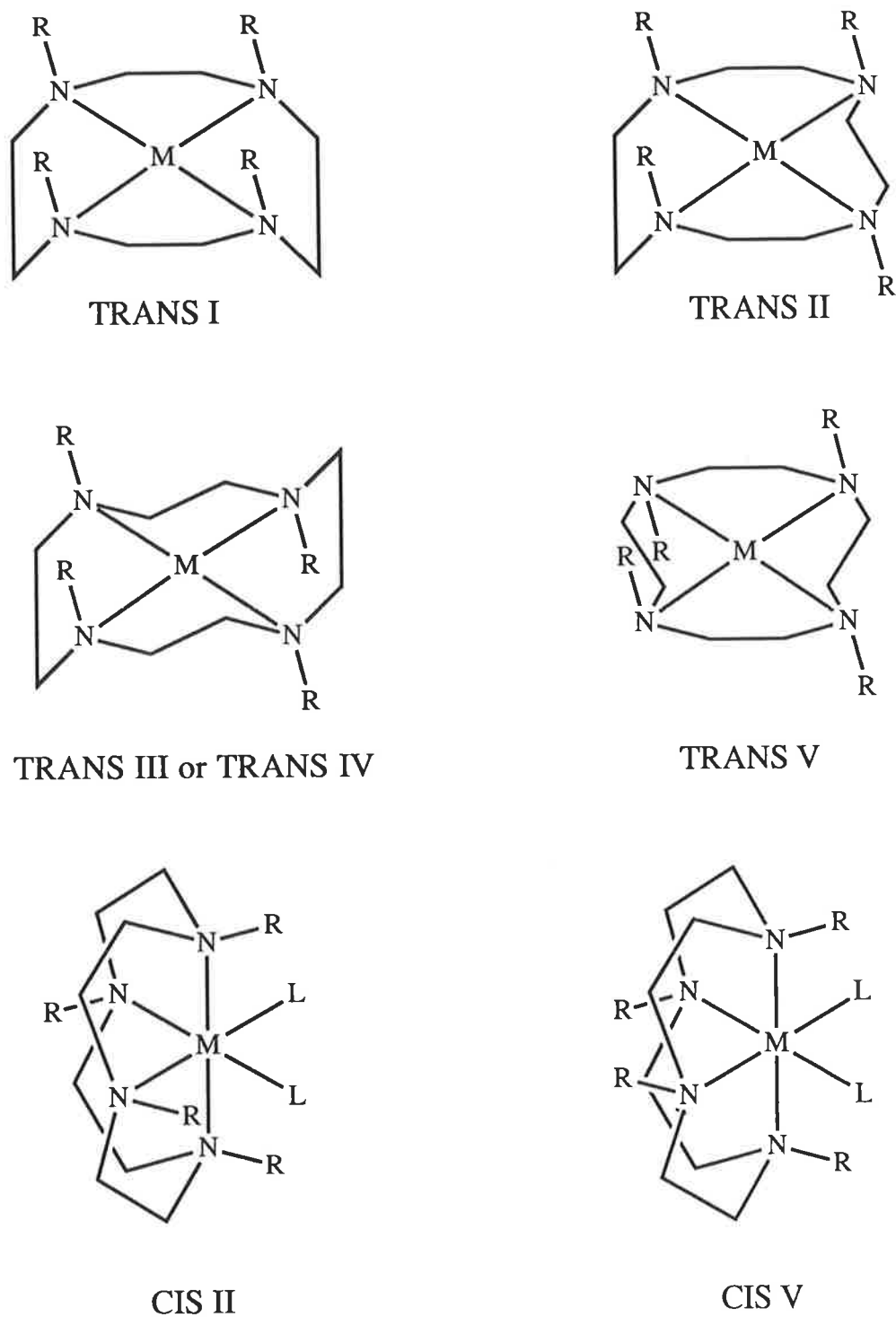


**Figure 7.1.** The possible configurational isomers of  $[M(\text{TMEC12})]^{n+}$ , where the methoxyethyl arms (R) are shown as uncoordinated. The TRANS III and the TRANS IV conformers are equivalent in the completely symmetrical TMEC12 system.

geometry of  $\text{Mg}^{2+}$ ,  $\text{Sr}^{2+}$  and  $\text{Ba}^{2+}$  are unknown, but it is probable that the larger  $\text{Sr}^{2+}$  and  $\text{Ba}^{2+}$  are also bound to all eight donor atoms of TMEC12 and possibly to one or more solvent molecules.

The stabilities of the alkaline earth complexes,  $[\text{M}(\text{TMEC12})]^{2+}$ , are in the sequence  $\text{Mg}^{2+} < \text{Ca}^{2+} > \text{Sr}^{2+} > \text{Ba}^{2+}$ , which is similar to the stability sequence  $\text{Li}^+ < \text{Na}^+ > \text{K}^+ > \text{Rb}^+ > \text{Cs}^+$  for the alkali metal complexes of TMEC12 in most solvents studied (Chapter 6). The greater stability of  $[\text{Ca}(\text{TMEC12})]^{2+}$  is probably consistent with  $\text{Ca}^{2+}$  establishing optimum bonding distances and minimising strain in  $[\text{Ca}(\text{TMEC12})]^{2+}$  compared with the other  $[\text{M}(\text{TMEC12})]^{2+}$  complexes. In  $[\text{Na}(\text{TMEC12})]^+$  and  $[\text{Ca}(\text{TMEC12})]^{2+}$ , both cations are eight coordinate and the tetraaza ring adopts the TRANS I conformation.<sup>13-14</sup> In aqueous solution, the selectivity of TMEC12 for  $\text{Na}^+$  ( $r = 1.18 \text{ \AA}$ ) and  $\text{Ca}^{2+}$  ( $r = 1.12 \text{ \AA}$ ), respectively, over the other alkali and alkaline earth metal ions, suggests that when TMEC12 adopts the TRANS I conformation, the optimum ionic radius for the metal ion is  $\sim 1.15 \text{ \AA}$ . The particularly low stability of  $[\text{Mg}(\text{TMEC12})]^{2+}$  relative to the other alkaline earth complexes probably results from a combination of a lower coordination number and the higher solvation energy of  $\text{Mg}^{2+}$ . The small selectivity of TMEC12 for  $\text{Ca}^{2+}$  over  $\text{Sr}^{2+}$  and  $\text{Ba}^{2+}$  is consistent with the flexibility of TMEC12 allowing it to readily adjust to these larger ions. However, as the ionic radius of  $\text{M}^{2+}$  increases from  $\text{Ca}^{2+}$  to  $\text{Ba}^{2+}$ , there is a concomitant decrease in the electrostatic attraction between  $\text{M}^{2+}$  and TMEC12, so that the stability of  $[\text{M}(\text{TMEC12})]^{2+}$  decreases in the sequence  $\text{Ca}^{2+} > \text{Sr}^{2+} > \text{Ba}^{2+}$ .

### 7.2.2 Complexes of the Heavy Metal Ions $\text{Cd}^{2+}$ , $\text{Hg}^{2+}$ and $\text{Pb}^{2+}$

<sup>13</sup>C NMR studies in *d*<sub>4</sub>-methanol (Chapter 9) have demonstrated that  $\text{M}^{2+}$  in  $[\text{M}(\text{TMEC12})]^{2+}$  is eight coordinate, lying above the plane of the tetraaza ring, bound to the four nitrogens and all four pendant arms, for  $\text{M}^{2+} = \text{Cd}^{2+}$ ,  $\text{Hg}^{2+}$  and  $\text{Pb}^{2+}$ . The tetraaza ring is in the TRANS I conformation, and the coordination geometry of  $\text{M}^{2+}$  is square antiprismatic. As discussed previously, it is apparent that when TMEC12 adopts the TRANS I conformation, the optimum ionic radius for the metal ion is  $\sim 1.15 \text{ \AA}$ . This is closest to the ionic radii of  $\text{Cd}^{2+}$  ( $r = 1.10 \text{ \AA}$ ) and  $\text{Hg}^{2+}$  ( $r = 1.14 \text{ \AA}$ ), but the stabilities of  $[\text{M}(\text{TMEC12})]^{2+}$  lie in the sequence  $\text{Cd}^{2+} < \text{Hg}^{2+} > \text{Pb}^{2+}$ . The greater stability of  $[\text{Hg}(\text{TMEC12})]^{2+}$  may result from the greater softness of  $\text{Hg}^{2+}$  by comparison with  $\text{Cd}^{2+}$  and  $\text{Pb}^{2+}$ , which allows it to bind more

strongly to the nitrogens of the tetraaza ring than the other two metal ions. The particularly high stability of  $[\text{Pb}(\text{TMEC12})]^{2+}$  compared with that of  $[\text{Cd}(\text{TMEC12})]^{2+}$ , despite the greater ionic radius of  $\text{Pb}^{2+}$ , may be attributed to the inert pair effect<sup>16,21</sup> and the smaller solvation energy of  $\text{Pb}^{2+}$  compared with that of  $\text{Cd}^{2+}$ .<sup>9</sup> The inert pair effect is a phenomenon where  $\text{Pb}^{2+}$  changes from a situation where the lone pair of electrons occupies the spherically symmetrical 6s orbital to a situation where it occupies a stereochemically active  $\text{sp}^n$  or  $\text{sp}^n\text{d}^n$  orbital. This results in an increase in the covalency of the nitrogen- $\text{Pb}^{2+}$  bonds, which shorten by  $\sim 0.3 \text{ \AA}$ . Thus, the effective ionic radius of  $\text{Pb}^{2+}$  is decreased and there is a resultant increase in the stability of the  $\text{Pb}^{2+}$  complex. The inert pair effect may be observed in macrocyclic complexes of  $\text{Pb}^{2+}$  in which the ligand has three or more nitrogen donor atoms.

### 7.2.3 Complexes of the First-Row Transition Metal Ions

The stabilities of the first-row transition metal complexes of TMEC12 vary in the sequence  $\text{Mn}^{2+} > \text{Co}^{2+} > \text{Ni}^{2+} < \text{Cu}^{2+} > \text{Zn}^{2+}$ . This contrasts with the Irving-Williams series,<sup>22-23</sup> which predicts the following variation in the stabilities of the first-row transition metal complexes of simple ligands;  $\text{Mn}^{2+} < \text{Co}^{2+} < \text{Ni}^{2+} < \text{Cu}^{2+} > \text{Zn}^{2+}$ . This sequence derives from ligand dipole-metal ion electrostatic effects and ligand field effects. The deviations of  $[\text{M}(\text{TMEC12})]^{2+}$  from the Irving-Williams series may result from steric effects, as discussed below.

The metal ions in this study are all too large to sit within the plane of the tetraaza ring of TMEC12.<sup>19</sup> Thus, octahedral or square planar coordination cannot occur for  $[\text{M}(\text{TMEC12})]^{2+}$  when the tetraaza ring is in any of the TRANS conformations, where the four nitrogens are coplanar. The TRANS I conformer may allow five, seven and eight coordinate complexes, as observed for  $[\text{Cu}(\text{cyclen})(\text{NO}_3)]\text{NO}_3$  (5) and  $[\text{Li}(\text{THEC12})]^+$  (5),  $[\text{Na}(\text{THEC12})]^+$  (7) and  $[\text{K}(\text{THEC12})]^+$  (8), respectively, in the solid state.<sup>24-27</sup> Octahedral coordination is achieved when the tetraaza ring adopts a folded conformation, where two of the nitrogen donor atoms occupy cis coordination sites and the other two nitrogens occupy trans coordination sites. The CIS II conformation (Figure 7.1) is observed in the solid state for several first-row transition metal complexes of cyclen,<sup>28-32</sup> whereas the CIS V (Figure 7.1) conformation is observed in the solid state structure of  $[\text{NiBr}(\text{H}_2\text{O})\text{L}]\text{Br}$ , where L is the ligand 1,7-dimethyl-1,4,7,10-tetraazacyclododecane.<sup>33</sup> However, the steric hindrance

resulting from the pendant arms of TMEC12 may cause considerable strain for octahedral coordination, and trigonal bipyramidal coordination may result, as observed for the  $\text{Co}^{2+}$  and  $\text{Ni}^{2+}$  complexes of 1,4,7,10-tetrabenzyl-1,4,7,10-tetraazacyclododecane.<sup>34-35</sup> This may account for the greater stabilities of  $[\text{Mn}(\text{TMEC12})]^{2+}$  and  $[\text{Zn}(\text{TMEC12})]^{2+}$ , compared with those of their  $\text{Co}^{2+}$  and  $\text{Ni}^{2+}$  analogues, which probably prefer the octahedral coordination which results from a folded CIS conformation, whereas  $\text{Mn}^{2+}$  and  $\text{Zn}^{2+}$  have no preferred coordination geometry.

### 7.3 Effect of the Pendant Arm on Complex Stability

The stabilities of  $[\text{M}(\text{TMEC12})]^{2+}$ , where  $\text{M}^{2+} = \text{Mg}^{2+}$  and  $\text{Ca}^{2+}$  are greater than those of  $[\text{M}(\text{cyclen})]^{2+}$ , consistent with an increase in the number of donor atoms in going from cyclen to TMEC12 increasing the binding of  $\text{M}^{2+}$ . The attachment of the methoxyethyl pendant arms to cyclen leads to an increase in steric crowding when  $\text{M}^{2+}$  is coordinated. Nevertheless, these pendant arms allow TMEC12 to encapsulate  $\text{M}^{2+}$  more effectively than the unsubstituted macrocycle. As a consequence, the selectivity of TMEC12 for  $\text{Ca}^{2+}$  over  $\text{Mg}^{2+}$  is greater than that of cyclen. A similar relationship was observed for the alkali metal ions in Chapter 6.

In contrast to the hard acid alkaline earth metal ions, the dominant interaction in the pendant arm tetraaza macrocyclic complexes of the first-row transition metal and heavy metal ions is between  $\text{M}^{2+}$  and the nitrogen donor atoms of the tetraaza ring. The steric hindrance caused by the pendant arms of TMEC12 reduces the flexibility of the tetraaza ring and the ability of TMEC12 to establish optimum metal-nitrogen bond lengths by folding is decreased in comparison with the parent macrocycle cyclen. Thus, the stabilities of  $[\text{M}(\text{TMEC12})]^{2+}$ , where  $\text{M}^{2+} = \text{Co}^{2+}$ ,  $\text{Ni}^{2+}$ ,  $\text{Cu}^{2+}$ ,  $\text{Zn}^{2+}$ ,  $\text{Cd}^{2+}$  and  $\text{Pb}^{2+}$  are lower than those of their  $[\text{M}(\text{cyclen})]^{2+}$  analogues, but the differences are largest for the smaller first-row transition metal ions  $\text{Co}^{2+}$ ,  $\text{Ni}^{2+}$ ,  $\text{Cu}^{2+}$  and  $\text{Zn}^{2+}$ . The effects of steric hindrance are greatest for smaller metal ions, and may also prevent TMEC12 from adopting the preferred coordination geometry for  $\text{Co}^{2+}$ ,  $\text{Ni}^{2+}$  and  $\text{Cu}^{2+}$ , as discussed in Section 7.2.3. Thus, the substantially lower stabilities of  $[\text{M}(\text{TMEC12})]^{2+}$  compared with those of  $[\text{M}(\text{cyclen})]^{2+}$ , for  $\text{M}^{2+} = \text{Co}^{2+}$ ,  $\text{Ni}^{2+}$  and  $\text{Cu}^{2+}$  may be a result of steric strain or a non-preferred coordination geometry. It is probable that steric hindrance prevents high coordination numbers for these first-row transition metal ions in  $[\text{M}(\text{TMEC12})]^{2+}$ . However, the larger  $\text{Cd}^{2+}$  and  $\text{Pb}^{2+}$  more readily adopt

higher coordination numbers and both are eight coordinate in  $[M(\text{TMEC12})]^{2+}$ . In addition, the methoxyethyl arms form five membered chelate rings when coordinated to  $M^{2+}$ , and five membered chelate rings coordinate large metal ions with less strain than smaller metal ions, as discussed in Section 6.1.<sup>36-37</sup> As a result, the binding of  $\text{Cd}^{2+}$  and  $\text{Pb}^{2+}$  by the four methoxyethyl arms in  $[M(\text{TMEC12})]^{2+}$  counteracts the effect of steric hindrance, and the differences in stability between  $[M(\text{cyclen})]^{2+}$  and  $[M(\text{TMEC12})]^{2+}$  are much smaller for  $\text{Cd}^{2+}$  and  $\text{Pb}^{2+}$ .

## 7.4 Effect of the Nature of the Pendant Arm on Complex Stability

The selectivity of TMEC12 for the alkaline earth ions is similar to that of THEC12. A similar relationship exists for the alkali metal complexes of these ligands. In *d*<sub>4</sub>-methanol, the  $\text{Na}^+$  and  $\text{Ca}^{2+}$  complexes of both TMEC12 and THEC12 are eight coordinate, with the tetraaza ring adopting the TRANS I conformation (Chapter 9).<sup>5,13-14</sup> This emphasises the selectivity of these pendant arm ligands for metal ions of similar size to  $\text{Na}^+$  and  $\text{Ca}^{2+}$ , when the tetraaza ring adopts the TRANS I conformation. However, while the stabilities of the alkali metal  $[M(\text{TMEC12})]^+$  complexes are more stable than their  $[M(\text{THEC12})]^+$  analogues, the reverse is true for the alkaline earth complexes of these ligands. Similarly, the stabilities of  $[M(\text{TMEC12})]^{2+}$  are also lower than those of their  $[M(\text{THEC12})]^{2+}$  analogues, when  $M^{2+}$  is a first-row transition metal or heavy metal ion (except for  $\text{Co}^{2+}$ ). The factors responsible for the greater stability of  $[M(\text{TMEC12})]^+$  over  $[M(\text{THEC12})]^+$  have been discussed in Chapter 6. However, it is apparent that additional factors are important for the divalent metal complexes of these ligands, as described below.

The steric hindrance caused by the pendant arms of TMEC12 and THEC12 influences the ability of these ligands to adopt the conformation which allows the preferred coordination geometry of  $\text{Co}^{2+}$  (octahedral<sup>12</sup>),  $\text{Ni}^{2+}$  (octahedral<sup>12</sup>) and  $\text{Cu}^{2+}$  (tetragonally distorted octahedral<sup>12</sup>). While  $\text{Zn}^{2+}$  has no preferred coordination geometry, steric hindrance may be particularly important because of its small size. This steric hindrance should generally be greater for the complexes of TMEC12 than those of THEC12, but this depends on the ligand conformation, the coordination geometry of  $M^{2+}$ , the number of pendant arms coordinated to  $M^{2+}$  and the ionic radius of  $M^{2+}$ . For the first-row transition metal ions, the difference between the stabilities of

$[M(\text{THEC12})]^{2+}$  and  $[M(\text{TMEC12})]^{2+}$  is largest for  $\text{Ni}^{2+}$  and  $\text{Zn}^{2+}$ , smaller for  $\text{Cu}^{2+}$ , and  $[\text{Co}(\text{TMEC12})]^{2+}$  is more stable than  $[\text{Co}(\text{THEC12})]^{2+}$ . This may be a reflection of the different ligand conformations and coordination geometries of  $\text{M}^{2+}$  in these complexes, which are determined by the relative effects of steric hindrance.

For  $[M(\text{TMEC12})]^{2+}$  and  $[M(\text{THEC12})]^{2+}$ ,  $\text{M}^{2+}$  is eight coordinate and the tetraaza ring adopts the TRANS I conformation when  $\text{M}^{2+} = \text{Ca}^{2+}$ ,  $\text{Cd}^{2+}$ , and  $\text{Pb}^{2+}$  (Chapter 9) and the same is probably true for  $\text{Sr}^{2+}$  and  $\text{Ba}^{2+}$ . Thus, the differences between the stabilities of  $[M(\text{TMEC12})]^{2+}$  and  $[M(\text{THEC12})]^{2+}$  do not result from differences in coordination numbers and geometries in these complexes. Another factor which may be important is the solvation of the metal complex. The ligand interposes a lipophilic layer between the metal ion and the solvent, and the thickness of this layer will influence the stability of the complex.<sup>38</sup> From molecular models, it is apparent that when TMEC12 and THEC12 adopt the TRANS I conformation, the methyl groups of the TMEC12 pendant arms result in the complexed metal ion being shielded from the solvent to a greater extent than in complexes of THEC12. This has a destabilising effect on  $[M(\text{TMEC12})]^{2+}$  relative to  $[M(\text{THEC12})]^{2+}$ .

Some support for this argument comes from consideration of the  $\text{K}^+$  ( $r = 1.51 \text{ \AA}$ ) and  $\text{Ba}^{2+}$  ( $r = 1.42 \text{ \AA}$ ) complexes of the cryptands C222 and DB-C222 (Figure 7.2). In 95 % methanol/water, the  $\text{K}^+$  complex of DB-C222 is only 7.1 times less stable than that of C222, whereas the  $\text{Ba}^{2+}$  complex of DB-C222 is 1000 times less stable than that of C222.<sup>39</sup> This is consistent with the presence of the two benzene rings in DB-C222 hindering the approach of solvent to the complexed cation, and as expected, this destabilising effect is greater for divalent  $\text{Ba}^{2+}$  than for monovalent  $\text{K}^+$ .<sup>39</sup> These results help to explain why differences in the solvation of the metal complexes of TMEC12 and THEC12 may be important for divalent metal ions, but appear to be less important for monovalent metal ions.



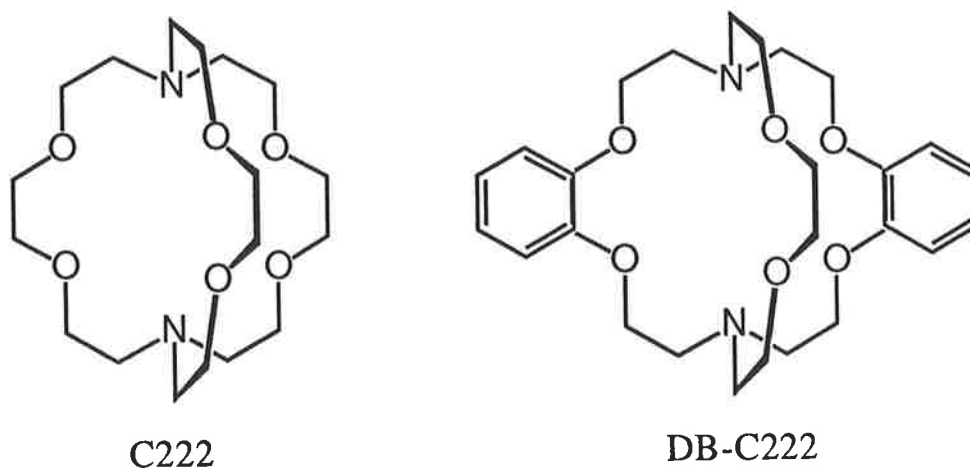


Figure 7.2. The cryptands C222 and DB-C222

## 7.5 Effect of Macrocyclic Ring Size on Complex Stability

In  $[M(\text{TMEC12})]^{2+}$ , there are four five membered chelate rings in which both donor atoms are nitrogen (nitrogen chelate rings), whereas in  $[M(\text{TMEC14})]^{2+}$ , there are two five membered and two six membered nitrogen chelate rings. As described previously, this should result in TMEC12 coordinating large metal ions with less strain than occurs with TMEC14. In qualitative agreement with this prediction, the difference between the stabilities of  $[M(\text{TMEC12})]^{2+}$  and  $[M(\text{TMEC14})]^{2+}$  tends to increase as the ionic radius of  $M^{2+}$  increases, where  $M^{2+}$  is a first-row transition metal or heavy metal ion, with the exception of  $\text{Cu}^{2+}$  and  $\text{Hg}^{2+}$ . However, the methoxyethyl arms of both ligands form five membered chelate rings when coordinated to  $M^{2+}$ , which could modify the effect of the change in the size of the nitrogen chelate rings in going from TMEC12 to TMEC14.

For the alkaline earth metal ions, the stabilities of  $[M(\text{TMEC12})]^{2+}$  are also considerably greater than those of  $[M(\text{TMEC14})]^{2+}$ . However, the differences between the stabilities of  $[M(\text{TMEC12})]^{2+}$  and  $[M(\text{TMEC14})]^{2+}$  are much lower for  $\text{Ca}^{2+}$  (eight coordinate ionic radius,  $r = 1.12 \text{ \AA}$ ),  $\text{Sr}^{2+}$  ( $r = 1.26 \text{ \AA}$ ) and  $\text{Ba}^{2+}$  ( $r = 1.42 \text{ \AA}$ ) than for the heavy metal ions  $\text{Cd}^{2+}$  ( $r = 1.10 \text{ \AA}$ ),  $\text{Hg}^{2+}$  ( $r = 1.14 \text{ \AA}$ ) and  $\text{Pb}^{2+}$  ( $r = 1.29 \text{ \AA}$ ). The size of the nitrogen chelate rings probably influences the relative stabilities of  $[M(\text{TMEC12})]^{2+}$  and

$[M(\text{TMEC14})]^{2+}$  to a smaller extent for the alkaline earth metal ions than for the other divalent metal ions in this study. This is because the alkaline earth cations bind preferentially with oxygen donor atoms over nitrogen donor atoms and there is a lack of directionality in the metal-ligand bonds, which are almost purely electrostatic in nature.<sup>37</sup>

## 7.6 $[M(\text{HTMEC12})]^{(n+1)+}$ and $[M(\text{OH})\text{TMEC12}]^+$ Complexes

Monoprotonated complexes of TMEC12,  $[M(\text{HTMEC12})]^{(n+1)+}$ , form for  $\text{Cd}^{2+}$ ,  $\text{Pb}^{2+}$  and  $\text{Ag}^+$ . The formation of these complexes is described by Equation 7.11.



$$\text{where } K_{\text{MH}} = \frac{[\text{M}(\text{HTMEC12})]^{(n+1)+}}{[\text{M}^{n+}][\text{HTMEC12}^+]} \quad 7.12$$

The values of  $K_{\text{MH}}$  appear in Table 7.3.

The monoprotonated complexes are less stable than the complexes of the neutral ligand. This is a consequence of electrostatic repulsion between the proton and the metal ion in  $[M(\text{HTMEC12})]^{(n+1)+}$ , and the decrease in the number of donor atoms coordinated to  $\text{M}^{n+}$ . It is probable that the protonated nitrogen is in the *exo* conformation, which would minimise the repulsion between the proton and  $\text{M}^{n+}$ . Thus, the formation of  $[M(\text{TMEC12})]^{n+}$  from  $[M(\text{HTMEC12})]^{(n+1)+}$  occurs through nitrogen inversion.

The equilibrium:



$$\text{where } K_{\text{OH}} = \frac{[\text{M}(\text{OH})\text{TMEC12}^+]}{[\text{M}^{2+}][\text{OH}^-][\text{TMEC12}]} \quad 7.14$$

is characterised by  $\log(K_{\text{OH}}/\text{dm}^6 \text{ mol}^{-2}) = 10.0 \pm 0.2$ ,  $11.4 \pm 0.2$ ,  $13.16 \pm 0.05$  and  $23.39 \pm 0.05$  when  $\text{M}^{2+} = \text{Mn}^{2+}$ ,  $\text{Co}^{2+}$ ,  $\text{Zn}^{2+}$  and  $\text{Hg}^{2+}$ , respectively. These species form either from the hydrolysis of a water molecule coordinated

to  $M^{2+}$  or from coordination of a hydroxide ion at high pH, but the two processes cannot be distinguished by the titration technique used to characterise these species. This contrasts with the  $[M(OH)TMEC12]^+$  complexes, which are thought to form through the deprotonation of a hydroxy group of the pendant arm.

The complex  $[M(TMEC12)]^{2+}$  acts as an acid, as expressed in Equation 7.15;



$$\text{where } K_a = \frac{[M(OH)TMEC12^+][H^+]}{[M(TMEC12)^{2+}]} \quad 7.16$$

$$\text{and } pK_a = -\log K_a \quad 7.17$$

The  $pK_a$  values for  $[M(TMEC12)]^{2+}$  appear in Table 7.3. The  $pK_a$  of a hydrated metal ion should decrease as the ionic radius decreases. However, there is no apparent trend in the  $pK_a$  values of  $[M(TMEC12)]^{2+}$  with ionic radius. This is consistent with the acidity of  $M^{2+}OH_2$  depending on its environment, being different when coordinated by TMEC12 than in the hydrated metal ion. A similar result was observed for the analogous complexes of C22C<sub>2</sub> and C22C<sub>8</sub> in Chapter 3.

**Table 7.3.** Stability Constants<sup>a</sup> for the Formation of [M(HTMEC12)]<sup>(n+1)+</sup> and [M(OH)TMEC12]<sup>+</sup> Complexes at 298.2 K in Aqueous Solution.

M <sup>2+</sup>	Ionic radius <sup>b</sup> (Å)	logK <sub>s</sub> (K <sub>s</sub> /dm <sup>3</sup> mol <sup>-1</sup> )	logK <sub>MH</sub> (K <sub>MH</sub> /dm <sup>3</sup> mol <sup>-1</sup> )	pK <sub>a</sub> (K <sub>a</sub> /mol dm <sup>-3</sup> )
Mn <sup>2+</sup>	0.83	7.1		10.9 ± 0.2
Co <sup>2+</sup>	0.75	6.6		9.0 ± 0.2
Zn <sup>2+</sup>	0.74	8.58		9.22 ± 0.05
Cd <sup>2+</sup>	0.95 (1.10)	12.6	5.9 ± 0.1	
Hg <sup>2+</sup>	1.02 (1.14)	18.57		8.98 ± 0.05
Pb <sup>2+</sup>	1.19 (1.29)	14.9	4.4 ± 0.1	
Ag <sup>+</sup>	1.15 (1.28)	12.62	4.09 ± 0.05	

<sup>a</sup> In 0.10 mol dm<sup>-3</sup> NEt<sub>4</sub>ClO<sub>4</sub> supporting electrolyte. <sup>b</sup> Reference 8. Ionic radii for six-coordination are quoted for all metal ions. The numbers in parentheses are the eight coordinate radii of these ions.

- 1 Micheloni, M.; Paoletti, P.; Vacca, A. *J. Chem. Soc., Perkin Trans 2.* **1978**, 945-947
- 2 Hay, R.W.; Pujari, M.P.; Moodie, W.T.; Craig, S.; Richens, D.T.; Perotti, A.; Ungaretti, L. *J. Chem. Soc., Dalton Trans.* **1987**, 2605.
- 3 Hancock, R.D. *J. Chem. Soc., Dalton Trans.* **1979**, 416-418.
- 4 Turonek, M.L. PhD Thesis, University of Adelaide, **1993**.
- 5 Lincoln, S.F.; Whitbread, S. Unpublished material.
- 6 Lincoln, S.F.; Lucas, J.B. Unpublished material.
- 7 Micheloni, M.; Sabatini, A.; Paoletti, P. *J. Chem. Soc., Perkin Trans.2* **1978**, 828.
- 8 Shannon, R.D. *Acta. Crystallogr., Sect. A: Cryst. Diffr., Theor. Gen. Crystallogr.* **1976**, A32, 751.
- 9 Burgess, J. "Metal Ions in Solution", Ellis Horwood, Chichester, **1978**.
- 10 Pearson, R.G. *J. Am. Chem. Soc.* **1963**, 85, 3533.
- 11 Pearson, R.G. *Coord. Chem. Rev.* **1990**, 100, 403.
- 12 Cotton, F.A.; Wilkinson, G. "Advanced Inorganic Chemistry", 4th ed, Interscience, New York, **1980**.
- 13 Lincoln, S.F.; Dhillon, R. Unpublished Material.
- 14 Lincoln, S.F.; Madbak, S. Unpublished Material.
- 15 Ruangpornvisuti, V.W.; Probst, M.M.; Rode, B.M. *Inorg. Chim. Acta.* **1988**, 144, 21-23.
- 16 Hancock, R.D.; Shaikjee, M.S.; Dobson, S.M.; Boeyons, J.C.A. *Inorg. Chim. Acta.* **1988**, 154, 229-238.
- 17 Kodama, M.; Kimura, E. *J. Chem. Soc., Dalton Trans.* **1980**, 327-333.
- 18 Thöm, V.J.; Hancock, R.D. *J. Chem. Soc., Dalton Trans.* **1985**, 1877-1880.
- 19 Thöm, V.J.; Hosken, G.D.; Hancock, R.D. *Inorg. Chem.* **1985**, 24, 3378-3381.
- 20 Hancock, R.D.; Dobson, S.M.; Evers, A.; Wade, P.W.; Ngwenya, M.P.; Boeyons, J.C.A.; Wainwright, K.P. *J. Am. Chem. Soc.* **1988**, 110, 2788-2794.
- 21 Hancock, R.D.; Bhavan, R.; Wade, P.W.; Boeyons, J.C.A.; Dobson, S.M. *Inorg. Chem.* **1989**, 28, 187-194.
- 22 Irving, H.; Williams, R.J.P. *Nature (London)*. **1948**, 162, 746.
- 23 Irving, H.; Williams, R.J.P. *J. Chem. Soc.* **1953**, 3192.
- 24 Clay, R.; Murray-Rust, P.; Murray-Rust, J. *Acta Cryst.* **1979**, B35, 1894-1895.
- 25 Buøen, S.; Dale, J.; Groth, Krane, J. *J. Chem. Soc., Chem Commun.* **1982**, 1172-174.

- 26 Groth, P. *Acta Chem. Scand.* **1983**, A37, 71-77.
- 27 Groth, P. *Acta Chem. Scand.* **1983**, A37, 283-291.
- 28 Iitaka, Y.; Shina, M.; Kimura, E. *Inorg. Chem.* **1974**, 13, 2886-2891.
- 29 Loehlin, J.H.; Fleischer, E.B. *Acta Cryst.* **1976**, B32, 3063-3066.
- 30 Matsumoto, N.; Hirano, A.; Hara, T.; Ohyoshi, A. *J. Chem. Soc., Dalton Trans.* **1983**, 2405-2410.
- 31 Scott, B.; Brewer, K.J.; Spreer, L.O.; Craig, C.A.; Otvos, J.W.; Calvin, M.; Taylor, S. *J. Coord. Chem.* **1990**, 21, 307-313.
- 32 Kojima, M.; Nakabayashi, K.; Ohba, S.; Okumoto, S.; Saito, Y.; Fujita, J. *Bull. Chem. Soc. Jpn.* **1986**, 59, 277-283.
- 33 Giusti, J.; Chimichi, S.; Ciampolini, M. *Inorg. Chim. Acta.* **1984**, 88, 51-54.
- 34 Sarther, C.M.; Blinn, E.L. *Inorg. Chem.* **1976**, 15, 3083-3087.
- 35 Smierciak, R.; Passariello, J.; Blinn, E.L. *Inorg. Chem.* **1977**, 16, 2646-2648.
- 36 Hancock, R.D.; *Prog. Inorg. Chem.* **1989**, 37, 187.
- 37 Hancock, R.D.; Wade, P.W.; Ngwenya, M.P.; de Sousa, A.S.; Damu, K.V. *Inorg. Chem.* **1990**, 29, 1968-1974.
- 38 Lehn, J-M. *Struct. Bonding (Berlin)*. **1973**, 16, 1-69.
- 39 Dietrich, B.; Lehn, J-M.; Sauvage, J-P. *J. Chem. Soc., Chem. Commun.* **1973**, 15-16.

# Chapter 8: Complexation Dynamics of [M(TMEC12)]<sup>+</sup>

## 8.1 Introduction

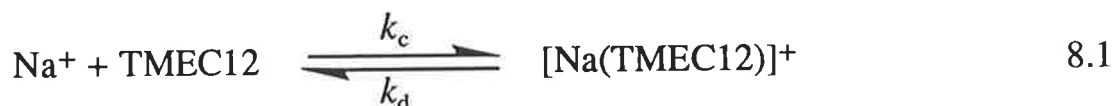
Metal complexes of unsubstituted tetraaza macrocyclic ligands are characterised by their kinetic inertness.<sup>1</sup> The initial research into pendant arm tetraaza macrocycles was stimulated by the effect of the pendant arms on the lability of their divalent metal complexes.<sup>2-5</sup> For ligands based on cyclam (Figure 5.1), metal complexation takes several hours to reach equilibrium, when the pendant arms have no donor atoms, as in 1,4,8,11-tetramethyl-1,4,8,11-tetraazacyclotetradecane, whereas equilibrium is reached in seconds when the pendant arms possess donor groups, as exemplified by the ligand THEC14 (Figure 5.1).<sup>2-3</sup>

In contrast, kinetic studies characterising alkali metal complexes of unsubstituted tetraaza macrocycles and their pendant arm derivatives are few in number.<sup>6</sup> Nevertheless, the discussion of mechanistic aspects of cryptates in Chapter 4 is applicable to the complexation and decomplexation of alkali metal complexes of all ionophores. Consequently, the formation of the alkali metal complexes of TMEC12 is expected to follow the step-wise desolvation of M<sup>+</sup>, bond formation between M<sup>+</sup> and TMEC12 and ligand conformational changes as described by the Eigen-Winkler mechanism<sup>7-9</sup> (Chapter 4). Thus, the lability of these complexes should depend on the solvation energy of the metal ion and the structure and flexibility of the ligand, as found for the cryptates studied in Chapter 4. This study seeks to provide a better understanding of the complexation of alkali metal ions by pendant arm tetraaza macrocyclic ligands through a study of the exchange of M<sup>+</sup> on [M(TMEC12)]<sup>+</sup>, where M<sup>+</sup> = Li<sup>+</sup> and Na<sup>+</sup>, in a range of solvents.

In Chapter 6, it was seen that TMEC12 shows properties similar to those of the Na<sup>+</sup> selective cryptands C221 and C22C<sub>2</sub> in its complexation of alkali metal ions. Nevertheless, its greater structural flexibility results in the stabilities of [M(TMEC12)]<sup>+</sup> being substantially lower than those of the cryptates of C221 and C22C<sub>2</sub>, and a lower selectivity for Na<sup>+</sup>, which is dependent on the nature of the solvent. This chapter examines the effect of this greater flexibility on the lability of the alkali metal complexes of TMEC12, and studies the kinetic origin of its selectivity for these ions.

## 8.2 Exchange Kinetics of $\text{Na}^+$ on $[\text{Na}(\text{TMEC12})]^+$

The temperature dependent coalescence of the  $^{23}\text{Na}$  resonances arising from solvated  $\text{Na}^+$  and  $[\text{Na}(\text{TMEC12})]^+$  in dimethylformamide, dimethylsulfoxide and water yields the kinetic parameters for the decomplexation of  $[\text{Na}(\text{TMEC12})]^+$  (Equation 8.1) shown in Table 8.1.



The temperature dependent coalescence of the  $^{23}\text{Na}$  resonances characterising this exchange in water appears in Figure 8.1. The kinetic parameters were obtained through the temperature dependence of  $\tau_c$ , the mean lifetime of  $[\text{Na}(\text{TMEC12})]^+$ , through Equation 4.14. The decomplexation rate constant is quoted at two temperatures; (i) the coalescence temperature, where the exchange induced modification of the spectra is at a maximum and hence the most reliable values of  $k_d$  are obtained and (ii) at 298.2 K, for the purpose of comparison with other systems. The  $\tau_c$  values were determined by complete lineshape analysis of the coalescing  $^{23}\text{Na}$  resonances observed for each of the solutions (i) - (x), whose compositions appear in Table 8.1. The magnitudes and temperature variations of  $\tau_c$  for each of the solutions studied for a given solvent are indistinguishable (Figure 8.2). Thus,  $\tau_c$  is independent of the concentration of solvated  $\text{Na}^+$ , consistent with the operation of a monomolecular mechanism for the decomplexation of  $\text{Na}^+$  from  $[\text{Na}(\text{TMEC12})]^+$  (Equation 4.3, Chapter 4) in dimethylformamide and dimethylsulfoxide. However, there is another possibility, Mechanism III,<sup>10</sup> in which a second TMEC12 may displace TMEC12 in  $[\text{Na}(\text{TMEC12})]^+$ , as shown in Equation 8.2. In this case,  $\tau_c$  shows a dependence on the free ligand concentration as described by Equation 8.3. In water, the low stability of  $[\text{Na}(\text{TMEC12})]^+$  results in significant concentrations of TMEC12 and  $\text{HTMEC12}^+$  for aqueous solutions (vii) - (x), as shown in Table 8.2. However, it is apparent that  $\tau_c$  is also independent of the concentration of TMEC12 and  $\text{HTMEC12}^+$ , consistent with the rate-determining step of the decomplexation of  $[\text{Na}(\text{TMEC12})]^+$  in water involving  $[\text{Na}(\text{TMEC12})]^+$  alone, which precludes any contribution from Mechanism III to the decomplexation of  $[\text{Na}(\text{TMEC12})]^+$ .



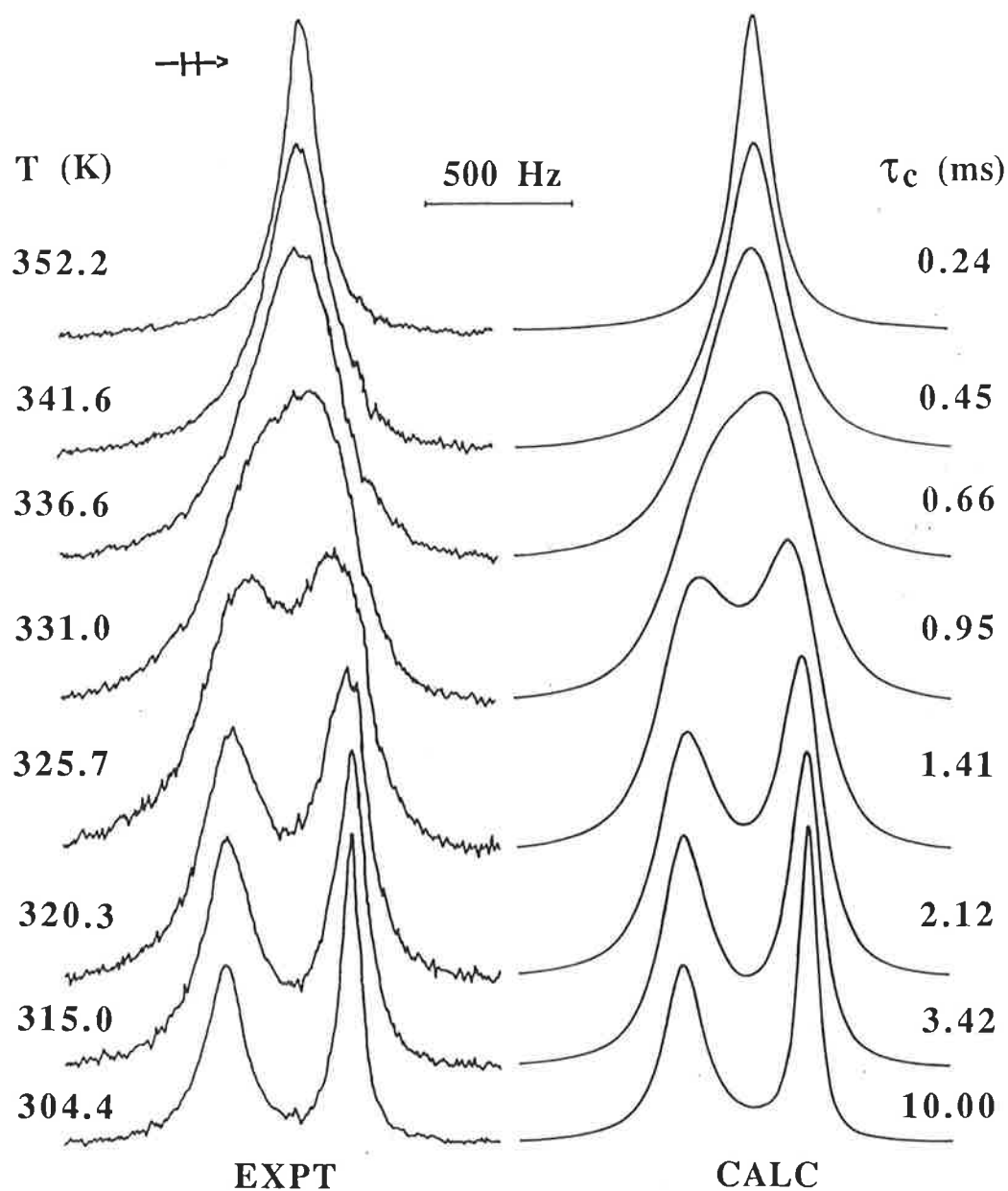


**Figure 8.1.** Typical exchange-modified 79.39 MHz  $^{23}\text{Na}$  NMR spectra of an aqueous solution of hydrated  $\text{Na}^+$  ( $0.0085 \text{ mol dm}^{-3}$ ),  $[\text{Na}(\text{TMEC12})]^+$  ( $0.0116 \text{ mol dm}^{-3}$ ), free TMEC12 ( $0.0087 \text{ mol dm}^{-3}$ ) and HTMEC12 $^+$  ( $0.0035 \text{ mol dm}^{-3}$ ). Experimental temperatures and spectra appear to the left of the figure and the best fit calculated line shapes and corresponding  $\tau_c$  values appear to the right. The resonance of  $[\text{Na}(\text{TMEC12})]^+$  appears downfield from that of solvated  $\text{Na}^+$ .

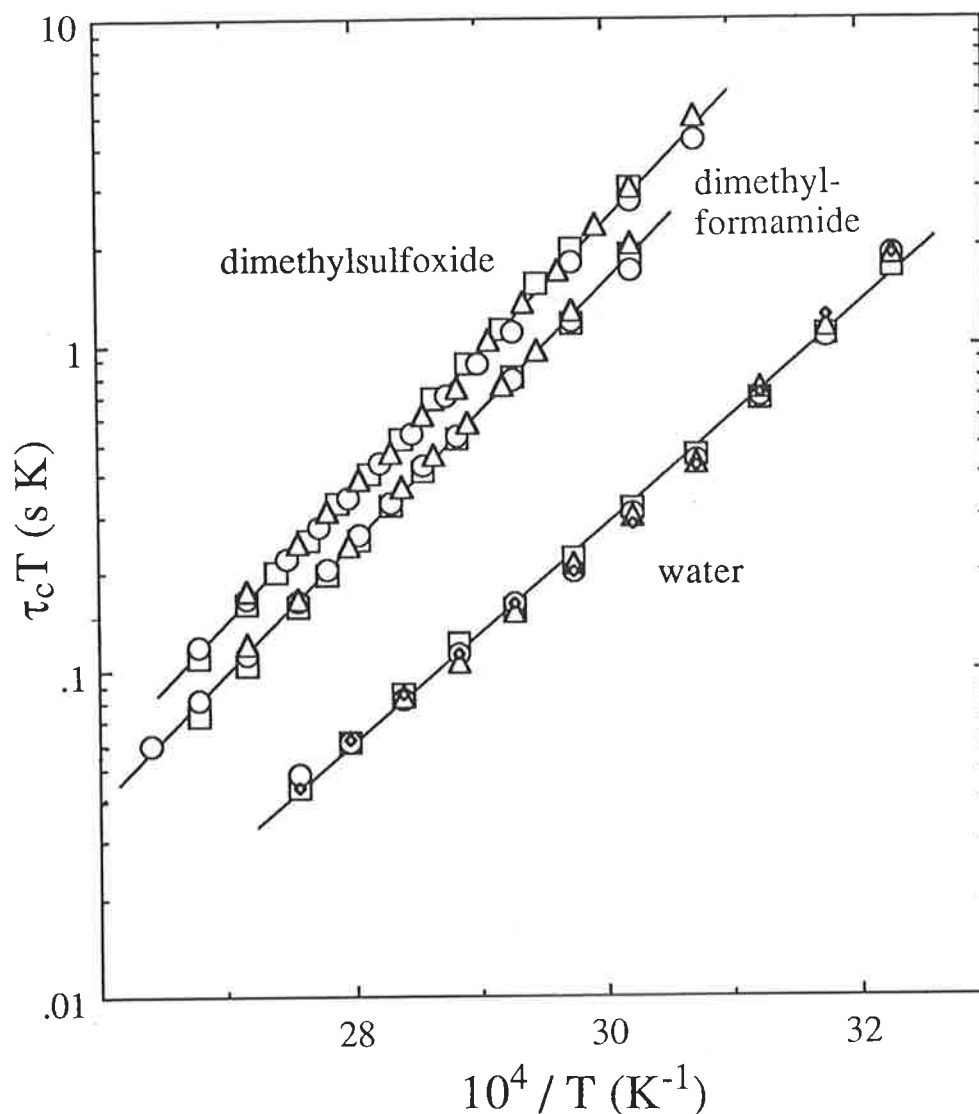
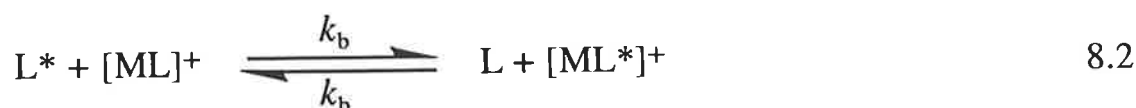


**Figure 8.2.** Temperature variation of  $\tau_c$  for  $[\text{Na}(\text{TMEC12})]^+$  in dimethylformamide, dimethylsulfoxide and water. Data points for dimethylformamide solutions i-iii are represented by triangles, squares and circles, respectively. Data points for dimethylsulfoxide solutions iv-vi are represented by triangles, squares and circles, respectively. Data points for aqueous solutions vii-x are represented by triangles, squares, diamonds and circles, respectively. The solid lines represent the best fit of the combined data for each group to Equation 4.14.

**Table 8.1.** Sodium Ion Exchange on [Na(TMEC12)]<sup>+</sup> in Dimethylformamide, Dimethylsulfoxide and Water. Solution Composition and Kinetic Parameters.<sup>a</sup>

soln.	solvent	[Na <sup>+</sup> <sub>solvated</sub> ] mol dm <sup>-3</sup>	[Na(TMEC12)] <sup>+</sup> mol dm <sup>-3</sup>	$k_d(T)$ s <sup>-1</sup>	$k_d(298.2 \text{ K})$ s <sup>-1</sup>	$\Delta H_d^\ddagger$ kJ mol <sup>-1</sup>	$\Delta S_d^\ddagger$ J mol <sup>-1</sup> K <sup>-1</sup>
				$k_d(356.6 \text{ K})$			
i	dimethyl- formamide	0.0259	0.0777	1340 ± 10	7.7 ± 0.3	76.8 ± 0.1	29.1 ± 1.8
ii		0.0549	0.0487	1424 ± 12	7.2 ± 0.3	77.6 ± 0.1	31.5 ± 2.0
iii		0.0730	0.0306	1382 ± 11	8.6 ± 0.4	74.3 ± 0.1	22.2 ± 1.8
(i - iii) <sup>b</sup>				1381 ± 10	7.6 ± 0.3	76.2 ± 0.1	27.7 ± 1.7
				$k_d(352.2 \text{ K})$			
(iv)	dimethyl- sulfoxide	0.0351	0.0653	661 ± 8	4.4 ± 0.2	78.3 ± 0.1	30.0 ± 2.8
(v)		0.0502	0.0502	670 ± 3	3.9 ± 0.1	80.4 ± 0.1	36.0 ± 1.2
(vi)		0.0673	0.0331	693 ± 4	5.5 ± 0.1	75.6 ± 0.1	22.7 ± 1.3
(iv - vi) <sup>b</sup>				675 ± 5	4.6 ± 0.2	78.1 ± 0.1	29.6 ± 1.6
				$k_d(325.7 \text{ K})$			
vii	water	0.0062	0.0139	676 ± 17	65 ± 4	66.3 ± 1.7	1.2 ± 4.8
viii		0.0085	0.0116	664 ± 15	68 ± 3	64.3 ± 1.1	5.8 ± 3.0
ix		0.0114	0.0087	689 ± 21	75 ± 5	62.7 ± 1.5	1.1 ± 4.3
x		0.0143	0.0056	680 ± 26	71 ± 6	63.9 ± 1.9	4.8 ± 5.1
(vii - x) <sup>b</sup>					677 ± 10	70 ± 2	64.0 ± 0.7

<sup>a</sup> Errors represent one standard deviation from the least-squares fit of the experimental  $\tau_c$  data to Equation 4.14. <sup>b</sup> Simultaneous fit of all data for this solvent.



where  $k_b$  is the bimolecular exchange rate constant.

$$\tau_c = \frac{1}{k_b[L]} \quad \text{and} \quad \frac{\tau_c}{\chi_c} = \frac{\tau_s}{\chi_s} \quad 8.3$$

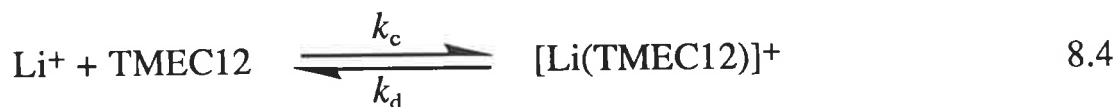
**Table 8.2.** Solution Compositions for [Na(TMEC12)]<sup>+</sup> in Aqueous Solution.

Solution	pH	[Na <sup>+</sup> ] <sub>hydrated</sub> mol dm <sup>-3</sup>	[Na(TMEC12)] <sup>+</sup> mol dm <sup>-3</sup>	[TMEC12] mol dm <sup>-3</sup>	[HTMEC12] <sup>+</sup> mol dm <sup>-3</sup>
(vii)	11.42	0.0062	0.0139	0.0141	0.0044
(viii)	11.32	0.0085	0.0116	0.0087	0.0035
(ix)	11.20	0.0114	0.0087	0.0048	0.0025
(x)	11.06	0.0143	0.0058	0.0025	0.0018

The <sup>23</sup>Na NMR spectra of solutions containing solvated Na<sup>+</sup> and [Na(TMEC12)]<sup>+</sup> in acetonitrile, propylene carbonate and methanol show two distinct resonances characterising solvated Na<sup>+</sup> and [Na(TMEC12)]<sup>+</sup>, which exhibit no apparent broadening at temperatures approaching the boiling point of these solvents. Thus, the rate of exchange of Na<sup>+</sup> between the solvated and complexed environments is in the very slow exchange region of the NMR timescale in these solvents (Chapter 12). However, conservative lower limits for  $\tau_c$  of 24.4 ms (355 K), 11.5 ms (400 K) and 17.2 ms (338 K) in acetonitrile, propylene carbonate and methanol, respectively, were determined using the slow-exchange approximation (Equation 12.23) by calculating the  $\tau_c$  value that would cause the width of the [Na(TMEC12)]<sup>+</sup> resonance to be broadened by a factor of 1.5. These results are summarised in Table 8.4.

### 8.3 Exchange Kinetics of Li<sup>+</sup> on [Li(TMEDC12)]<sup>+</sup>

The exchange of Li<sup>+</sup> on [Li(TMEDC12)]<sup>+</sup> (Equation 8.4) falls within the NMR timescale in methanol, dimethylformamide and dimethylsulfoxide.



The temperature dependent coalescence of the <sup>7</sup>Li resonances characterising this exchange in dimethylsulfoxide appears in Figure 8.3. The kinetic parameters shown in Table 8.3 were obtained through the temperature dependence of  $\tau_c$ , the mean lifetime of [Li(TMEDC12)]<sup>+</sup>, through Equation 4.14. The  $\tau_c$  values were determined by complete lineshape analysis of the coalescing <sup>7</sup>Li resonances observed for each of the solutions (i) - (ix), whose compositions appear in Table 8.3. The magnitudes and temperature variations of  $\tau_c$  for each of the solutions studied for a given solvent are indistinguishable (Figure 8.4). Thus,  $\tau_c$  is independent of the concentration of solvated Li<sup>+</sup>, consistent with the operation of a monomolecular mechanism for the decomplexation of Li<sup>+</sup> from [Li(TMEDC12)]<sup>+</sup> (Equation 4.3).

The <sup>7</sup>Li NMR spectra of solutions containing solvated Li<sup>+</sup> and [Li(TMEDC12)]<sup>+</sup> in acetonitrile and propylene carbonate show two distinct resonances characterising solvated Li<sup>+</sup> and [Li(TMEDC12)]<sup>+</sup>, which exhibit no apparent broadening at temperatures approaching the boiling point of these solvents. Thus, the rate of exchange of Li<sup>+</sup> between the solvated and complexed environments is in the very slow exchange region of the NMR timescale in these solvents (Chapter 12). However, conservative lower limits for  $\tau_c$  of 118 ms (355 K) and 84 ms (400 K) in acetonitrile and propylene carbonate, respectively, could be estimated using the slow-exchange approximation (Equation 12.23) by calculating the  $\tau_c$  value that would cause the width of the [Li(TMEDC12)]<sup>+</sup> resonance to be broadened by a factor of 1.5. These results are summarised in Table 8.4.

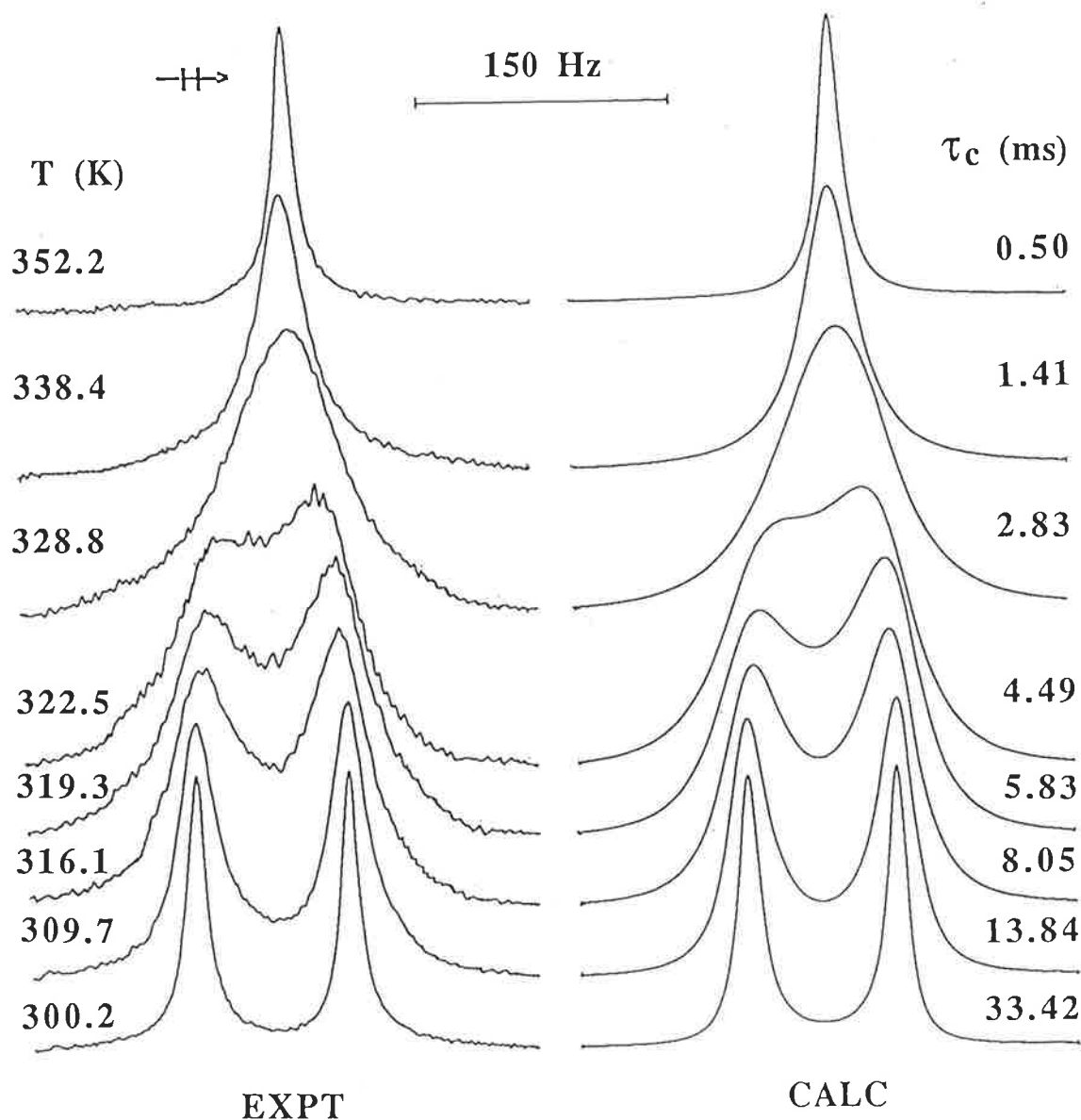


**Figure 8.3.** Typical exchange-modified 116.59 MHz  $^7\text{Li}$  NMR spectra of a dimethylsulfoxide solution of solvated  $\text{Li}^+$  ( $0.0474 \text{ mol dm}^{-3}$ ) and  $[\text{Li}(\text{TMEC12})]^+$  ( $0.0534 \text{ mol dm}^{-3}$ ). Experimental temperatures and spectra appear to the left of the figure and the best fit calculated line shapes and corresponding  $\tau_c$  values appear to the right. The resonance of  $[\text{Li}(\text{TMEC12})]^+$  appears downfield from that of solvated  $\text{Li}^+$ .

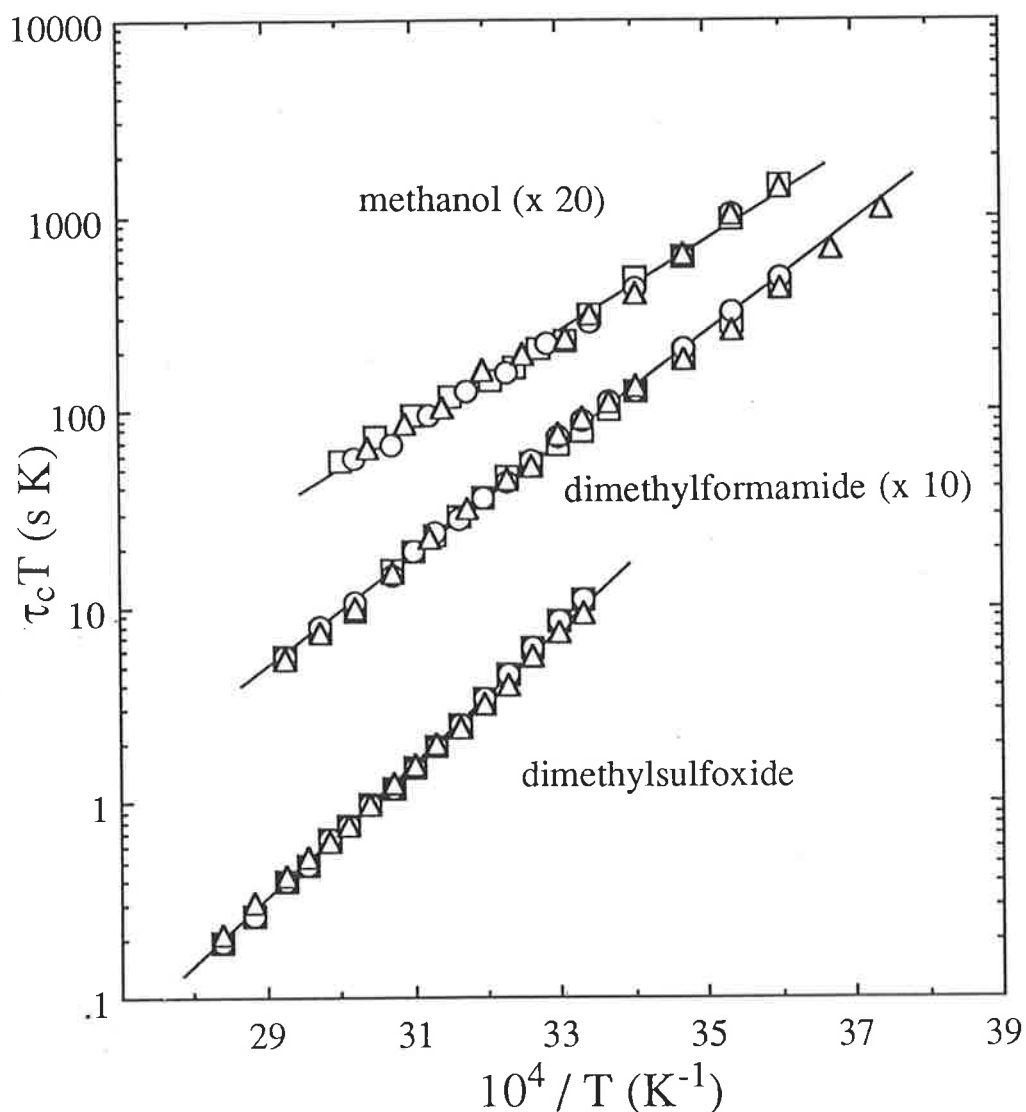


**Figure 8.4.** Temperature variation of  $\tau_c$  for  $[\text{Li}(\text{TMEC12})]^+$  in dimethylformamide, dimethylsulfoxide and methanol. Data points for dimethylformamide solutions i-iii are represented by triangles, squares and circles, respectively. Data points for dimethylsulfoxide solutions iv-vi are represented by triangles, squares, and circles, respectively. Data points for methanol solutions vii-ix are represented by triangles, squares and circles, respectively. The solid lines represent the best fit of the combined data for each group to Equation 4.14.

**Table 8.3.** Lithium Ion Exchange on [Li(TMEC12)]<sup>+</sup> in Dimethylformamide, Dimethylsulfoxide and Methanol. Solution Composition and Kinetic Parameters.<sup>a</sup>

soln.	solvent	[Li <sup>+</sup> <sub>solvated</sub> ] mol dm <sup>-3</sup>	[Li(TMEC12)] <sup>+</sup> mol dm <sup>-3</sup>	$k_d(T)$ s <sup>-1</sup>	$k_d(298.2 \text{ K})$ s <sup>-1</sup>	$\Delta H_d^\ddagger$ kJ mol <sup>-1</sup>	$\Delta S_d^\ddagger$ J mol <sup>-1</sup> K <sup>-1</sup>
				$k_d(316.1 \text{ K})$			
i	dimethyl- formamide	0.0250	0.0749	116 ± 3	31.4 ± 0.4	53.7 ± 0.8	-35.9 ± 2.6
ii		0.0454	0.0544	117 ± 2	31.7 ± 0.7	54.3 ± 0.9	-34.1 ± 2.6
iii		0.0639	0.0360	112 ± 2	30.0 ± 0.6	55.3 ± 0.7	-31.4 ± 2.1
(i - iii) <sup>b</sup>				115 ± 1	31.4 ± 0.4	54.3 ± 0.5	-34.3 ± 1.5
				$k_d(322.5 \text{ K})$			
(iv)	dimethyl- sulfoxide	0.0272	0.0736	202 ± 2	26.7 ± 0.6	64.2 ± 0.7	-2.4 ± 1.9
(v)		0.0474	0.0534	210 ± 2	26.1 ± 0.6	66.2 ± 0.7	4.2 ± 1.9
(vi)		0.0600	0.0408	202 ± 2	23.9 ± 0.6	67.8 ± 0.7	8.7 ± 2.1
(iv - vi) <sup>b</sup>				205 ± 2	25.6 ± 0.4	66.0 ± 0.5	3.3 ± 1.4
				$k_d(308.7 \text{ K})$			
vii	methanol	0.0065	0.0141	34 ± 1	17.9 ± 0.5	44.8 ± 1.3	-70.8 ± 4.7
viii		0.0090	0.0115	34 ± 1	17.9 ± 0.7	44.1 ± 1.5	-73.2 ± 5.3
ix		0.0128	0.0077	36 ± 1	18.8 ± 0.6	45.7 ± 1.3	-67.4 ± 4.7
(vii - ix) <sup>b</sup>				34.7 ± 0.6	18.2 ± 0.4	44.8 ± 0.8	-70.5 ± 2.9

<sup>a</sup> Errors represent one standard deviation from the least-squares fit of the experimental  $\tau_c$  data to Equation 4.14. <sup>b</sup> Simultaneous fit of all data for this solvent.



**Table 8.4.** Kinetic Parameters for M<sup>+</sup> Exchange on [M(TMEDC12)]<sup>+</sup> in a Range of Solvents at 298.2 K.

Solvent	$D_N^a$	$10^{-5} k_c^b$ dm <sup>3</sup> mol <sup>-1</sup> s <sup>-1</sup>	$k_d$ s <sup>-1</sup>	$\log K_s$ ( $K_s/\text{dm}^3 \text{ mol}^{-1}$ )
[Na(TMEDC12)] <sup>+</sup>				
acetonitrile	14.1		<41 <sup>c</sup>	9.13
propylene-carbonate	15.1		<87 <sup>c</sup>	8.2
methanol	19.0 (23.5) <sup>d</sup>		<58 <sup>c</sup>	6.2
dimethyl-formamide	26.6	36.4	7.6	5.68
dimethyl-sulfoxide	29.8	4.1	4.6	4.95
water	18.0 (33.0) <sup>d</sup>	0.11	70	2.20
[Li(TMEDC12)] <sup>+</sup>				
acetonitrile	14.1		<8.5 <sup>c</sup>	9.34
propylene-carbonate	15.1		<11.9 <sup>c</sup>	8.0
methanol	19.0 (23.5) <sup>d</sup>	2.3	18.2	4.1
dimethyl-formamide	26.6	1.3	31.4	3.61
dimethyl-sulfoxide	29.8	0.17	25.6	2.82

<sup>a</sup> Gutmann donor numbers from Reference 11. <sup>b</sup>  $k_c = k_d K_s$ . <sup>c</sup> Calculated from Equation 12.23. The widths at half height of the <sup>23</sup>Na resonances of [Na(TMEDC12)]<sup>+</sup> ( $W_{1/2a}$ ) in acetonitrile, propylene carbonate and methanol are 26.1 Hz, 55.4 Hz and 37.0 Hz, respectively. The widths at half height of the <sup>7</sup>Li resonances of [Li(TMEDC12)]<sup>+</sup> ( $W_{1/2a}$ ) in acetonitrile and propylene carbonate are 5.4 Hz and 7.6 Hz, respectively. <sup>d</sup> Gutmann donor number from references 12 and 13.

## 8.4 Mechanism of Exchange of $M^+$ on $[M(\text{TMEC12})]^+$

Two possible pathways for the exchange of  $M^+$  on  $[M(\text{TMEC12})]^+$  are shown in Figure 8.5. The ground state  $[M(\text{TMEC12})]^+$  species is based on  $^{13}\text{C}$  NMR studies which show that both  $\text{Li}^+$  and  $\text{Na}^+$  are eight coordinate in methanol and the coordination geometry of  $M^+$  is square antiprismatic (Chapter 9).<sup>14</sup> The reaction pathway for complexation and decomplexation includes solvational changes in  $M^+$  and conformational changes in TMEC12, as described by the Eigen-Winkler mechanism in Chapter 4.<sup>7-9</sup> However, in Figure 8.5, these are omitted for the sake of simplicity. Pathway A involves initial coordination of  $M^+$  to the four ligand nitrogens, where  $M^+$  lies above the plane of the tetraaza ring. This is followed by the sequential coordination of the four methoxyethyl arms. Pathway B involves initial coordination of  $M^+$  by two nitrogens and two methoxyethyl pendant arms so that  $M^+$  is bound perpendicular to the plane of the tetraaza ring. This is followed by coordination of the remaining ring nitrogens and the other two methoxyethyl pendant arms. Decomplexation is the reverse of either of these two processes. The formation of stable  $[M(\text{cyclen})]^+$  complexes indicates that pathway A is plausible, but the experimental results do not distinguish between these two pathways, although  $k_d$  represents the slowest step in the sequential decomplexation of  $[M(\text{TMEC12})]^+$  depicted in Figure 8.5. It is possible that  $k_d$  characterises an inversion about an amine nitrogen of TMEC12, as has been suggested for complexation and decomplexation of divalent metal ions by 1,4,7,10-tetramethyl-1,4,7,10-tetraazacyclododecane.<sup>15</sup> (Similar rate-limiting conformational changes are postulated in the Eigen-Winkler mechanism<sup>7-9</sup> and have been proposed for the complexation of alkali metal ions by crown ethers, diaza crown ethers and lariat ethers<sup>16-23</sup>).

## 8.5 Effect of Solvent on the Lability of $[M(\text{TMEC12})]^+$

As may be seen from Table 8.4, there is a significant variation in  $k_c$  and  $k_d$  characterising  $[\text{Li}(\text{TMEC12})]^+$  and  $[\text{Na}(\text{TMEC12})]^+$  with the nature of the solvent. The variation in magnitude of  $k_d$  characterising  $[\text{Na}(\text{TMEC12})]^+$  is in the sequence methanol < dimethylformamide < water. For  $[\text{Li}(\text{TMEC12})]^+$ , a similar trend is observed, with  $k_d$  increasing in the sequence acetonitrile < methanol < dimethylformamide. This is similar to the variation of  $k_d$  with the nature of the solvent discussed in Chapter 4 for the  $\text{Na}^+$  complexes of  $\text{C22C2}$

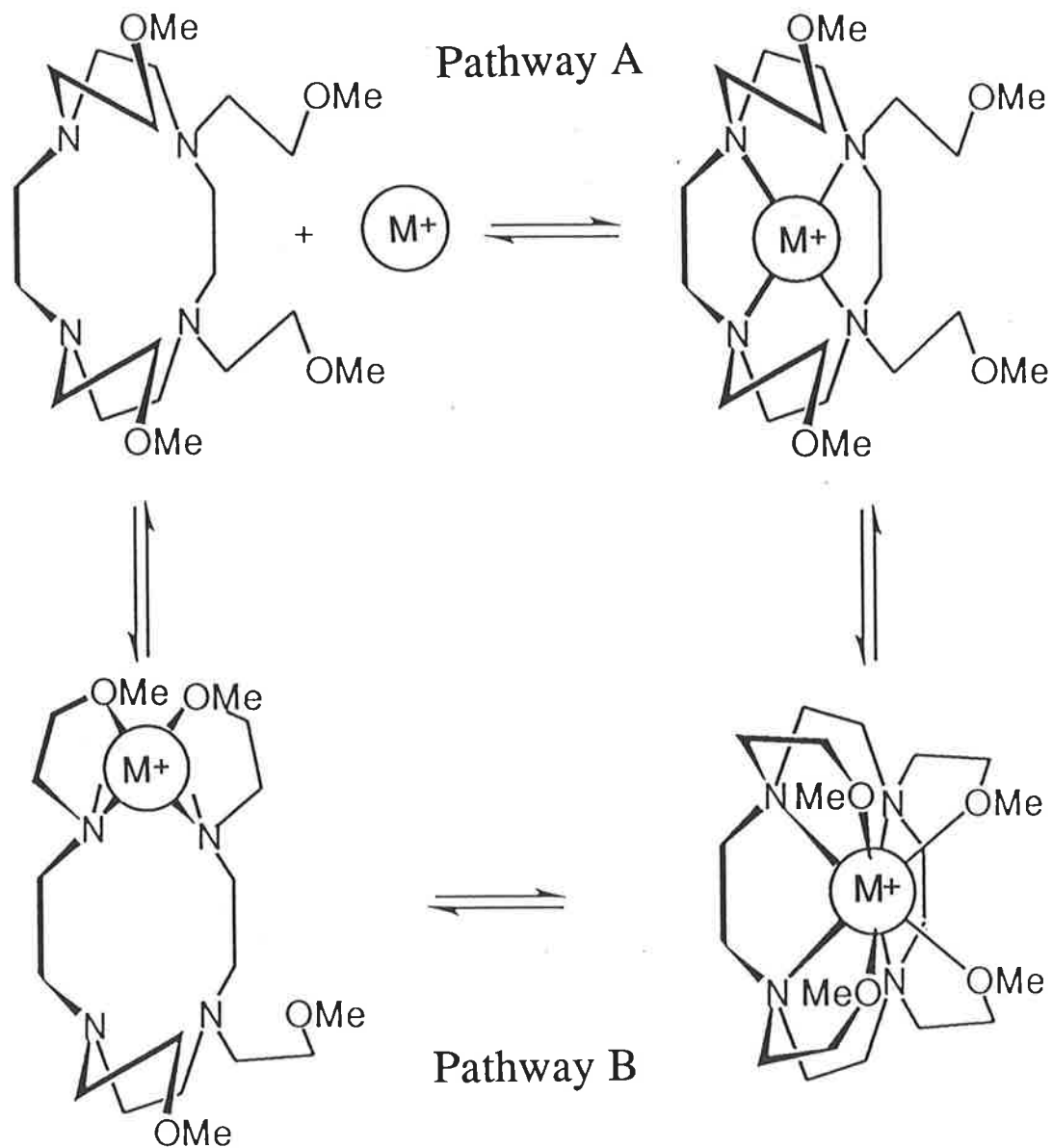


**Figure 8.5.** Possible pathways for the exchange of  $M^+$  on  $[M(\text{TMEC12})]^+$ . Pathway A involves initial coordination of  $M^+$  to the four ligand nitrogens, followed by the coordination of the four methoxyethyl pendant arms. Pathway B involves the initial coordination of  $M^+$  by two nitrogens and two methoxyethyl pendant arms, followed by the coordination of the remaining ring nitrogens and the other two methoxyethyl pendant arms. This scheme does not show solvational changes in  $M^+$  or conformational changes in TMEC12.

and C22C8, where it was found that  $k_d$  increases as the solvent  $D_N$  increases. However, for the range of solvents for which quantitative data for  $[M(\text{TMEC12})]^+$  is available,  $k_c$  varies more significantly than  $k_d$  with the nature of the solvent, with the result that variations in the stability of  $[M(\text{TMEC12})]^+$  are determined predominantly by variations in  $k_c$ . The variation of  $k_c$  (298.2 K) characterising  $[\text{Li}(\text{TMEC12})]^+$  is in the sequence dimethylsulfoxide < dimethylformamide < methanol and the variation of  $k_c$  (298.2 K) characterising  $[\text{Na}(\text{TMEC12})]^+$  is in the sequence water < dimethylsulfoxide < dimethylformamide. Thus,  $k_c$  decreases as solvent  $D_N$  increases, consistent with the rate-determining step for complex formation involving substantial desolvation of  $M^+$ . Conversely, there is little involvement of solvent in the rate-determining step for decomplexation, as demonstrated by the small solvent variation in  $k_d$  characterising  $[\text{Li}(\text{TMEC12})]^+$  and  $[\text{Na}(\text{TMEC12})]^+$  in these solvents. (Nevertheless, the similar  $k_d$  values characterising  $[\text{Li}(\text{TMEC12})]^+$  result from different, but compensating values of  $\Delta H_d^\ddagger$  and  $\Delta S_d^\ddagger$ , which may reflect the different contributions of conformational and solvational changes to the decomplexation process in each solvent). This implies that the transition state is more similar to the complex than to the solvated  $M^+$  and free TMEC12. Similar variations in  $k_c$  (298.2 K) and  $k_d$  (298.2 K) with the nature of the solvent are observed for the related  $[\text{Na}(\text{THEC12})]^+$  system.<sup>6,24</sup> This contrasts with the behaviour exhibited by the alkali metal cryptates, where  $k_d$  varies with the nature of the solvent far more than  $k_c$ ,<sup>25-26</sup> which may be a reflection of the greater rigidity of the cryptands by comparison with TMEC12 and THEC12.

As discussed in Chapter 6,  $[\text{Na}(\text{TMEC12})]^+$  is more stable than  $[\text{Li}(\text{TMEC12})]^+$  in the oxygen donor solvents studied, but in acetonitrile, this selectivity is reversed and  $[\text{Li}(\text{TMEC12})]^+$  is more stable than  $[\text{Na}(\text{TMEC12})]^+$ . Unfortunately, no quantitative kinetic data for these complexes could be obtained in acetonitrile, so that it is not certain to what extent this selectivity reversal results from changes in  $k_c$  and  $k_d$ .

In aqueous solution,  $k_c$  characterising  $[\text{Na}(\text{TMEC12})]^+$  is particularly small. As discussed in Chapter 4, this may be a result of the hydrogen bonding ability of water. Any hydrogen bonding between water molecules and TMEC12 must be disrupted during the complexation process, which tends to slow the rate of complex formation. Conversely, the hydrogen bonding ability of water also facilitates the decomplexation process, since solvation of the ligand during the decomplexation of  $\text{Na}^+$  from  $[\text{Na}(\text{TMEC12})]^+$  will stabilise

the transition state. This is consistent with the smaller  $\Delta H_d^\ddagger$  and  $\Delta S_d^\ddagger$ , and the larger  $k_d$  characterising  $[\text{Na}(\text{TMEC12})]^+$  in water, compared with these parameters in dimethylformamide and dimethylsulfoxide.

## 8.6 Exchange Kinetics of $[M(\text{TMEC12})]^+$ and Related Systems

The kinetic parameters characterising  $[\text{Li}(\text{TMEC12})]^+$  and  $[\text{Na}(\text{TMEC12})]^+$  appear in Table 8.5. In dimethylformamide, the 117 fold greater stability of  $[\text{Na}(\text{TMEC12})]^+$  compared with  $[\text{Li}(\text{TMEC12})]^+$  results from  $k_c$  and  $k_d$  characterising  $[\text{Na}(\text{TMEC12})]^+$  being 28.0 times larger and 4.1 times smaller, respectively, than those characterising  $[\text{Li}(\text{TMEC12})]^+$ . In dimethylsulfoxide, the 135 fold greater stability of  $[\text{Na}(\text{TMEC12})]^+$  compared with  $[\text{Li}(\text{TMEC12})]^+$  results from  $k_c$  and  $k_d$  characterising  $[\text{Na}(\text{TMEC12})]^+$  being 24.1 times larger and 5.6 times smaller, respectively, than those characterising  $[\text{Li}(\text{TMEC12})]^+$ . This is similar to the behaviour exhibited by alkali metal cryptates (Chapter 4), in which the most stable cryptate is generally the least labile toward decomplexation.<sup>25</sup> However, the variation in  $k_c$  is the dominant factor determining variations in  $K_s$  among the  $\text{Li}^+$  and  $\text{Na}^+$  complexes of TMEC12. As discussed in Section 8.5, it is apparent that the rate-determining step for the formation of  $[M(\text{TMEC12})]^+$  involves considerable desolvation of  $M^+$ . Thus, the smaller  $k_c$  characterising  $[\text{Li}(\text{TMEC12})]^+$  are consistent with the greater solvation energy of  $\text{Li}^+$  compared with  $\text{Na}^+$ , which gives rise to a more significant contribution from desolvation to the activation energy for the complexation process.

The greater  $k_d$  characterising  $[\text{Li}(\text{TMEC12})]^+$ , compared with those of  $[\text{Na}(\text{TMEC12})]^+$  in dimethylformamide and dimethylsulfoxide, is a result of a much smaller  $\Delta H_d^\ddagger$ , despite a more negative  $\Delta S_d^\ddagger$ . In methanol,  $\text{Li}^+$  and  $\text{Na}^+$  in  $[M(\text{TMEC12})]^+$  are both eight coordinate<sup>14</sup> (Chapter 9) and it is probable that this coordination number is maintained in all solvents studied, as discussed in Chapter 6. As a result, it may be concluded that the different  $\Delta H_d^\ddagger$  and  $\Delta S_d^\ddagger$  characterising  $[\text{Na}(\text{TMEC12})]^+$  and  $[\text{Li}(\text{TMEC12})]^+$  do not arise from a difference in the number of pendant arms binding  $\text{Li}^+$  and  $\text{Na}^+$ . Thus, the smaller  $k_d$  and larger  $\Delta H_d^\ddagger$  characterising  $[\text{Na}(\text{TMEC12})]^+$  probably result from the optimum size of  $\text{Na}^+$  and the minimisation of strain in  $[\text{Na}(\text{TMEC12})]^+$ , compared with  $[\text{Li}(\text{TMEC12})]^+$  (see discussion in Sections 6.2 and 6.4, Chapter 6). The smaller size of  $\text{Li}^+$  may result in greater steric hindrance between coordinated methoxyethyl pendant arms in  $[\text{Li}(\text{TMEC12})]^+$ ,

**Table 8.5.** Kinetic Parameters for M<sup>+</sup> Exchange on [M(TMEC12)]<sup>+</sup> and Other Complexes.

complex	solvent	$D_N^a$	$10^{-5} k_c^b$ (298.2 K) $\text{dm}^3 \text{mol}^{-1} \text{s}^{-1}$	$k_d$ (298.2 K) $\text{s}^{-1}$	$\Delta H_d^\ddagger$ $\text{kJ mol}^{-1}$	$\Delta S_d^\ddagger$ $\text{J mol}^{-1} \text{K}^{-1}$	$\log K_s$ ( $\text{K}_s/\text{dm}^3 \text{mol}^{-1}$ )
[Li(TMEC12)] <sup>+</sup> <sup>c</sup>	methanol	19.0 (23.5) <sup>d</sup>	2.3	18.2	44.8	-70.5	4.1
[Li(TMEC12)] <sup>+</sup> <sup>c</sup>	dimethyl- formamide	26.6	1.3	31.4	54.3	-34.3	3.61
[Li(TMEC12)] <sup>+</sup> <sup>c</sup>	dimethyl sulfoxide	29.8	0.17	25.6	66.0	3.3	2.82
[Na(TMEC12)] <sup>+</sup> <sup>c</sup>	acetonitrile	14.1		<41			9.13
[Na(TMEC12)] <sup>+</sup>	propylene- carbonate	15.1		<87 <sup>c</sup>			8.2 <sup>e</sup>
[Na(TMEC12)] <sup>+</sup> <sup>c</sup>	dimethyl- formamide	26.6	36.4	7.6	76.2	27.7	5.68
[Na(TMEC12)] <sup>+</sup> <sup>c</sup>	dimethyl- sulfoxide	29.8	4.1	4.6	78.1	29.6	4.95
[Na(TMEC12)] <sup>+</sup> <sup>c</sup>	water	18.0 (33.0) <sup>d</sup>	0.11	70	64.0	5.1	2.20
[Li(THEC12)] <sup>+</sup> <sup>e</sup>	methanol	19.0 (23.5) <sup>d</sup>	8.97	729	38.0	-62.8	3.09
[Li(THEC12)] <sup>+</sup> <sup>e</sup>	dimethyl- formamide	26.6	5.74	587	41.8	-51.9	2.99
[Na(THEC12)] <sup>+</sup> <sup>e</sup>	methanol	19.0 (23.5) <sup>d</sup>	70.8	209	68.3	28.4	4.53
[Na(THEC12)] <sup>+</sup> <sup>e</sup>	dimethyl- formamide	26.6	7.00	299	56.4	-8.4	3.37

**Table 8.5** continued.

[Na(cyclen)] <sup>+f</sup>	acetonitrile	14.1		>704			3.60
[Na(cyclen)] <sup>+f</sup>	propylene-carbonate	15.1		>2440			5.45
[Na(TMEC14)] <sup>+g</sup>	acetonitrile	14.1	1018	9500	25.0	-85.1	4.03
[LiC22C2] <sup>+h</sup>	methanol	19.0 (23.5) <sup>d</sup>	97.1	971	31.0	-84.0	4.0
[LiC22C2] <sup>+h</sup>	dimethyl-formamide	26.6	7.60	240	22.5	-124	3.5
[NaC22C2] <sup>+c</sup>	dimethyl-formamide	26.6	155	12.3	64.0	-9.5	6.1
[NaC22C2] <sup>+c</sup>	dimethyl-sulfoxide	29.8	44.2	11.1	65.8	-4.1	5.6
[NaC22C2] <sup>+c</sup>	water	18.0 (33.0) <sup>d</sup>	4.04	255	56.6	-9.4	3.2
[LiC221] <sup>+</sup>	methanol	19.0 (23.5) <sup>d</sup>	192 <sup>i</sup>	78.4 <sup>i</sup>	23.8 <sup>i</sup>	-129 <sup>i</sup>	5.38 <sup>j</sup>
[NaC221] <sup>+</sup>	dimethyl-formamide	26.6	180 <sup>k</sup>	0.25 <sup>k</sup>	73.0 <sup>l</sup>	-9 <sup>l</sup>	7.93 <sup>j</sup>
[NaC221] <sup>+</sup>	dimethyl-sulfoxide	29.8	72 <sup>k</sup>	0.75 <sup>k</sup>	70.4 <sup>l</sup>	-11 <sup>l</sup>	6.98 <sup>j</sup>
[NaC221] <sup>+</sup>	water	18.0 (33.0) <sup>d</sup>	36 <sup>k</sup>	14.5 <sup>k</sup>			5.4 <sup>j</sup>

<sup>a</sup> Gutmann donor numbers from reference 11. <sup>b</sup>  $k_c = k_d K_s$ . <sup>c</sup> This work. <sup>d</sup> Gutmann donor number from references 12 and 13.

<sup>e</sup> Reference 6. <sup>f</sup> Reference 24. <sup>g</sup> Reference 27. <sup>h</sup> Reference 28. <sup>i</sup> Reference 29. <sup>j</sup> Reference 30. <sup>k</sup> Reference 25. <sup>l</sup> Reference 31

by comparison with  $[\text{Na}(\text{TMEC12})]^+$ . This factor should also contribute to the smaller  $k_c$  characterising  $[\text{Li}(\text{TMEC12})]^+$ .

The  $[\text{M}(\text{TMEC12})]^+$  kinetic data may now be compared with those characterising  $[\text{Li}(\text{THEC12})]^+$ ,  $[\text{Na}(\text{THEC12})]^+$  and other complexes for which monomolecular decomplexation mechanisms operate. In methanol and dimethylformamide, it is apparent that the greater stability of  $[\text{Li}(\text{TMEC12})]^+$  compared with that of  $[\text{Li}(\text{THEC12})]^+$  is largely a result of a much smaller  $k_d$  characterising  $[\text{Li}(\text{TMEC12})]^+$ , despite its smaller  $k_c$ . This is a result of the much larger  $\Delta H_d^\ddagger$  characterising  $[\text{Li}(\text{TMEC12})]^+$ . Similarly, the greater stability of  $[\text{Na}(\text{TMEC12})]^+$  in dimethylformamide, by comparison with that of  $[\text{Na}(\text{THEC12})]^+$ , results mainly from the much smaller  $k_d$  characterising  $[\text{Na}(\text{TMEC12})]^+$ , which is a consequence of the much larger  $\Delta H_d^\ddagger$ .

The factors that effect the relative labilities of  $[\text{M}(\text{TMEC12})]^+$  and  $[\text{M}(\text{THEC12})]^+$  are the same as those affecting their relative stabilities, which are as follows; i) the inductive effect of the methyl group of the methoxyethyl arm of TMEC12; ii) the steric effect of the methyl group and iii) the hydrogen bonding capacity of THEC12. In Chapter 6, it was seen that the balance between these effects resulted in both  $[\text{Li}(\text{TMEC12})]^+$  and  $[\text{Na}(\text{TMEC12})]^+$  being more stable than their THEC12 analogues and the difference in stabilities was greater for the  $\text{Na}^+$  complexes than for the  $\text{Li}^+$  complexes. The smaller  $k_d(298.2 \text{ K})$  and larger  $\Delta H_d^\ddagger$  characterising  $[\text{M}(\text{TMEC12})]^+$  compared with those characterising  $[\text{M}(\text{THEC12})]^+$  are consistent with the methoxy donor group being a stronger electron pair donor than the hydroxy donor group, which results in a greater electrostatic attraction between  $\text{M}^+$  and TMEC12 compared with THEC12. The greater steric hindrance resulting from the methyl group would tend to decrease  $k_c$  characterising  $[\text{M}(\text{TMEC12})]^+$  compared with that characterising  $[\text{M}(\text{THEC12})]^+$ . Conversely, the hydrogen bonding capacity of THEC12, (which may result in intramolecular hydrogen bonds between the pendant arms<sup>32</sup> or intermolecular hydrogen bonds between the pendant arms and the solvent) would tend to decrease  $k_c$  for  $[\text{M}(\text{THEC12})]^+$ . The balance between these two effects results in  $k_c(298.2 \text{ K})$  characterising  $[\text{Na}(\text{TMEC12})]^+$  in dimethylformamide being greater than that characterising  $[\text{Na}(\text{THEC12})]^+$ . In contrast,  $k_c(298.2 \text{ K})$  characterising  $[\text{Li}(\text{TMEC12})]^+$  in methanol and dimethylformamide are smaller than those characterising  $[\text{Li}(\text{THEC12})]^+$ , probably because the effect of steric hindrance is greater for the smaller  $\text{Li}^+$  than for  $\text{Na}^+$ .



In acetonitrile and propylene carbonate, the lower stability of  $[\text{Na}(\text{cyclen})]^+$  compared with that of  $[\text{Na}(\text{TMEC}12)]^+$  results from the much larger  $k_d$  characterising the former complex. As a result of its coordinating pendant arms, TMEC12 can form a three dimensional cavity which can encapsulate  $\text{Na}^+$  more effectively than can cyclen, with the consequence that  $[\text{Na}(\text{TMEC}12)]^+$  is considerably less labile than  $[\text{Na}(\text{cyclen})]^+$ . The lower lability of  $[\text{Na}(\text{TMEC}12)]^+$  also reflects the greater electrostatic attraction between  $\text{Na}^+$  and TMEC12, which possesses eight donor atoms, compared with that between  $\text{Na}^+$  and cyclen, which possesses only four donor atoms.

In acetonitrile, the lower stability of  $[\text{Na}(\text{TMEC}14)]^+$  compared with that of  $[\text{Na}(\text{TMEC}12)]^+$  results from the much larger  $k_d$  characterising  $[\text{Na}(\text{TMEC}14)]^+$ . The lower lability of  $[\text{Na}(\text{TMEC}12)]^+$  is consistent with the lower flexibility of TMEC12 and the optimum size of  $\text{Na}^+$  for TMEC12, whereas TMEC14 selectively complexes the larger  $\text{K}^+$  in most solvents.

Kinetic data for the  $\text{Na}^+$  selective ligands C22C<sub>2</sub> and C221 is available for all solvents in which data were obtained for  $[M(\text{TMEC}12)]^+$ . In dimethylformamide, dimethylsulfoxide and water,  $k_d$  characterising  $[\text{Na}(\text{TMEC}12)]^+$  is 0.62, 0.41 and 0.27 times  $k_d$  characterising  $[\text{NaC}22\text{C}_2]^+$ , but in each case,  $k_c$  characterising  $[\text{NaC}22\text{C}_2]^+$  is significantly larger, so that  $[\text{NaC}22\text{C}_2]^+$  is more stable than  $[\text{Na}(\text{TMEC}12)]^+$ . In dimethylformamide, dimethylsulfoxide and water,  $k_c$  characterising  $[\text{Na}(\text{TMEC}12)]^+$  is 0.20, 0.057 and 0.003 times  $k_c$  characterising  $[\text{NaC}221]^+$  and  $k_d$  characterising  $[\text{NaC}221]^+$  is always smaller, so that  $[\text{NaC}221]^+$  is more stable than  $[\text{Na}(\text{TMEC}12)]^+$ . The selectivity of C221 for  $\text{Na}^+$  results from the matching of the size of  $\text{Na}^+$  to that of the preformed cavity of C221, whereas the selectivity of C22C<sub>2</sub> for  $\text{Na}^+$  results from the similar jaw-angles in  $[\text{NaC}22\text{C}_2]^+$  and free C22C<sub>2</sub>. Thus, in both C221 and C22C<sub>2</sub>, the array of donor atoms are particularly well positioned for sequential coordination of  $\text{Na}^+$ . No such preformed arrangement of donor atoms exists for the more flexible TMEC12, where all conformations readily interconvert in solution. Thus, complexation of  $\text{Na}^+$  by TMEC12 probably involves considerably more conformational changes, when compared with the two cryptands, which may result in the lower  $k_c$  observed for this complex. The larger variation of  $k_c$  with solvent  $D_N$  for  $[\text{Na}(\text{TMEC}12)]^+$  compared with that of its C221 analogues may also indicate the greater importance of desolvation of  $\text{Na}^+$  in the rate-determining step for complexation which would also contribute to the lower  $k_c$  characterising  $[\text{Na}(\text{TMEC}12)]^+$ . These observations are also consistent with the significantly

lower  $k_c$  characterising  $[\text{Li}(\text{TMEC12})]^+$  by comparison with its C221 and C22C<sub>2</sub> analogues.

The differences between  $k_d$  characterising  $[\text{Li}(\text{TMEC12})]^+$  and  $[\text{Na}(\text{TMEC12})]^+$  are considerably lower than the 3000 fold difference in  $k_d$  characterising  $[\text{LiC221}]^+$  and  $[\text{NaC221}]^+$  in methanol, which demonstrates the more incisive influence of the rigid preformed cavity of C221 on selectivity in its complexes and which largely accounts for the much greater stability of the latter cryptate. In dimethylformamide,  $k_d$  characterising  $[\text{LiC22C}_2]^+$  is ~20 times  $k_d$  characterising  $[\text{NaC22C}_2]^+$ , which together with the ~20 fold greater  $k_c$  of the latter cryptate accounts for its greater stability by comparison with  $[\text{LiC22C}_2]^+$ . These variations in  $k_c$  and  $k_d$  are consistent with flexible TMEC12 adapting to the different sizes of Li<sup>+</sup> and Na<sup>+</sup> more readily than the less flexible C221 and C22C<sub>2</sub>. As a consequence, the selectivity of TMEC12 for Na<sup>+</sup> over Li<sup>+</sup> is considerably less than that of C221 and C22C<sub>2</sub>. A similar relationship exists for THEC12.<sup>6</sup>

- 1 Lindoy, L.F. *"The Chemistry of Macrocyclic Ligand Complexes"*, Cambridge University Press, Cambridge, U.K, **1989**.
- 2 Madeyski, C.M.; Michael, J.P.; Hancock, R.D. *Inorg. Chem.* **1984**, *23*, 1487-1489.
- 3 Hay, R.W.; Pujari, M.P.; Moodie, W.T.; Craig, S.; Richens, D.T.; Perotti, A.; Ungaretti, L. *J. Chem. Soc., Dalton Trans.* **1987**, 2605-2613.
- 4 Wainwright, K.P. *J. Chem. Soc., Dalton Trans.* **1980**, 2117-2120.
- 5 Kasprzyk, S.P.; Wilkins, R.G. *Inorg. Chem.* **1982**, *21*, 3349.
- 6 Turonek, M.L.; Clarke, P.; Laurence, G.S.; Lincoln, S.F.; Pittet, P-A.; Politis, S.; Wainwright, K.P. *Inorg. Chem.* **1993**, *32*, 2195-2198.
- 7 Burgermeister, W.; Winkler-Oswatitsch, R. *Top. Curr. Chem.* **1977**, *69*, 91-196.
- 8 Eigen, M.; Winkler, R. *"The Neurosciences, Second Study Program"*, New York, Rockefeller University Press, **1970**.
- 9 Cox, B.G.; Schneider, H. *Pure Appl. Chem.* **1990**, *62*, 2259-2268.
- 10 Cox, B.G.; van Truong, N.; Schneider, H. *J. Chem. Soc., Faraday Trans 1.* **1984**, *80*, 3285-3293.
- 11 Gutmann, V. *"Coordination Chemistry in Non-Aqueous Solutions"*, Springer-Verlag, Wien, **1968**.
- 12 Erlich, R.H.; Roach, E.; Popov, A.I. *J. Am. Chem. Soc.* **1970**, *92*, 4989-4990.
- 13 Dewitte, W.J.; Popov, A.I. *J. Soln. Chem.* **1976**, *5*, 231-240.
- 14 Lincoln, S.F.; Dhillon, R. Unpublished material.
- 15 Röper, J.R.; Elias, H. *Inorg. Chem.* **1992**, *31*, 1202.
- 16 Chen, C.C.; Petrucci, S. *J. Phys. Chem.* **1982**, *86*, 2601-2605.
- 17 Maynard, K.J.; Irish, D.E.; Eyring, E.M.; Petrucci, S. *J. Phys. Chem.* **1984**, *88*, 729-736.
- 18 Wallace, W.; Chen, C.; Eyring, E.M.; Petrucci, S. *J. Phys. Chem.* **1985**, *89*, 1357-1366.
- 19 Petrucci, S.; Adamic, R.J.; Eyring, E.M. *J. Phys. Chem.* **1986**, *90*, 1677-1683.
- 20 Xu, M.; Inoue, N.; Eyring, E.M.; Petrucci, S. *J. Phys. Chem.* **1988**, *92*, 2789-2798.
- 21 Cobranchi, D.P.; Phillips, G.R.; Johnson, D.E.; Barton, R.M.; Rose, D.J.; Eyring, E.M.; Rodriguez, L.J.; Petrucci, S. *J. Phys. Chem.* **1989**, *93*, 1396-1398.
- 22 Rodriguez, L.J.; Eyring, E.M.; Petrucci, S. *J. Phys. Chem.* **1989**, *93*, 5916-5924.

- 23 Rodopoulos, T.; Pittet, P-A.; Lincoln, S.F. *J. Chem. Soc., Dalton Trans.* **1993**, 1055.
- 24 Lincoln, S.F.; Whitbread, S. Unpublished material.
- 25 Cox, B.G.; Garcia-Rosas, J.; Schneider, H. *J. Am. Chem. Soc.* **1981**, 103, 1054-1059.
- 26 Lincoln, S.F.; Brereton, I.M.; Spotswood, T.M. *J. Am. Chem. Soc.* **1986**, 108, 8134-8138.
- 27 Lincoln, S.F.; Lucas, J.B. Unpublished material.
- 28 Lincoln, S.F.; Abou-Hamdan, A. *Inorg. Chem.* **1991**, 30, 462-466.
- 29 Shamsipur, M.; Popov, A.I. *J. Phys. Chem.* **1986**, 90, 5997-5999.
- 30 Cox, B.G.; Garcia-Rosas, J.; Schneider, H. *J. Am. Chem. Soc.* **1981**, 103, 1384-1389.
- 31 Ishihara, K.; Miura, H.; Funahashi, S.; Tanaka, M. *Inorg. Chem.* **1988**, 27, 1706-1710.
- 32 Grace, D.S.B.; Krane, J. *J. Chem. Research (S)*. **1983**, 162-163.

# Chapter 9: Intramolecular Exchange in Metal Complexes of TMEC12

## 9.1 Introduction

The substitution of pendant arms containing donor atoms onto polyaza macrocyclic ligands generates possibilities for stereochemistries and intramolecular processes in its metal complexes which are not available to the complexes formed by the parent ligand.<sup>1-3</sup> In Chapter 2, the solid state structures of the alkali metal cryptates of C22C<sub>2</sub> were used to explain the selectivity of C22C<sub>2</sub> for Na<sup>+</sup> over the other alkali metal ions in solution. However, it cannot always be assumed that the solid state structures of metal complexes are retained in solution and the solid state structures are often unable to account for behaviour of a metal complex in solution. Variable temperature <sup>13</sup>C NMR spectroscopy has proved a useful tool in determining the solution structures of a number of tetraaza macrocyclic complexes, where the coordination geometry and macrocyclic ring conformation can often be deduced when separate isomers of the complex are observed in slow exchange with each other on the NMR timescale.<sup>1-6</sup> This chapter examines how the solution structures of some metal complexes of TMEC12 were determined using variable temperature <sup>13</sup>C NMR spectroscopy.

## 9.2 Solution Structures of Heavy Metal [M(TMEC12)]<sup>2+</sup>

The natural abundance broad-band <sup>1</sup>H decoupled 75.47 MHz <sup>13</sup>C NMR spectra of TMEC12, [Cd(TMEC12)]<sup>2+</sup>, [Hg(TMEC12)]<sup>2+</sup> and [Pb(TMEC12)]<sup>2+</sup> in <sup>13</sup>C depleted *d*<sub>4</sub>-methanol at ambient temperature consist of four resonances (Table 9.1). The four observed <sup>13</sup>C resonances obtained for the fast exchange (high temperature) spectra of [M(TMEC12)]<sup>2+</sup> arise from the four chemically different environments in TMEC12. For TMEC12, the resonances at 71.14, 58.76, and 55.13 ppm are assigned to the carbons of the 2-methoxyethyl arms (sites A, B and C in Figure 9.1) and the resonance at 52.77 ppm is assigned to the 1,2-diaminoethane moiety of the macrocyclic ring (site D). For the [Cd(TMEC12)]<sup>2+</sup> spectrum, these correspond to the resonances at 66.25, 59.25, 50.52 and 47.26 ppm, respectively. For the [Hg(TMEC12)]<sup>2+</sup> spectrum, these correspond to the resonances at 66.64,

59.22, 51.60 and 47.04 ppm, respectively. For the  $[\text{Pb}(\text{TMEC12})]^{2+}$  spectrum, these correspond to the resonances at 66.68, 57.23, 52.69 and 49.99 ppm, respectively.

As the temperature is decreased, the  $^{13}\text{C}$  spectra of  $[\text{Cd}(\text{TMEC12})]^{2+}$ ,  $[\text{Hg}(\text{TMEC12})]^{2+}$  and  $[\text{Pb}(\text{TMEC12})]^{2+}$  show that the resonance characterising the carbons of the macrocyclic ring broadens and then splits into two resonances of equal intensity, whereas the resonances characterising the carbons of the 2-methoxyethyl arms remain as singlets (Table 9.2). This is consistent with the carbons of the tetraaza ring of TMEC12 exchanging between two magnetically inequivalent environments in  $[\text{M}(\text{TMEC12})]^{2+}$ . With the  $^{13}\text{C}$  NMR spectrum of TMEC12, all four resonances remain unchanged as the temperature is decreased.

**Table 9.1.**  $^{13}\text{C}$  Chemical Shifts of TMEC12 and its Heavy Metal Complexes  $[\text{M}(\text{TMEC12})]^{2+}$  in  $d_4$ -methanol at High Temperature.

complex	T(K)	Conc. mol dm <sup>-3</sup>		$\delta$ (ppm) <sup>a</sup>		
TMEC12	295	0.050	71.14	58.76	55.13	52.77
$[\text{Cd}(\text{TMEC12})]^{2+}$	295	0.101	66.25	59.25	50.52	47.26
$[\text{Hg}(\text{TMEC12})]^{2+}$	295	0.107	66.64	59.22	51.60	47.04
$[\text{Pb}(\text{TMEC12})]^{2+}$	335	0.101	66.68	57.23	52.69	49.99

<sup>a</sup>  $^{13}\text{C}$  chemical shifts are referenced to external natural abundance  $d_4$ -methanol, which was assigned a chemical shift of 47.05 ppm.

**Table 9.2.** Slow-Exchange  $^{13}\text{C}$  Chemical Shifts of  $[\text{M}(\text{TMEC12})]^{2+}$  in  $d_4$ -methanol at 195 K.

complex	Conc. mol dm <sup>-3</sup>		$\delta$ (ppm) <sup>a</sup>			
$[\text{Cd}(\text{TMEC12})]^{2+}$	0.101	62.71	58.92	49.66	48.35	44.82
$[\text{Hg}(\text{TMEC12})]^{2+}$	0.107	66.32	59.04	50.94	47.16	46.06
$[\text{Pb}(\text{TMEC12})]^{2+}$	0.101	66.39	56.96	51.98	51.55	47.12

<sup>a</sup>  $^{13}\text{C}$  chemical shifts are referenced to external natural abundance  $d_4$ -methanol, which was assigned a chemical shift of 47.05 ppm.

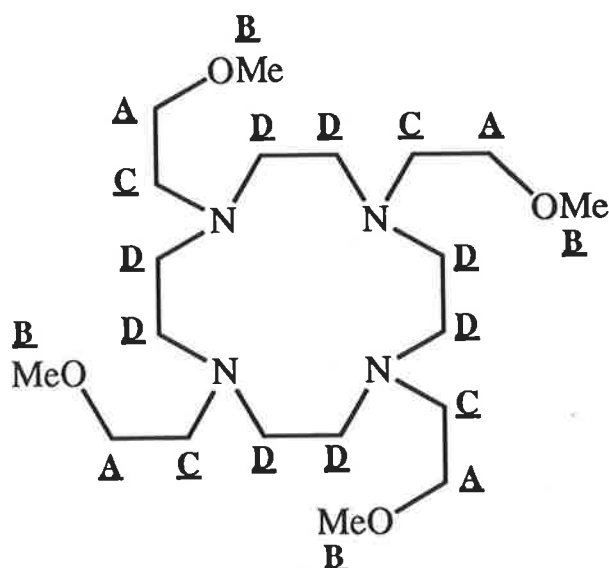


**Figure 9.1.** Assignment of the  $^{13}\text{C}$  resonances for TMEC12 and the heavy metal complexes  $[\text{M}(\text{TMEC12})]^{2+}$ , where  $\text{M}^{2+} = \text{Cd}^{2+}, \text{Hg}^{2+}$  and  $\text{Pb}^{2+}$ .

The solution structures of  $[\text{M}(\text{TMEC12})]^{2+}$  may be assigned from the slow exchange spectra of these complexes. The 2-methoxyethyl pendant arms may exchange between being coordinated to the metal ion and being uncoordinated. If this were true, then the resonances observed at sites A, B, and C would be the weighted average of the resonances characterising these sites for the coordinated and uncoordinated pendant arms. However, if fewer than four pendant arms are involved in the coordination of  $\text{M}^{2+}$ , then this is not demonstrated by the appearance of additional resonances in the low temperature  $^{13}\text{C}$  NMR spectra of the  $[\text{M}(\text{TMEC12})]^{2+}$  complexes. Thus, the exchange mechanism that results in the coalescence of the two resonances at site D does not alter the magnetic environment of the carbons at sites A, B and C. This requirement implies that the metal ion must be bound by all four methoxyethyl arms and the four coplanar nitrogens of the tetraaza ring. The conformations of the tetraaza ring which allow coordination of  $\text{M}^{2+}$  by the four coplanar nitrogens are TRANS I-V (Figure 7.1, Chapter 7). However, the metal ions in this study are too large to sit within the plane of the tetraaza ring of TMEC12 and thus, eight coordination is not possible for  $\text{M}^{2+}$  if TMEC12 adopts any of the TRANS II - TRANS V conformations.<sup>7</sup> The observed  $^{13}\text{C}$  NMR spectra of  $[\text{M}(\text{TMEC12})]^{2+}$  are consistent only with the TRANS I conformation, in which  $\text{M}^{2+}$  lies above the plane of the tetraaza ring and is

coordinated by the four nitrogens and the four oxygens of the methoxyethyl arms.

### 9.3 Intramolecular Exchange in Heavy Metal [M(TMEC12)]<sup>2+</sup>

The temperature dependent <sup>13</sup>C NMR spectra of [Cd(TMEC12)]<sup>2+</sup>, [Hg(TMEC12)]<sup>2+</sup> and [Pb(TMEC12)]<sup>2+</sup> appear in Figures 9.2, 9.3 and 9.4, respectively. These spectra are consistent with the intramolecular exchange of [M(TMEC12)]<sup>2+</sup> between two square antiprismatic enantiomers of C<sub>4v</sub> symmetry in which M<sup>2+</sup> is coordinated by the four oxygens of the 2-methoxyethyl pendant arms and by the four nitrogens of the tetraaza ring. This mechanism is demonstrated in Figure 9.5. It is seen that the macrocyclic carbons exchange between the inequivalent sites (a) and (b), whereas the carbons of the 2-methoxyethyl arms experience no change in magnetic environment when the enantiomers interconvert. Some support for this mechanism comes from the observation of enantiomeric, approximately square antiprismatic, structures for [K(THEC12)]<sup>+</sup> in the solid state.<sup>8-9</sup> The mean site lifetimes ( $\tau$ ) for the macrocyclic carbons were determined by complete lineshape analysis (Chapter 12) of their coalescing <sup>13</sup>C resonances. The kinetic parameters for this exchange process were derived from the temperature variation of  $\tau$  through Equation 4.14, as illustrated in Figure 9.6, and appear in Table 9.3, together with those for [Li(TMEC12)]<sup>+</sup> and [Na(TMEC12)]<sup>+</sup>, which also undergo the same intramolecular exchange process characterising the heavy metal complexes of TMEC12.<sup>10</sup>

If all eight TMEC12 donor atoms remain coordinated during the exchange then the geometry of the transition state will be square prismatic and  $\Delta H^\ddagger$  and  $\Delta S^\ddagger$  represent the differences between the square antiprismatic and prismatic geometries. However, it is also possible that one or more of the pendant arms are uncoordinated in the transition state. The differences between the square antiprismatic ground state and the transition state arise from differences in i) metal-ligand bond lengths; ii) coordination geometry; iii) steric crowding; iv) conformational strain and v) change in coordination number if any metal-ligand bonds are broken. These factors will largely depend on the ionic radius of the metal ion and the metal-ligand bond strengths.



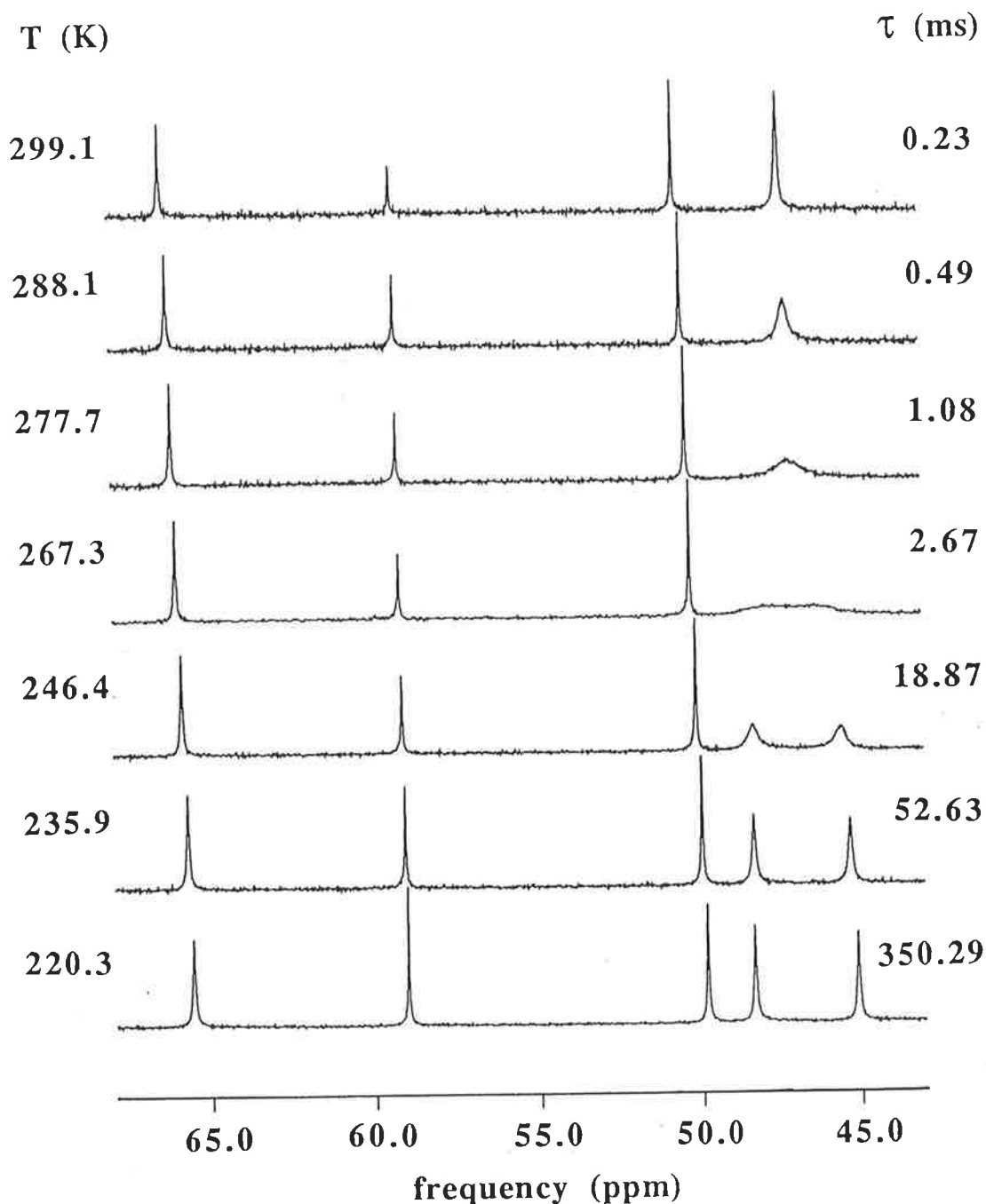


**Figure 9.2.** Temperature variation of the 75.47 MHz,  $^{13}\text{C}$  NMR spectra of  $[\text{Cd}(\text{TMEC12})]^{2+}$  ( $0.101 \text{ mol dm}^{-3}$ ) in  $d_4$ -methanol. The values of the site lifetimes,  $\tau$ , were derived from complete lineshape analyses of the exchange modified high field resonances arising from the macrocyclic ring carbons. The broadening of the low field resonances arising from the 2-methoxyethyl pendant arms is a consequence of the increase in solution viscosity with a decrease in temperature.

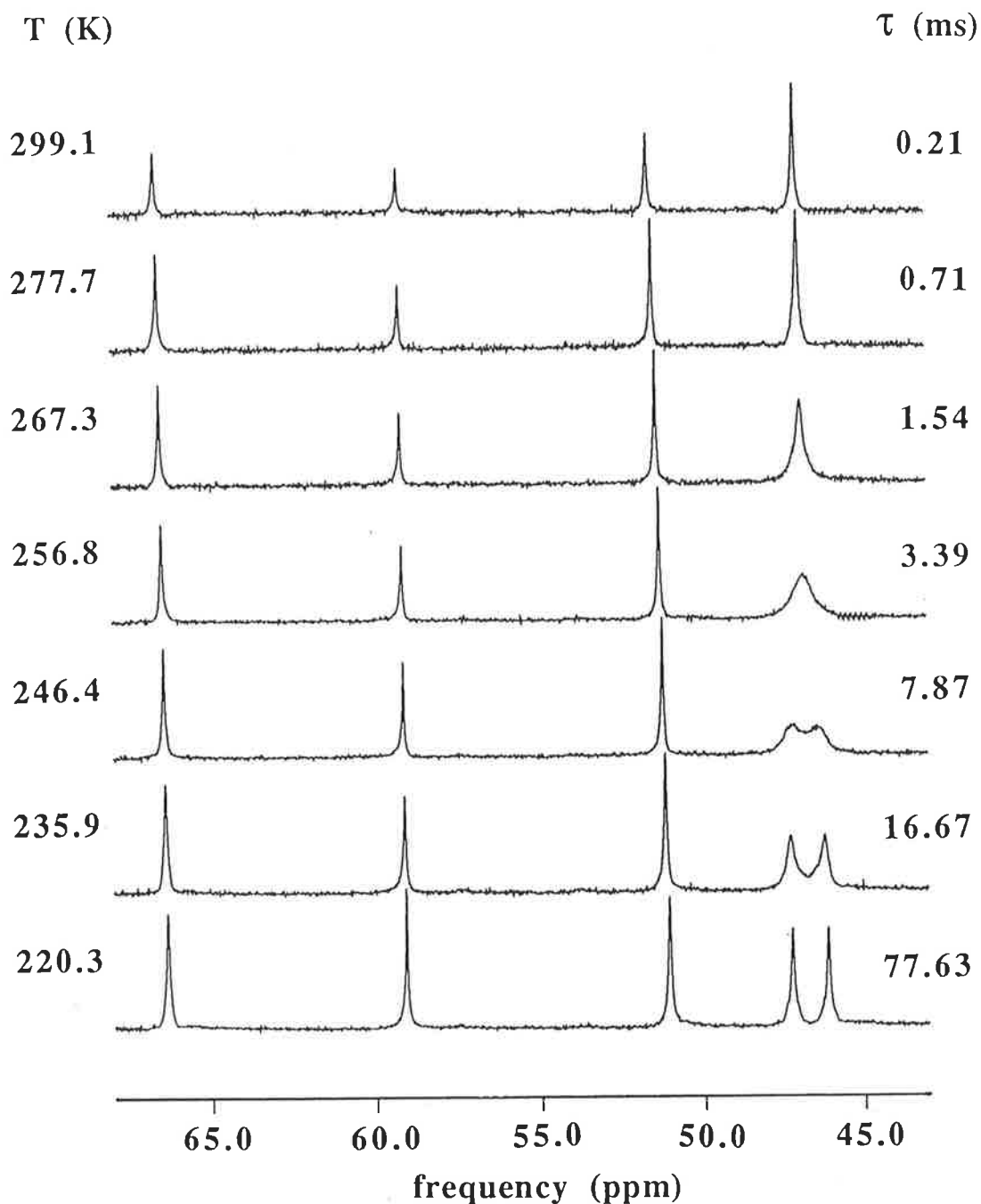


**Figure 9.3.** Temperature variation of the 75.47 MHz,  $^{13}\text{C}$  NMR spectra of  $[\text{Hg}(\text{TMEC12})]^{2+}$  ( $0.107 \text{ mol dm}^{-3}$ ) in  $d_4$ -methanol. The values of the site lifetimes,  $\tau$ , were derived from complete lineshape analyses of the exchange modified high field resonances arising from the macrocyclic ring carbons. The broadening of the low field resonances arising from the 2-methoxyethyl pendant arms is a consequence of the increase in solution viscosity with a decrease in temperature.

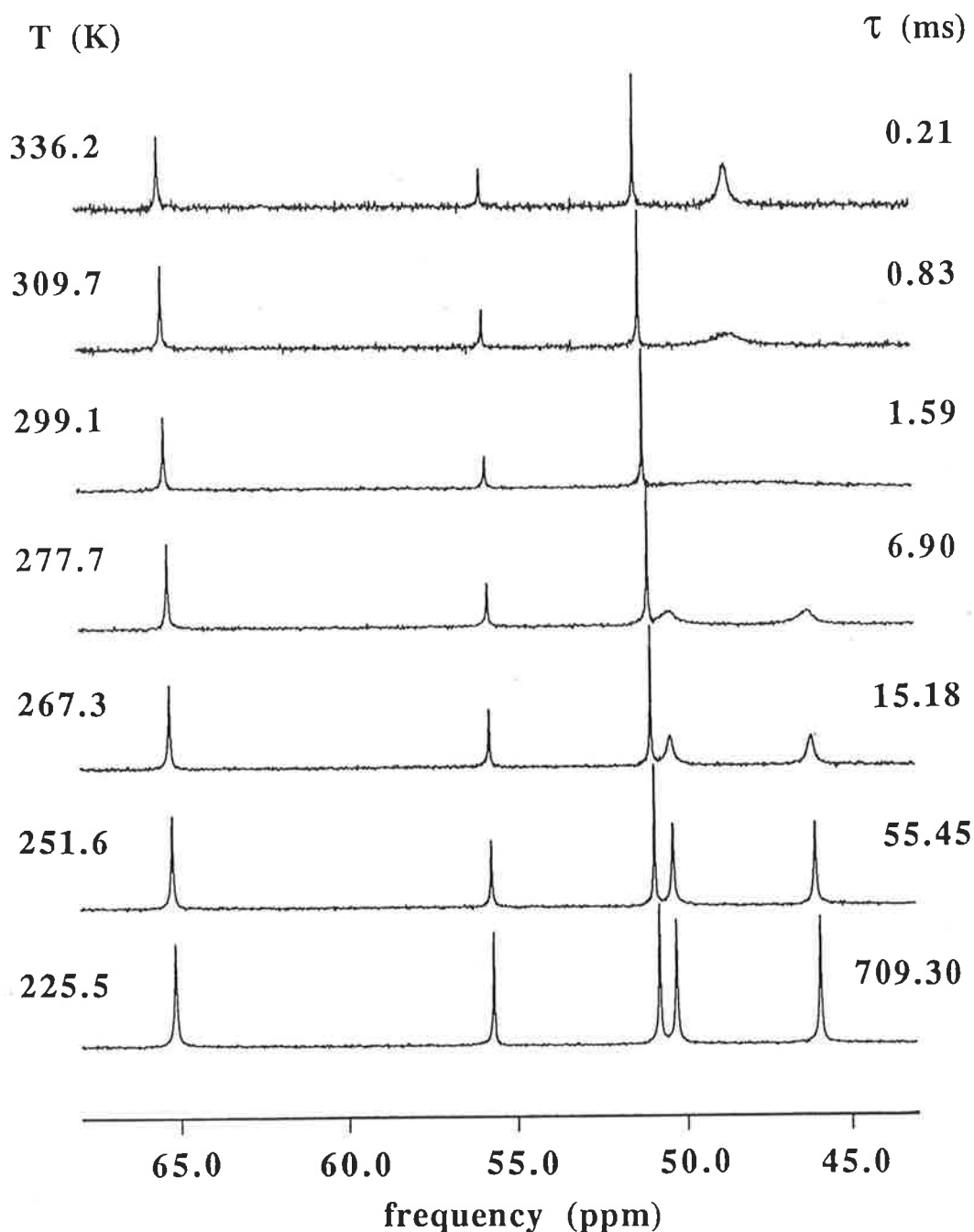


**Figure 9.4.** Temperature variation of the 75.47 MHz,  $^{13}\text{C}$  NMR spectra of  $[\text{Pb}(\text{TMEC12})]^{2+}$  ( $0.101 \text{ mol dm}^{-3}$ ) in  $d_4$ -methanol. The values of the site lifetimes,  $\tau$ , were derived from complete lineshape analyses of the exchange modified high field resonances arising from the macrocyclic ring carbons. The broadening of the low field resonances arising from the 2-methoxyethyl pendant arms is a consequence of the increase in solution viscosity with a decrease in temperature.

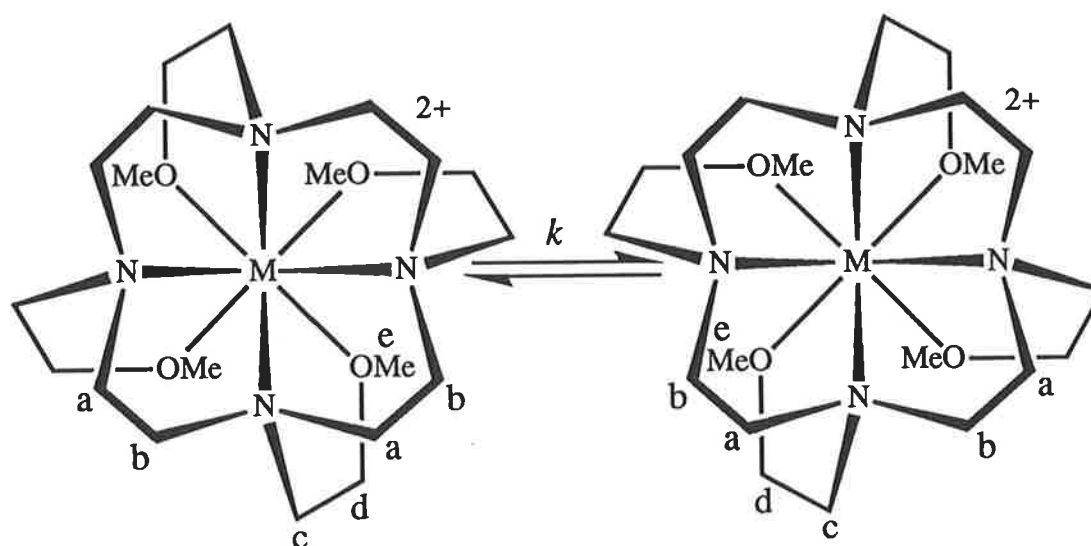


**Figure 9.5.** Proposed mechanism for the interconversion of the square antiprismatic enantiomers of  $[M(\text{TMEC12})]^{2+}$  (where  $M^{2+} = \text{Cd}^{2+}, \text{Hg}^{2+}$  and  $\text{Pb}^{2+}$ ), viewed from above the tetraaza macrocyclic plane.

**Table 9.3.** Kinetic Parameters<sup>a</sup> for Intramolecular Exchange in  $[M(\text{TMEC12})]^{n+}$  Complexes.

complex	$k$ (T) $\text{s}^{-1}$	$10^{-3} k$ (298.2 K) $\text{s}^{-1}$	$\Delta H^\ddagger$ ( $\text{kJ mol}^{-1}$ )	$\Delta S^\ddagger$ ( $\text{J mol}^{-1} \text{K}^{-1}$ )
$[\text{Cd}(\text{TMEC12})]^{2+}$	$378.2 \pm 4.4$ (267.3 K)	$4.13 \pm 0.09$	$48.9 \pm 0.4$	$-11.7 \pm 1.5$
$[\text{Hg}(\text{TMEC12})]^{2+}$	$209.4 \pm 4.5$ (251.6 K)	$4.57 \pm 0.20$	$39.1 \pm 0.7$	$-43.9 \pm 2.6$
$[\text{Pb}(\text{TMEC12})]^{2+}$	<i>c</i>	$0.57 \pm 0.02$	$44.1 \pm 1.1$	$-44.2 \pm 3.8$
$[\text{Na}(\text{TMEC12})]^+$	<i>b</i>	1.47	31.4	-78.8
$[\text{Li}(\text{TMEC12})]^+$	<i>b</i>	32.75	41.4	-19.6

<sup>a</sup> Errors represent one standard deviation of the fit of the experimental  $\tau$  data to Equation 4.14.

<sup>b</sup> Reference 10. <sup>c</sup> Coalescence at 299.1 K.

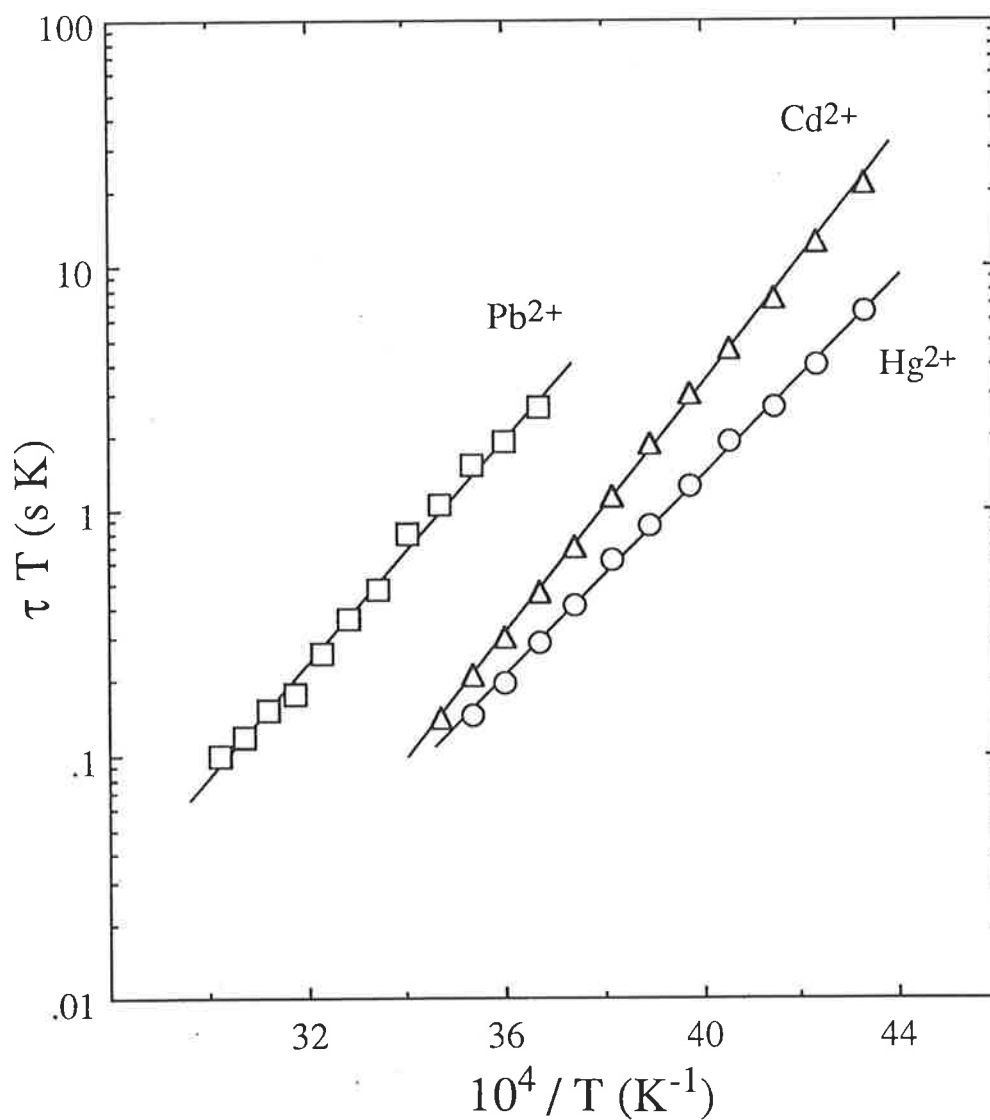


**Figure 9.6.** The temperature variation of  $\tau$  for the intramolecular exchange between square antiprismatic enantiomers for  $[Cd(TMEC12)]^{2+}$  (triangles),  $[Hg(TMEC12)]^{2+}$  (circles) and  $[Pb(TMEC12)]^{2+}$  (squares). The solid lines represent the best fit of the data to Equation 4.14 for each system.

The eight coordinate ionic radii of  $\text{Cd}^{2+}$ ,  $\text{Hg}^{2+}$  and  $\text{Pb}^{2+}$  are 1.10 Å, 1.14 Å and 1.29 Å, respectively.<sup>11</sup> The metal ions closest in size ( $\text{Cd}^{2+}$  and  $\text{Hg}^{2+}$ ) have similar  $k$  (298.2 K) values, but this is a result of different but compensating  $\Delta H^\ddagger$  and  $\Delta S^\ddagger$  values. The largest heavy metal ion,  $\text{Pb}^{2+}$ , is characterised by the smallest  $k$  value at 298.2 K, but this is largely a result of a high  $\Delta H^\ddagger$  and a large negative  $\Delta S^\ddagger$ . The soft acid heavy metal ions  $\text{Cd}^{2+}$ ,  $\text{Hg}^{2+}$  and  $\text{Pb}^{2+}$  will interact predominantly with the nitrogens of the tetraaza ring. The smaller heavy metal ions  $\text{Cd}^{2+}$  and  $\text{Hg}^{2+}$  will have smaller metal-ligand bond lengths and may cause greater steric crowding between the pendant arms, whereas the larger  $\text{Pb}^{2+}$  will cause less steric crowding but may prove a tighter fit for the ligand topology. This factor is also complicated by the lone-pair effect discussed in Chapter 7, whereby  $\text{Pb}^{2+}$  may behave as a smaller metal ion.<sup>12-13</sup> It is extremely difficult to predict the relative contributions of factors i) - v) and the net effect is that the activation parameters for  $\text{Cd}^{2+}$ ,  $\text{Hg}^{2+}$  and  $\text{Pb}^{2+}$  are not greatly different.

The hard acid alkali metal ions  $\text{Li}^+$  and  $\text{Na}^+$  will interact more strongly with the oxygen donor atoms rather than the nitrogen donor atoms of TMEC12. In addition, as a result of their hard acid and monovalent nature, the metal-ligand bond strengths will be considerably weaker than those of their heavy metal analogues. However, the nature of the metal ion does not appear to have a major effect on the rate of intramolecular exchange.  $\text{Na}^+$  ( $r = 1.18$  Å) is intermediate in size between  $\text{Cd}^{2+}$  and  $\text{Pb}^{2+}$  and  $[\text{Na}(\text{TMEC12})]^+$  is characterised by  $k$  (298.2 K) which lies between those characterising  $[\text{Cd}(\text{TMEC12})]^{2+}$  and  $[\text{Pb}(\text{TMEC12})]^{2+}$ . The smallest metal ion in Table 9.3 is  $\text{Li}^+$  (0.92 Å), with  $k$  (298.2 K) for  $[\text{Li}(\text{TMEC12})]^+$  considerably larger than  $k$  (298.2 K) characterising the other complexes in Table 9.3. It is apparent that the rate of intramolecular exchange is largely controlled by the size of  $\text{M}^{n+}$ , but the large variation in  $\Delta H^\ddagger$  and  $\Delta S^\ddagger$  characterising  $[\text{M}(\text{TMEC12})]^{n+}$  is consistent with a large number of underlying factors contributing to the observed activation parameters for these metal complexes.

#### 9.4 Intramolecular and Intermolecular Exchange in $[\text{Li}(\text{TMEC12})]^+$ and $[\text{Na}(\text{TMEC12})]^+$

The variable temperature  $^{13}\text{C}$  NMR spectra of  $[\text{Li}(\text{TMEC12})]^+$  and  $[\text{Na}(\text{TMEC12})]^+$  in  $d_4$ -methanol are similar to those characterising their heavy metal  $[\text{M}(\text{TMEC12})]^{2+}$  analogues (Figure 9.7).<sup>10</sup> This demonstrates that both  $\text{Li}^+$  and  $\text{Na}^+$  are coordinated in square antiprismatic geometry by the eight

TMEC12 donor atoms, with the tetraaza ring in the TRANS I conformation. The parameters characterising the intramolecular exchange process appear in Table 9.4, together with the kinetic parameters characterising the intermolecular exchange of  $\text{Li}^+$  and  $\text{Na}^+$  on  $[\text{Li}(\text{TMEC12})]^+$  and  $[\text{Na}(\text{TMEC12})]^+$ , respectively, in methanol. The temperature dependence of  $\tau$ , the mean lifetime of the macrocyclic ring carbons for these systems, appears in Figure 9.8.

The decomplexation rate constants,  $k_d$  (298.2 K), characterising  $[\text{Li}(\text{TMEC12})]^+$  and  $[\text{Na}(\text{TMEC12})]^+$  in methanol are much smaller than the rate constants,  $k$ , for the intramolecular exchange in  $[\text{Li}(\text{TMEC12})]^+$  and  $[\text{Na}(\text{TMEC12})]^+$ . This demonstrates that intramolecular exchange in these complexes is not the rate-determining step for their decomplexation and that the two processes occur independently.

**Table 9.4.** Kinetic Parameters for Intramolecular<sup>a</sup> and Intermolecular<sup>b</sup> Exchange in Alkali  $[\text{M}(\text{TMEC12})]^+$  Complexes.

	$[\text{Li}(\text{TMEC12})]^+$	$[\text{Na}(\text{TMEC12})]^+$
Intramolecular Exchange		
$k$ (298.2 K) $\text{s}^{-1}$	32750	1468
$\Delta H^\ddagger$ $\text{kJ mol}^{-1}$	41.4	31.4
$\Delta S^\ddagger$ $\text{J mol}^{-1} \text{K}^{-1}$	-19.6	-78.8
Intermolecular Exchange		
$k_d$ (298.2 K) $\text{s}^{-1}$	18.2	<58
$\Delta H_d^\ddagger$ $\text{kJ mol}^{-1}$	44.8	
$\Delta S_d^\ddagger$ $\text{J mol}^{-1} \text{K}^{-1}$	-70.5	

<sup>a</sup> Reference 10. <sup>b</sup> This work.

Similar variable temperature  $^{13}\text{C}$  NMR studies have shown the following complexes to be eight coordinate, with the coordination geometry square antiprismatic and the ligand adopting the TRANS I conformation;  $[\text{Ca}(\text{TMEC12})]^{2+}$ ,  $[\text{Na}(\text{THEC12})]^+$ ,  $[\text{Ca}(\text{THEC12})]^{2+}$ , and the  $\text{Cd}^{2+}$ ,  $\text{Hg}^{2+}$  and  $\text{Pb}^{2+}$  complexes of THEC12 and *S*-THPC12 (where *S*-THPC12 is the

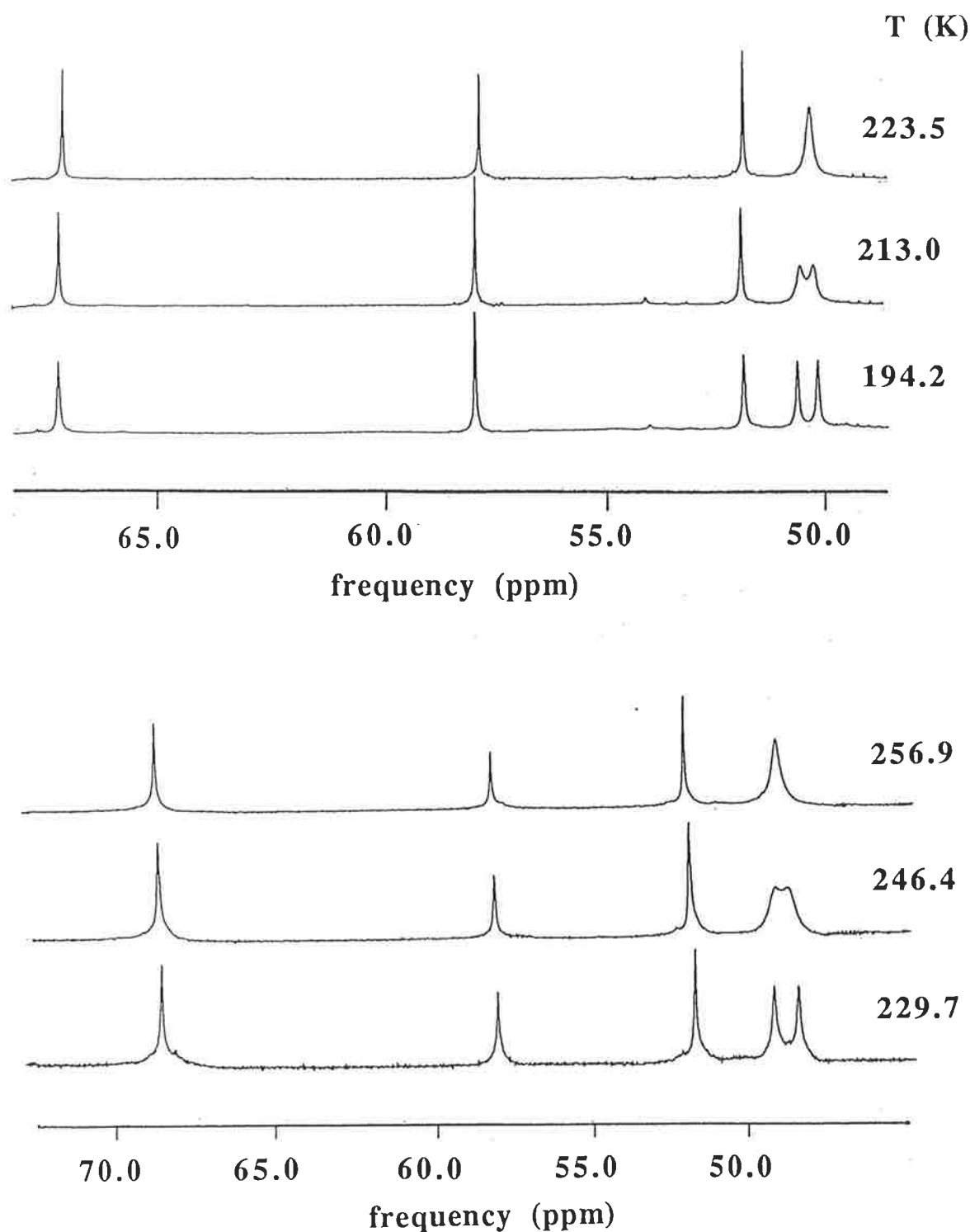


**Figure 9.7.** (From reference 10). Selected 75.47 MHz,  $^{13}\text{C}$  NMR spectra of  $[\text{Li}(\text{TMEC12})]^+$  (top) and  $[\text{Na}(\text{TMEC12})]^+$  (bottom) in  $d_4$ -methanol. The broadening of the low field resonances arising from the 2-methoxyethyl pendant arms is a consequence of the increase in solution viscosity with a decrease in temperature.



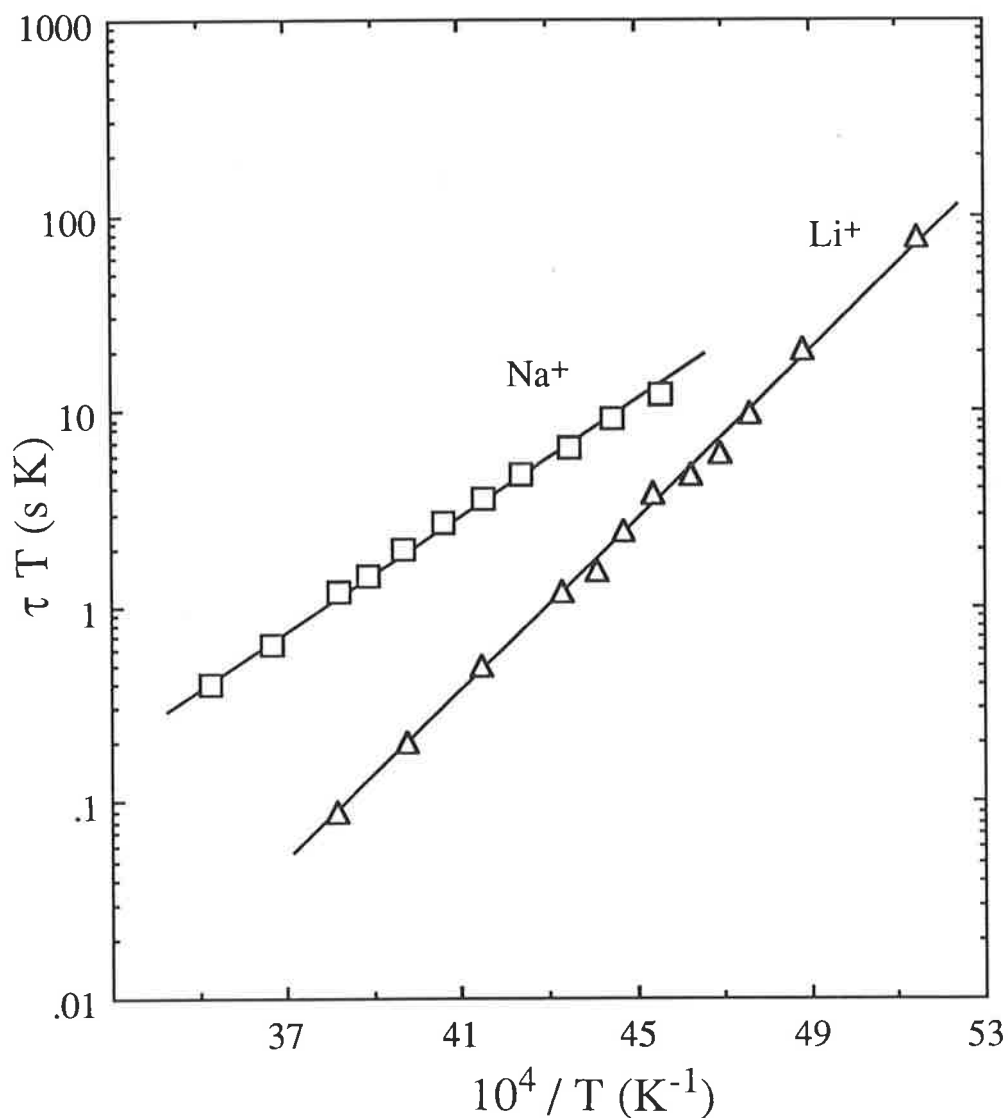


**Figure 9.8.** (From reference 10). The temperature variation of  $\tau$  for the intramolecular exchange between square antiprismatic enantiomers for  $[\text{Li(TMEC12)}]^+$  (triangles) and  $[\text{Na(TMEC12)}]^+$  (squares). The solid lines represent the best fit of the data to Equation 4.14 for each system.

analogue of THEC12 and TMEC12 with (*S*-) 2-hydroxypropyl pendant arms).<sup>6,10,14-15</sup> The predominance of the TRANS I conformation in these complexes is consistent with molecular mechanics calculations<sup>16</sup> which have shown that the TRANS I conformation is lower in energy than the other conformations for the 1,4,7,10-tetraazacyclododecane ring and will be adopted in all complexes where the metal ion does not require octahedral coordination.

The heavy metal complexes,  $[M(\text{THEC14})]^{2+}$  and  $[M(\text{TMEC14})]^{2+}$ , show contrasting behaviour in solution to that exhibited by the smaller ring size  $[M(\text{TMEC12})]^{2+}$ ,  $[M(\text{THEC12})]^{2+}$  and  $[M(\text{S-THPC12})]^{2+}$  systems.<sup>1-2,17</sup> The variable temperature  $^{13}\text{C}$  NMR spectra of  $[M(\text{THEC14})]^{2+}$  and  $[M(\text{TMEC14})]^{2+}$  in  $d_4$ -methanol are consistent with  $M^{2+}$  being coordinated by the four ring nitrogens and two of the four pendant arms in a trigonal prismatic stereochemistry, with the macrocyclic ring in the TRANS III conformation. These complexes undergo an exchange process that results from the oscillation of  $M^{2+}$  through the macrocyclic annulus of THEC14 and TMEC14, where  $M^{2+}$  alternates between being bound above and below the plane of the tetraaza ring. The differing behaviour exhibited by these twelve and fourteen membered pendant arm macrocyclic complexes are indicative of the importance of the macrocyclic ring size, the conformation of the macrocyclic ring and the orientation of the pendant arms in determining complex stereochemistry and the coordination number of  $M^{2+}$ . These factors also determine the consequent possibilities for intramolecular rearrangement.

### 9.5 A $^{13}\text{C}$ NMR Study of $[\text{Zn}(\text{TMEC12})]^{2+}$

The  $^{13}\text{C}$  NMR spectrum of  $[\text{Zn}(\text{TMEC12})]^{2+}$  in  $d_4$ -methanol at 295 K is more complicated than that of its  $\text{Cd}^{2+}$ ,  $\text{Hg}^{2+}$  and  $\text{Pb}^{2+}$  analogues, with eight resonances between 48.05 and 68.51 ppm (Table 9.5). The resonances at 68.51, 66.70, 57.80, 57.27, 51.80 and 51.58 ppm are assigned to the carbons of the 2-methoxyethyl pendant arms. The resonances at 48.78 and 48.05 ppm are assigned to the carbons of the macrocyclic ring. As the temperature is decreased, the pair of resonances characterising the ring carbons broaden, with the resonance at 48.78 ppm resolving into two resonances of equal population at ~246 K, and the resonance at 48.05 ppm resolving into two resonances of equal population at ~226 K. At 190 K, the first pair of these resonances are at 48.93 ppm and 47.97 ppm, whereas the second pair of resonances are at 50.37 ppm and 46.02 ppm. The spectrum at 295 K is consistent with the presence of two isomers in slow exchange with each other on the NMR timescale. On

lowering the temperature, the spectra are consistent with each of these isomers exchanging between two different conformations, with the rate of exchange being different for each isomer. Only the carbons of the macrocyclic ring are effected by these exchange processes; the resonances characterising the methoxyethyl pendant arms remain as singlets over the temperature range 190-330 K. The relative intensities of the corresponding resonances characterising each isomer vary with the temperature, and it is apparent that the isomers are of unequal stability. The coordination geometries of  $Zn^{2+}$  and the conformations adopted by TMEC12 in these isomers are not immediately apparent from these results, and it is hoped that further studies may resolve this problem.

**Table 9.5.**  $^{13}C$  Chemical Shifts of  $[Zn(TMEC12)]^{2+}$  in  $d_4$ -methanol.

T (K)	Conc. mol dm <sup>-3</sup>	$\delta$ (ppm) <sup>a</sup>				
295	0.103	68.51	66.70	57.80	57.27	51.80
		51.58	48.78		48.05	
190	0.103	68.32	66.66	57.86	57.35	51.66
		51.31	50.37	48.93	47.97	46.02

<sup>a</sup>  $^{13}C$  chemical shifts are referenced to external natural abundance  $d_4$ -methanol, which was assigned a chemical shift of 47.05 ppm.

- 1 Clarke, P.; Hounslow, A.M.; Keough, R.A.; Lincoln, S.F.; Wainwright, K.P. *Inorg. Chem.* **1990**, *29*, 1793.
- 2 Clarke, P.; Lincoln, S.F.; Wainwright, K.P. *Inorg. Chem.* **1991**, *30*, 134.
- 3 Alcock, N.W.; Herron, N.; Moore, P. *J. Chem. Soc., Dalton Trans.* **1978**, 1282-1288.
- 4 Alcock, N.W.; Herron, N.; Moore, P. *J. Chem. Soc., Dalton Trans.* **1979**, 1486-1491.
- 5 Alcock, N.W.; Curson, E.H.; Herron, N.; Moore, P. *J. Chem. Soc., Dalton Trans.* **1979**, 1987-1993.
- 6 Pittet, P.-A.; Laurence, G.S.; Lincoln, S.F.; Turonek, M.L.; Wainwright, K.P. *J. Chem. Soc., Chem Commun.* **1991**, 1205-1206.
- 7 Thöm, V.J.; Hosken, G.D.; Hancock, R.D.; *Inorg. Chem.* **1985**, *24*, 3378-3381.
- 8 Buøen, S.; Dale, J.; Groth, P.; Krane, J. *J. Chem. Soc., Chem Commun.* **1982**, 1172.
- 9 Groth, P. *Acta Chem. Scand.* **1983**, *A37*, 283.
- 10 Lincoln, S.F.; Dhillon, R. Unpublished material.
- 11 Shannon, R.D.; *Acta Crystallogr., Sect. A.: Cryst. Phys. Diffr., Theor. Gen. Crystallogr.* **1976**, *A32*, 751-767.
- 12 Hancock, R.D.; Shaikjee, M.S.; Dobson, S.M.; Boeyens, J.C.A. *Inorg. Chim. Acta.* **1988**, *154*, 229-238.
- 13 Hancock, R.D.; Bhavan, R.; Wade, P.W.; Boeyens, J.C.A.; Dobson, S.M. *Inorg. Chem.* **1989**, *28*, 187-194.
- 14 Lincoln, S.F.; Whitbread, S.W. Unpublished material.
- 15 Lincoln, S.F.; Madbak, S. Unpublished material.
- 16 Thöm, V.J.; Fox, C.C.; Boeyens, J.C.A.; Hancock, R.D. *J. Am. Chem. Soc.* **1984**, *106*, 5947-5955.
- 17 Lincoln, S.F.; Lucas, J.B. Unpublished material.

# Chapter 10: Experimental

## 10.1 Non-Aqueous Titrations

### 10.1.1 Materials

Acetonitrile (Ajax), dimethylformamide (BDH), dimethylsulfoxide (Ajax), methanol (CSR), propylene carbonate (Aldrich) and pyridine (BDH) were purified and dried by literature methods.<sup>1</sup> Deionized water was ultrapurified with a MilliQ-Reagent system to produce water with a resistance of  $>15 \text{ M}\Omega \text{ cm}$ . All solvents except water were stored over appropriate Linde molecular sieves and kept under dry nitrogen.  $\text{NaClO}_4$  (Fluka),  $\text{LiClO}_4$  (Fluka), and  $\text{AgClO}_4$  (Aldrich) were used as received.  $\text{KClO}_4$  (BDH) was recrystallized from water.  $\text{CsClO}_4$  was prepared by the addition of concentrated  $\text{HClO}_4$  to  $\text{CsCl}$  (BDH) and was recrystallized from water until free of acid and chloride.  $\text{RbNO}_3$  (BDH) was converted to  $\text{RbOH}$  using an ion exchange column. Concentrated  $\text{HClO}_4$  was added to the  $\text{RbOH}$  solution and the resultant precipitate of  $\text{RbClO}_4$  was recrystallized from water until free from acid.  $\text{TlClO}_4$  was prepared by the addition of excess concentrated  $\text{HClO}_4$  to  $\text{Tl}_2\text{CO}_3$  and was recrystallized from water until free from acid. All metal perchlorate salts were vacuum dried at 353-363 K for 48 hours and stored over  $\text{P}_2\text{O}_5$  under vacuum.  $\text{NEt}_4\text{ClO}_4$  was prepared by addition of  $\text{HClO}_4$  to  $\text{NEt}_4\text{Br}$  (BDH) or  $\text{NEt}_4\text{OH}$  (Fluka). The resulting precipitate of  $\text{NEt}_4\text{ClO}_4$  was recrystallized from water until free from bromide and acid, dried under vacuum at 353-365 K for 24 hours and stored over  $\text{P}_2\text{O}_5$  under vacuum.  $\text{AgNO}_3$  (Matthey-Garrett) was dried under vacuum at 353-363 K for 48 hours and was stored over  $\text{P}_2\text{O}_5$  under vacuum.

### 10.1.2 Determination of Stability Constants

Stability constants for  $[\text{ML}]^+$  (where  $\text{L} = \text{C22C}_2$ ,  $\text{C22C}_8$ ,  $\text{TMEC12}$  or cyclen) were determined by potentiometric titration. Stability constants for  $\text{Na}^+$  complexes (except where stated) were determined by titration of  $20 \text{ cm}^3$   $0.001 \text{ mol dm}^{-3}$   $\text{NaClO}_4$  solution (in vessel) with  $5 \text{ cm}^3$   $0.01 \text{ mol dm}^{-3}$   $\text{L}$  solution (in burette), with free  $\text{Na}^+$  concentration monitored using a Radiometer G502NA sodium selective electrode. The reference solution was either  $0.01 \text{ mol dm}^{-3}$   $\text{AgNO}_3$  or  $\text{AgClO}_4$  and the reference electrode was silver. The  $\text{Na}^+$  selective electrode was calibrated using  $\text{NaClO}_4$  solutions of appropriate concentration as described below. Stability constants for  $\text{Ag}^+$

complexes were determined by direct titration of 20 cm<sup>3</sup> of 0.001 mol dm<sup>-3</sup> AgNO<sub>3</sub> or AgClO<sub>4</sub> solution (in vessel) with 5 cm<sup>3</sup> of 0.01 mol dm<sup>-3</sup> L solution (in burette). The stability constants of the Li<sup>+</sup>, K<sup>+</sup>, Rb<sup>+</sup>, Cs<sup>+</sup> and Tl<sup>+</sup> complexes were determined through competitive titrations of 20 cm<sup>3</sup> of 0.001 mol dm<sup>-3</sup> AgNO<sub>3</sub> or AgClO<sub>4</sub> solution (in vessel) with 5 cm<sup>3</sup> of a solution of 0.01 mol dm<sup>-3</sup> L and 0.05 mol dm<sup>-3</sup> MClO<sub>4</sub> (in burette). For these titrations, both the titration and reference electrodes were silver and the reference solution was 0.01 mol dm<sup>-3</sup> in either AgNO<sub>3</sub> or AgClO<sub>4</sub>. The electrode was calibrated using Ag<sup>+</sup> solutions of appropriate concentration as described below. As a result of the low solubilities of KClO<sub>4</sub>, RbClO<sub>4</sub> and CsClO<sub>4</sub>, titrations involving these metal ions in acetonitrile and methanol were carried out using concentrations 1/5th and 1/10th, respectively, of those stated previously.

Solutions were prepared by volume under dry nitrogen in a glove box. All titrations were carried out under dry nitrogen in a thermostatted reference vessel connected to a thermostatted titration vessel by a salt bridge. For a given experiment, the titration and reference vessels and the salt bridge contained solutions made up in the same solvent, with all solutions 0.050 mol dm<sup>-3</sup> in NEt<sub>4</sub>ClO<sub>4</sub>. A stream of dry nitrogen was bubbled through the titration solution to prevent ingress of atmospheric gases and moisture and also served to stir the solution. An Orion Research 720 digital analyser was used to measure the potential during the titration. In general, all stability constants were determined using these methods. Any exceptions are discussed below.

**C22C<sub>2</sub>**: The stability constants of [NaC22C<sub>2</sub>]<sup>+</sup> were determined using a Na<sup>+</sup> selective electrode except in methanol and acetonitrile. The poor behaviour of this electrode in methanol necessitated the use of the competitive titration method using silver electrodes as described above. The stability of [NaC22C<sub>2</sub>]<sup>+</sup> in acetonitrile was too high to be reliably determined using the Na<sup>+</sup> selective electrode. Thus, the stability of [NaC22C<sub>2</sub>]<sup>+</sup> and also [TlC22C<sub>2</sub>]<sup>+</sup> were determined using a modification of the competitive titration method in which 20 cm<sup>3</sup> of a solution of 0.001 mol dm<sup>-3</sup> NaClO<sub>4</sub> or TlClO<sub>4</sub> (in vessel) was titrated with a solution of 0.01 mol dm<sup>-3</sup> [AgC22C<sub>2</sub>]<sup>+</sup> (in burette). However the similarities between the stabilities of these two complexes and that of [AgC22C<sub>2</sub>]<sup>+</sup> decreased the accuracy of the determination of the stability constant values (hence the larger errors cited in Table 2.2).

**C22C<sub>8</sub>**: The stability constants of [NaC<sub>22</sub>C<sub>8</sub>]<sup>+</sup> were determined by the competitive titration method except for that of [NaC<sub>22</sub>C<sub>8</sub>]<sup>+</sup> in pyridine, where the Na<sup>+</sup> selective electrode was used.

**TMEC12**: The stability constants of [Na(TMEC12)]<sup>+</sup> were determined by the competitive titration method except for that of [Na(TMEC12)]<sup>+</sup> in dimethylsulfoxide, where the Na<sup>+</sup> selective electrode was used.

The electrode response to metal ion concentration was determined by titration of a solution of known concentration of Na<sup>+</sup> (Na<sup>+</sup> ion selective electrode) or Ag<sup>+</sup> (Ag<sup>+</sup> selective electrode) into a known volume of a solution of 0.050 mol dm<sup>-3</sup> NEt<sub>4</sub>ClO<sub>4</sub> in the appropriate solvent, and measuring the corresponding potential. The electrode response to metal ion concentration is pseudo Nernstian and is given by Equation 10.1

$$E = E_0 + C \ln[M^+] \quad 10.1$$

The constants  $E_0$  and  $C$  may simply be determined from a plot of the potential  $E$  against the logarithm of the metal ion concentration,  $\ln[M^+]$ . The values of  $E_0$  and  $C$  vary with solvent, with  $C$  lying in the range 19 to 28 mV, consistent with values found in the literature.<sup>2</sup>

The detection limit for the metal ion concentration by the relevant ion selective electrode was dependent on the solvent used. In the case of the Na<sup>+</sup> ion selective electrode, it has been reported that stability constants in the range 10<sup>2</sup> - 10<sup>7</sup> dm<sup>3</sup> mol<sup>-1</sup> could be determined,<sup>2</sup> although it was found that the limit was lower than this in methanol and somewhat higher in pyridine. Surprisingly, initial attempts to measure the stability of [NaC<sub>22</sub>C<sub>2</sub>]<sup>+</sup> in acetonitrile using the Na<sup>+</sup> ion selective electrode gave  $\log(K_s/\text{dm}^3 \text{ mol}^{-1}) = 9.4$ , the same as the result determined using the competitive method. Similarly high stability constants have been successfully determined using an Na<sup>+</sup> ion selective electrode in acetonitrile and pyridine.<sup>3-5</sup> In all solvents studied, the response of the Ag<sup>+</sup> ion selective electrode obeyed equation 10.1 over all concentration ranges encountered during the titrations, allowing stability constants as high as 10<sup>16</sup> to be determined. For the competitive titrations, it is necessary for the Ag<sup>+</sup> and M<sup>+</sup> stability constants to differ by a factor of 10 or more, for accurate determination of the M<sup>+</sup> complex stability constant.

## 10.2 Aqueous Titrations

### 10.2.1 Materials

Deionized water was ultrapurified with a MilliQ-Reagent system to produce water with a resistance of  $>15 \text{ M}\Omega \text{ cm}$  and was used for the preparation of all solutions. Lead, cadmium, calcium, strontium and barium perchlorates were prepared by the addition of concentrated  $\text{HClO}_4$  to the corresponding metal carbonate. Due to the potentially hazardous nature of  $\text{Hg}(\text{ClO}_4)_2$ , no attempt was made to isolate the salt. Instead, concentrated  $\text{HClO}_4$  was added to red  $\text{HgO}$  (BDH) to produce a solution of  $0.1 \text{ mol dm}^{-3}$   $\text{Hg}(\text{ClO}_4)_2$  in approximately  $0.1 \text{ mol dm}^{-3}$   $\text{HClO}_4$  (a  $\text{pH} < 2$  was necessary to prevent the reformation of  $\text{HgO}$ ). Cobalt, nickel, copper, zinc, and magnesium perchlorates were purchased. In both cases the perchlorate salts were twice recrystallized from water and were dried over  $\text{P}_2\text{O}_5$  under vacuum. Solutions of  $\text{HClO}_4$  and  $\text{NEt}_4\text{OH}$  were standardized by conventional methods. Metal perchlorate solutions were standardized by EDTA titration.<sup>6</sup>  $\text{MClO}_4$  salts (where  $\text{M}^+ = \text{Li}^+, \text{Na}^+, \text{K}^+, \text{Rb}^+, \text{Cs}^+, \text{Ag}^+$  or  $\text{Tl}^+$ ) and  $\text{NEt}_4\text{ClO}_4$  were prepared as described previously in Section 10.1.1.

### 10.2.2 Determination of Stability Constants

The stability constants for the divalent metal complexes in aqueous solution were determined by potentiometric titration using a Metrohm E665 Dosimat autoburette interfaced to a Laser XT/3-8086 PC. Changes in hydrogen ion concentration were monitored using an Orion Ross Sureflow 81-72 BN combination electrode connected to an Orion SA720 potentiometer. All titrations were carried out at  $298.2 \pm 0.1 \text{ K}$  in a water jacketed vessel. A stream of nitrogen was bubbled through the titration solution to prevent the ingress of atmospheric  $\text{CO}_2$  and the solution was stirred with a magnetic stirrer. Prior to entering the vessel, the nitrogen was bubbled through a solution of  $0.1 \text{ mol dm}^{-3}$   $\text{NEt}_4\text{ClO}_4$ , in order to prevent evaporation from the vessel.

The protonation constants  $K_1$  and  $K_2$  of  $\text{C}_{22}\text{C}_2$  and  $\text{C}_{22}\text{C}_8$  were determined by the titration of a solution of  $0.1 \text{ mol dm}^{-3}$   $\text{NEt}_4\text{OH}$  with  $10 \text{ cm}^3$  of a solution of  $0.001 \text{ mol dm}^{-3}$  ligand and  $0.004 \text{ mol dm}^{-3}$   $\text{HClO}_4$ . The protonation constants  $K_1, K_2, K_3$ , and  $K_4$  of the ligand TMEC12 were determined by the titration of a solution of  $0.1 \text{ mol dm}^{-3}$   $\text{NEt}_4\text{OH}$  with  $10 \text{ cm}^3$



of a solution of  $0.001 \text{ mol dm}^{-3}$  ligand and  $0.005 \text{ mol dm}^{-3}$   $\text{HClO}_4$ . Both the stock  $\text{HClO}_4$  and ligand solutions were  $0.10 \text{ mol dm}^{-3}$  in  $\text{NEt}_4\text{ClO}_4$ . Complex stability constants were determined through the titration of a solution of  $0.1 \text{ mol dm}^{-3}$   $\text{NEt}_4\text{OH}$  with  $10 \text{ cm}^3$  of a solution of  $0.001 \text{ mol dm}^{-3}$  ligand and  $0.004$  or  $0.005 \text{ mol dm}^{-3}$   $\text{HClO}_4$  and containing  $\text{M}(\text{ClO}_4)_2$  or  $\text{MClO}_4$ . For each metal ion at least three titrations were performed in which the metal ion / ligand ratio was varied. The addition of titrant was computer controlled so that either constant volume aliquots could be delivered, or successive additions of titrant were added to cause a decrease in potential of approximately  $4 \text{ mV}$ . For most titrations, a delay of up to  $300 \text{ s}$  was sufficient for equilibrium to be attained, but for situations in which slow complexation of the metal ion occurred, a delay of up to  $3000 \text{ s}$  was allowed. In the the case of  $[\text{NiC}_2\text{C}_2]^{2+}$  even this delay was insufficient because the complexation of the metal ion was extremely slow. Thus, accurate determination of the stabilities of this complex was impossible.

The electrode was regularly calibrated by the titration of  $0.1 \text{ mol dm}^{-3}$   $\text{NEt}_4\text{OH}$  from the autoburette with  $10 \text{ cm}^3$  of  $0.004 \text{ mol dm}^{-3}$   $\text{HClO}_4$ . The resulting data was fitted to the Nernst equation (Equation 10.2);

$$E = E_0 + \frac{RT}{F} \ln [\text{H}^+] \quad 10.2$$

where;

$E$  is the observed potential (Volts)

$E_0$  is the standard electrode potential (Volts)

$R$  is the gas constant ( $8.314 \text{ J mol}^{-1} \text{ K}^{-1}$ )

$T$  is the temperature (K)

$F$  is Faradays constant ( $9.6487 \times 10^4 \text{ Coulombs mol}^{-1}$ )

$[\text{H}^+]$  is the hydrogen ion concentration

At  $298.2 \text{ K}$ , with  $E$  in millivolts (mV) equation 10.2 becomes;

$$\text{pH} = \frac{E_0 - E}{59.15} \quad 10.3$$

where;

$$K_w = [\text{H}^+][\text{OH}^-]$$

$$\text{p}K_w = \text{pH} + \text{pOH}$$

$$\text{pH} = -\log[\text{H}^+] \text{ and } \text{pOH} = -\log[\text{OH}^-]$$

The constants  $E_0$  and  $\text{p}K_w$  were determined using the program MINQUAD,<sup>7</sup> with the appropriate diffusion correction terms for 0.10 mol dm<sup>-3</sup> NEt<sub>4</sub>ClO<sub>4</sub> in water.<sup>8</sup> For C22C<sub>2</sub> and C22C<sub>8</sub>, the ligand protonation constants and the stability constants of the metal complexes were determined by fitting the titration data using the program MINQUAD. For TMEC12, the ligand protonation constants and the stability constants of the metal complexes were determined using the program SUPERQUAD.<sup>9</sup>

## 10.3 Heavy Metal Complexes of TMEC12

### 10.3.1 Materials

Cd(CF<sub>3</sub>SO<sub>3</sub>)<sub>2</sub>, Zn(CF<sub>3</sub>SO<sub>3</sub>)<sub>2</sub> and Pb(CF<sub>3</sub>SO<sub>3</sub>)<sub>2</sub> were prepared by the addition of concentrated trifluoromethanesulfonic acid (Aldrich) to an excess of the respective carbonates. The excess carbonate was filtered off and the volume was reduced until the triflate salt precipitated from solution. In the case of Hg(CF<sub>3</sub>SO<sub>3</sub>)<sub>2</sub>, it was necessary to add excess acid to prevent the formation of HgO. The salts were filtered off under an atmosphere of dry N<sub>2</sub> and were dried for 48 hours under high vacuum over P<sub>2</sub>O<sub>5</sub>.

### 10.3.2 Preparation of Complexes

The complexes [M(TMEC12)](CF<sub>3</sub>SO<sub>3</sub>)<sub>2</sub> could not be crystallized from solution due to their extremely high solubility. Instead, a 1 cm<sup>3</sup> solution of approximately 0.1 mol dm<sup>-3</sup> of the complex in <sup>13</sup>C depleted *d*<sub>4</sub>-methanol (Aldrich) was prepared by addition of equimolar amounts of TMEC12 and the metal triflate. The <sup>13</sup>C depleted *d*<sub>4</sub>-methanol was used in preference to natural abundance *d*<sub>4</sub>-methanol to avoid problems of overlap between the <sup>13</sup>C NMR resonances of the complex and those arising from *d*<sub>4</sub>-methanol.

## 10.4 NMR Measurements

### 10.4.1 $^7\text{Li}$ and $^{23}\text{Na}$ NMR Measurements of Intermolecular Metal Ion Exchange

The preparation of materials used in this section has already been described in Section 10.1.1. Solutions for  $^{23}\text{Na}$  NMR were prepared using  $0.1 \text{ mol dm}^{-3}$   $\text{NaClO}_4$  except in the cases where the low solubility of the  $\text{Na}^+$  complex necessitated the use of a more dilute solution. Such was the case with  $[\text{NaC}_{22}\text{C}_2]^+$  and  $[\text{Na}(\text{TMEC}_{12})]^+$  in water and with  $[\text{NaC}_{22}\text{C}_8]^+$  in acetonitrile (where the total  $\text{NaClO}_4$  concentrations were  $0.05 \text{ mol dm}^{-3}$ ,  $0.02 \text{ mol dm}^{-3}$  and  $0.05 \text{ mol dm}^{-3}$  respectively). The concentration of  $\text{LiClO}_4$  used for  $^7\text{Li}$  NMR measurements depended on the signal to noise ratio obtained with test solutions. All solutions were prepared under dry nitrogen to prevent the ingress of moisture and were degassed and sealed under vacuum in 5 mm outer diameter NMR tubes. These were coaxially mounted in 10 mm NMR tubes containing either  $\text{D}_2\text{O}$ ,  $d_6$ -acetone or  $d_6$ -dimethylsulfoxide which acted as the lock solvent.  $^7\text{Li}$  and  $^{23}\text{Na}$  spectra were recorded on a Bruker CXP-300 NMR spectrometer at 116.59 and 79.39 MHz respectively. For  $^7\text{Li}$  measurements, an average of 1000 - 6000 transients were accumulated in a 8192 point data base over a 1000 Hz spectral width prior to Fourier transformation. For  $^{23}\text{Na}$  measurements, an average of 1000 - 6000 transients were collected in a 2048 point data base over an 8000 Hz spectral width prior to Fourier transformation. The sample temperature was controlled to within  $\pm 0.3 \text{ K}$  using a Bruker B-VT1000 variable temperature unit which was calibrated using the temperature dependence of the  $^1\text{H}$  chemical shifts of ethylene glycol ( $T > 300 \text{ K}$ ) and methanol ( $T < 300 \text{ K}$ ).<sup>10-12</sup> Twenty minutes was allowed for sample equilibration at each new temperature.

The Fourier transformed data were transferred to a VAX 11-780 mainframe computer and were subject to complete lineshape analysis (see Chapter 12) to obtain the kinetic parameters. The temperature dependence of linewidths and chemical shifts pertaining in the absence of exchange used in the lineshape analysis were determined from a combination of extrapolation from the spectra at low temperatures where no exchange induced broadening occurred and from the linewidths and chemical shifts of solutions containing purely solvated or purely complexed  $\text{Na}^+$  or  $\text{Li}^+$ .

### 10.4.2 $^{13}\text{C}$ NMR Measurements of Intramolecular Exchange in Metal Complexes of TMEC12

Broad-band  $^1\text{H}$  decoupled  $^{13}\text{C}$  spectra were run on a Bruker CXP-300 spectrometer at 75.47 MHz. An average of 2000 transients were accumulated in an 8192 point data base over a 2500 Hz spectral width at temperature intervals of 5 K prior to Fourier transformation. The sample temperature was controlled to within  $\pm 0.3$  K using a Bruker B-VT1000 variable temperature unit. The Fourier transformed data were transferred to a VAX 11-780 computer and the kinetic parameters characterising the intramolecular exchange were derived from complete lineshape analysis (Chapter 12). The temperature dependences of chemical widths and shifts in the absence of exchange required in the lineshape analysis were extrapolated from low temperatures where no exchange induced modification of the spectra occurred. Since an accurate extrapolation was required, spectra were recorded starting from the lowest temperature obtainable (190 K).  $^{13}\text{C}$  chemical shifts were referenced to external natural abundance  $d_4$ -methanol, which was assigned a chemical shift of 47.05 ppm.<sup>13</sup>

## 10.5 Synthesis of Ligands

### 10.5.1 Synthesis of the Cryptand C22C<sub>2</sub>

The synthesis of cryptands with aliphatic bridges through the reaction of a diaza crown ether with a diacid chloride, followed by reduction of the amide groups to give the desired cryptand is well established.<sup>14-16</sup> However, Dale and co-workers have developed an alternative method, whereby two aza or diaza crown ethers were linked via the nitrogens by an ethylene bridge, by the reaction of the macrocycle with ethylene glycol ditosylate in refluxing acetonitrile containing suspended  $\text{Na}_2\text{CO}_3$ .<sup>17-18</sup> Using this technique, they developed the following synthesis of the ligand C22C<sub>2</sub>.<sup>19</sup>

Two separate solutions, one of ethylene glycol ditosylate (4.17g, 11.3 mmol) in 100 cm<sup>3</sup> of dry acetonitrile and another of Cryptofix 22 (Merck) (2.98g, 11.2 mmol) in 100 cm<sup>3</sup> dry acetonitrile were added synchronously over 32 hours by perfusor syringe to a solution of  $\text{Na}_2\text{CO}_3$  in refluxing acetonitrile (100 cm<sup>3</sup>). Stirring and refluxing continued for 7 days, then the solid salts were removed and washed with acetonitrile and the combined solvents were removed. The residue was taken up in chloroform (50 cm<sup>3</sup>) and

water (5 cm<sup>3</sup>) and the aqueous phase further extracted with CHCl<sub>3</sub> (3 x 50 cm<sup>3</sup>). After removal of the CHCl<sub>3</sub>, the residue was refluxed with NaOCH<sub>3</sub> / CH<sub>3</sub>OH to destroy any unreacted tosyl functions and the methanol was evaporated. The residue was taken up in water (50 cm<sup>3</sup>) and the aqueous layer was extracted with CHCl<sub>3</sub> (3 x 10 cm<sup>3</sup>). The aqueous layer was concentrated and further extractions with CHCl<sub>3</sub> (4 x 50 cm<sup>3</sup>) yielded the sodium tosylate complex of C<sub>22</sub>C<sub>2</sub>. The free ligand was obtained on pyrolysis in a Kugelrohr at 473.2 K / 0.01mm Hg. Yield 2.1g, 65%, m.p = 60-65°C, <sup>13</sup>C NMR (CDCl<sub>3</sub>): δ (ppm) 52.5 (NCH<sub>2</sub>), 56.3 (NCH<sub>2</sub>), 70.0 (CH<sub>2</sub>O), 70.8 (CH<sub>2</sub>O).

Ethylene glycol ditosylate was prepared according to the literature<sup>20</sup> and was dried under vacuum and stored under nitrogen prior to use.

### 10.5.2 Synthesis of the Cryptand C<sub>22</sub>C<sub>8</sub>

The synthesis of this cryptand was a combination of the original method of synthesis by Lehn<sup>14</sup> and that of C<sub>21</sub>C<sub>5</sub>.<sup>15</sup> A reaction scheme for the synthesis appears in Figure 10.1.

A solution of Cryptofix 22 (Merck) (3.0 g, 11.44 mmol) and triethylamine (3.66 g, 36.17 mmol) in dry benzene (150 cm<sup>3</sup>) and a solution of suberoyl dichloride (2.21 g, 10.47 mmol) in dry benzene (150 cm<sup>3</sup>) were added simultaneously to dry benzene (1500 cm<sup>3</sup>) with continuous stirring over 8 hours using Perfusor motor driven syringes. The resultant Et<sub>3</sub>NHCl was filtered off and the solvent was removed under vacuum. The residue was chromatographed on 'flash' silica (Merck, 230-400 mesh, 4% methanol / dichloromethane, R<sub>f</sub> = 0.15) and removal of the solvent yielded the C<sub>22</sub>C<sub>8</sub> diamide as a white solid. Yield 4.3 g, 92.6 %.

The C<sub>22</sub>C<sub>8</sub> diamide (4.3 g, 10.74 mmol) was dissolved in dry tetrahydrofuran (40 cm<sup>3</sup>) and heated to 323.2 K under dry nitrogen. Boron trifluoride etherate (3.13 g, 22.1 mmol) was added dropwise over three minutes. The reaction mixture was heated to reflux and borane-dimethylsulfide complex (2.84 g, 37.2 mmol) was added over fifteen minutes and the solution was allowed to reflux for a further three hours. The solvent was then removed under vacuum yielding a white residue to which 40 cm<sup>3</sup> of 6 mol dm<sup>-3</sup> HCl was added. The resultant solution was refluxed for twelve hours and then evaporated to dryness. Due to the low solubility of C<sub>22</sub>C<sub>8</sub> in water, the cryptand could not be obtained by ion exchange. Instead, concentrated NEt<sub>4</sub>OH was added to the hydrochloride salt until the solution was strongly basic,

followed by extraction with benzene (6 x 100 cm<sup>3</sup>). The benzene was removed under vacuum and recrystallization from benzene yielded the pure ligand. Yield 2.16 g, 50.1%, <sup>1</sup>H NMR (CDCl<sub>3</sub>): δ (ppm) 1.38 (m) (12H, aliphatic -CH<sub>2</sub>-), 2.47 (m) (12H, NCH<sub>2</sub>), 3.48 (m) (8H, CH<sub>2</sub>O), 3.63 (m) (8H, CH<sub>2</sub>O). <sup>13</sup>C NMR (CDCl<sub>3</sub>): δ (ppm) 25.8 (aliphatic -CH<sub>2</sub>-), 27.7 (aliphatic -CH<sub>2</sub>-), 28.8 (aliphatic -CH<sub>2</sub>-), 54.0 (NCH<sub>2</sub>), 55.3 (NCH<sub>2</sub>), 68.9 (OCH<sub>2</sub>), 70.7 (OCH<sub>2</sub>).

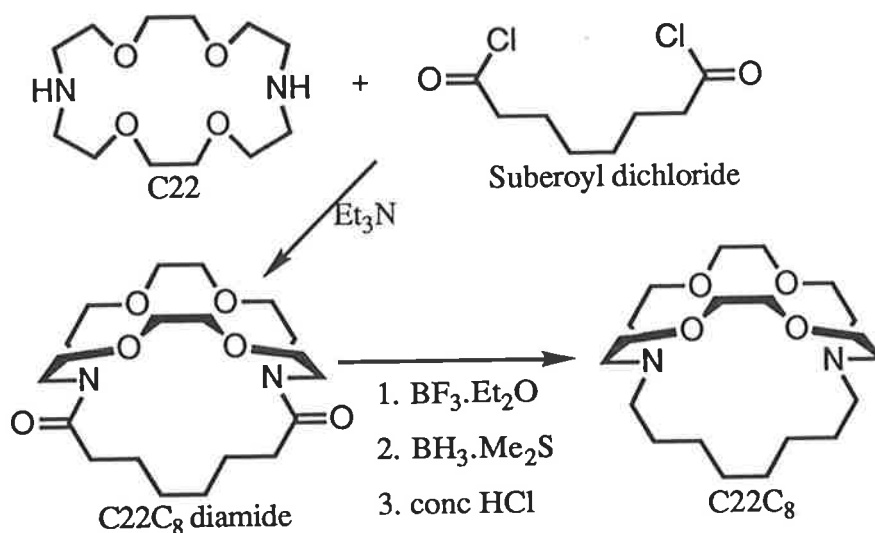


Figure 10.1. Synthesis of C22C<sub>8</sub>.

### 10.5.3 Synthesis of 1,4,7,10-Tetrakis(2-methoxyethyl)-1,4,7,10-Tetraazacyclododecane (TMEC12)

The synthesis of TMEC12 (using THEC12 as a starting material) has been reported in the literature,<sup>21</sup> but a far simpler method is to synthesise the ligand directly from the parent tetraaza macrocycle cyclen. The synthesis of *N* functionalized azamacrocycles has been reviewed in the literature and in many cases is straightforward.<sup>22</sup> The unsubstituted macrocycle is reacted with an excess of alkylating agent in the presence of a base to neutralise the acid liberated by this reaction. This method has been successfully used in the synthesis of a number of pendant arm tetraaza macrocycles<sup>23-28</sup> and was thus chosen as the method of synthesising TMEC12. The cyclen used in the synthesis was prepared according to the method described by Richman and Atkins.<sup>29</sup>

The starting materials used in this synthesis; *NOO'*-tris(toluene-*p*-sulphonyl)bis(2-hydroxyethyl)amine and the disodium salt of 1,4,7-tris(toluene-*p*-sulphonyl)-1,4,7-triazaheptane were both synthesised according to the literature<sup>30</sup> as described below.

#### 10.5.3.1 Synthesis of *NOO'*-tris(toluene-*p*-sulphonyl)bis(2-hydroxyethyl)amine

A solution of *p*-toluenesulphonyl chloride (BDH) (114.4 g, 0.6 mol) in diethylether (600 cm<sup>3</sup>) was added dropwise to a stirred solution of bis(2-hydroxyethyl)amine (BDH) (20.4 g, 0.2 mol) in triethylamine (200 cm<sup>3</sup>) at room temperature. When the addition was complete, the solution was stirred for a further 1 hour. Water (900 cm<sup>3</sup>) was added and the solution was stirred for another 8 hours. A white precipitate (*NOO'*-tris(toluene-*p*-sulphonyl)bis(2-hydroxyethyl)amine) was filtered from solution, washed with diethylether (200 cm<sup>3</sup>) and air dried overnight. Yield 40.9 g, 37%.

#### 10.5.3.2 Synthesis of 1,4,7-tris(toluene-*p*-sulphonyl)-1,4,7-triazaheptane and its Disodium Salt

A solution of *p*-toluenesulphonyl chloride (BDH) (114.4 g, 0.6 mol) in diethylether (600 cm<sup>3</sup>) was added dropwise to a vigorously stirred solution of diethylenetriamine (BDH) (20.6 g, 0.2 mol) and NaOH (24 g, 0.6 mol) in water (200 cm<sup>3</sup>) at room temperature. When the addition was complete, the solution was further stirred for 1 hour. The resulting white solid (1,4,7-tris(toluene-*p*-sulphonyl)-1,4,7-triazaheptane) was filtered and recrystallised from ethanol. Yield 73.5 g, 65.3 %. The disodium salt was prepared by the addition of 1,4,7-tris(toluene-*p*-sulphonyl)-1,4,7-triazaheptane in small portions to a stirred solution of sodium in ethanol (700 cm<sup>3</sup>) under dry N<sub>2</sub>. The resultant white pasty precipitate was filtered under dry N<sub>2</sub> and washed with large portions of diethylether. The white solid was then dried under vacuum. Yield 60.4 g, 66.1%

#### 10.5.3.3 Synthesis of 1,4,7,10-tetraazacyclododecane (Cyclen)

A solution of *NOO'*-tris(toluene-*p*-sulphonyl)bis(2-hydroxyethyl)amine (48.8 g, 0.086 mol) in anhydrous dimethylformamide (325 cm<sup>3</sup>) was added dropwise to a stirred solution of the disodium salt of 1,4,7-tris(toluene-*p*-sulphonyl)-1,4,7-triazaheptane (60.4 g, 0.086 mol) in anhydrous dimethyl-

formamide (650 cm<sup>3</sup>) at 383.2 K under dry N<sub>2</sub>. When addition was complete (2 hours), the solution was cooled and water was added dropwise to the mechanically stirred solution until the volume was 3 dm<sup>3</sup> and the solution was stirred for 8 hours. The tetratosyl cyclen was collected by filtration, then washed with ethanol (2 x 200 cm<sup>3</sup>) and diethylether (200 cm<sup>3</sup>) and then dried under vacuum. Yield 59.8 g, 88.4%.

The tosyl functional groups were removed by dissolving tetratosyl cyclen (59.8 g, 0.076 mol) in a stirred solution of deoxygenated concentrated H<sub>2</sub>SO<sub>4</sub> (220 cm<sup>3</sup>) and water (5 cm<sup>3</sup>) at 373.2 K under dry N<sub>2</sub> and stirring for 50 hours. The solution was ice cooled, and diethylether was added (550 cm<sup>3</sup>). The resulting grey precipitate was filtered from solution and washed with diethylether (200 cm<sup>3</sup>). The crude cyclen was dissolved in water (100 cm<sup>3</sup>) and NaOH (50 g) was slowly added. The cyclen was extracted with CHCl<sub>3</sub> (5 x 200 cm<sup>3</sup>), dried with anhydrous MgSO<sub>4</sub> and taken to dryness on a rotary evaporator. Yield 7.2 g, 56.3 %, <sup>1</sup>H NMR. (CDCl<sub>3</sub>): δ (ppm) 2.59, <sup>13</sup>C NMR (CDCl<sub>3</sub>): δ (ppm) 45.95.

#### 10.5.3.4 Synthesis of TMEC12

Cyclen (1,4,7,10-tetraazacyclododecane) (0.6 g, 3.48 mmol), NaOH (0.53 g, 13.25 mmol) and 2-chloroethylmethyl ether (12.4 g, 131.16 mmol) were dissolved in 25 cm<sup>3</sup> 50% ethanol/water and the solution refluxed under N<sub>2</sub> for several days. Because of the side reaction between the chloride and NaOH it was necessary to add NaOH intermittently in order to maintain the pH above 11. The solvent was removed under vacuum and the solid residue dissolved in 25 cm<sup>3</sup> water, basicified with NaOH and extracted with CHCl<sub>3</sub> (5 x 50 cm<sup>3</sup>). The CHCl<sub>3</sub> was removed under vacuum leaving a yellow solid, impure [Na(TMEC12)]Cl. Heating under vacuum yielded an observable dissociation of the complex at 373.2 K, 0.05 mm Hg, and the free ligand was distilled at 413.2 K, 0.015 mm Hg. Yield 0.78 g, 55.4%, <sup>1</sup>H NMR (CDCl<sub>3</sub>): δ (ppm) 2.57 (t) (8H, NCH<sub>2</sub>), 2.62 (s) (16H, NCH<sub>2</sub>), 3.27 (s) (12H, OCH<sub>3</sub>), 3.41 (t) (8H, CH<sub>2</sub>O), <sup>13</sup>C NMR (CDCl<sub>3</sub>): δ (ppm) 52.59 (NCH<sub>2</sub>), 55.02 (NCH<sub>2</sub>), (58.71) (OCH<sub>3</sub>), 71.01 (CH<sub>2</sub>O). A reaction scheme for this synthesis appears in Figure 10.2.



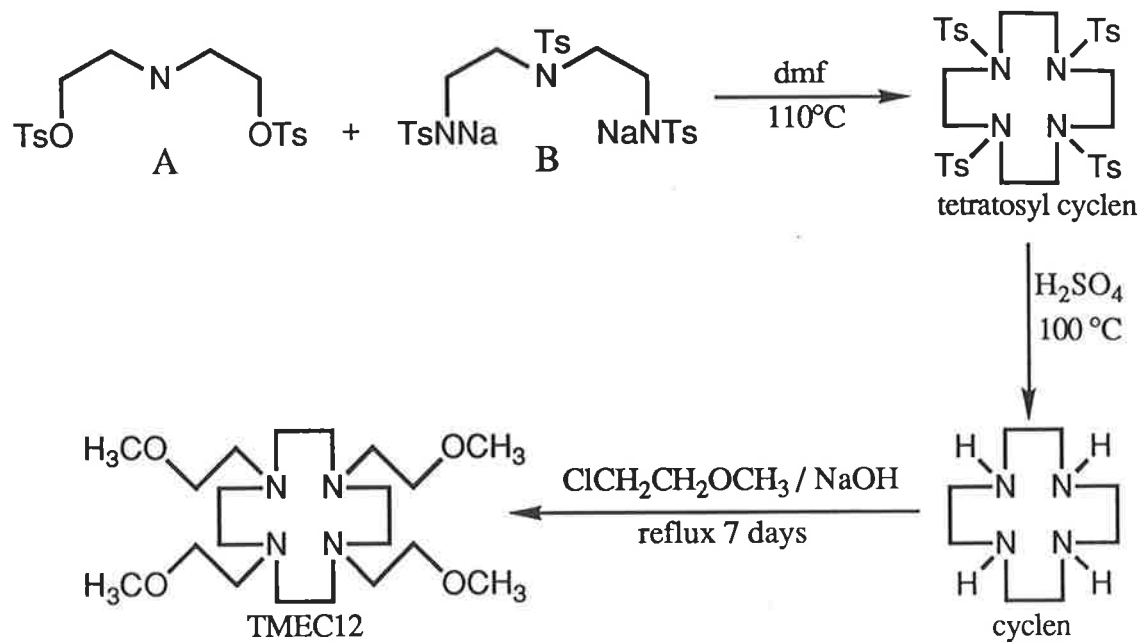


**Figure 10.2.** Synthesis of 1,4,7,10-Tetrakis(2-methoxyethyl)-1,4,7,10-tetraazacyclododecane (TMEC12). Here A is *NOO'*-tris(toluene-*p*-sulphonyl)bis(2-hydroxyethyl)amine and B is the disodium salt of 1,4,7-tris(toluene-*p*-sulphonyl)-1,4,7-triazaheptane.

- 1 Perrin, D.D.; Aramaego, W.L.F.; Perrin, D.R. *"Purification of Laboratory Chemicals"*, 2nd ed, Pergamon, Oxford, U.K, 1980.
- 2 Lehn, J-M.; Sauvage, J-P. *J. Am. Chem. Soc.* **1975**, 97, 6700-6707.
- 3 Nakamura, T.; Yumoto, Y.; Izutsu, K. *Bull. Chem. Soc. Jpn.* **1982**, 55, 1850-1853.
- 4 Lincoln, S.F.; Lucas, J.B. *J. Chem. Soc., Dalton Trans.* **1994**, 423-427.
- 5 Rodopoulos, T.; Pittet, P-A.; Lincoln, S.F. *J. Chem. Soc., Dalton Trans.* **1993**, 1055.
- 6 Vogel, A.I., *"Quantitative Inorganic Analysis"*, Longmans, Green and Co., London, **1955**.
- 7 Sabatini, A.; Vacca, A.; Gans, P. *Talanta.* **1974**, 21, 53-77.
- 8 Kulstad, S.; Malmsten, L.A. *J. Inorg. Nucl. Lett.* **1980**, 42, 573-578.
- 9 Gans, P.; Sabatini, A.; Vacca, A. *J. Chem. Soc., Dalton. Trans.* **1985**, 1195-1200.
- 10 Raiford, D.S.; Fisk, C.L.; Becker, E.D. *Anal. Chem.* **1979**, 51, 2050.
- 11 van Geet, A.L. *Anal. Chem.* **1970**, 42, 679-680.
- 12 van Geet, A.L. *Anal. Chem.* **1968**, 40, 2227.
- 13 Breitmaier, E.; Haas, G.; Voelter, W. *"Atlas of Carbon-13 NMR Data"*, Volume 1, Heyden, London, **1979**.
- 14 Dietrich, B.; Lehn, J-M.; Sauvage, J-P.; Blanzat, J. *Tetrahedron* . **1973**, 29, 1629-1645.
- 15 Lincoln, S.F.; Horn, E.; Snow, M.R.; Hambley, T.W.; Brereton, I.M.; Spotswood, T.M. *J. Chem. Soc., Dalton Trans.* **1986**, 1075-1080.
- 16 Clarke, P. PhD Thesis, University of Adelaide, **1992**
- 17 Calverley, M.J.; Dale, J. *J. Chem. Soc., Chem. Commun.* **1981**, 684-686
- 18 Calverley, M.J.; Dale, J. *J. Chem. Soc., Chem. Commun.* **1981**, 1084-1086.
- 19 Alfheim, T.; Dale, J.; Krautwurst, K.D. *Acta Chem. Scand.* **1986**, B40, 40-49.
- 20 Dale, J.; Kristiansen, P.O. *Acta Chem. Scand.* **1972**, 26, 1471.
- 21 Buoen, S.; Dale, J. *Acta Chem. Scand.* **1986**, B40, 278-282.
- 22 Kaden, T.A. *Top. Curr. Chem.* **1984**, 121, 157-179.
- 23 Hafliger, H.; Kaden, T.A. *Helv. Chim. Acta.* **1979**, 62, 683-688.
- 24 Alcock, N.W.; Balakrishnan, K.P.; Moore, P. *J. Chem. Soc., Dalton. Trans.* **1986**, 1743-1745.
- 25 Chia, P.S.K.; Elkstrom, A.; Liepa, I.; Lindoy, L.F.; McPartlin, M.; Smith, S.V.; Tasker, P.A. *Aust. J. Chem.* **1991**, 44, 737.
- 26 Stetter, H.; Frank, W.; Mertens, R. *Tetrahedron.* **1981**, 37, 767.

- 27 Takahashi, M.; Takamoto, S. *Bull. Chem. Soc. Japan.* **1977**, 50, 3413-3414.
- 28 Weitzel, F.L.; Raymond, K.N. *J. Am. Chem. Soc.* **1979**, 101, 2728-2731.
- 29 Richman, J.E.; Atkins, T.J. *J. Am. Chem. Soc.* **1974**, 96, 2268.
- 30 Fabbrizzi, L. *J. Chem. Soc., Dalton. Trans.* **1979**, 1857.

# Chapter 11: Analysis of Data from Potentiometric Titrations

## 11.1 Determination of Stability Constants of Metal Complexes in Non-Aqueous Solution

A wide variety of methods have been used to determine the stability constants of metal complexes in non-aqueous solution, including NMR spectroscopy, calorimetry and polarography, but the most common method is that of potentiometric titration. This simply involves directly titrating a solution of the ligand into a solution of the metal ion of interest and measuring the free metal ion concentration with an ion selective electrode (ISE). The relationship between electrode potential and free metal ion concentration is pseudo-Nernstian and is given by Equation 11.1.

$$E = E_0 + C \ln[M^+] \quad 11.1$$



$$K_s = \frac{[ML^+]}{[M^+][L]} \quad 11.3$$

Having determined the constants  $E_0$  and  $C$  by electrode calibration (Chapter 10), free metal ion concentration and thus  $K_s$  may be determined from Equation 11.3. The stability constants  $K_s$  for the  $Na^+$  and  $Ag^+$  complexes in this study were determined by this method. When no suitable ion selective electrode is available, the stability constant of the desired metal complex may be determined by a competitive titration method<sup>1</sup> which involves measuring the stability constant of the silver complex in the presence of a competing metal ion  $M^+$ . A solution of  $Ag^+$  is titrated with a solution of  $[ML]^+$  and the competition between  $Ag^+$  and  $M^+$  for the ligand  $L$  (Equation 11.4) is monitored with an  $Ag^+$  ISE.



$$K_e = \frac{[\text{AgL}^+][\text{M}^+]}{[\text{Ag}^+][\text{ML}^+]} \quad 11.5$$

Thus, if the stability constant of the silver complex,  $K_s(\text{Ag}^+)$ , is known, the stability constant of the metal complex,  $K_s(\text{M}^+)$ , can be determined from;

$$K_s(\text{M}^+) = \frac{K_s(\text{Ag}^+)}{K_e} \quad 11.6$$

The stability constants of the  $\text{Li}^+$ ,  $\text{K}^+$ ,  $\text{Rb}^+$ ,  $\text{Cs}^+$  and  $\text{Tl}^+$  complexes in this study were determined by this method. In systems where  $K_s > 10^6 \text{ dm}^3 \text{ mol}^{-1}$  then the free  $\text{Na}^+$  concentration may be too low to be reliably determined by the  $\text{Na}^+$  ISE whose response no longer obeys equation Equation 11.1 below certain  $\text{Na}^+$  concentrations.<sup>1-2</sup> Thus, the competitive titration method was employed in determining the stabilities of  $[\text{NaC22C}_2]^+$  in methanol and acetonitrile.

The following sections describe in detail how stability constants are obtained from potentiometric titration data. Examples of titration data and the subsequent analysis of this data for both direct and competitive titration methods are included to illustrate the discussion. The method used follows that of Rossotti and Rossotti<sup>3</sup> and for the formation of 1:1 metal complexes is straightforward.

### 11.1.1 Direct Titration

The equilibrium constant  $K_s$  determined at each point  $i$  of the titration is given by;

$$K_s(i) = \frac{[\text{ML}^+(i)]}{[\text{M}^+(i)][\text{L}(i)]} \quad 11.7$$

Rearrangement of Equation 11.7 gives;

$$\frac{[\text{ML}^+(i)]}{[\text{M}^+(i)]} = K_s(i) [\text{L}(i)] \quad 11.8$$

or equivalently;

$$\frac{1-\alpha(i)}{\alpha(i)} = K_s(i) [L(i)] \quad 11.9$$

where  $\alpha(i) = \frac{[M^+(i)]}{[M^+(i)]_t}$  and is the proportion of total metal ion in the form  $M^+$ .

Thus, a plot of  $\frac{1-\alpha(i)}{\alpha(i)}$  versus  $[L(i)]$  is a straight line which passes through the origin and has a slope of  $K_s$ . The various concentrations in Equation 11.8 are obtainable from known or measurable quantities. At each point  $i$  in the titration the potential  $E(i)$  is related to the free  $M^+$  concentration  $[M^+(i)]$  by Equation 11.1.

$$\text{Thus } [M^+(i)] = \exp\left(\frac{E(i) - E_0}{C}\right) \quad 11.10$$

The concentrations  $[ML^+(i)]$  and  $[L(i)]$  may be calculated from the mass balance equations;

$$[M^+(i)]_t = [M^+(i)] + [ML^+(i)] \quad 11.11$$

$$[L(i)]_t = [L(i)] + [ML^+(i)] \quad 11.12$$

where  $[M^+(i)]_t$  and  $[L(i)]_t$  are the total metal and ligand concentrations, respectively, and refer to the alkali metal ion of interest or  $Ag^+$ . For the addition of  $V_{\text{titre}}$   $\text{cm}^3$  of a solution of L to  $20 \text{ cm}^3$  of a solution of  $M^+$  (at point  $i$  of the titration) the following relations hold;

$$[M^+(i)]_t = \frac{20 \times [M^+]_{\text{in}}}{20 + V_{\text{titre}}} \quad 11.13$$

$$[L(i)]_t = \frac{V_{\text{titre}} \times [L]_{\text{in}}}{20 + V_{\text{titre}}} \quad 11.14$$

where  $[M^+]_{\text{in}}$  and  $[L]_{\text{in}}$  are the initial concentrations of  $M^+$  and L.

A simple FORTRAN-77 program, STAB,<sup>4</sup> was used to calculate the values of  $[L(i)]$  and  $\frac{1-\alpha(i)}{\alpha(i)}$  using these mass balance equations and the known electrode

calibration parameters  $C$  and  $E_0$  (Equation 11.1). Simple linear regression of Equation 11.9 yielded  $K_s$ .

### 11.1.2 Competitive Titration

Equation 11.5 can be rewritten as;

$$\frac{[\text{AgL}^{+(i)}] [\text{M}^{+(i)}]}{[\text{Ag}^{+(i)}]} = K_e [\text{ML}^{+(i)}] \quad 11.15$$

$$\text{or } \frac{1-\alpha(i)}{\alpha(i)} [\text{M}^{+(i)}] = K_e [\text{ML}^{+(i)}] \quad 11.16$$

$$\text{where } \alpha(i) = \frac{[\text{Ag}^{+(i)}]}{[\text{Ag}^{+(i)}]_t}$$

Thus, a plot of  $\frac{1-\alpha(i)}{\alpha(i)} [\text{M}^{+(i)}]$  versus  $[\text{ML}^{+(i)}]$  is a straight line of slope  $K_e$ . Values of  $[\text{Ag}^{+(i)}]$  are calculated from the measured EMF values using Equation 11.1. The other concentrations can be calculated using the mass balance equations which for the competitive situation become;

$$[\text{Ag}^{+(i)}]_t = [\text{Ag}^{+(i)}] + [\text{AgL}^{+(i)}] \quad 11.17$$

$$[\text{M}^{+(i)}]_t = [\text{M}^{+(i)}] + [\text{ML}^{+(i)}] \quad 11.18$$

$$[\text{L}(i)]_t = [\text{L}(i)] + [\text{AgL}^{+(i)}] + [\text{ML}^{+(i)}] \quad 11.19$$

where  $[\text{Ag}^{+(i)}]_t$ ,  $[\text{M}^{+(i)}]_t$  and  $[\text{L}(i)]_t$  are the total concentrations of  $\text{Ag}^+$ ,  $\text{M}^+$  and  $\text{L}$ , respectively. However, under the conditions  $[\text{M}^+]_t > [\text{L}]_t$  and  $\log(K_s/\text{dm}^3 \text{ mol}^{-1}) > 2$ , the free ligand concentration  $[\text{L}]$  is negligible so that Equation 11.19 becomes;

$$[\text{L}(i)]_t = [\text{AgL}^{+(i)}] + [\text{ML}^{+(i)}] \quad 11.20$$

The following relations also hold;

$$[\text{Ag}^{+(i)}]_t = \frac{20 \times [\text{Ag}^+]_{\text{in}}}{20 + V_{\text{titre}}} \quad 11.21$$

$$[M^{+}(i)]_t = \frac{V_{\text{titre}} \times [M^{+}]_{\text{in}}}{20 + V_{\text{titre}}} \quad 11.22$$

$$[L(i)]_t = \frac{V_{\text{titre}} \times [L]_{\text{in}}}{20 + V_{\text{titre}}} \quad 11.23$$

where  $[Ag^{+}]_{\text{in}}$ ,  $[M^{+}]_{\text{in}}$  and  $[L]_{\text{in}}$  are the initial concentrations of  $Ag^{+}$ ,  $M^{+}$  and  $L$  respectively. The program STAB was used to calculate values of  $\frac{1-\alpha(i)}{\alpha(i)} [M^{+}(i)]$  and  $[ML^{+}(i)]$  and subsequent linear regression of Equation 11.16 yielded  $K_e$  and hence  $K_s$ . The titration data and parameters calculated by STAB for the determination of the stability constants of  $[NaC22C2]^{+}$  in dimethylsulfoxide and  $[AgC22C8]^{+}$  in dimethylformamide appear in Tables 11.1 and 11.3, respectively. Plots of  $\frac{1-\alpha(i)}{\alpha(i)}$  versus  $[L(i)]$  for these systems appear in Figures 11.1 and 11.3 respectively. Similar data used in the determination of the stability constant of  $[TlC22C8]^{+}$  in dimethylformamide appears in Table 11.5 and a plot of  $\frac{1-\alpha(i)}{\alpha(i)} [M^{+}(i)]$  versus  $[ML^{+}(i)]$  appears in Figure 11.5. The  $K_s$  values quoted in Tables 2.2, 2.4 and 6.1 are the average values determined from two titration experiments. The experimental conditions for these titrations are included below. All stability constants were determined at 298.2 K and ionic strength  $I = 0.050 \text{ mol dm}^{-3}$  ( $NEt_4ClO_4$ ). For a complete description of experimental details see Chapter 10.

### $[NaC22C2]^{+}$ in Dimethylsulfoxide

A solution of  $5 \text{ cm}^3$  of  $1.260 \times 10^{-2} \text{ mol dm}^{-3}$   $C22C2$  was titrated with  $20 \text{ cm}^3$  of  $1.06 \times 10^{-3} \text{ mol dm}^{-3}$   $NaClO_4$  solution. The  $Na^{+}$  ISE used to measure  $[Na^{+}]$  was calibrated over the concentration range  $2.0 \times 10^{-6} \text{ mol dm}^{-3}$  to  $2.0 \times 10^{-3} \text{ mol dm}^{-3}$ . The calibration constants  $C$  and  $E_0$  (Equation 11.1) were 24.39 mV and -104.5 mV respectively. From linear regression of Equation 11.9, the value  $\log(K_s/\text{dm}^3 \text{ mol}^{-1}) = 5.62 \pm 0.01$  was obtained.

### $[AgC22C8]^{+}$ in Dimethylformamide

A solution of  $5 \text{ cm}^3$  of  $8.90 \times 10^{-3} \text{ mol dm}^{-3}$   $C22C8$  was titrated with  $20 \text{ cm}^3$  of  $1.07 \times 10^{-3} \text{ mol dm}^{-3}$   $AgNO_3$  solution. The  $Ag^{+}$  electrode used to measure  $[Ag^{+}]$  was calibrated over the concentration range  $1.0 \times 10^{-8} \text{ mol dm}^{-3}$  to  $2.0 \times 10^{-3} \text{ mol dm}^{-3}$ . The calibration constants  $C$  and  $E_0$  were 26.38



mV and 132.8 mV respectively. From linear regression of Equation 11.9, the value  $\log(K_s/\text{dm}^3 \text{ mol}^{-1}) = 7.78 \pm 0.01$  was obtained.

### [TIC22C<sub>8</sub>]<sup>+</sup> in Dimethylformamide

A solution of 5 cm<sup>3</sup> of  $9.10 \times 10^{-3} \text{ mol dm}^{-3}$  C22C<sub>8</sub> and  $4.794 \times 10^{-2} \text{ mol dm}^{-3}$  TiClO<sub>4</sub> was titrated with 20 cm<sup>3</sup> of  $1.15 \times 10^{-3} \text{ mol dm}^{-3}$  AgNO<sub>3</sub> solution. The Ag<sup>+</sup> electrode was calibrated over the concentration range  $1.0 \times 10^{-8} \text{ mol dm}^{-3}$  to  $2.0 \times 10^{-3} \text{ mol dm}^{-3}$  and the calibration constants *C* and *E*<sub>0</sub> were 26.38 mV and 132.0 mV respectively. From linear regression of Equation 11.16, the value  $\log K_e = 4.67 \pm 0.01$  was obtained. Thus, from Equation 11.6,  $\log K_s(\text{Ti}^+) (\text{dm}^3 \text{ mol}^{-1}) = \log K_s(\text{Ag}^+) - \log K_e = 3.02 \pm 0.02$ .

### 11.1.3 Determination of Stability Constants by Curve Fitting

Complexes with high stability constants result in very small free ligand concentrations [L] before the equivalence point. Similarly, in competitive titrations, a large difference in stabilities between [AgL]<sup>+</sup> and [ML]<sup>+</sup> results in very small [ML]<sup>+</sup> concentrations before the equivalence point. As a result, any experimental uncertainties in the parameters used to calculate these concentrations (Equations 11.11 - 11.12 and 11.17 - 11.19) give very large relative errors for these points which thus could not be used in calculating *K*<sub>s</sub>. It was decided that a method that used all data points to determine *K*<sub>s</sub> was more appropriate and thus the method of curve fitting described by Rossotti and Rossotti<sup>3</sup> was used to confirm all values of *K*<sub>s</sub> determined by use of Equations 11.9 and 11.16. The FORTRAN-77 program VIS<sup>4</sup> calculates a theoretical titration curve which is a function of known concentrations, the calibrated electrode response and the stability constant *K*<sub>s</sub> for direct or *K*<sub>e</sub> for competitive titrations. Derivation of this theoretical curve is described below.

Substitution of the mass balance Equations 11.11 and 11.12 into Equation 11.3 gives;

$$K_s = \frac{[\text{M}^+(i)]_t - [\text{M}^+]}{([\text{L}(i)]_t - [\text{M}^+(i)]_t + [\text{M}^+(i)]) \times [\text{M}^+(i)]} \quad 11.24$$

Let  $[\text{M}^+(i)]_t = M_t$ ,  $[\text{L}(i)]_t = L_t$  and  $[\text{M}^+(i)] = M$   
ie

$$K_s = \frac{M_t - M}{(L_t - M_t + M) \times M} \quad 11.25$$

Rearrangement of Equation 11.25 gives a quadratic in M;

$$K_s M^2 + (K_s L_t - K_s M_t + 1)M - M_t = 0 \quad 11.26$$

This may be solved to give M;

$$M = \frac{-b \pm \sqrt{b^2 - 4ac}}{2a} \quad 11.27$$

where  $a = K_s$ ,  $b = (K_s L_t - K_s M_t + 1)$  and  $c = -M_t$

Obviously, only solutions for which  $b^2 - 4ac > 0$  and  $0 < M < M_t$  are physically meaningful. The former requirement is always satisfied under experimental conditions and the latter may be satisfied by taking only the positive root of Equation 11.27.

For the competitive case, substitution of the mass balance Equations 11.17 - 11.19 into Equation 11.5 gives;

$$K_e = \frac{(A_t - A) \times (M_t - L_t + A_t - A)}{A \times (L_t - A_t + A)} \quad 11.28$$

where  $A_t = [Ag^+(i)]_t$ ,  $M_t = [M^+(i)]_t$ ,  $L_t = [L(i)]_t$  and  $A = [Ag^+(i)]$

Since  $[Ag^+]$  is the variable determined experimentally, it is necessary to solve for A and thus rearranging Equation 11.28 gives;

$$A^2(K_e - 1) + A(K_e L_t - K_e A_t + 2A_t - L_t + M_t) + A_t(L_t - M_t - A_t) = 0 \quad 11.29$$

This may be solved to give A;

$$A = \frac{-b \pm \sqrt{b^2 - 4ac}}{2a} \quad 11.30$$

where  $a = K_e - 1$ ,  $b = K_e L_t - K_e A_t + 2A_t - L_t + M_t$  and  $c = A_t(L_t - M_t - A_t)$

As before, the conditions  $b^2 - 4ac > 0$  and  $0 < A < A_t$  must be satisfied. VISP generates a theoretical titration curve (EMF versus titre) by determining free metal ion concentration,  $[M^+]$  (Equation 11.27), or free silver ion concentration,  $[Ag^+]$  (Equation 11.30), for an initial estimate of  $K_s$  (or  $K_e$ ). Substitution of this concentration into Equation 11.1 yields a theoretical EMF. The value of  $K_s$  (or  $K_e$ ) may be systematically varied until the best fit of the experimental EMF data to the theoretical curve is obtained. Experimental and calculated EMF values calculated by VISP used in the determination of the stability constants of  $[NaC22C2]^+$  in dimethylsulfoxide,  $[AgC22C8]^+$  in dimethylformamide and  $[TlC22C8]^+$  in dimethylformamide appear in Tables 11.2, 11.4 and 11.6 respectively. The fit of the experimental EMF to the curve calculated by VISP for these systems appear in Figures 11.2, 11.4 and 11.6 respectively. The results obtained are identical within experimental error to those obtained using Equations 11.9 and 11.16.

**Table 11.1.** Experimental Data and Concentrations Calculated Using STAB Used to Determine the Stability Constant of  $[\text{NaC22C}_2]^+$  in Dimethylsulfoxide at 298.2 K and  $I = 0.050 \text{ mol dm}^{-3}$  ( $\text{NEt}_4\text{ClO}_4$ ).

titre ( $\text{cm}^3$ )	EMF (expt) mV	$[\text{Na}^+]$ $\times 10^5$ mol $\text{dm}^{-3}$	$[\text{NaC22C}_2^+]$ $\times 10^4$ mol $\text{dm}^{-3}$	$[\text{C22C}_2]$ $\times 10^4$ mol $\text{dm}^{-3}$	$\frac{1-\alpha}{\alpha}$
1.46	-322.3	13.237	8.555	0.017	6.46
1.54	-328.3	10.350	8.807	0.201	8.51
1.6	-334.9	7.897	9.025	0.308	11.43
1.66	-342.6	5.759	9.212	0.445	16.00
1.72	-353.2	3.729	9.388	0.590	25.18
1.78	-360.2	2.799	9.454	0.844	33.78
1.84	-367.0	2.118	9.495	1.120	44.84
1.9	-372.4	1.697	9.511	1.421	56.04
1.96	-376.9	1.411	9.513	1.733	67.41
2.02	-381.0	1.193	9.508	2.050	79.71
2.08	-384.5	1.033	9.498	2.371	91.92
2.14	-387.6	0.910	9.484	2.694	104.22
2.2	-390.5	0.808	9.469	3.018	117.19
2.26	-392.9	0.732	9.451	3.342	129.06
2.32	-395.0	0.672	9.431	3.666	140.37
2.38	-397.5	0.606	9.412	3.987	155.21
2.44	-399.5	0.559	9.392	4.309	168.11
2.5	-401.4	0.517	9.371	4.629	181.32
2.6	-404.2	0.461	9.334	5.161	202.59
2.7	-406.8	0.414	9.298	5.689	224.50
2.8	-409.2	0.375	9.261	6.213	246.72
2.9	-411.3	0.344	9.223	6.733	267.82
3.0	-413.3	0.317	9.186	7.249	289.52
3.1	-415.1	0.295	9.148	7.761	310.42
3.2	-416.8	0.275	9.110	8.269	331.46
3.3	-418.3	0.258	9.073	8.773	351.03
3.4	-419.9	0.242	9.036	9.272	373.29
3.5	-421.3	0.229	8.998	9.768	393.72
3.6	-422.7	0.216	8.961	10.259	415.27
3.7	-423.9	0.205	8.925	10.746	434.42
3.8	-425.2	0.195	8.888	11.230	456.32
3.9	-426.5	0.185	8.852	11.709	479.34
4.0	-427.5	0.177	8.816	12.184	497.36
4.1	-428.4	0.171	8.780	12.656	513.95
4.2	-429.5	0.163	8.744	13.124	535.48
4.3	-430.6	0.156	8.709	13.588	557.92
4.4	-431.4	0.151	8.673	14.048	574.19
4.5	-432.4	0.145	8.639	14.504	595.82
4.6	-433.3	0.140	8.604	14.957	615.73
4.7	-434.1	0.135	8.569	15.406	633.72
4.8	-434.9	0.131	8.535	15.852	652.24
4.9	-435.8	0.126	8.501	16.294	674.07
5.0	-436.5	0.123	8.468	16.732	690.94

**Table 11.2.** Experimental and Calculated EMF Values Calculated Using VISP Used to Determine the Stability Constant of  $[\text{NaC}_2\text{C}_2]^+$  in Dimethylsulfoxide at 298.2 K and  $I = 0.050 \text{ mol dm}^{-3}$  ( $\text{NEt}_4\text{ClO}_4$ ).

titre ( $\text{cm}^3$ )	EMF (expt) mV	EMF (calc) mV	titre ( $\text{cm}^3$ )	EMF (expt) mV	EMF (calc) mV
0.0	-268.6	-271.59	2.14	-387.6	-388.43
0.1	-270.9	-273.21	2.20	-390.5	-391.23
0.2	-273.4	-274.92	2.26	-392.9	-393.75
0.3	-275.8	-276.74	2.32	-395.0	-396.05
0.4	-277.9	-278.68	2.38	-397.5	-398.15
0.5	-280.2	-280.78	2.44	-399.5	-400.09
0.56	-281.7	-282.11	2.50	-401.4	-401.90
0.62	-283.3	-283.51	2.60	-404.2	-404.64
0.68	-284.9	-284.99	2.70	-406.8	-407.10
0.74	-286.6	-286.56	2.80	-409.2	-409.35
0.80	-288.3	-288.22	2.90	-411.3	-411.40
0.86	-290.3	-289.98	3.00	-413.3	-413.30
0.92	-292.4	-291.88	3.10	-415.1	-415.06
0.98	-294.5	-293.91	3.20	-416.8	-416.71
1.04	-296.9	-296.11	3.30	-418.3	-418.25
1.10	-299.5	-298.51	3.40	-419.9	-419.70
1.16	-302.3	-301.14	3.50	-421.3	-421.06
1.22	-305.3	-304.06	3.60	-422.7	-422.36
1.28	-308.4	-307.32	3.70	-423.9	-423.59
1.34	-312.5	-311.02	3.80	-425.2	-424.76
1.40	-317.2	-315.28	3.90	-426.5	-425.88
1.46	-322.3	-320.25	4.00	-427.5	-426.95
1.54	-328.3	-328.33	4.10	-428.4	-427.98
1.60	-334.9	-335.69	4.20	-429.5	-428.96
1.66	-342.6	-344.00	4.30	-430.6	-429.91
1.72	-353.2	-352.55	4.40	-431.4	-430.82
1.78	-360.2	-360.42	4.50	-432.4	-431.69
1.84	-367.0	-367.17	4.60	-433.3	-432.54
1.90	-372.4	-372.84	4.70	-434.1	-433.36
1.96	-376.9	-377.63	4.80	-434.9	-434.15
2.02	-381.0	-381.72	4.90	-435.8	-434.92
2.08	-384.5	-385.29	5.00	-436.5	-435.66

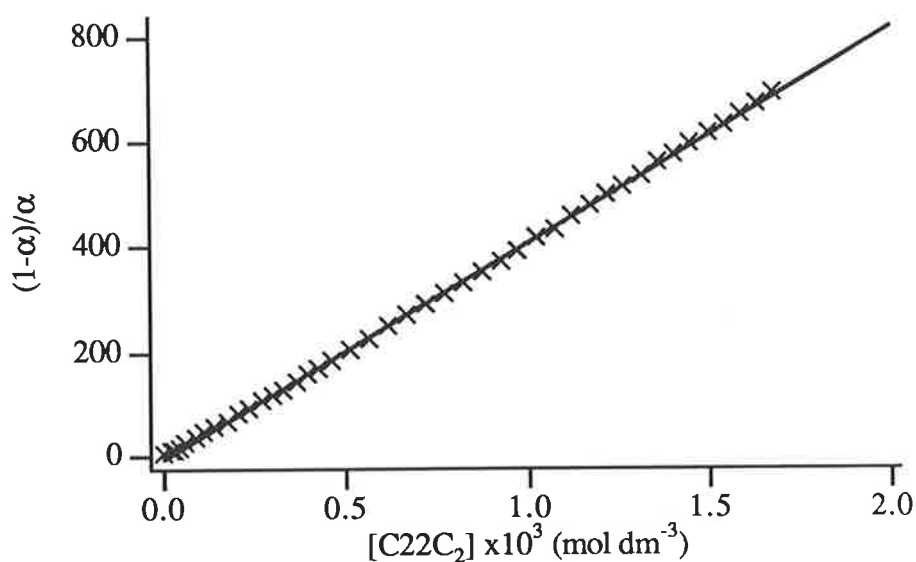


**Figure 11.1.** Plot of  $\frac{1-\alpha}{\alpha}$  versus  $[C_{22}C_2]$  for the titration of  $C_{22}C_2$  with  $Na^+$  in dimethylsulfoxide at 298.2 K and  $I = 0.050 \text{ mol dm}^{-3}$  ( $NEt_4ClO_4$ ). The straight line is the best fit of the data to Equation 11.9.

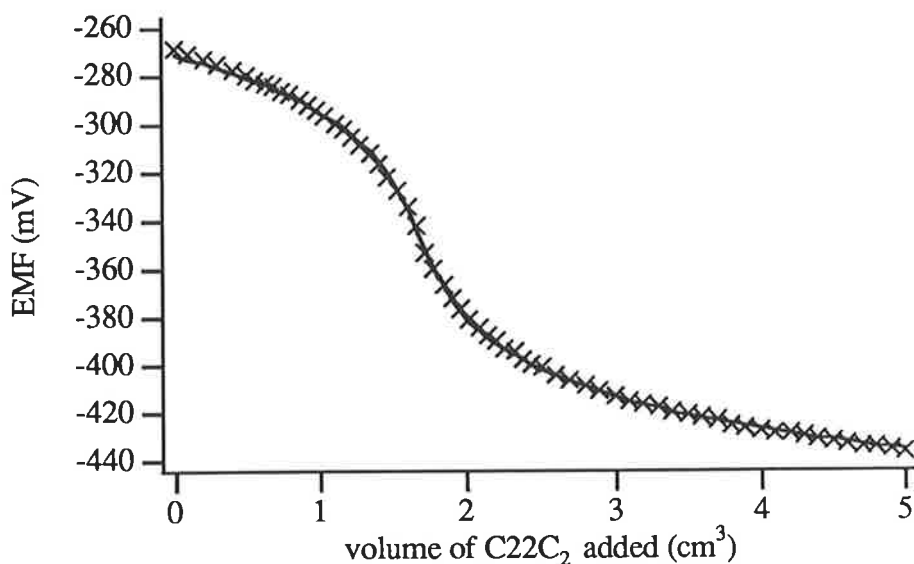


**Figure 11.2.** Plot of experimental (x) and calculated (solid curve) EMF versus titre for the titration of  $C_{22}C_2$  with  $Na^+$  in dimethylsulfoxide at 298.2 K and  $I = 0.050 \text{ mol dm}^{-3}$  ( $NEt_4ClO_4$ ).

**Table 11.3.** Experimental Data and Concentrations Calculated Using STAB Used to Determine the Stability Constant of  $[\text{AgC}_{22}\text{C}_8]^+$  in Dimethylformamide at 298.2 K and  $I = 0.050 \text{ mol dm}^{-3}$  ( $\text{NEt}_4\text{ClO}_4$ ).

titre ( $\text{cm}^3$ )	EMF (expt) mV	$[\text{Ag}^+]$ $\times 10^7$ $\text{mol dm}^{-3}$	$[\text{AgC}_{22}\text{C}_8^+]$ $\times 10^4$ $\text{mol dm}^{-3}$	$[\text{C}_{22}\text{C}_8]$ $\times 10^4$ $\text{mol dm}^{-3}$	$\frac{1-\alpha}{\alpha}$
2.7	-272.2	2.151	9.407	1.179	4373
2.8	-280.5	1.570	9.366	1.564	5964
2.9	-288.5	1.160	9.325	1.945	8042
3.0	-295.5	0.889	9.285	2.323	10441
3.1	-299.5	0.764	9.245	2.699	12098
3.2	-303.5	0.657	9.205	3.070	14018
3.3	-307.7	0.560	9.166	3.439	16367
3.4	-310.3	0.507	9.127	3.805	17985
3.5	-312.5	0.467	9.088	4.167	19467
3.6	-315.4	0.418	9.050	4.527	21637
3.7	-317.9	0.380	9.011	4.883	23687
3.8	-320.3	0.347	8.974	5.236	25834
3.9	-322.5	0.320	8.936	5.587	27964
4.0	-324.4	0.297	8.899	5.934	29927
4.1	-326.3	0.277	8.862	6.279	32029
4.2	-328.1	0.258	8.825	6.621	34149
4.3	-329.8	0.242	8.789	6.960	36272
4.4	-331.4	0.228	8.753	7.296	38382
4.5	-332.9	0.215	8.717	7.630	40462
4.6	-334.7	0.201	8.682	7.960	43143
4.7	-336.0	0.192	8.647	8.288	45139
4.8	-337.0	0.184	8.612	8.614	46694
4.9	-338.2	0.176	8.577	8.937	48671
5.0	-339.3	0.169	8.543	9.257	50540

**Table 11.4.** Experimental and Calculated EMF Values Calculated Using VISP Used to Determine the Stability Constant of  $[\text{AgC}_{22}\text{C}_8]^+$  in Dimethylformamide at 298.2 K and  $I = 0.050 \text{ mol dm}^{-3}$  ( $\text{NEt}_4\text{ClO}_4$ ).

titre ( $\text{cm}^3$ )	EMF (expt) mV	EMF (calc) mV	titre ( $\text{cm}^3$ )	EMF (expt) mV	EMF (calc) mV
0.0	-47.7	-47.70	2.6	-256.3	-268.89
0.1	-48.4	-48.96	2.7	-272.2	-279.53
0.2	-49.3	-50.26	2.8	-280.5	-287.10
0.3	-51.2	-51.62	2.9	-288.5	-292.97
0.4	-52.6	-53.04	3.0	-295.5	-297.77
0.5	-53.9	-54.52	3.1	-299.5	-301.83
0.6	-55.3	-56.07	3.2	-303.5	-305.35
0.7	-56.9	-57.71	3.3	-307.7	-308.46
0.8	-58.7	-59.44	3.4	-310.3	-311.24
0.9	-60.7	-61.26	3.5	-312.5	-313.75
1.0	-62.7	-63.21	3.6	-315.4	-316.04
1.1	-65.0	-65.29	3.7	-317.9	-318.15
1.2	-67.4	-67.53	3.8	-320.3	-320.11
1.3	-70.1	-69.95	3.9	-322.5	-321.93
1.4	-72.9	-72.58	4.0	-324.4	-323.63
1.5	-76.2	-75.49	4.1	-326.3	-325.23
1.6	-79.7	-78.72	4.2	-328.1	-326.74
1.7	-83.6	-82.36	4.3	-329.8	-328.16
1.8	-88.4	-86.55	4.4	-331.4	-329.52
1.9	-94.1	-91.48	4.5	-332.9	-330.80
2.0	-101.1	-97.48	4.6	-334.7	-332.03
2.1	-110.6	-105.18	4.7	-336.0	-333.20
2.2	-125.1	-115.96	4.8	-337.0	-334.32
2.3	-150.9	-134.16	4.9	-338.2	-335.40
2.4	-194.7	-192.83	5.0	-339.3	-336.44
2.5	-235.9	-250.88			



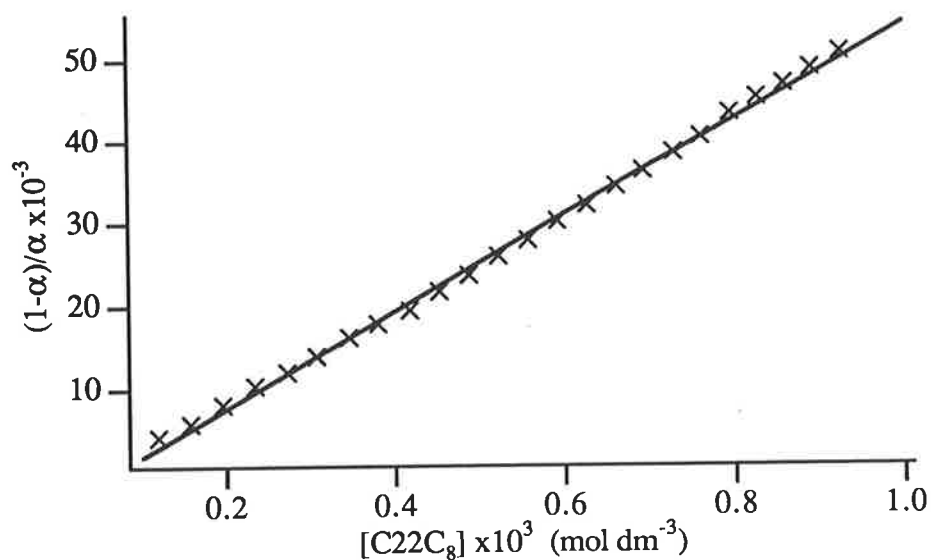


**Figure 11.3.** Plot of  $\frac{1-\alpha}{\alpha}$  versus  $[C_{22}C_8]$  for the determination of the stability constant of  $[AgC_{22}C_8]^+$  in dimethylformamide at 298.2 K and  $I = 0.050 \text{ mol dm}^{-3}$  ( $NEt_4ClO_4$ ). The straight line is the best fit of the data to Equation 11.9.

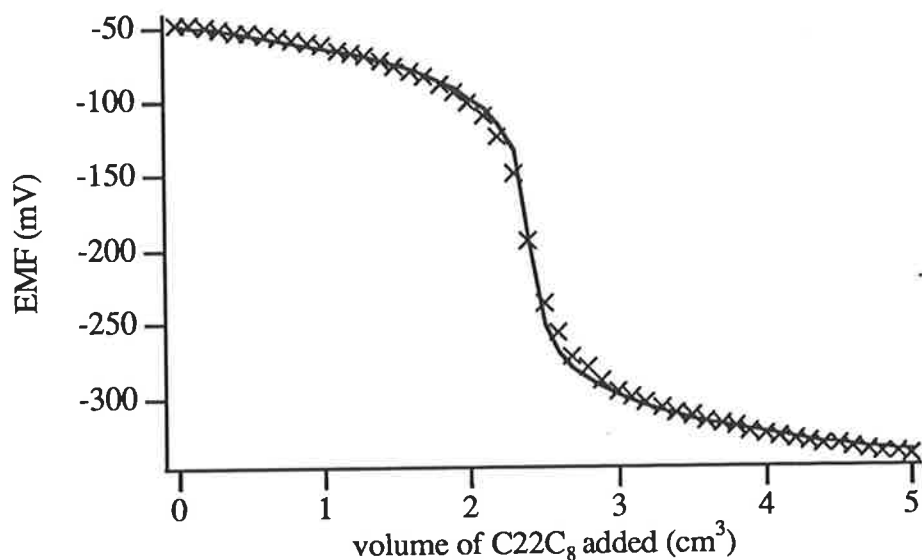


**Figure 11.4.** Plot of experimental (x) and calculated (solid curve) EMF versus titre for the titration of  $C_{22}C_8$  with  $Ag^+$  in dimethylformamide at 298.2 K and  $I = 0.050 \text{ mol dm}^{-3}$  ( $NEt_4ClO_4$ ).

**Table 11.5.** Experimental Data and Concentrations Calculated Using STAB Used to Determine the Stability Constant of  $[\text{TIC22C}_8]^+$  in Dimethylformamide at 298.2 K and  $I = 0.050 \text{ mol dm}^{-3}$  ( $\text{NEt}_4\text{ClO}_4$ ).

titre $\text{cm}^3$	EMF (expt) (mV)	$[\text{Ag}^+]$ $\times 10^7$ $\text{mol dm}^{-3}$	$[\text{Tl}^+]$ $\times 10^3$ $\text{mol dm}^{-3}$	$[\text{AgC22C}_8^+]$ $\times 10^4$ $\text{mol dm}^{-3}$	$[\text{TIC22C}_8^+]$ $\times 10^4$ $\text{mol dm}^{-3}$	$\frac{1-\alpha}{\alpha} \times [\text{Tl}^+]$ $\text{mol dm}^{-3}$
2.4	-127.7	530.540	5.133	9.718	0.032	0.094
2.5	-154.6	191.365	5.316	10.011	0.100	0.278
2.6	-185.3	59.765	5.478	10.098	0.371	0.925
2.7	-206.7	26.555	5.628	10.086	0.738	2.138
2.8	-219.9	16.100	5.775	10.052	1.123	3.605
2.9	-228.8	11.490	5.919	10.013	1.511	5.159
3.0	-235.6	8.879	6.063	9.972	1.898	6.809
3.1	-240.8	7.290	6.205	9.930	2.282	8.452
3.2	-245.7	6.055	6.346	9.889	2.663	10.364
3.3	-248.7	5.404	6.485	9.847	3.041	11.817
3.4	-251.7	4.823	6.623	9.805	3.417	13.466
3.5	-254.5	4.337	6.761	9.764	3.789	15.220
3.6	-257.0	3.945	6.896	9.723	4.158	16.997
3.7	-259.0	3.657	7.031	9.682	4.524	18.616
3.8	-259.6	3.575	7.165	9.642	4.888	19.325
3.9	-261.1	3.377	7.297	9.602	5.248	20.747
4.0	-264.5	2.969	7.429	9.562	5.605	23.927
4.1	-266.8	2.721	7.559	9.523	5.959	26.456
4.2	-267.8	2.620	7.688	9.483	6.310	27.832
4.3	-268.9	2.513	7.817	9.444	6.658	29.380
4.4	-270.0	2.410	7.944	9.406	7.004	31.002
4.5	-271.0	2.320	8.070	9.367	7.347	32.578
4.6	-272.0	2.234	8.195	9.329	7.687	34.222
4.7	-273.0	2.151	8.319	9.292	8.024	35.936
4.8	-274.5	2.032	8.442	9.254	8.358	38.446
4.9	-275.3	1.971	8.564	9.217	8.690	40.042
5.0	-275.9	1.927	8.685	9.180	9.020	41.376

**Table 11.6.** Experimental and Calculated EMF Values Calculated Using VISIP Used to Determine the Stability Constant of  $[\text{TlC}_2\text{C}_8]^+$  in Dimethylformamide at 298.2 K and  $I = 0.050 \text{ mol dm}^{-3}$  ( $\text{NEt}_4\text{ClO}_4$ ).

titre $\text{cm}^3$	EMF (expt) mV	EMF (calc) mV	titre $\text{cm}^3$	EMF (expt) mV	EMF (calc) mV
0.0	-48.6	-46.60	2.6	-185.3	-196.66
0.1	-49.1	-47.80	2.7	-206.7	-215.39
0.2	-49.3	-49.04	2.8	-219.9	-226.10
0.3	-49.6	-50.33	2.9	-228.8	-233.42
0.4	-50.5	-51.68	3.0	-235.6	-238.93
0.5	-51.5	-53.08	3.1	-240.8	-243.30
0.6	-52.7	-54.54	3.2	-245.7	-246.90
0.7	-54.0	-56.08	3.3	-248.7	-249.95
0.8	-55.5	-57.70	3.4	-251.7	-252.57
0.9	-57.0	-59.40	3.5	-254.5	-254.87
1.0	-58.7	-61.20	3.6	-257.0	-256.91
1.1	-60.6	-63.12	3.7	-259.0	-258.74
1.2	-62.6	-65.17	3.8	-259.6	-260.39
1.3	-64.8	-67.36	3.9	-261.1	-261.89
1.4	-67.3	-69.74	4.0	-264.5	-263.27
1.5	-69.5	-72.32	4.1	-266.8	-264.53
1.6	-72.5	-75.15	4.2	-267.8	-265.71
1.7	-75.6	-78.30	4.3	-268.9	-266.80
1.8	-79.0	-81.83	4.4	-270.0	-267.81
1.9	-83.2	-85.87	4.5	-271.0	-268.77
2.0	-87.9	-90.59	4.6	-272.0	-269.99
2.1	-93.9	-96.28	4.7	-273.0	-270.50
2.2	-101.1	-103.45	4.8	-274.5	-271.30
2.3	-111.4	-113.15	4.9	-275.3	-272.05
2.4	-127.7	-128.14	5.0	-275.9	-272.77
2.5	-154.6	-157.87			

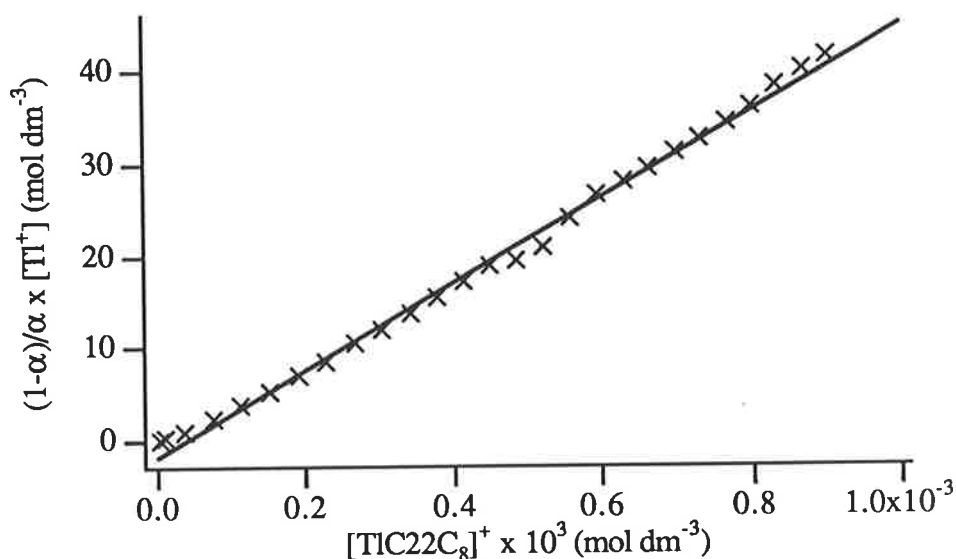


**Figure 11.5.** Plot of  $\frac{1-\alpha}{\alpha} \times [\text{Tl}^+]$  versus  $[\text{TlC}_{22}\text{C}_8]^+$  for the titration of  $[\text{TlC}_{22}\text{C}_8]^+$  with  $\text{Ag}^+$  at 298.2 K and  $I = 0.050 \text{ mol dm}^{-3}$  ( $\text{NEt}_4\text{ClO}_4$ ). The straight line is the best fit of the data to Equation 11.16.

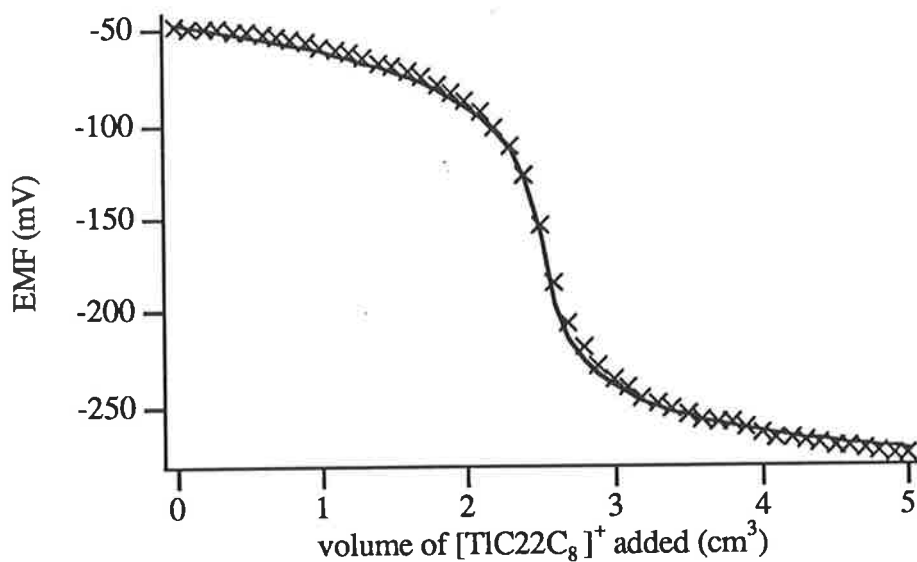


**Figure 11.6.** Plot of experimental (x) and calculated (solid curve) EMF versus titre for the titration of  $[\text{TlC}_{22}\text{C}_8]^+$  with  $\text{Ag}^+$  in dimethylformamide at 298.2 K and  $I = 0.050 \text{ mol dm}^{-3}$  ( $\text{NEt}_4\text{ClO}_4$ ).

## 11.2 Determination of Stability Constants of Metal Complexes in Aqueous Solution

The determination of stability constants in aqueous solution is similar to that in non-aqueous solution, but is complicated by the protonation equilibria of the dibasic cryptands C22C<sub>2</sub> and C22C<sub>8</sub> (Chapter 3) and the tetrabasic tetraazamacrocyclic TMEC12 (Chapter 7). When the total ligand, metal and acid concentrations are known, measurement of the solution pH establishes the extent of the metal ion-ligand equilibria and allows determination of the stability constant of the metal complex. The general procedure involves the titration of an acidified solution of the ligand with a base, with analysis of the resultant titration curve yielding the ligand p*K*<sub>a</sub> values (Equation 11.31), which must be known before the stability constants, *K*<sub>s</sub>, (Equation 11.32) of the metal complex may be determined.

$$K_n = \frac{[\text{LH}_n^{n+}]}{[\text{LH}_{n-1}^{(n-1)+}][\text{H}^+]} \quad \text{p}K_{\text{an}} = -\log(K_{\text{an}}) \quad 11.31$$

$$K_s = \frac{[\text{ML}^{n+}]}{[\text{M}^{n+}][\text{L}]} \quad 11.32$$

The stability constants, *K*<sub>s</sub>, of the metal complexes are determined by the titration of an acidified solution of the ligand with a base but in the presence of the relevant metal ion. The resulting titration curves are modified by the formation of metal complexes and may be analysed to give their stability constants. In this study, the protonation constants *K*<sub>1</sub> and *K*<sub>2</sub> of C22C<sub>2</sub> and C22C<sub>8</sub> and the stability constants of the various metal complexes (Chapter 3) were determined from titration data using the program MINQUAD.<sup>5</sup> The corresponding data for TMEC12 (Chapter 7) were determined using the program SUPERQUAD.<sup>6</sup> The experimental detail for these titrations is described in Chapter 10.

The protonation constant values and stability constant values quoted in Tables 3.1, 3.2, 7.1 and 7.2 are the average values determined from at least three titration experiments. In determining these values, only data points in the titration where significant concentrations of the relevant species had formed were used in the refining process. In some cases, metal hydroxide precipitation occurred at high pH, so that data points obtained in this region were discarded.

For each metal ion studied, an attempt to fit the data to a number of models was made. The simplest model includes only the  $[ML]^{n+}$  species but species such as  $[M(LH)]^{(n+1)+}$  and  $[M(OH)L]^{(n-1)+}$  may also exist (Chapters 3 and 7). The criterion for including such species was that their presence greatly improved the fit of the data, and that such species existed in concentrations  $\geq 10\%$  of the total metal ion concentration. In MINQUAD, a better fit is defined by a lower  $R$ -factor  $R$ , where a value of  $R \leq 0.004$  was taken to mean that the titration data fitted the protonation or complexation model satisfactorily. For SUPERQUAD, the corresponding parameter is  $c^2$ , with  $c^2 \leq 12.60$  implying that the titration data fitted the protonation or complexation model satisfactorily. Included below are the details of some typical titration experiments to illustrate this discussion.

Figure 11.7 shows the titration curve obtained from the titration of  $10.00 \text{ cm}^3$  of a solution of  $1.011 \times 10^{-3} \text{ mol dm}^{-3}$  C22C<sub>2</sub> in  $4.107 \times 10^{-3} \text{ mol dm}^{-3}$  HClO<sub>4</sub> ( $0.10 \text{ mol dm}^{-3}$  NEt<sub>4</sub>ClO<sub>4</sub> background electrolyte) with  $1.222 \times 10^{-1} \text{ mol dm}^{-3}$  NEt<sub>4</sub>OH solution. The electrode calibration parameters for this titration were  $pK_w = 13.744$  and  $E_0 = 497.228 \text{ mV}$ . For C22C<sub>2</sub>, the values of  $K_1$  and  $K_2$  were refined separately, because the two  $pK_a$  values are at opposite ends of the pH scale. Thus, for this titration, points lying between pH 5 and pH 9 were not used in the determination of these values. The results calculated using MINQUAD for this titration were  $\log(K_1/\text{dm}^3 \text{ mol}^{-1}) = 10.88 \pm 0.02$  ( $R = 0.0029$ ) and  $\log(K_2/\text{dm}^3 \text{ mol}^{-1}) = 3.45 \pm 0.02$  ( $R = 0.0019$ ).

Figure 11.8 shows the titration curve obtained for the titration of  $10.08 \text{ cm}^3$  of a solution of  $1.003 \times 10^{-3} \text{ mol dm}^{-3}$  C22C<sub>2</sub> and  $8.81 \times 10^{-4} \text{ mol dm}^{-3}$  Ca(ClO<sub>4</sub>)<sub>2</sub> in  $4.074 \times 10^{-3} \text{ mol dm}^{-3}$  HClO<sub>4</sub> ( $0.10 \text{ mol dm}^{-3}$  NEt<sub>4</sub>ClO<sub>4</sub> background electrolyte) with  $1.222 \times 10^{-1} \text{ mol dm}^{-3}$  NEt<sub>4</sub>OH solution. The electrode calibration parameters for this titration were  $pK_w = 13.736$  and  $E_0 = 571.772 \text{ mV}$  and the protonation constants  $\log K_1$  and  $\log K_2$  used in the refinement were 10.92 and 3.42, respectively. The results calculated using MINQUAD for this titration were  $\log(K_s/\text{dm}^3 \text{ mol}^{-1}) = 4.63 \pm 0.04$  ( $R = 0.0039$ ). The data points used in the determination of this value lay between pH 7 and pH 11.

Figure 11.9 shows the titration curve obtained for the titration of  $10.00 \text{ cm}^3$  of a solution of  $1.100 \times 10^{-3} \text{ mol dm}^{-3}$  C22C<sub>8</sub> in  $4.107 \times 10^{-3} \text{ mol dm}^{-3}$  HClO<sub>4</sub> ( $0.10 \text{ mol dm}^{-3}$  NEt<sub>4</sub>ClO<sub>4</sub> background electrolyte) with  $1.015 \times 10^{-1} \text{ mol dm}^{-3}$  NEt<sub>4</sub>OH solution. The electrode calibration parameters for this

titration were  $pK_w = 13.818$  and  $E_0 = 414.364$  mV. The results calculated using MINIQUAD for this titration were  $\log(K_1/\text{dm}^3 \text{ mol}^{-1}) = 11.08 \pm 0.02$  and  $\log(K_2/\text{dm}^3 \text{ mol}^{-1}) = 8.44 \pm 0.03$  ( $R = 0.00231$ ). Points at  $\text{pH} < 6$  were not used in this calculation and above  $\text{pH} 11$ , precipitation of C22C8 occurred.

Figure 11.10 shows the titration curve obtained for the titration of  $10.09 \text{ cm}^3$  of a solution of  $9.64 \times 10^{-4} \text{ mol dm}^{-3}$  C22C8 and  $9.02 \times 10^{-4} \text{ mol dm}^{-3}$   $\text{Pb}(\text{ClO}_4)_2$  in  $4.070 \times 10^{-3} \text{ mol dm}^{-3}$   $\text{HClO}_4$  ( $0.10 \text{ mol dm}^{-3}$   $\text{NEt}_4\text{ClO}_4$  background electrolyte) with  $1.015 \times 10^{-1} \text{ mol dm}^{-3}$   $\text{NEt}_4\text{OH}$  solution. The electrode calibration parameters for this titration were  $pK_w = 13.754$  and  $E_0 = 396.218$  mV and the protonation constants  $\log K_1$  and  $\log K_2$  used in the refinement were 11.06 and 8.41, respectively. The results calculated using MINIQUAD for this titration were  $\log(K_s/\text{dm}^3 \text{ mol}^{-1}) = 7.98 \pm 0.01$  and  $\log(K_{\text{OH}}/\text{dm}^6 \text{ mol}^{-2}) = 13.85 \pm 0.02$  ( $R = 0.0018$ ). The data points used in the determination of these values lay between  $\text{pH} 6$  and  $\text{pH} 9$ .

$$K_{\text{OH}} = \frac{[[\text{Pb}(\text{OH})\text{C22C8}]^+]}{[\text{Pb}^{2+}][\text{OH}^-][\text{C22C8}]} \quad 11.33$$

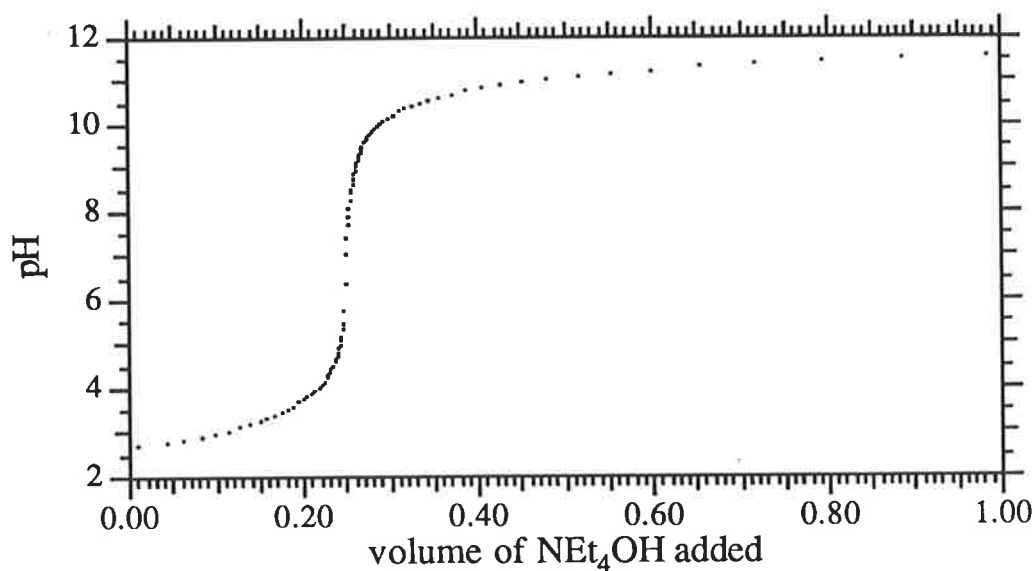
Figure 11.11 shows the titration curve obtained for the titration of  $10.00 \text{ cm}^3$  of a solution of  $1.090 \times 10^{-3} \text{ mol dm}^{-3}$  TMEC12 in  $4.960 \times 10^{-3} \text{ mol dm}^{-3}$   $\text{HClO}_4$  ( $0.10 \text{ mol dm}^{-3}$   $\text{NEt}_4\text{ClO}_4$  background electrolyte) with  $1.047 \times 10^{-1} \text{ mol dm}^{-3}$   $\text{NEt}_4\text{OH}$  solution. The electrode calibration parameters for this titration were  $pK_w = 13.774$  and  $E_0 = 446.213$  mV. The results calculated using SUPERQUAD for this titration were  $\log(K_1/\text{dm}^3 \text{ mol}^{-1}) = 10.96 \pm 0.01$ ,  $\log(K_2/\text{dm}^3 \text{ mol}^{-1}) = 7.98 \pm 0.01$  and  $(\log K_3/\text{dm}^3 \text{ mol}^{-1}) = 2.24 \pm 0.09$  ( $c^2 = 12.58$ ). The value of the fourth protonation constant,  $\log(K_4/\text{dm}^3 \text{ mol}^{-1})$ , was too low to be determined. The best fit curve obtained by SUPERQUAD is represented by the solid curve in Figure 11.5 and the experimental data is represented by an x.

Figure 11.12 shows the titration curve obtained for the titration of  $10.95 \text{ cm}^3$  of a solution of  $1.080 \times 10^{-3} \text{ mol dm}^{-3}$  TMEC12 and  $9.23 \times 10^{-4} \text{ mol dm}^{-3}$   $\text{AgClO}_4$  in  $4.913 \times 10^{-3} \text{ mol dm}^{-3}$   $\text{HClO}_4$  ( $0.10 \text{ mol dm}^{-3}$   $\text{NEt}_4\text{ClO}_4$  background electrolyte) with  $1.047 \times 10^{-1} \text{ mol dm}^{-3}$   $\text{NEt}_4\text{OH}$  solution. The electrode calibration parameters for this titration were  $pK_w = 13.776$  and  $E_0 = 406.950$  mV and the protonation constants  $\log K_1$ ,  $\log K_2$  and  $\log K_3$  used in the refinement were 10.92, 8.04 and 2.17, respectively. The results calculated using SUPERQUAD for this titration were  $\log(K_s/\text{dm}^3 \text{ mol}^{-1}) = 12.63 \pm 0.01$

and  $\log(K_{MH}/\text{dm}^6 \text{ mol}^{-2}) = 16.73 \pm 0.05$  ( $c^2 = 11.93$ ). The best fit curve obtained by SUPERQUAD is represented by the solid curve in Figure 11.6 and the experimental data is represented by an x.

$$K_{MH} = \frac{[\text{Ag}(\text{HTMEC12})^{2+}]}{[\text{Ag}^+][\text{H}^+][\text{TMEC12}]} \quad 11.34$$





**Figure 11.7.** A typical titration curve for the determination of the protonation constants of C<sub>22</sub>C<sub>2</sub> at 298.2 K and  $I = 0.10 \text{ mol dm}^{-3}$  (NEt<sub>4</sub>ClO<sub>4</sub>).

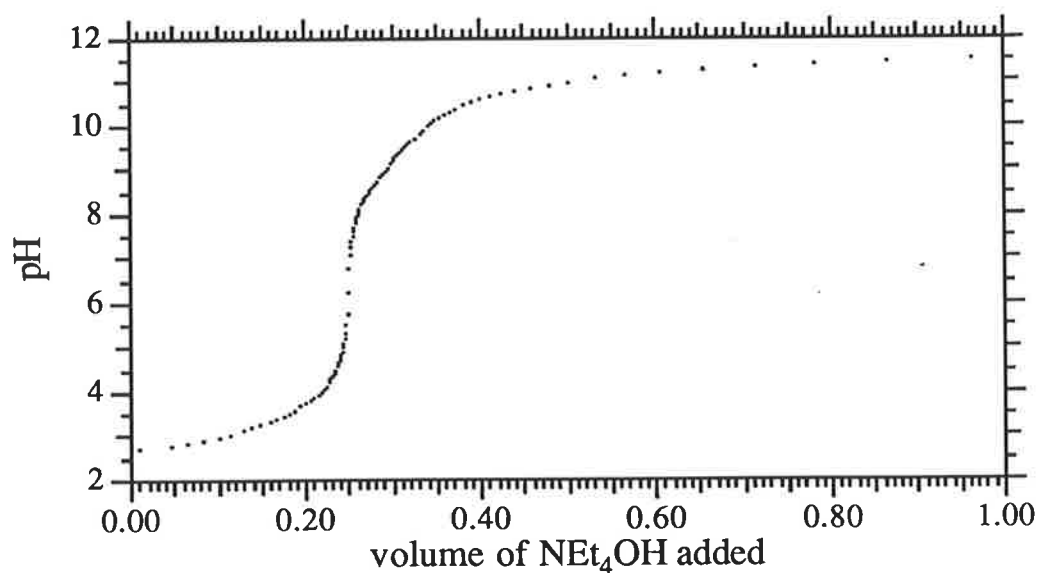


**Figure 11.8.** A typical titration curve for the determination of the stability constant  $K_s$  of [CaC<sub>22</sub>C<sub>2</sub>]<sup>2+</sup> at 298.2 K and  $I = 0.10 \text{ mol dm}^{-3}$  (NEt<sub>4</sub>ClO<sub>4</sub>).

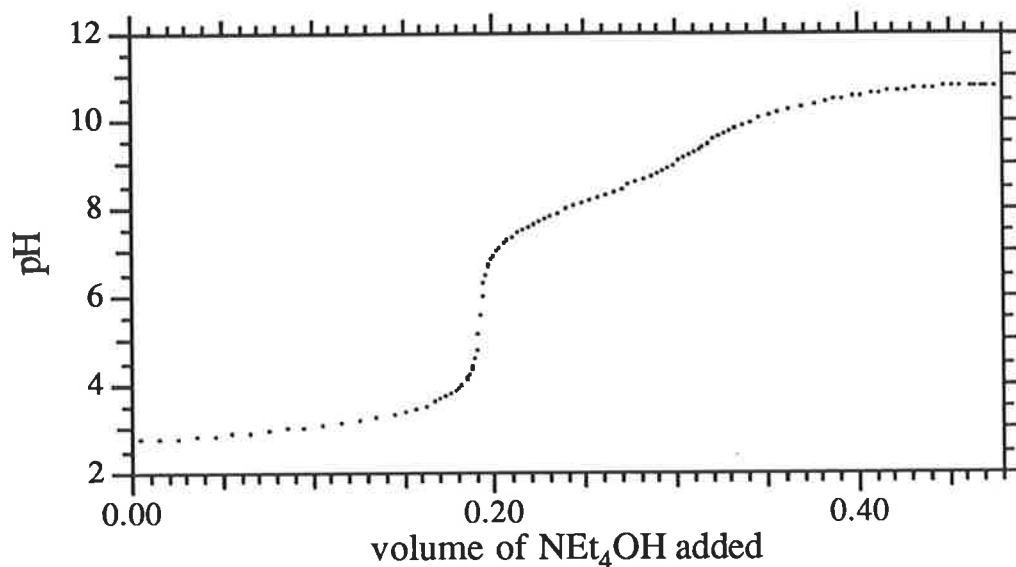


**Figure 11.9.** A typical titration curve for the determination of the protonation constants of C22C<sub>8</sub> at 298.2 K and  $I = 0.10 \text{ mol dm}^{-3}$  (NEt<sub>4</sub>ClO<sub>4</sub>).

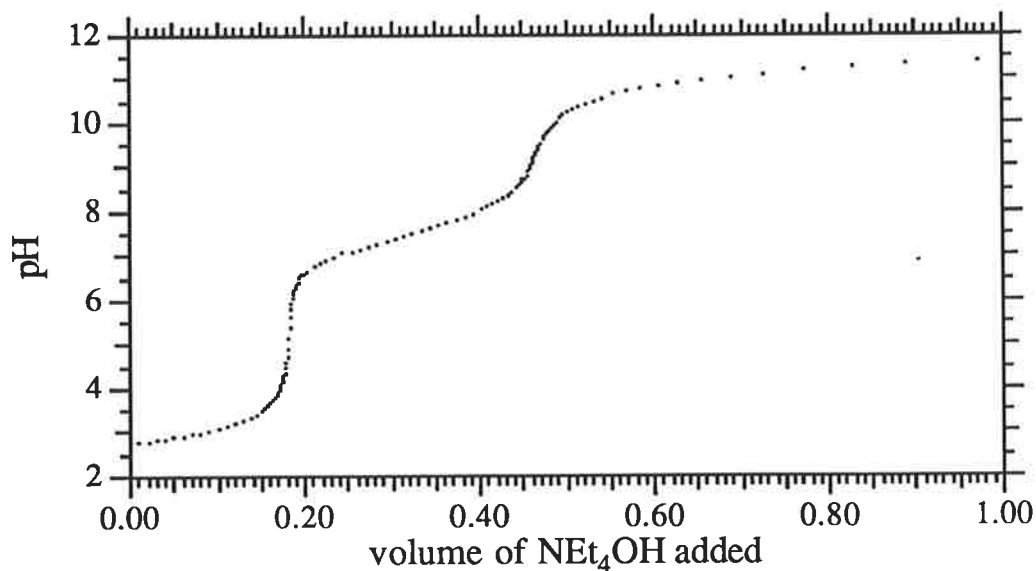


**Figure 11.10.** A typical titration curve for the determination of the stability constants  $K_s$  and  $K_{OH}$  of [PbC22C<sub>8</sub>]<sup>2+</sup> at 298.2 K and  $I = 0.10 \text{ mol dm}^{-3}$  (NEt<sub>4</sub>ClO<sub>4</sub>).

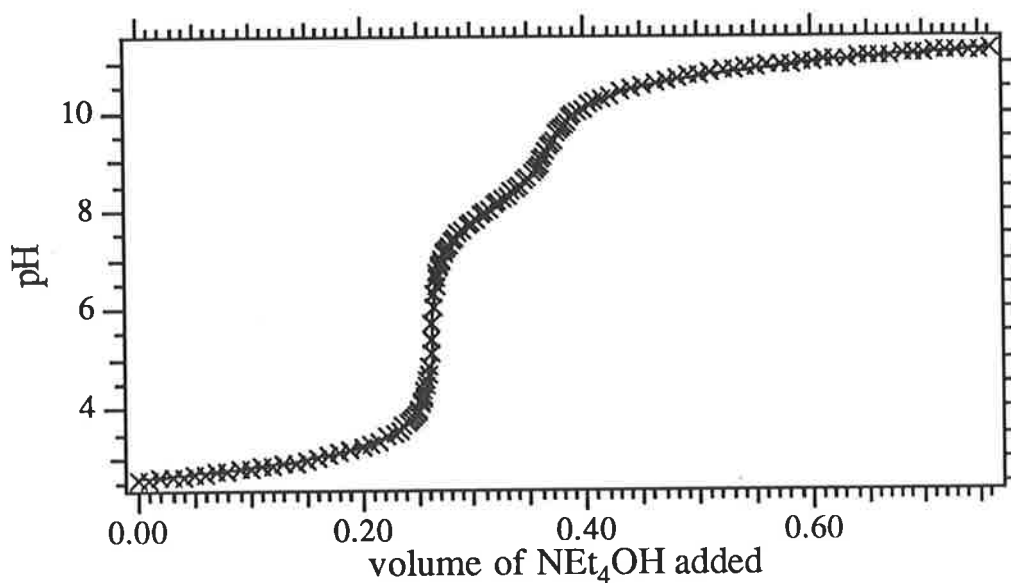


**Figure 11.11.** A part of the titration curve for the determination of the protonation constants of TMEC12 at 298.2 K and  $I = 0.10 \text{ mol dm}^{-3}$  ( $\text{NEt}_4\text{ClO}_4$ ). The experimental data is represented by an x and the solid curve is the best fit of the data by SUPERQUAD.

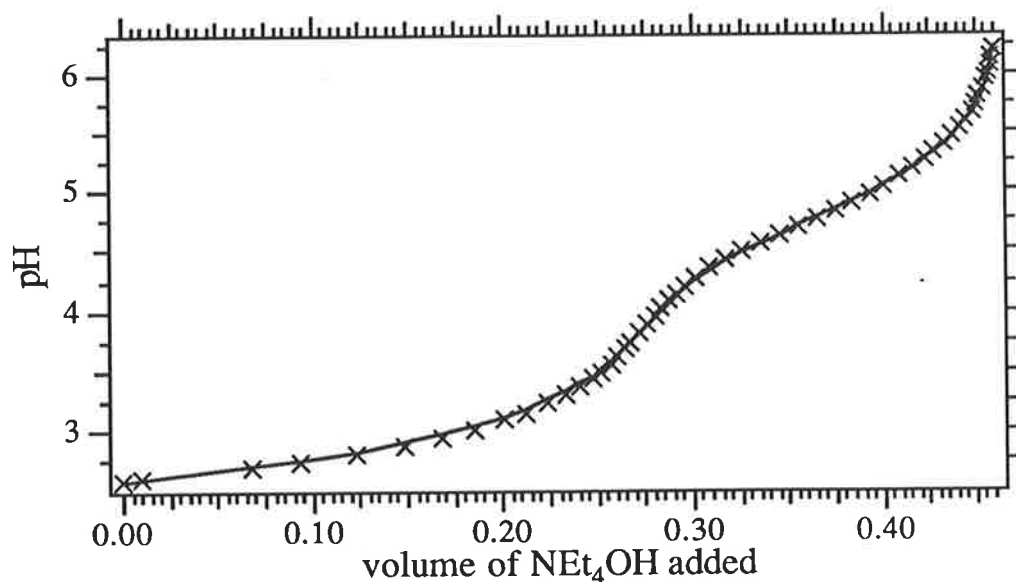


**Figure 11.12.** A part of the titration curve for the determination of the stability constants  $K_s$  and  $K_{MH}$  of  $[\text{Ag}(\text{TMEC12})]^+$  at 298.2 K and  $I = 0.10 \text{ mol dm}^{-3}$  ( $\text{NEt}_4\text{ClO}_4$ ). The experimental data is represented by an x and the solid curve is the best fit of the data by SUPERQUAD.

- 1 Cox, B.G.; Schneider, H.; Stroka, J. *J. Am. Chem. Soc.* **1978**, 100, 4746-4749.
- 2 Lehn, J-M.; Sauvage, J-P. *J. Am. Chem. Soc.* **1975**, 97, 6700-6707.
- 3 Rossotti, F.J.C.; Rossotti, H. *"The Determination of Stability Constants"*, McGraw-Hill, New York, **1961**.
- 4 Clarke, P. PhD Thesis, University of Adelaide, **1992**.
- 5 Sabatini, A.; Vacca, A.; Gans, P. *Talanta*. **1974**, 21, 53-77.
- 6 Gans, P.; Sabatini, A.; Vacca, A. *J. Chem. Soc., Dalton. Trans.* **1985**, 1195-1200.

# Chapter 12: Kinetic Applications of NMR Spectroscopy

## 12.1 Theory of Two-Site Chemical Exchange

Nuclear magnetic resonance spectroscopy is one of the most widely used methods for following rapid inter and intramolecular chemical exchange processes in solution. In Chapters 4 and 8, the intermolecular exchange of  $\text{Li}^+$  and  $\text{Na}^+$  between the solvated and complexed states was studied by  $^7\text{Li}$  and  $^{23}\text{Na}$  NMR, respectively. In Chapter 9, the intramolecular exchange between two conformers of some heavy metal complexes of TMEC12 was studied by broad-band decoupled  $^{13}\text{C}$  NMR. The basic theory underlying the NMR studies in these chapters is now outlined.

The observation of chemical exchange of systems at thermal equilibrium is conveniently studied by NMR spectroscopy. As a kinetic process is involved, such studies are referred to as Dynamic NMR studies (DNMR). DNMR is founded on the effects of chemical exchange processes on the NMR lineshape and is the basis of numerous studies and literature reviews.<sup>1-8</sup> This technique may be used to derive exchange rate constants in the range  $10^{-1} - 10^6 \text{ s}^{-1}$  and may also be used to determine activation parameters from the temperature dependence of the exchange modified NMR spectrum.<sup>9</sup> The theoretical treatment of DNMR is extensively covered in the literature,<sup>6,9-13</sup> but the approach taken and the level of treatment may vary. The following treatment, using a classical mechanical model, applies only for simple two-site exchange between uncoupled nuclei. For more complex situations, such as multi-site intramolecular exchange, or exchange between coupled spin systems, the quantum mechanical density matrix method must be employed.<sup>9,13-17</sup>

In a typical NMR experiment, a magnetic field  $B_0$  is applied to the sample along the  $z$  axis causing the individual magnetic moments  $\mu$  of the sample nuclei to precess about the  $z$  axis at the Larmor frequency  $\omega_0$ . The lowest energy state is that which occurs when the nuclear spins of the sample are aligned with  $B_0$ . This state is favoured by the Boltzmann distribution and gives rise to a net magnetic moment  $M$  with  $z$  component  $M_z$ , with the  $x$  and  $y$  components  $M_x$  and  $M_y$  being zero. The application of a second and smaller oscillating magnetic field  $B_1$  rotating clockwise in the  $xy$  plane at frequency  $\omega$ , gives rise to a total magnetic field  $B$ ;

$$B = (B_1 \cos \omega t, -B_1 \sin \omega t, B_0) \quad 12.1$$

This causes  $M$  to tilt away from the  $z$  axis into the  $xy$  plane and results in non-zero components  $M_x$  and  $M_y$  (which exhibit maximum values when  $\omega = \omega_0$ ) while  $M_z$  diminishes. The relaxation process whereby  $M_z$  regains its initial (equilibrium) value  $M_{zeq}$  is a first order process characterised by  $T_1$ , the spin-lattice or longitudinal relaxation time. The decay of the transverse components of  $M$ ;  $M_x$  and  $M_y$ , to an equilibrium value of zero as a result of dephasing is also a first order process characterised by  $T_2$ , the transverse relaxation time. The time dependence of  $M$  in the stationary frame (with stationary Cartesian co-ordinates  $(x, y, z)$ ) is described by the Bloch equations,<sup>18</sup> which incorporate the effect of  $B_1$  on  $M$  and also the effects of longitudinal and transverse relaxation.

$$\frac{dM_x}{dt} = \gamma(M_y B_0 + M_z B_1 \sin \omega t) - \frac{M_x}{T_2} \quad 12.2$$

$$\frac{dM_y}{dt} = \gamma(-M_x B_0 + M_z B_1 \cos \omega t) - \frac{M_y}{T_2} \quad 12.3$$

$$\frac{dM_z}{dt} = \gamma(-M_x B_1 \sin \omega t - M_y B_1 \cos \omega t) - \frac{(M_z - M_{zeq})}{T_1} \quad 12.4$$

It is more convenient to reformulate these expressions by replacing the stationary set of Cartesian axes  $(x, y, z)$  by a rotating frame of reference  $(x', y', z')$ , with the co-ordinates rotating at frequency  $\omega$  about the  $z$  axis, so that the Bloch equations may be expressed as;

$$\frac{dM_{xy}}{dt} = -\alpha M_{xy} - i\gamma B_1 M_{zeq} \quad 12.5$$

$$\frac{dM_z}{dt} = \gamma \nu B_1 + \frac{(M_{zeq} - M_z)}{T_1} \quad 12.6$$

where;

$M_{xy}$  is the transverse magnetization

$\nu$  is the component of  $M$  along the  $y'$  axis  $90^\circ$  out of phase with  $B_1$

$$\alpha = \frac{1}{T_2} - i(\omega_0 - \omega).$$

Thus, the variation of  $M_z$  and hence the energy of the system is dependent on  $\nu$ , which therefore corresponds to the absorption mode of the NMR signal.

The NMR measurements performed in this work were carried out using the pulsed Fourier transform technique. The NMR absorption mode lineshape obtained from the pulsed Fourier transform experiment is equivalent to that obtained from the continuous wave slow passage experiment (as is discussed in Section 12.2). However, the continuous wave slow passage experiment is easier to visualise and so the following discussions are based on this technique. Under continuous wave slow passage conditions,  $\omega$  is swept slowly through  $\omega_0$  so that  $\frac{dM_{xy}}{dt}$  and  $\frac{dM_z}{dt} = 0$ . If  $B_1$  is small, so that  $M_z \sim M_{zeq}$  and  $M_{xy}$  is small, the form of the absorption mode lineshape is given by;

$$\nu = -M_{zeq} \frac{\gamma B_1 T_2}{1 + T_2^2 (\omega_0 - \omega)^2 + \gamma^2 B_1^2 T_1 T_2} \quad 12.7$$

Generally,  $B_1$  is so small that the term  $\gamma^2 B_1^2 T_1 T_2$  is negligible and can be ignored so that the absorption mode lineshape  $\nu$  is described by a Lorentzian function;

$$\nu = -M_{zeq} \frac{\gamma B_1 T_2}{1 + T_2^2 (\omega_0 - \omega)^2} \quad 12.8$$

The Bloch equations may now be modified to incorporate the effects of chemical exchange.<sup>19-20</sup> These modifications are only applicable where the exchange of nuclear spins induces transverse relaxation only (adiabatic exchange) and where no spin-spin coupling between exchanging nuclear spins occurs. In the uncoupled two site exchange case, the nucleus exchanges between sites **a** and **b** at a rate;

$$k_a \chi_a = k_b \chi_b; k_a = \frac{1}{\tau_a}, k_b = \frac{1}{\tau_b} \quad 12.9$$

where  $\chi_a$  and  $\chi_b$  are the relative populations and  $\tau_a$  and  $\tau_b$  are the mean lifetimes of the nucleus at sites **a** and **b**, respectively.

It is assumed that the time required for a nuclear spin to transfer from site **a** to site **b** is so small that no nuclear spin precession occurs in that time, and that a nucleus arrives at site **b** with its phase memory of site **a** intact and vice versa. This transfer causes dephasing of the nuclear spins at site **b** and an increase in  $M_{xyb}$ , the transverse magnetization of site **b** at the rate  $M_{xya}/\tau_a$  and a decrease in  $M_{xya}$  at the same rate. Similarly, transfer of a nuclear spin from site **b** to **a** causes dephasing at site **a**, increases  $M_{xya}$  at the rate  $M_{xyb}/\tau_b$  and decreases  $M_{xyb}$  at the same rate;

$$\frac{dM_{xya}}{dt} = \frac{M_{xyb}}{\tau_b} - \frac{M_{xya}}{\tau_a} \quad 12.10$$

$$\frac{dM_{xyb}}{dt} = \frac{M_{xya}}{\tau_a} - \frac{M_{xyb}}{\tau_b} \quad 12.11$$

Incorporation of these effects into the Bloch equations results in;

$$\frac{dM_{xya}}{dt} = -\alpha_a M_{xya} - i\gamma B_1 M_{zeqa} + \frac{M_{xyb}}{\tau_b} - \frac{M_{xya}}{\tau_a} \quad 12.12$$

$$\frac{dM_{xyb}}{dt} = -\alpha_b M_{xyb} - i\gamma B_1 M_{zeqb} + \frac{M_{xya}}{\tau_a} - \frac{M_{xyb}}{\tau_b} \quad 12.13$$

where;

$$\alpha_a = \frac{1}{T_{2a}} - i(\omega_{0a} - \omega)$$

$$\alpha_b = \frac{1}{T_{2b}} - i(\omega_{0b} - \omega)$$

Under continuous wave slow passage conditions, the  $M_z$  components do not differ significantly from  $M_{zeq}$  and therefore;

$$M_{za} = M_{zeqa} = \chi_a M_{zeq} \text{ and } M_{zb} = M_{zeqb} = \chi_b M_{zeq} \quad 12.14$$

$$\frac{dM_{xya}}{dt} = \frac{dM_{xyb}}{dt} = 0 \quad 12.15$$



The total transverse magnetization  $M_{xy} = M_{xya} + M_{xyb}$  may now be expressed in terms of  $\tau_a$  and  $\tau_b$ ;

$$M_{xy} = \frac{-i\gamma B_1 M_{zeq} [\tau_a + \tau_b + \tau_a \tau_b (\alpha_a \chi_a + \alpha_b \chi_b)]}{(1 + \alpha_a \tau_a)(1 + \alpha_b \tau_b) - 1} \quad 12.16$$

The NMR absorption lineshape  $\nu$  at frequency  $\omega$  (rad s<sup>-1</sup>) is proportional to the imaginary part of  $M_{xy}$  and can be expressed in the form;<sup>21-22</sup>

$$\nu = \frac{-\gamma B_1 M_{zeq} \left\{ Y \left[ 1 + \tau \left( \frac{\chi_b}{T_{2a}} + \frac{\chi_a}{T_{2b}} \right) \right] + Q R \right\}}{Y^2 + R^2} \quad 12.17$$

where;

$$\tau = \chi_b \tau_a + \chi_a \tau_b$$

$$\Delta\omega = \omega_{0a} - \omega_{0b}$$

$$\delta\omega = \frac{1}{2} |\omega_{0a} - \omega_{0b}| - \omega$$

$$Y = \tau \left( \frac{1}{T_{2a} T_{2b}} - \delta\omega^2 + \frac{\Delta\omega^2}{4} \right) + \frac{\chi_a}{T_{2a}} + \frac{\chi_b}{T_{2b}}$$

$$Q = \tau \left( \delta\omega - \frac{\Delta\omega}{2} (\chi_a - \chi_b) \right)$$

$$R = \delta\omega \left[ 1 + \tau \left( \frac{1}{T_{2a}} + \frac{1}{T_{2b}} \right) \right] + \frac{\Delta\omega}{2} \tau \left( \frac{1}{T_{2b}} - \frac{1}{T_{2a}} \right) + \frac{\Delta\omega}{2} (\chi_a - \chi_b)$$

The NMR lineshape for systems undergoing chemical exchange may be calculated from Equation 12.17. When the rate of exchange is slow ( $\tau_a$  and  $\tau_b$  are very large) the NMR spectrum consists of two Lorentzian lineshapes centred at  $\omega_{0a}$  and  $\omega_{0b}$ . As the rate of exchange increases,  $\tau_a$  and  $\tau_b$  decrease with the result that the two resonances broaden and coalesce to form a single resonance. The very slow exchange limit occurs when the rate of exchange between sites **a** and **b** is too slow to cause any measurable broadening of the two resonances. The very fast exchange limit occurs when the rate of exchange is so fast, that the coalesced lineshape is characterised by a chemical shift and linewidth that is simply the weighted average of those characterising sites **a** and **b** in the absence of exchange. The variation in lineshape as a function of exchange rate is now considered in more detail.

### 12.1.1 Slow exchange

#### Very Slow Exchange Limit;

Under these conditions;

$$\tau_a^{-1}, \tau_b^{-1} \ll |\omega_{0a} - \omega_{0b}|, T_{2a}^{-1}, T_{2b}^{-1}$$

ie the rate of exchange between sites **a** and **b** is sufficiently small compared with the chemical shift difference (frequency separation) between the two sites and Equation 12.17 approximates to;

$$\nu = \frac{-\gamma B_1 \chi_a M_{zeq} T_{2a}^{-1}}{T_{2a}^{-2} + (\omega_{0a} - \omega)^2} + \frac{-\gamma B_1 \chi_b M_{zeq} T_{2b}^{-1}}{T_{2b}^{-2} + (\omega_{0b} - \omega)^2} \quad 12.18$$

Equation 12.18 contains no chemical exchange parameters and describes two Lorentzian line shapes centred at  $\omega_{0a}$  and  $\omega_{0b}$ .

#### Slow Exchange Limit;

Under these conditions;

$$\tau_a^{-1}, \tau_b^{-1} \ll |\omega_{0a} - \omega_{0b}|, \tau_a^{-1} \approx T_{2a}^{-1}, \tau_b^{-1} \approx T_{2b}^{-1}$$

The exchange rate is now greater than the previous case, although still small compared with the chemical shift difference between sites **a** and **b**. In this case the NMR lineshape becomes;

$$\nu = \frac{-\gamma B_1 \chi_a M_{zeq} T'_{2a}^{-1}}{T'_{2a}^{-2} + (\omega_{0a} - \omega)^2} + \frac{-\gamma B_1 \chi_b M_{zeq} T'_{2b}^{-1}}{T'_{2b}^{-2} + (\omega_{0b} - \omega)^2} \quad 12.19$$

where  $T'_{2a}$  and  $T'_{2b}$  are the observed transverse relaxation times of sites **a** and **b**;

$$T'_{2a}^{-1} = T_{2a}^{-1} + \tau_a^{-1} \text{ and } T'_{2b}^{-1} = T_{2b}^{-1} + \tau_b^{-1} \quad 12.20$$

Equation 12.19 once again describes two Lorentzian lineshapes centred at  $\omega_{0a}$  and  $\omega_{0b}$  but because the observed transverse relaxation times are shorter than

$T_{2a}$  and  $T_{2b}$ , the transverse relaxation times characterising these sites in the absence of exchange, as a result of the dephasing effect of the exchange process. Thus, the resonances characterising sites **a** and **b** are broader than those in the absence of exchange. The difference between  $W_{1/2a}$ , the full width at half maximum amplitude in the absence of exchange and  $W'_{1/2a}$ , the corresponding width of the exchange broadened resonance can be used to estimate  $\tau_a$ :

$$\pi W_{1/2a} = \frac{1}{T_{2a}} \quad 12.21$$

$$\pi W'_{1/2a} - \pi W_{1/2a} = \frac{1}{T'_{2a}} - \frac{1}{T_{2a}} = \frac{1}{\tau_a} \quad 12.22$$

For exchanging systems in the very slow exchange limit of the NMR timescale, Equation 12.22 may be used to provide an estimate of the lower limit of either  $\tau_a$  or  $\tau_b$  (and hence an upper limit of  $k$ , the exchange rate constant) by calculating the lifetime which would cause a broadening of each resonance by 50%;

$$W'_{1/2a} = 1.5W_{1/2a} \text{ and hence } \tau_a = \frac{2}{\pi W_{1/2a}} \quad 12.23$$

A similar expression applies for  $\tau_b$ . Equation 12.23 was used to estimate lower limits of  $\tau_c$  ( $\equiv \tau_a$ ) in Chapters 4 and 8 for  $\text{Li}^+$  and  $\text{Na}^+$  exchanging systems in the very slow exchange limit.

### 12.1.2 Intermediate Rates of Exchange; Coalescence

From the slow exchange limit, the resonances characterising sites **a** and **b** broaden further and coalesce to form a single resonance when the lifetimes  $\tau_a$  and  $\tau_b$  are of the order  $(\omega_{0a} - \omega_{0b})^{-1}$ . From this point, the fast exchange limit is experienced, with  $\tau_a$  and  $\tau_b$  decreasing further until the very fast exchange limit is met. If the restraints  $\chi_a = \chi_b$  and  $\tau_a = \tau_b$  are introduced and  $\frac{1}{T_{2a}} = \frac{1}{T_{2b}} = 0$ , then;

$$M_{za} = M_{zb} = \frac{1}{2}M_{zeq} \quad 12.24$$

Thus, the NMR absorption mode lineshape becomes;

$$v = \frac{\frac{1}{2}\gamma B_1 M_{zeq} \tau_a (\omega_{0a} - \omega_{0b})^2}{(\omega_{0a} + \omega_{0b} - 2\omega)^2 + \tau_a^2 (\omega_{0a} - \omega)^2 (\omega_{0b} - \omega)^2} \quad 12.25$$

In frequency units  $\nu(\text{Hz}) (= \omega/2\pi)$

$$g(\nu) = \frac{2\tau_a (\nu_a - \nu_b)^2}{[\nu - \frac{1}{2}(\nu_a + \nu_b)]^2 + \pi^2 \tau_a^2 (\nu - \nu_a)^2 (\nu - \nu_b)^2} \quad 12.26$$

Equation 12.26 may be simplified<sup>23</sup> by expressing the absorption lineshape as a function of the dimensionless quantity  $x = \frac{\Delta\nu}{\Delta}$ , where  $\Delta\nu = \nu - \frac{1}{2}(\nu_a + \nu_b)$ ,  $q = \pi\tau_a\Delta$  and  $\Delta = \frac{1}{2}(\nu_a - \nu_b)$ ;

$$g(x) = \frac{2\tau_a}{[x^2 + q^2(x^2 - 1)^2]} \quad 12.27$$

The lineshapes predicted by Equation 12.27 are, of course, identical to those derived from Equation 12.17 (with  $\chi_a = \chi_b$ ). For  $q \gg 1$  (slow exchange), Equation 12.27 predicts two Lorentzian signals centred at  $\nu_a$  and  $\nu_b$ . As  $q$  decreases ( $\tau_a$  decreases), the two signals broaden and their maxima draw closer together until  $q = \frac{1}{\sqrt{2}}$ , where the two resonances coalesce to form a single broad signal with maximum amplitude at the mean of the frequency of the individual resonances  $\frac{1}{2}(\nu_a + \nu_b)$ . For conditions of faster exchange ( $q \ll 1$ , fast exchange), Equation 12.27 predicts that the single broad resonance centred at  $\frac{1}{2}(\nu_a + \nu_b)$  narrows further until the fast exchange limit is reached. Thus for systems undergoing chemical exchange, an estimate of the lifetime of the exchanging species  $\tau_a = \tau_b$ , may be calculated at the coalescence temperature, where the two resonances of the spectrum coalesce into a single broad resonance;

At coalescence;

$$q = \frac{1}{\sqrt{2}} \text{ and } \tau_a = \tau_b = \frac{\sqrt{2}}{\pi(\nu_a - \nu_b)} \quad 12.28$$

If the chemical shifts characterising sites **a** and **b** in the absence of exchange ( $\nu_a$  and  $\nu_b$ ) are known, then an approximate value of  $\tau_a$  may be calculated using Equation 12.28. This method was used in Chapter 4 to estimate  $\tau_c$  ( $\equiv \tau_a$ ), the mean lifetime of  $\text{Li}^+$  in  $[\text{LiC}_2\text{C}_8]^+$  in propylene carbonate at the coalescence temperature.

### 12.1.3 Fast Exchange

#### Very Fast Exchange Limit;

Under these conditions;

$$\tau_a^{-1}, \tau_b^{-1} \gg |\omega_{0a} - \omega_{0b}|, T_{2a}^{-1}, T_{2b}^{-1}$$

Here, the two broadened resonances centred at  $\omega_{0a}$  and  $\omega_{0b}$  have coalesced to form a single Lorentzian resonance centred at  $\omega = \chi_a \omega_{0a} + \chi_b \omega_{0b}$  (the population weighted mean of the individual resonances  $\omega_{0a}$  and  $\omega_{0b}$ ) and with linewidth also the weighted average of the individual resonances in the absence of exchange;

$$W_{1/2} = \frac{1}{\pi T'_2} = \frac{\chi_a}{\pi T_{2a}} + \frac{\chi_b}{\pi T_{2b}} \quad 12.29$$

The absorption mode lineshape is given by;

$$\nu = \frac{-\gamma B_1 M_{zeq} T'_2}{1 + (T'_2)^2 (\chi_a \omega_{0a} + \chi_b \omega_{0b} - \omega)^2} \quad 12.30$$

$$\text{where } \frac{1}{T'_2} = \frac{\chi_a}{T_{2a}} + \frac{\chi_b}{T_{2b}} \quad 12.31$$

As in the very slow exchange limit, Equation 12.30 contains no chemical exchange information; the rate of exchange is so fast that the exchanging nuclear spins experience the weighted average of the environments **a** and **b**. If the rate of exchange is slightly slower ( $\tau_a^{-1}, \tau_b^{-1} > |\omega_{0a} - \omega_{0b}|$ ; the fast exchange limit) then a single Lorentzian lineshape centred at  $\omega = \chi_a \omega_{0a} + \chi_b \omega_{0b}$  is observed but the linewidth  $W'_{1/2}$  will be greater than that given in Equation 12.29;

$$\frac{1}{T'_2} = \frac{\chi_a}{T_{2a}} + \frac{\chi_b}{T_{2b}} + \chi_a^2 \chi_b^2 (\omega_{0a} - \omega_{0b})^2 (\tau_a + \tau_b) \quad 12.32$$

$$\pi W'_{1/2} = \pi \chi_a W_{1/2a} + \pi \chi_b W_{1/2b} + \chi_a^2 \chi_b^2 \Delta \omega_0^2 (\tau_a + \tau_b) \quad 12.33$$

where  $\Delta \omega_0 = |\omega_{0a} - \omega_{0b}|$

In frequency units  $\nu(\text{Hz}) (= \omega/2\pi)$ ;

$$\pi W'_{1/2} = \pi \chi_a W_{1/2a} + \pi \chi_b W_{1/2b} + 4\pi^2 \chi_a^2 \chi_b^2 \Delta \nu_0^2 (\tau_a + \tau_b) \quad 12.34$$

where  $\Delta \nu_0 = |\nu_{0a} - \nu_{0b}|$

If the linewidths,  $W_{1/2a}$  and  $W_{1/2b}$ , and the chemical shift difference,  $\Delta \nu_0$ , of the two resonances in the absence of exchange are known, then  $\tau_a$  (and  $\tau_b$ ) may be determined from Equation 12.34 and the relationship;  $\frac{\tau_a}{\chi_a} = \frac{\tau_b}{\chi_b}$ . Equation 12.34 was used in Chapter 4 to determine an estimate of  $\tau_c (\equiv \tau_a)$ , the mean lifetime of  $\text{Li}^+$  in  $[\text{LiC}_{22}\text{C}_8]^+$  in acetonitrile.

## 12.2 Pulsed Fourier Transform NMR

Under pulsed NMR conditions (in the rotating frame  $(x', y', z')$ ),  $B_0$  is still applied continuously along the  $z'$  axis but now  $B_1$  is applied along the  $x'$  axis in a high intensity pulse of short duration ( $10^{-6}$  -  $10^{-4}$  s), whose frequency is centred about  $\omega_0$ . This applies a torque to  $M$ , causing it to rotate towards the  $y'$  axis (about  $x'$ ) and thus generating a transverse component of  $M$ ;  $M_{xy}$ . Immediately after the cessation of the pulse ( $B_1 = 0$ ), spin-lattice relaxation causes  $M$  to relax back to its equilibrium position aligned along the  $z'$  axis. Transverse relaxation causes the transverse component of  $M$ ,  $M_{xy}$  to decay to zero, generating a free induction decay signal (FID). By setting  $B_1 = 0$ , the modified Bloch equations may be solved to give an equation describing the FID;<sup>24</sup>

$$M_{xy} = C_1 e^{-\phi+t} + C_2 e^{-\phi-t} \quad 12.35$$

where  $C_1$  and  $C_2$  are constants of integration and;

$$2\phi_{\pm} = \left( \alpha_a + \frac{1}{\tau_a} + \alpha_b + \frac{1}{\tau_b} \right) \pm \left[ \left( \alpha_a + \frac{1}{\tau_a} - \alpha_b - \frac{1}{\tau_b} \right)^2 + \frac{4}{\tau_a \tau_b} \right]^{1/2} \quad 12.36$$

The Fourier transform of the FID,  $S$ , is given by;

$$S = \int_0^{\infty} M_{zeq} e^{-i(\omega - \omega_1)t} dt \quad 12.37$$

$$= \frac{iM_{zeq}(\tau_a + \tau_b + \tau_a \tau_b (\alpha_a \chi_a + \alpha_b \chi_b))}{(1 + \alpha_a \tau_a)(1 + \alpha_b \tau_b) - 1} \quad 12.38$$

where;

$$\alpha_a = \frac{1}{T_{2a}} + i(\omega_{0a} - \omega)$$

$$\alpha_b = \frac{1}{T_{2b}} + i(\omega_{0b} - \omega)$$

$\omega$  = the variable frequency

$\omega_1$  = the fixed pulse carrier frequency

The absorption mode lineshape is derived from the imaginary part of Equation 12.37 and is the same as that derived from the continuous wave slow passage case (Equation 12.17). In general, the lineshape obtained for a pulsed Fourier transform experiment for an uncoupled spin system undergoing chemical exchange is equivalent to that obtained under continuous wave slow passage conditions.<sup>24-28</sup> All systems undergoing chemical exchange in this study fall into this category.

### 12.3 Lineshape Analysis

For two-site uncoupled intermolecular exchange or intramolecular exchange, a theoretical NMR spectrum was generated using the non-interactive FORTRAN-77 program LINSHP,<sup>29</sup> using the following input parameters;

$\nu_a$  and  $\nu_b$ , the frequency (Hz) of the two coalescing resonances characterising sites **a** and **b** in the absence of exchange

$W_{1/2a}$  and  $W_{1/2b}$ , the full width at half maximum amplitude of each resonance in the absence of exchange

$\chi_a$  and  $\chi_b$ , the relative populations (mole fraction) of each site and

$R$ , the estimated rate of exchange, where  $R = (\tau_a \chi_b)^{-1} = (\tau_b \chi_a)^{-1}$

In order to minimise the introduction of systematic errors, the chemical shifts and linewidths of the site resonances in the absence of exchange must be known accurately over the temperature range over which NMR measurements of the exchange process are carried out. Thus, the variations in these parameters were determined by extrapolation from data in the very slow exchange region ( $^7\text{Li}$ ,  $^{23}\text{Na}$  and  $^{13}\text{C}$  NMR measurements) together with these data determined from measurements of solutions containing the complexed metal ion or the solvated metal ion alone ( $^7\text{Li}$  and  $^{23}\text{Na}$  NMR measurements only).

The intra or intermolecular exchange rate constant,  $k$ , was determined at each temperature by complete lineshape analysis of the corresponding experimental spectrum. The theoretical spectrum created by LINSHP was calculated from the value of  $R$  that minimised the residuals of the fit between the theoretical and experimental spectra. Both theoretical and experimental spectra could be displayed simultaneously on a VDU for comparison purposes. Examples of the best fit theoretical spectra and the corresponding experimental spectra are shown in Figures 4.1, 4.3, 8.1 and 8.3.

## 12.4 Calculation of Activation Parameters

The variation of the exchange rate constant  $k$  with temperature is given by the Eyring equation of transition state theory;<sup>30-31</sup>

$$k = \frac{1}{\tau} = \frac{k_B T}{h} \exp\left(\frac{-\Delta H^\ddagger}{RT} + \frac{\Delta S^\ddagger}{R}\right) \quad 12.39$$

where;

$k_B$  = Boltzmann's constant ( $1.38062 \times 10^{-23} \text{ J K}^{-1}$ )

$h$  = Planck's constant ( $6.62620 \times 10^{-34} \text{ J s}$ )

$R$  = Gas constant ( $8.31434 \text{ J mol}^{-1} \text{ K}^{-1}$ )

$\Delta H^\ddagger$  = enthalpy of activation ( $\text{J mol}^{-1}$ )

$\Delta S^\ddagger$  = entropy of activation ( $\text{J mol}^{-1} \text{ K}^{-1}$ )

$T$  = temperature (K)



Equation 12.39 may be expressed in a linear form, Equation 12.40;

$$\ln(T\tau) = \ln\left(\frac{h}{k_B}\right) - \frac{\Delta S^\ddagger}{R} + \frac{\Delta H^\ddagger}{RT} \quad 12.40$$

Thus, a plot of  $\ln(T\tau)$  against  $\frac{1}{T}$  yields a straight line with slope of  $\frac{\Delta H^\ddagger}{R}$  and an intercept of  $\left( \frac{-\Delta S^\ddagger}{R} + \ln\left(\frac{h}{k_B}\right) \right)$ . Examples of these plots appear in Figures 4.2, 4.4, 8.2, 8.4, 9.6 and 9.8.

For the calculation of  $\Delta H^\ddagger$ ,  $\Delta S^\ddagger$  and  $k$ , a non-linear, weighted least squares method of fitting was employed, using the program DATAFIT<sup>32-33</sup> on a VAX 11-780. This program was used to fit the experimentally determined variation of  $k$  with temperature using equation 12.39. DATAFIT minimises the residual differences in an  $n$ -dimensional sum of squares space between a calculated and experimental surface ( $n$ -dimensional) using the method of Pitha and Jones.<sup>34</sup> The errors quoted for the activation parameters derived by this method (Tables 4.1, 4.4, 8.1, 8.3 and 9.3) are the standard deviations for each parameter in the sum of squares space. These errors take into account only the errors between the input parameters and not any systematic errors associated with the individual input parameters  $k$  and  $T$ .

- 1 Lincoln, S.F.; Brereton, I.M.; Spotswood, T.M. *J. Chem. Soc., Faraday Trans. 1*, **1985**, 81, 1623-1630.
- 2 Lincoln, S.F.; White, A.; Hounslow, A.M. *J. Chem. Soc., Faraday Trans. 1*, **1987**, 83, 2459-2466.
- 3 Clarke, P.; Lincoln, S.F.; Wainright, K.P. *Inorg. Chem.* **1991**, 30, 134-139.
- 4 Cahen, Y.M.; Dye, J.L.; Popov, A.I. *J. Phys. Chem.* **1975**, 79, 1292-1295.
- 5 Ceraso, J.M.; Smith, P.B.; Landers, J.S.; Dye, J.L. *J. Phys. Chem.* **1977**, 81, 760-766.
- 6 Sutherland, I.O. *Ann. Reports. NMR Spectros.* **1971**, 4, 71-235.
- 7 Orrell, K.; Sik, V.; Stephenson, D. *Prog. NMR Spec.* **1990**, 22, 141-208.
- 8 Perrin, C.L.; Dwyer, T.J. *Chem. Rev.* **1990**, 90, 935-967.
- 9 Lincoln, S.F. *Prog. React. Kinetics.* **1977**, 9, 1-91.
- 10 Sandstrom, J. *"Dynamic NMR Spectroscopy"*, Academic Press, London, **1982**.
- 11 Kaplan, J.I.; Fraenkel, G. *"NMR of Chemically Exchanging Systems"*, Academic Press, New York, **1980**.
- 12 Gamliel, D.; Luz, Z.; Vega, S. *J. Chem. Phys.* **1988**, 88, 25-42.
- 13 Lynden-Bell, R.M. *Prog. NMR Spectros.* **1967**, 2, 163-204.
- 14 Kaplan, J.I. *J. Chem. Phys.* **1958**, 28, 278-282.
- 15 Kaplan, J.I. *J. Chem. Phys.* **1958**, 28, 462.
- 16 Alexander, S. *J. Chem. Phys.* **1962**, 37, 967-974.
- 17 Alexander, S. *J. Chem. Phys.* **1962**, 37, 974-980.
- 18 Bloch, F. *Phys. Rev.* **1946**, 70, 460-474.
- 19 Hahn, E.L.; Maxwell, D.E. *Phys. Rev.* **1952**, 88, 1070.
- 20 McConnell, H.M. *J. Chem. Phys.* **1958**, 28, 430.
- 21 Rogers, M.T.; Woodbrey, J.C. *J. Phys. Chem.* **1962**, 66, 540
- 22 Sutherland, I.O. *Ann Reports NMR Spectros.* **1971**, 4, 71.
- 23 Harris, R.K. *"Nuclear Magnetic Resonance Spectroscopy"*, Pittman, London, U.K, **1983**.
- 24 Gupta, R.K.; Pitner, T.P.; Wasylshen, R. *J. Mag. Reson.* **1974**, 13, 383-385.
- 25 Kaplan, J.I. *J. Chem. Phys.* **1972**, 57, 5615-5616.
- 26 Ernst, R.R. *J. Chem. Phys.* **1973**, 59, 989
- 27 Kaplan, J.I. *J. Chem. Phys.* **1973**, 59, 990.
- 28 Farrer, T.C.; Becker, E.D. *"Pulse and Fourier Transform NMR"*, Academic Press, New York, **1971**.

- 29 LINSHP; a Fortran-77 program by Clarke, P. PhD Thesis, University of Adelaide, **1992**.
- 30 Wynne-Jones, W.F.K.; Eyring, H. *J. Chem. Phys.* **1935**, 3, 492.
- 31 Glasstone, S.; Laidler, K.J.; Eyring, H. "*Theory of Rate Processes*", McGraw-Hill, New York, **1941**.
- 32 Kuruscev, T. *J. Chem. Educ.* **1978**, 55, 128.
- 33 Kuruscev, T. Unpublished Material, 1990, University of Adelaide.
- 34 Pitha, J.; Jones, R.N. *Can. J. Chem.* **1966**, 44, 3031.

## Appendix i: The Gutmann Donor Number

The majority of solvents are electron pair donors, with the ability to donate electron density to an electron pair acceptor such as a metal ion. Thus, in solution, the complexation of a metal ion by a ligand involves a competition between the ligand and the solvent for coordination of the metal ion. The Gutmann donor number  $D_N$ , is an empirical measurement of the electron pair donating power or donor strength of the solvent, which has been successfully used to correlate the results of a number of kinetic and equilibrium studies of metal complexes in non-aqueous solution.<sup>1-4</sup>  $D_N$  is defined as the enthalpy of formation ( $-\Delta H / \text{kJ mol}^{-1}$ ) of the 1:1 adduct between a solvent molecule and the reference electron pair acceptor antimony (V) chloride ( $\text{SbCl}_5$ ) in the non-coordinating solvent 1,2-dichloroethane (Equation A.1). Thus, as solvent donor strength increases,  $D_N$  increases. The  $D_N$  values for the solvents used in this study appear in Table A.1

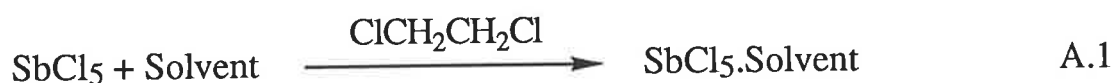


Table A.1.  $D_N$  Values for Solvents Used in This Study.

Solvent	$D_N^a$	$D_N^b$
1,2-dichloroethane	0.0	
acetonitrile	14.1	
propylene carbonate	15.1	
methanol	19.0	23.5
dimethylformamide	26.6	
dimethylsulfoxide	29.8	
water	18.0	33.0
pyridine	33.1	

<sup>a</sup> References 5-6. <sup>b</sup> References 7-8.

It has been suggested that for bulk water and methanol, the values  $D_N = 33.0$  and  $23.5$ , respectively, are more appropriate<sup>7-8</sup> than  $D_N = 18.0$  and  $19.0$ , respectively, obtained for water and methanol in 1,2-dichloroethane, where the hydrogen bonding structure of these protic solvents is disrupted. However, as discussed in Section 2.5, it is probable that neither  $D_N = 18.0$  nor  $D_N = 33.0$  are accurate measures of metal ion hydration energies.

In this study,  $D_N$  has been successfully used as a measure of the strength of cation-solvent interactions in solution. There is a good correlation between  $D_N$  and the stabilities and labilities of the metal complexes studied. However, one drawback in using  $D_N$  is that no allowance has been made for specific interactions which may exist between certain donor-acceptor species. Thus, there is a good correlation between  $D_N$  and the stabilities of the  $Ag^+$  complexes in the oxygen donor solvents, but not in the nitrogen donor solvents, because of the high affinity of  $Ag^+$  for nitrogen donor atoms. Since  $D_N$  is calculated on the basis of electron pair donation by a single solvent molecule, it does not take into account steric effects which may occur when a metal ion is coordinated to several bulky solvent molecules. Thus, in pyridine, the relationship between  $D_N$  and the solvation energy of  $M^+$  appears to be disrupted, probably because the incorporation of the nitrogen donor atom within the aromatic ring results in steric hindrance between adjacent pyridines in the first coordination sphere of  $M^+$ .

- 1 Cox, B.G.; Garcia-Rosas, J.; Schneider, H. *J. Am. Chem. Soc.* **1981**, 103, 1054-1059.
- 2 Lincoln, S.F.; Brereton, I.M.; Spotswood, T.M.; *J. Am. Chem. Soc.* **1986**, 108, 8134-8138.
- 3 Lincoln, S.F.; Abou-Hamdan, A. *Inorg. Chem.* **1990**, 30, 462-466.
- 4 Shamsipur, M.; Popov, A.I. *Inorg. Chim. Acta.* **1980**, 43, 243-247.
- 5 Mayer, U.; Gutmann, V. *Top. Curr. Chem.* **1972**, 27, 113-140.
- 6 Gutmann, V. *"Coordination Chemistry in Non-Aqueous Solvents"*, Springer-Verlag, Wien, **1968**.
- 7 Erlich, R.H.; Roach, E.; Popov, A.I. *J. Am. Chem. Soc.* **1970**, 92, 4989-4990.
- 8 Dewitte, W.J.; Popov, A.I. *J. Soln. Chem.* **1976**, 5, 231-240.

## Publications:

"Complexation of Sodium (I) and Other Monovalent Ions by 4,7,13,16-Tetraoxa-1,10-diazabicyclo[8.8.2]eicosane in a Range of Solvents. A Potentiometric Titration and  $^{23}\text{Na}$  Nuclear Magnetic Resonance Study"

Stephen F. Lincoln and Ashley K. W. Stephens. *Inorg. Chem.* **1991**, 30, 3529-3537.

"Complexation of Monovalent Metal Ions by 4,7,13,16-Tetraoxa-1,10-diazabicyclo[8.8.8]hexacosane in a Range of Solvents. A Potentiometric Titration and Nuclear Magnetic Resonance Study"

Stephen F. Lincoln and Ashley K. W. Stephens. *Inorg. Chem.* **1992**, 31, 5067-5071.

"The Complexation of Divalent Metal Ions by the Cryptands 4,7,13,16-Tetraoxa-1,10-diazabicyclo[8.8.2]eicosane, -[8.8.5]tricosane and -[8.8.8]hexacosane in Aqueous Solution"

Rameshpal S. Dhillon, Stephen F. Lincoln, Ashley K. W. Stephens and Paul A. Duckworth. *Inorg. Chim. Acta.* **1994**, 215, 79-84.

"Complexation of the Sodium Ion by a Pendant-Arm Tetraaza Macrocyclic Ligand in Aqueous Solution"

Ashley K. W. Stephens and Stephen F. Lincoln. *J. Chem. Soc., Dalton Trans.* **1993**, 2123-2126.

"Cyclodextrin Inclusion Complexes of Two Non-Steroidal Antiinflammatory Drugs and of an Analgesic Drug"

Susan E. Brown, John H. Coates, Christopher J. Easton, Stephen F. Lincoln, Yin Luo and Ashley K.W. Stephens. *Aust. J. Chem.* **1991**, 44, 855-862.

"Isomerization and Sodium(I) Exchange in N,N',N'',N'''-Tetrakis-(hydroxyethyl)-1,4,7,10-tetraazacyclododecane sodium(I) and its methoxyethyl and (*S*-) 2-hydroxypropyl Analogues"

Ramesh Dhillon, Ashley K.W. Stephens, Sonya Whitbread, Stephen F. Lincoln and Kevin P. Wainwright. Submitted for Publication.

**"Isomerism in the Cadmium (II), Mercury (II) and Lead (II) Complexes of Two Isomeric Pendant Arm Tetraaza Macrocyclic Ligands"**

Ashley K.W. Stephens, Ramesh Dhillon, Stephen F. Lincoln and Kevin P. Wainwright. Submitted for Publication.